EFFECT OF COMPRESSIBILITY, SUCTION, AND HEAT TRANSFER ON THE NONPARALLEL STABILITY OF BOUNDARY-LAYER FLOWS

by

Nabil Mohamed El-Hady

Dissertation submitted to the Graduate Faculty of the
Virginia Polytechnic Institute and State University
in partial fulfilment of the requirements for the degree of
DOCTOR OF PHILOSOPHY
in
Engineering Mechanics

APPROVED:

Ali H. Nayfeh, Chairman

William S. Saric

Dean T. Mook

Mark S. Cramer

Chih B. Ling

December, 1978

Blacksburg, Virginia

TO MY PARENTS

ACKNOWLEDGEMENTS

I would like to express my sincere gratitude to the Chairman of my committee, Dr. Ali H. Nayfeh, whose guidance, encouragement, knowledge and understanding were indispensable throughout this work. His invaluable help and constructive criticism in the preparation of this manuscript is deeply appreciated. I would also like to express my appreciation to Dr. William S. Saric who served as a guide in the initial stages of the research and provided early numerical assistance. I would also like to thank Dr. John E. Kaiser whose classroom lectures in viscous flows has been of great help. Thanks are also extended to other members of my committee.

Thanks are extended to the United States National Aeronautics and Space Administration, Langely Research Center for supporting this work. The aid of Langley Research Center, in running the computer program for the cases of suction is greatly appreciated. Thanks are due to who suffered through the typing of this work.

Finally, a profound debt of gratitude is expressed to my wife, for her support throughout these graduate school years. Without her sacrifice, loyalty and patience this dissertation would not have been possible.

TABLE OF CONTENTS

Table of Contents Con't

Table of Contents Con't

LIST OF TABLES

LIST OF FIGURES

List of Figures (Con't)

List of Figures (Con't)

List of Figures (Con't)

List of Figures (Con't)

List of Figures (Con't)

List of Figures (Con't)

List of Figures (Con't)

CHAPTER 1

INTRODUCTION

It was an early view of Reynolds, developed by Rayleigh, that transition to turbulence is a consequence of the instability of laminar flows. This approach has stimulated much theoretical and experimental work in boundary-layer stability.

In a boundary layer, the theory predicts and the experiments verify that the initial instability takes the form of two-dimensional velocity and pressure disturbances known as Tollmien-Schlichting waves (Schubauer and Skramstad, 1947). These disturbances have small amplitudes and do not affect the mean flow. Their growth rates are independent of the disturbance amplitudes. However, three-dimensionality soon appears as the Tollmien-Schlichting waves quickly begin to show spanwise variations as observed by Klebanoff et al (1962). With the generated streamwise vortices, nonlinear effects begin. The disturbances continue to grow downstream and when they significantly distort the mean flow, secondary instabilities take place (Kovasznay et al, 1962; Sato, 1970; Miksad, 1973; Kelly, 1967; Morkovin, 1978; Kachanov et al, 1977; Nayfeh and Bozatli, 1978). From then on the process is more of a breakdown rather than a continual growth. Hama and Nutant (1963) have observed the disintegration of streamwise vortices into families of smaller and smaller vortices with random frequencies and amplitudes. Then spots of turbulent flow appear from intense local fluctuations and grow in size as they move downstream. Finally, the turbulent spots coalesce, resulting in a fully turbulent mean flow.

It is an accepted fact that transition is the result of several instability mechanisms (Dryden, 1955; Morkovin, 1958, 1969; Reshotko, 1976; Tani, 1969). Since the linear instability of small-amplitude disturbances is one of the major roads leading to natural transition, boundary-layer stability has received considerable attention in an attempt to develop a better understanding of this aspect of the transition process. The fair agreement between the boundary-layer experiments of Schubauer and Skramstad (1947), Liepmann (1943), Laufer and Vrebalovich (1960), Kendall (1967), and others with appropriate theories has provided a basis for further development. However, transition to turbulence is generally found to occur at Reynolds numbers much greater than the critical value predicted by linear theory. Thus, the problems of calculating the stability of a shear layer and predicting the actual transition are distinct problems.

A shear layer, like any other continuous system, is capable of free oscillations around its mean state. The linear stability investigations are usually concerned with these free oscillations (normal modes), whereby infinitesimal disturbances are introduced in the boundary-layer. These disturbances tend to excite the normal modes of the boundary layer which are often referred to as Tollmien-Schlichting waves. A solution of the eigenvalue problem arising from the linearized disturbance equations with the appropriate boundary conditions determines the nature of these normal modes.

The linear stability theory predicts the growth and decay of the free oscillations, but like any other linear theory it cannot predict

the amplitude of the free-oscillation terms. It identifies the range of unstable frequencies under given flow conditions and the overall growth of a disturbance of constant frequency as it travels through the unstable region. Also, it determines the critical Reynolds number below which all disturbances are damped and the effects of the different flow parameters on the stability. Such parametric studies can be used to direct efforts for stabilizing the flow and hence delaying transition. Since nonlinearities and secondary instabilities precede transition, the linear stability theory is not expected to be valid there. In the absence of well developed nonlinear theories, a number of researchers have used the linear theory to correlate the location of transition. One of these correlations, the e^N criterion, calculates the amplitude ratio of a constant frequency disturbance and determines the so-called amplification factor $N = \ln \frac{a}{a_0}$, where a_0 is the initial amplitude. Smith and Gamberoni (1956) proposed this criterion for flight data and suggested that the transition location corresponds to the Reynolds number and frequency range where N = 9. This value was modified later to N = 10 by Jaffe, et al (1970). This method is semi-empirical. Its general success in giving satisfactory results for incompressible two-dimensional and axisymmetric flows (Van Ingen, 1956; Kaups, 1975) indicates that in these cases the initial disturbance level is low and linear instability is the road leading to transition. For supersonic flows, wind-tunnel data do not correspond to flight data because of the high noise levels in ground facilities. Consequently there is no direct criterion to predict transition. Reshotko (1969) and Mack (1975)

attempted to use linear stability theory to clarify this issue. Reshotko invoked dimensional analysis and results of linear stability theory to identify all factors possibly affecting transition. He concluded that the dimentionless frequency of the disturbance and the wave orientation are relevant parameters. Mack examined detailed numerical results in the light of supersonic wind tunnel transition measurements. He concluded that changes in the transition Reynolds number with changes in the freestream Mach number and wall temperature can be accounted for by the linear stability theory. As pointed out by Morkovin (1969), still there is a need for more accumulation of complete transition data. With such data, linear stability theory can aid in clarifying the subject of supersonic boundary-layer transition.

A principle application of linear stability investigations is the design of laminar-flow vehicles. By reducing the friction drag, a high performance is achieved with respect to range and economy of vehicle operation. The optimum amount of suction, or cooling (in air), or heating (in water) required to maintain laminar flow depends on accurate stability calculations.

The first analytical solutions for the stability of the Blasius boundary layer were obtained by Tollmien (1929) and Schlichting (1935). These solutions were continually refined as analytical and numerical techniques improved so that the later work (e.g., Mack, 1969) has rendered much of the literature before 1965 quite obsolete. Classical linear stability theories treat the basic flows as quasi-parallel flows. A summary of the parallel stability calculations for the Blasius profile

is given by Jordinson (1970). For a flow past a flat plate, the critical Reynolds number predicted by parallel stability theories is about 30% larger than the experimental results of Schubauer and Skramstad (1947), Wortmann (1955), Ross et al (1970), Kachanov et al (1975), and Strazisar et al (1975, 1977). Various investigators (e.g., Barry and Ross, 1970; Ling and Reynolds, 1973; Lanchon and Eckhaus, 1964; Volodin, 1973; Boehman, 1971; Wazzan et al, 1974) have made incomplete attempts to account for the nonparallel-flow effects by retaining the normal velocity component or some of the streamwise derivatives of the basic flow in the stability equations. However, the full nonparallel incompressible problem has been solved recently by Bouthier (1972, 1973), Nayfeh et al (1974), and Gaster (1974). Saric and Nayfeh (1975) presented a critical review of the prior work, together with a treatment of the nonparallel stability theory. They analyzed the spatial stability of two-dimensional incompressible boundary-layer flows and applied this analysis to the Blasius and Falkner-Skan flows. Their results show that the nonparallel effects are insignificant for flows with a favorable pressure gradient, are quite noticeable for the Blasius flow, and become more pronounced as the pressure gradient becomes more adverse. Saric and Nayfeh (1977) extended their nonparallel investigations to boundary-layer flows with pressure gradients and suction.

The earliest compressible stability analyses were of Lees and Lin (1946) and Lees (1947). They were extended by Dunn and Lin (1955), Reshotko (1960), and Lees and Reshotko (1962). These early theories were asymptotic or approximate in nature and proved to be valid only up

to low supersonic Mach numbers. The use of direct computer solutions to exploit the full compressible stability equations was initiated by Mack (1960, 1965, 1967) and Brown (1961, 1962, 1967). An extensive treatment of the parallel stability theory for compressible flows is given by Mack (1969).

In the case of compressible flows, the stability problem is more complex. It is necessary to account for the rate of heat transfer between the fluid and the wall. When the fluid is incompressible, heat can be exchanged between the wall and the fluid only if the temperature of the wall is higher or lower than that of the fluid. In either case a thermal boundary layer develops in addition to the velocity boundary layer, and it plays an important role in the determination of the stability of the flow.

The aim of this study is to demonstrate the effect of heating, suction, and compressiblity on the stability characteristics of boundary-layer flows within the framework of a complete nonparallel linear stability theory.

In Chapter 2, we introduce a formulation of the linear nonparallel stability theory. We consider the spatial, three-dimensional stability of laminar incompressible and compressible two-dimensional steady viscous flows. In Chapter 3, we describe the numerical procedures and techniques used in solving the disturbance equations. Chapter 4 is devoted to the investigation of the nonparallel stability of heated water boundary layers on a flat plate. Cases of uniform as well as nonuniform plate heating are considered. Theoretical results are com-

pared with the experimental results of Strazisar et al (1975, 1977) and Strazisar and Reshotko (1978). In Chapter 5, we analyze the linear nonparallel stability of two-dimensional disturbances in two-dimensional subsonic laminar boundary layers. Stability characteristics are examined for boundary-layer flows over an adiabatic flat plate to study the effect of slight compressibility of the mean flow. We compare the effects of continuous suction and suction through porous strips on the stability characteristics. In Chapter 6, we investigate the linear stability of three-dimensional disturbances in two-dimensional supersonic laminar boundary layers; we ascertain the nonparallel effects on the stability of oblique disturances. The theoretical results are compared with the experimental results of Laufer and Vrebalovich (1960) and Kendall (1967, 1975). In Chapter 7, the mean flow used for the stability calculations is discussed. Similar and nonsimilar solutions of the steady boundary-layer equations are presented. Finally Chapter 8 contains summary and conclusions.

CHAPTER 2

FORMULATION OF THE STABILITY THEORY

In this chapter, we consider the spatial, three-dimensional, stability of laminar incompressible and compressible two-dimensional steady viscous flows to small-amplitude disturbances.

The flow field is described by the Navier-Stokes, energy, and state equations. Lengths, velocities, and time are made dimensionless using a suitable reference length L^*, the freestream velocity U_∞^*, and L^*/U_∞^*, respectively. The pressure is made dimensionless using $\rho_\infty^* U_\infty^{*2}$. The temperature, density, specific heats, viscosity, and thermal conductivity are made dimensionless using their corresponding freestream values. In terms of these dimensionless quantities and in a vectorial form, the governing equations are

continuity

$$\frac{\partial \rho}{\partial t} + \nabla \cdot (\rho \vec{v}) = 0 \tag{2.1}$$

momentum

$$\rho\left(\frac{\partial \vec{v}}{\partial t} + \vec{v} \cdot \nabla \vec{v}\right) = -\nabla p + \frac{1}{R} \nabla \cdot \tau \tag{2.2}$$

energy

$$\rho\left(\frac{\partial T}{\partial t} + \vec{v} \cdot \nabla T\right) = Ec\left[\left(\frac{\partial p}{\partial t} + \vec{v} \cdot \nabla p\right) + \frac{1}{R} \Phi\right] + \frac{1}{RPr_\infty c_p} \nabla \cdot (\kappa \nabla T) \tag{2.3}$$

and the state equation, which will be considered seperately for a perfect gas or a heated liquid. In these equations τ is the dimension-

less stress tensor, Φ is the dimensionless dissipation function, $R = \rho_\infty U_\infty L/\mu_\infty$ is the Reynolds number, $Pr_\infty = c_{p_\infty} \mu_\infty/\kappa_\infty$ is the Prandtl number, $Ec = U_\infty^2/c_{p_\infty} T_\infty$ is the Eckert number, which becomes equivalent to the Mach number [$Ec = (\gamma-1)M_\infty^2$] for the case of high freestream velocity.

2.1 Governing Equations for Disturbances

To study the linear stability of a steady two-dimensional, boundary-layer flow (basic flow), we superpose a small time dependent disturbance on each mean-flow, thermodynamic, and transport quantity. Thus we let

$$\hat{q}(x,y,z,t) = Q_0(x,y) + q(x,y,z,t) \qquad (2.4)$$

where $Q_0(x,y)$ is a two-dimensional basic-state quantity and $q(x,y,z,t)$ is a three-dimensional unsteady disturbance quantity. Here, q or $\hat{q}$ stands for the velocity components (u,v, and w), temperature T, pressure p, density ρ, specific heat c_p, viscosity μ, and thermal conductivity κ. The total flow satisfies the equation of state and the time- dependent conservation laws of mass, momentum, and energy, whereas the basic state satisfies a more restricted set of equations; namely, the steady, laminar boundary-layer equations. Substituting Eq. (2.4) into Eqs. (2.1)-(2.3), subtracting the basic-state quantities, and linearizing the resulting equations in the q's, we obtain the following disturbance equations:

$$\frac{\partial \rho}{\partial t} + \frac{\partial}{\partial x}(\rho_0 u + \rho U_0) + \frac{\partial}{\partial y}(\rho_0 v + \rho V_0) + \rho_0 \frac{\partial w}{\partial z} = 0 \qquad (2.5)$$

$$\rho_0\left(\frac{\partial u}{\partial t} + U_0 \frac{\partial u}{\partial x} + u \frac{\partial U_0}{\partial x} + V_0 \frac{\partial u}{\partial y} + v \frac{\partial U_0}{\partial y}\right) + \rho\left(U_0 \frac{\partial U_0}{\partial x} + V_0 \frac{\partial U_0}{\partial y}\right) = -\frac{\partial p}{\partial x} + \frac{1}{R}\left\{\frac{\partial}{\partial x}\left[\mu_0\left(r \frac{\partial u}{\partial x} + s \frac{\partial v}{\partial y} + s \frac{\partial w}{\partial z}\right) + \mu\left(r \frac{\partial U_0}{\partial x} + s \frac{\partial V_0}{\partial y}\right)\right] + \frac{\partial}{\partial y}\left[\mu_0\left(\frac{\partial u}{\partial y} + \frac{\partial v}{\partial x}\right) + \mu\left(\frac{\partial U_0}{\partial y} + \frac{\partial V_0}{\partial x}\right)\right] + \mu_0 \frac{\partial}{\partial z}\left(\frac{\partial w}{\partial x} + \frac{\partial u}{\partial z}\right)\right\} \tag{2.6}$$

$$\rho_0\left(\frac{\partial v}{\partial t} + U_0 \frac{\partial v}{\partial x} + u \frac{\partial V_0}{\partial x} + V_0 \frac{\partial v}{\partial y} + v \frac{\partial V_0}{\partial y}\right) + \rho\left(U_0 \frac{\partial V_0}{\partial x} + V_0 \frac{\partial V_0}{\partial y}\right) = -\frac{\partial p}{\partial y} + \frac{1}{R}\left\{\frac{\partial}{\partial x}\left[\mu_0\left(\frac{\partial u}{\partial y} + \frac{\partial v}{\partial x}\right) + \mu\left(\frac{\partial U_0}{\partial y} + \frac{\partial V_0}{\partial x}\right)\right] + \frac{\partial}{\partial y}\left[\mu_0\left(s \frac{\partial u}{\partial x} + r \frac{\partial v}{\partial y} + s \frac{\partial w}{\partial z}\right) + \mu\left(r \frac{\partial V_0}{\partial y} + s \frac{\partial U_0}{\partial x}\right)\right] + \mu_0 \frac{\partial}{\partial z}\left(\frac{\partial v}{\partial z} + \frac{\partial w}{\partial y}\right)\right\} \tag{2.7}$$

$$\rho_0\left(\frac{\partial w}{\partial t} + U_0 \frac{\partial w}{\partial x} + V_0 \frac{\partial w}{\partial y}\right) = -\frac{\partial p}{\partial z} + \frac{1}{R}\left\{\frac{\partial}{\partial x}\left[\mu_0\left(\frac{\partial w}{\partial x} + \frac{\partial u}{\partial z}\right)\right] + \frac{\partial}{\partial y}\left[\mu_0\left(\frac{\partial v}{\partial z} + \frac{\partial w}{\partial y}\right)\right] + \mu_0 \frac{\partial}{\partial z}\left(s \frac{\partial u}{\partial x} + s \frac{\partial v}{\partial y} + r \frac{\partial w}{\partial z}\right) + \frac{\partial}{\partial z}\mu\left(s \frac{\partial U_0}{\partial x} + s \frac{\partial V_0}{\partial y}\right)\right\} \tag{2.8}$$

$$\rho_0\left[\frac{\partial T}{\partial t} + u \frac{\partial T_0}{\partial x} + U_0 \frac{\partial T}{\partial x} + v \frac{\partial T_0}{\partial y} + V_0 \frac{\partial T}{\partial y}\right] + \left(\rho_0 \frac{c_p}{c_{p_0}} + \rho\right) \times \left[U_0 \frac{\partial T_0}{\partial x} + V_0 \frac{\partial T_0}{\partial y}\right] = Ec\left[\frac{\partial p}{\partial t} + u \frac{\partial p_0}{\partial x} + U_0 \frac{\partial p}{\partial x} + V_0 \frac{\partial p}{\partial y} + \frac{1}{R}\phi\right] + \frac{1}{RPr_\infty c_{p_0}}\left[\frac{\partial}{\partial x}\left(\kappa_0 \frac{\partial T}{\partial x} + \kappa \frac{\partial T_0}{\partial x}\right) + \frac{\partial}{\partial y}\left(\kappa_0 \frac{\partial T}{\partial y} + \kappa \frac{\partial T_0}{\partial y}\right) + \kappa_0 \frac{\partial}{\partial z}\left(\frac{\partial T}{\partial z}\right)\right] \tag{2.9}$$

where ϕ, the perturbation dissipation function, is defined as

$$\phi = \mu_0 \left\{ 2r\left(\frac{\partial U_0}{\partial x}\frac{\partial u}{\partial x} + \frac{\partial V_0}{\partial y}\frac{\partial v}{\partial y}\right) + 2s\left[\frac{\partial U_0}{\partial x}\left(\frac{\partial v}{\partial y} + \frac{\partial w}{\partial z}\right) + \frac{\partial V_0}{\partial y}\left(\frac{\partial u}{\partial x} + \frac{\partial w}{\partial z}\right)\right] \right.$$
$$\left. + 2\left(\frac{\partial u}{\partial y} + \frac{\partial v}{\partial x}\right)\left(\frac{\partial U_0}{\partial y} + \frac{\partial V_0}{\partial x}\right) \right\} + \mu \left\{ r\left[\left(\frac{\partial U_0}{\partial x}\right)^2 + \left(\frac{\partial V_0}{\partial y}\right)^2\right] \right.$$
$$\left. + 2s\,\frac{\partial U_0}{\partial x}\frac{\partial V_0}{\partial y} + \left(\frac{\partial U_0}{\partial y} + \frac{\partial V_0}{\partial x}\right)^2 \right\} \qquad (2.10)$$

Moreover,

$$r = \frac{2}{3}(\ell + 2),\ s = \frac{2}{3}(\ell - 1),\ f = \frac{1}{3}(2\ \ + 1),\ \hat{\lambda}_0 = \frac{2}{3}\mu_0(\ell - 1) \qquad (2.11)$$

where ℓ is the ratio of the second to the first viscosity coefficients; $\ell = 0$ is the Stokes hypothesis.

Equations (2.5)-(2.10) represent the stability equations for a three-dimensional disturbance in a two-dimensional, basic flow. Although the basic-state velocity component W_0 is absent, a z-momentum disturbance equation is included. In the presence of the dissipation terms in the energy equation involving the disturbance velocity component w, the z-momentum equation is coupled with the other equations, and the order of the system is eight, in contrast with the sixth-order system that governs two-dimensional disturbances.

2.2 Boundary Conditions for Disturbances

The analysis presented here is applicable to cases with suction or blowing as well as cases with uniform or nonuniform wall heating or cooling. The stability problem is completed by the specification of the appropriate initial and boundary conditions. We consider next the boundary conditions.

At the wall, we require the vanishing of the component of the relative velocity of the fluid/solid surface that is parallel to the interface, even in the region of perforations. This is a reasonable assumption provided that the percentage of the permeable area is small and most of the flow there is directed normal to the wall. The normal velocity and thermal boundary conditions at the wall need careful consideration.

For an impermeable wall, both the mean and disturbance velocities normal to the surface must vanish, whereas for a permeable wall this is not the case. The mean normal velocity component is not zero. For different disturbance normal velocities at the wall, Gaponov (1971, 1975) showed a destabilizing effect of a nonzero value for the normal component of the disturbance velocity at the wall. His results are based on the calculation of the neutral stability curves. Such curves are not directly related to transition. Moreover the boundary condition used by Gaponov is not of a practical application. Of more interest are the results of Lekoudis (1978), who examined the effect of the normal component of the disturbance velocity on the growth rates of disturbances. This boundary condition is given in the form of an admittance calculated for different configurations. He concluded that the condition of zero normal velocity at the wall is a reasonable approximation when the surface permeability is very small.

The thermal boundary condition for the disturbances needs an analysis of the heat conduction problem in the region very close to the wall (e.g., Dunn and Lin, 1955). This analysis results in a thermal boundary condition for the disturbance in the form

$$\frac{\partial T}{\partial y}(0) + g\,T(0) = 0$$

where g is a constant that depends on the disturbance frequency, and the physical properties of the liquid and the adjacent solid wall. This condition holds for very low frequencies because the thermal fluctuations can penetrate large distances into the solid wall. On the other hand, for very high frequencies, the thermal inertia of the solid makes the thermal fluctuations die out in the solid very close to the surface, and the wall remains at the temperature of the basic flow. In this case the condition $T(0) = 0$ is a very accurate approximation.

In the freestream, it is assumed that all disturbance quantities die out for subsonic disturbances and satisfy a radiation condition for supersonic disturbances. For boundary layers in subsonic flows, disturbances have amplitudes that decay exponentially in the freestream. For boundary layers in supersonic flows, we restrict our discussion to subsonic disturbances, that is to disturbances that move subsonically with respect to the freestream. The amplitudes of these disturbances decay also exponentially in the freestream.

In this work, we consider walls of small permeability and subsonic disturbances of sufficiently high frequencies. With these assumptions, the disturbance boundary conditions become

$$u = v = w = T = 0 \quad \text{at } y = 0 \tag{2.12}$$

$$u,v,w,T \to 0 \qquad \text{as } y \to \infty \tag{2.13}$$

2.3 Nonparallel-Flow Considerations

We consider weakly nonparallel flows. Thus, to account for the nonparallelism of the mean flow, we require that all mean-flow variables be weak functions of the streamwise position. Moreover, we require that the normal velocity component be small compared with the streamwise velocity component. These assumptions are expressed mathematically by writing the mean-flow variables in the form

$$U_0 = U_0(x_1,y),\ V_0 = \varepsilon V_0(x_1,y),\ p_0 = p_0(x_1),\ T_0 = T_0(x_1,y),$$
$$\rho_0 = \rho_0(x_i,y),\ c_{p_0} = c_{p_0}(x_1,y),\ \mu_0 = \mu_0(x_1,y),\ \kappa_0 = \kappa_0(x_1,y) \tag{2.14}$$

where

$$x_1 = \varepsilon x \tag{2.15}$$

and ε is a small dimensionless parameter characterizing the nonparallelism of the mean flow. In the parallel-flow approximation, $V_0 = 0$ and all variables in Eqs. (2.14) are independent of x_1. The main idea behind the nonparallel-flow analysis is to make a perturbation about the parallel-flow solution (Bouthier, 1973; Gaster, 1974; Nayfeh et al, 1974). The method of multiple scales (Nayfeh, 1973) is used to effect this perturbation. Accordingly different streamwise scales x, x_1, z, and z_1 are introduced. The fast scales x and z are used to describe the relatively rapid streamwise and spanwise variations of the traveling wave disturbance. The slow scales $x_1 = \varepsilon x$ and $z_1 = \varepsilon z$ are used to describe the relatively slow variations of the mean-flow quantities, the disturbance wavenumber, the growth rate, and the amplitude. Since the mean

flow is independent of z_1, the disturbance quantities are independent of z_1 unless the amplitude and wavenumber of the initial disturbance depend on z_1.

Since the coefficients in Eqs. (2.5)-(2.10) vary slowly in the streamwise direction and are independent of time, we use the method of multiple scales and seek a first-order expansion for the nine disturbance variables u, v, w, p, T, ρ, c_p, μ, and κ in the form of a traveling harmonic wave; that is

$$q(x_1,y,z_1,t;\varepsilon) = [q_1(x_1,y,z_1) + \varepsilon q_2(x_1,y,z_1) + \ldots]\exp(i\theta) \tag{2.16}$$

We note that because of the nonparallelism, the amplitudes of the disturbance quantities are functions of the slow scales x_1 and z_1 as well as y. In Eq. (2.16) the phase function θ is defined by

$$\nabla\theta = \vec{K}_0 = [\alpha_0(x_1,z_1),\ \beta_0(x_1,z_1)] \tag{2.17a}$$

$$\frac{\partial\theta}{\partial t} = -\omega \tag{2.17b}$$

Here α_0 and β_0 are the quasi-parallel components of the wavenumber vector $\vec{K}_0$ and ω is the circular frequency.

For the case of quasi-parallel spatial stability ω is real and α_0 and β_0 are complex, while for the case of quasi-parallel temporal stability, α_0 and β_0 are real and ω is complex. For the general case, α_0, β_0, and ω are complex. The present study is limited to spatial stability so that ω is a known real quantity.

In terms of x_1, z_1, and θ, the spatial and temporal derivatives are transformed as

$$\frac{\partial}{\partial x} = \alpha_0 \frac{\partial}{\partial \theta} + \varepsilon \frac{\partial}{\partial x_1} \tag{2.18a}$$

$$\frac{\partial}{\partial z} = \beta_0 \frac{\partial}{\partial \theta} + \varepsilon \frac{\partial}{\partial z_1} \tag{2.18b}$$

$$\frac{\partial}{\partial t} = - \omega \frac{\partial}{\partial \theta} \tag{2.18c}$$

Substituting Eqs. (2.16)-(2.18) into Eqs. (2.5)-(2.10) and equating the coefficients of ε^0 and ε on both sides, we obtain problems describing the q_1 and q_2 disturbance quantities. These problems are referred to as the first- and second-order problems, and they are discussed in the next two sections.

The disturbances of the fluid properties c_p, μ, and κ are related to the temperature disturbance by

$$q(x_1,y,z_1,t;\varepsilon) = \frac{dQ_0}{dT_0} [T_1(x_1,y,z_1) + \varepsilon T_2(x_1,y,z_1) + \ldots]\exp(i\theta) \tag{2.19}$$

while the density disturbance is related to the temperature disturbance by the state equation.

2.4 The First-Order Problem

Substituting Eqs. (2.16)-(2.19) into Eqs. (2.5)-(2.10) and equating the coefficients of ε^0 on both sides, we obtain

$$L_1(u_1,v_1,w_1,p_1,T_1) = i\rho_0(\alpha_0 u_1 + \beta_0 w_1) + i(\alpha_0 U_0 - \omega)\rho_1$$

$$+ \frac{\partial}{\partial y}(\rho_0 v_1) = 0 \tag{2.20}$$

$$L_2(u_1,v_1,w_1,p_1,T_1) = [i\rho_0(\alpha_0 U_0 - \omega) + \frac{\mu_0}{R}(r\alpha_0^2 + \beta_0^2)]u_1$$
$$+ (\rho_0 \frac{\partial U_0}{\partial y} - \frac{i}{R}\frac{\partial \mu_0}{\partial y}\alpha_0)v_1 + \frac{f}{R}\mu_0\alpha_0\beta_0 w_1 + i\alpha_0 p_1$$
$$- \frac{T_1}{R}\frac{\partial}{\partial y}(\frac{d\mu_0}{dT_0}\frac{\partial U_0}{\partial y}) - \frac{1}{R}\frac{\partial \mu_0}{\partial y}\frac{\partial u_1}{\partial y} - \frac{if}{R}\mu_0\alpha_0\frac{\partial v_1}{\partial y}$$
$$- \frac{1}{R}\frac{d\mu_0}{dT_0}\frac{\partial U_0}{\partial y}\frac{\partial T_1}{\partial y} - \frac{1}{R}\mu_0\frac{\partial^2 u_1}{\partial y^2} = 0 \qquad (2.21)$$

$$L_3(u_1,v_1,w_1,p_1,T_1) = [i\rho_0(\alpha_0 U_0 - \omega) + \frac{\mu_0}{R}(\alpha_0^2 + \beta_0^2)]v_1$$
$$- \frac{is}{R}\alpha_0\frac{\partial \mu_0}{\partial y}u_1 - \frac{is}{R}\beta_0\frac{\partial \mu_0}{\partial y}w_1 - \frac{i}{R}\alpha_0\frac{d\mu_0}{dT_0}\frac{\partial U_0}{\partial y}T_1$$
$$- \frac{if}{R}\mu_0\alpha_0\frac{\partial u_1}{\partial y} - \frac{r}{R}\frac{\partial \mu_0}{\partial y}\frac{\partial v_1}{\partial y} - \frac{if}{R}\mu_0\beta_0\frac{\partial w_1}{\partial y}$$
$$+ \frac{\partial p_1}{\partial y} - \frac{r}{R}\mu_0\frac{\partial^2 v_1}{\partial y^2} = 0 \qquad (2.22)$$

$$L_4(u_1,v_1,w_1,p_1,T_1) = [i\rho_0(\alpha_0 U_0 - \omega) + \frac{\mu_0}{R}(\alpha_0^2 + r\beta_0^2)]w_1$$
$$+ \frac{f}{R}\mu_0\alpha_0\beta_0 u_1 - \frac{i}{R}\beta_0\frac{\partial \mu_0}{\partial y}v_1 + i\beta_0 p_1 - \frac{if}{R}\mu_0\beta_0\frac{\partial v_1}{\partial y}$$
$$- \frac{1}{R}\frac{\partial \mu_0}{\partial y}\frac{\partial w_1}{\partial y} - \frac{\mu_0}{R}\frac{\partial^2 w_1}{\partial y^2} = 0 \qquad (2.23)$$

$$L_5(u_1,v_1,w_1,p_1,T_1) = \Big\{i\rho_0(\alpha_0 U_0 - \omega) - \frac{Ec}{R}\frac{d\mu_0}{dT_0}(\frac{\partial U_0}{\partial y})^2$$
$$+ \frac{1}{RPr_\infty c_{p_0}}[\kappa_0(\alpha_0^2 + \beta_0^2) - \frac{\partial^2 \kappa_0}{\partial y^2}]\Big\}T_1 + (\rho_0\frac{\partial T_0}{\partial y}$$
$$- \frac{2iEc}{R}\mu_0\alpha_0\frac{\partial U_0}{\partial y})v_1 - iEc(\alpha_0 U_0 - \omega)p_1 - \frac{2}{RPr_\infty c_{p_0}}\frac{\partial \kappa_0}{\partial y}\frac{\partial T_1}{\partial y}$$
$$- \frac{2Ec}{R}\mu_0\frac{\partial U_0}{\partial y}\frac{\partial u_1}{\partial y} - \frac{\kappa_0}{RPr_\infty c_{p_0}}\frac{\partial^2 T_1}{\partial y^2} = 0 \qquad (2.24)$$

The boundary conditions are

$$u_1 = v_1 = w_1 = T_1 = 0 \quad \text{at } y = 0 \tag{2.25}$$

$$u_1 , v_1, w_1, T_1 \to 0 \quad \text{as } y \to \infty \tag{2.26}$$

The operators, L_1, L_2, L_3, L_4, and L_5 correspond to the continuity, x-momentum, y-momentum, z-momentum, and energy equations, respectively.

The scales x_1 and z_1 appear implicitly in these equations due to the dependence of the mean-flow quantities on x_1 and the assumed dependence of the initial disturbance on z_1. It is convenient to express Eqs. (2.20)-(2.24) as a set of eight, first-order equations by introducing the new variables Z_{1_n} defined by

$$Z_{11} = u_1, \quad Z_{12} = \frac{\partial u_1}{\partial y}, \quad Z_{13} = v_1, \quad Z_{14} = p_1,$$

$$Z_{15} = w_1, \quad Z_{16} = \frac{\partial w_1}{\partial y}, \quad Z_{17} = T_1, \quad Z_{18} = \frac{\partial T_1}{\partial y} \tag{2.27}$$

Then, Eqs. (2.20)-(2.26) can be rewritten in the compact form

$$\frac{\partial Z_{1_i}}{\partial y} - \sum_{j=1}^{8} a_{ij} Z_{1_j} = 0 \quad \text{for } i = 1,2,\ldots,8 \tag{2.28}$$

$$Z_{11} = Z_{13} = Z_{15} = Z_{17} = 0 \quad \text{at } y = 0 \tag{2.29}$$

$$Z_{11}, Z_{13}, Z_{15}, Z_{17} \to 0 \quad \text{as } y \to \infty \tag{2.30}$$

where the a_{ij} are the elements of an 8 x 8 variable-coefficient matrix. Equations (2.28)-(2.30) consitute an eigenvalue problem that is solved numerically. The numerical solution is discussed in detail in the next chapter, and the solution of Eqs. (2.28)-(2.30) can be expressed in the form

$$Z_{1_i} = A(x_1,z_1)\zeta_i(x_1,y,z_1) \quad \text{for } i = 1,2,\ldots,8 \tag{2.31}$$

where A is still an undetermined function at this level of approximation. It is determined by imposing the solvability condition at the next level of approximation.

2.5 The Second-Order Problem

Substituting Eqs. (2.16)-(2.19) into Eqs. (2.5)-(2.10) and equating the coefficients of ε on both sides, we obtain

$$L_1(u_2,v_2,w_2,p_2,T_2) = I_m \tag{2.32}$$

$$L_2(u_2,v_2,w_2,p_2,T_2) = I_x \tag{2.33}$$

$$L_3(u_2,v_2,w_2,p_2,T_2) = I_y \tag{2.34}$$

$$L_4(u_2,v_2,w_2,p_2,T_2) = I_z \tag{2.35}$$

$$L_5(u_2,v_2,w_2,p_2,T_2) = I_e \tag{2.36}$$

The boundary conditions are

$$u_2 = v_2 = w_2 = T_2 = 0 \quad \text{at } y = 0 \tag{2.37}$$

$$u_2,v_2,w_2,T_2 \to 0 \qquad \text{as } y \to \infty \tag{2.38}$$

where the operators L_1-L_5 are defined by Eqs. (2.20)-(2.24) and I_m, I_x, I_y, I_z, and I_e are the inhomogeneous terms in the continuity, x-momentum, y-momentum, z-momentum, and energy equations, respectively. These inhomogeneous terms reflect the effects of the streamwise and spanwise variations of the disturbance amplitude, the normal basic-velocity component and the streamwise and spanwise variations of the wavenumber. These terms are tabulated in the appendices for the specific physical problems considered.

With the solution of the first-order problem given by Eq. (2.31), the second-order problem can be rewritten as

$$\frac{\partial Z_{2_i}}{\partial y} - \sum_{j=1}^{8} a_{ij} Z_{2_j} = G_i \frac{\partial A}{\partial x_1} + E_i \frac{\partial A}{\partial z_1} + D_i A \quad \text{for } i = 1,2,\ldots,8 \tag{2.39}$$

$$Z_{21} = Z_{23} = Z_{25} = Z_{27} = 0 \quad \text{at } y = 0 \tag{2.40}$$

$$Z_{21}, Z_{23}, Z_{25}, Z_{27} \to 0 \quad \text{as } y \to \infty \tag{2.41}$$

where the G_i, E_i, and D_i are known functions of the ζ_i, α_0, β_0, and the basic-flow quantities. They are defined in the specific chapters for the physical problems considered. The new variables Z_{2_n} are defined in the same way the Z_{1_n} are defined in Eq. (2.27).

2.6 Adjoint Problem and Solvability Condition

Since the homogeneous parts of Eqs. (2.39)-(2.41) are the same as Eqs. (2.28)-(2.30) and since the latter have a nontrivial solution, the inhomogenous Eqs. (2.39)-(2.41) have a solution if, and only if, a solvability condition is satisfied. In this case the solvability condition demands the inhomogeneous terms to be orthogonal to every solution of the adjoint homogeneous problem; that is,

$$\int_0^{\infty} \sum_{i=1}^{8} \left[G_i \frac{\partial A}{\partial x_1} + E_i \frac{\partial A}{\partial z_1} + D_i A\right] W_i \, dy = 0 \tag{2.42}$$

where the $W_i(x_1,y,z_1)$ are the solutions of the adjoint homogeneous problem corresponding to the same eigenvalue. Thus, they are the solutions of

$$\frac{\partial W_i}{\partial y} + \sum_{j=1}^{8} a_{ji} W_j = 0 \quad \text{for } i = 1,2,\ldots,8 \tag{2.43}$$

$$W_2 = W_4 = W_6 = W_8 = 0 \quad \text{at } y = 0 \tag{2.44}$$

$$W_2,\ W_4,\ W_6,\ W_8 \to 0 \quad \text{as } y \to \infty \tag{2.45}$$

2.7 Amplitude Equation

Substituting for G_i, E_i, and D_i into the solvability conditions (2.42), we obtain the following equation for the modulation of the wave amplitude A with position:

$$Q_1 \frac{\partial A}{\partial x_1} + Q_2 \frac{\partial A}{\partial z_1} = Q_3 A \tag{2.46}$$

where

$$Q_1 = \int_0^\infty \sum_{i=1}^{8} G_i W_i \, dy \tag{2.47}$$

$$Q_2 = \int_0^\infty \sum_{i=1}^{8} E_i W_i \, dy \tag{2.48}$$

$$Q_3 = -\int_0^\infty \sum_{i=1}^{8} D_i W_i \, dy \tag{2.49}$$

Here, Q_1 and Q_2 are proportional to the components of the group velocity $(\frac{\partial \omega}{\partial \alpha_0}, \frac{\partial \omega}{\partial \beta_0})$.

To determine Q_3, we need to evaluate $\partial\alpha_0/\partial x_1$, $\partial\alpha_0/\partial z_1$, $\partial\beta_0/\partial x_1$, $\partial\beta_0/\partial z_1$, $\partial\zeta_i/\partial x_1$, and $\partial\zeta_i/\partial z_1$. To accomplish this, we replace Z_i by ζ_i in Eqs. (2.28)-(2.30), differentiate the result with respect to x_1, and obtain

$$\frac{\partial}{\partial y}\left(\frac{\partial \zeta_i}{\partial x_1}\right) = \sum_{j=1}^{8} a_{ij}\left(\frac{\partial \zeta_j}{\partial x_1}\right) + G_i \frac{\partial \alpha_0}{\partial x_1} + E_i \frac{\partial \beta_0}{\partial x_1} + S_i \quad \text{for } i = 1,2,\ldots,8 \tag{2.50}$$

$$\frac{\partial \zeta_1}{\partial x_1} = \frac{\partial \zeta_3}{\partial x_1} = \frac{\partial \zeta_5}{\partial x_1} = \frac{\partial \zeta_7}{\partial x_1} = 0 \quad \text{at } y = 0 \tag{2.51}$$

$$\frac{\partial \zeta_1}{\partial x_1}, \frac{\partial \zeta_3}{\partial x_1}, \frac{\partial \zeta_5}{\partial x_1}, \frac{\partial \zeta_7}{\partial x_1} \to 0 \quad \text{as } y \to \infty \tag{2.52}$$

Similarly, differentiation of Eqs. (2.28)-(2.30) with respect to z_1 yields

$$\frac{\partial}{\partial y}\left(\frac{\partial \zeta_i}{\partial z_1}\right) = \sum_{j=1}^{8} a_{ij}\left(\frac{\partial \zeta_j}{\partial z_1}\right) + G_i \frac{\partial \alpha_0}{\partial z_1} + E_i \frac{\partial \beta_0}{\partial z_1} \quad \text{for } i = 1,2,\ldots,8 \tag{2.53}$$

$$\frac{\partial \zeta_1}{\partial z_1} = \frac{\partial \zeta_3}{\partial z_1} = \frac{\partial \zeta_5}{\partial z_1} = \frac{\partial \zeta_7}{\partial x_1} = 0 \quad \text{at } y = 0 \tag{2.54}$$

$$\frac{\partial \zeta_1}{\partial z_1}, \frac{\partial \zeta_3}{\partial z_1}, \frac{\partial \zeta_5}{\partial z_1}, \frac{\partial \zeta_7}{\partial z_1} \to 0 \quad \text{as } y \to \infty \tag{2.55}$$

Here, G_i, E_i, and S_i are known functions of ζ_i, α_0, β_0, and the basic-flow quantities, they are given by

$$G_i = \sum_{j=1}^{8} \zeta_j \left.\frac{\partial a_{ij}}{\partial x_1}\right|_{\beta_0} = \sum_{j=1}^{8} \zeta_j \left.\frac{\partial a_{ij}}{\partial z_1}\right|_{\beta_0} \quad \text{for } i = 1,2,\ldots,8 \tag{2.56}$$

$$E_i = \sum_{j=1}^{8} \zeta_j \left.\frac{\partial a_{ij}}{\partial x_1}\right|_{\alpha_0} = \sum_{j=1}^{8} \zeta_j \left.\frac{\partial a_{ij}}{\partial z_1}\right|_{\alpha_0} \quad \text{for } i = 1,2,\ldots,8 \tag{2.57}$$

$$S_i = \sum_{j=1}^{8} \zeta_j \left.\frac{\partial a_{ij}}{\partial x_1}\right|_{\alpha_0,\beta_0} \quad \text{for } i = 1,2,\ldots,8 \tag{2.58}$$

We note that Eqs. (2.53) do not contain terms corresponding to the S_i in Eqs. (2.50) because the basic flow is two dimensional.

Again, applying the solvability condition to Eqs. (2.50)-(2.52) and Eqs. (2.53)-(2.55), we obtain

$$Q_1 \frac{\partial \alpha_0}{\partial x_1} + Q_2 \frac{\partial \alpha_0}{\partial z_1} = Q_4 \tag{2.59}$$

$$Q_1 \frac{\partial \beta_0}{\partial x_1} + Q_2 \frac{\partial \beta_0}{\partial z_1} = 0 \tag{2.60}$$

where Q_1 and Q_2 are given in Eqs. (2.47) and (2.48) and Q_4 is given by

$$Q_4 = -\int_0^\infty \sum_{i=1}^{8} S_i W_i dy \tag{2.61}$$

Note that we used in Eqs. (2.59) and (2.60) the fact that θ is twice differentiable; that is,

$$\nabla \times \vec{K}_0 = 0 \tag{2.62}$$

In the spatial theory α_0 and β_0 are complex and ω is real. We define a real wavenumber vector of magnitude k_0 and direction ψ according to

$$\vec{k}_0 = (\alpha_{0_r}, \beta_{0_r}), \qquad \psi = \tan^{-1}(\beta_{0_r}/\alpha_{0_r}) \tag{2.63}$$

and a real spatial amplification-rate vector of magnitude σ_0 and direction $\overline{\psi}$ according to

$$\vec{\sigma}_0 = (\alpha_{0_i}, \beta_{0_i}), \quad \overline{\psi} = \tan^{-1}(\beta_{0_i}/\alpha_{0_i}) \tag{2.64}$$

The solution of the eigenvalue problem Eqs. (2.28)-(2.30) gives the complex dispersion relation

$$\omega = \omega(\vec{k}_0, \vec{\sigma}_0, x, z) \tag{2.65}$$

For fixed ω, x, and z, there are four real parameters k_0, ψ, σ, and $\bar{\psi}$. Two of them can be determined from the eigenvalue calculation.

In general, the direction of the wave propagation ψ is different from the direction of the wave amplification $\bar{\psi}$. The propagation angle ψ can be used as an input parameter, while the question of determining the direction of the amplification $\bar{\psi}$ is still open. Mack (1977) chose the direction of the group velocity $(\frac{\partial \omega}{\partial \alpha_0}, \frac{\partial \omega}{\partial \beta_0})$ to be the direction of amplification. He showed that for two-dimensional basic flows, the direction of the group velocity deviates by a few degrees from the streamwise direction. This deviation decreases as the Mach number increases. In the absence of any clear criterion for determining the direction of wave amplification, and to compare our results with available experiments, which measure the amplification in the streamwise direction, we take $\bar{\psi} = 0$ in the stability analysis. In Chapter 6, we use the transformation developed by Nayfeh and Padhye (1978) to relate the spatial amplifications of a disturbance along two directions. Thus, Eqs. (2.46), (2.59), and (2.60) reduce to

$$Q_1 \frac{dA}{dx_1} = Q_3 A \tag{2.66}$$

$$Q_1 \frac{d\alpha_0}{dx_1} = Q_4 \tag{2.67}$$

$$\frac{d\beta_0}{dx_1} = 0 \tag{2.68}$$

Equations (2.66) can be written as

$$\frac{1}{A} \frac{dA}{dx_1} = iK_1(x_1) \tag{2.69}$$

The solution of Eq. (2.69) can be written as

$$A = A_0 \exp[i\varepsilon \int K_1(x_1)dx] \tag{2.70}$$

where A_0 is a constant of integration.

Therefore, to the first approximation

$$Z_{11} = A_0 \zeta_1(x_1, y)\exp[i \int (K_0 + \varepsilon K_1)dx - i\omega t] + O(\varepsilon) \tag{2.71}$$

where the Z_{1_i} are related to the disturbance variables by Eq. (2.27) and the constant A_0 is determined from the initial conditions. It is clear from Eq. (2.71) that, in addition to the dependence of the eigensolution on x, the eigenvalue K_0 is modified by εK_1.

CHAPTER 3

NUMERICAL PROCEDURE AND SOLUTION

The first-order stability problem is reduced to the solution of the following set of eight first-order equations and eight homogeneous boundary conditions:

$$\frac{\partial Z_{1i}}{\partial y} - \sum_{j=1}^{8} a_{ij} Z_{1j} = 0 \quad \text{for } i = 1,2,\ldots,8 \tag{3.1}$$

$$Z_{11} = Z_{13} = Z_{15} = Z_{17} = 0 \quad \text{at } y = 0 \tag{3.2}$$

$$Z_{11}, Z_{13}, Z_{15}, Z_{17} \to 0 \qquad \text{as } y \to \infty \tag{3.3}$$

This set constitutes an eigenvalue problem and it has nontrivial solutions only for certain combinations of the parameters α_0, β_0, ω and R. The solution of this eigenvalue problem is obtained numerically.

For the spatial stability problem, we assign values to ω and R and two relations among α_{0_r}, α_{0_i}, β_{0_r} and β_{0_i}, where $\alpha_0 = \alpha_{0_r} + i\alpha_{0_i}$ and $\beta_0 = \beta_{0_r} + i\beta_{0_i}$. Then, we guess the remaining two relations. Since the problem is linear, one can calculate eight linearly independent solutions. Then, the general solution is a linear combination of these eight linearly independent solutions. Application of the boundary conditions yields the desired constatns in the linear combination and hence the desired solution when the eigenvalues are known.

The linearly independent solutions are calculated by first converting the problem into an initial value problem. The form of the boundary conditions at $y = \infty$ makes it more convenient to start the integration at an arbitrary point outside the boundary layer because satisfaction of

these boundary conditions demands that four of the eight linearly independent solutions vanish, leaving only four nonvanishing linearly independent solutions to be calculated. Although all of the integrators use double precision arithmatic, a straightforward integration fails to produce four linearly independent solutions because of the buildup of parasitic errors among the different solutions. One of the most successful and efficient methods that overcome this difficulty is the method of orthonormalization. The linearly independent solutions of the equations are orthonormalized whenever a loss of linear independence is detected. The computer code used here is called SUPORT, which was developed by Scott and Watts (1977). It is based primarily on the method of Godunov (1961). Among the different integrators and orthonormalization tests included in SUPORT, we choose the RKF integrator, a variable-step-size integrator based on the Runge-Kutta-Fehlburg fifth-order formulas. This integrator is used in conjunction with the modified Gram-Schmidt orthonormalization procedure. SUPORT combined with a Newton-Raphson iterative scheme is used to solve the eigenvalue problem as follows.

3.1 Eigenvalues and Vectors

Outside the boundary layer (at $y = y_e > \delta$, where δ is the boundary-layer thickness), the mean-flow quantities are independent of y and the nonzero elements of the coefficient matrix $[a_{ij}]$ given by Eq. (3.1) are constants. They become

$$\hat{a}_{21} = iR(\alpha_0 - \omega) + \alpha_0^2 + \beta_0^2,\ \hat{a}_{24} = iR\alpha_0 - f\gamma M_e^2\alpha_0(\alpha_0 - \omega),$$

$$\hat{a}_{25} = f\alpha_0(\alpha_0 - \omega),\ \hat{a}_{31} = -i\alpha_0,\ \hat{a}_{34} = -i\gamma M_e^2(\alpha_0 - \omega),$$

$$\hat{a}_{35} = i(\alpha_0 - \omega),\ \hat{a}_{37} = -i\beta_0,\ \hat{a}_{42} = -i\chi\alpha_0,$$

$$\hat{a}_{43} = -\chi[iR(\alpha_0 - \omega) + \alpha_0^2 + \beta_0^2],\ \hat{a}_{46} = i\chi r(\alpha_0 - \omega),$$

$$\hat{a}_{48} = -i\chi\beta_0,\ \hat{a}_{64} = -iRPr_eEcM_e^2(\alpha_0 - \omega),$$

$$\hat{a}_{65} = iRPr_e(\alpha_0 - \omega) + \alpha_0^2 + \beta_0^2,\ \hat{a}_{84} = iR\beta_0 - f\gamma M_e^2\beta_0(\alpha_0 - \omega),$$

$$\hat{a}_{85} = f\beta_0(\alpha_0 - \omega),\ \hat{a}_{87} = \hat{a}_{21}$$

where

$$\chi = 1/[R + ir\gamma M_e^2(\alpha_0 - \omega)]$$

Equations (3.1) with a constant coefficient matrix $[\hat{a}_{ij}]$ permit a solution that can be expressed in the general form

$$Z_{1i} = \sum_{j=1}^{8} \Lambda_{ij}c_j\exp(\lambda_j y) \text{ for } i = 1,2,\ldots,8 \qquad (3.4)$$

where the λ_j are eigenvalues of the matrix $[\hat{a}_{ij}]$, the Λ_{ij} are the elements of the corresponding eight eigenvectors, and the c_j are arbitrary constants.

The values λ_j and Λ_{ij} can be derived analytically be rewriting the eight first-order equations (3.1) with constant coefficients as four second-order equations in the form

$$\frac{d^2J_i}{dy^2} - \sum_{j=1}^{8} b_{ji}J_i = 0 \text{ for } i = 1,2,\ldots,4 \qquad (3.5)$$

where

$$J_1 = Z_{11},\ J_2 = Z_{14},\ J_3 = Z_{15},\ J_4 = Z_{17} \qquad (3.6)$$

and the coefficients b_{ij} are given by

$$b_{11} = \hat{a}_{21},\ b_{12} = \hat{a}_{24},\quad b_{13} = \hat{a}_{25},$$

$$b_{22} = \hat{a}_{24}\hat{a}_{42} + \hat{a}_{34}\hat{a}_{43} + \hat{a}_{46}\hat{a}_{64} + \hat{a}_{48}\hat{a}_{84},$$

$$b_{23} = \hat{a}_{25}\hat{a}_{42} + \hat{a}_{35}\hat{a}_{43} + \hat{a}_{46}\hat{a}_{65} + \hat{a}_{48}\hat{a}_{85},$$

$$b_{32} = \hat{a}_{64},\ b_{33} = \hat{a}_{65},\quad b_{42} = \hat{a}_{84},\ b_{43} = \hat{a}_{85},\ b_{44} = \hat{a}_{21}$$

The solution of Eqs. (3.5) has the form

$$J_i = \sum_{j=1}^{8} B_{ij} d_j \exp(\lambda_j y) \text{ for } i = 1,2,\ldots,4 \tag{3.7}$$

where the λ_j are the same as the eigenvalues of Eqs. (3.1) with constant coefficients, the B_{ij} are the elements of the corresponding eight eigenvectors, and the d_j are arbitrary constants. From the characteristic determinant, it follows that the eigenvalues are

$$\lambda_{1,5} = \mp (b_{11})^{1/2} \tag{3.8}$$

$$\lambda_{2,6} = \mp \left\{ \frac{1}{2}(b_{22} + b_{33}) + \left[\frac{1}{4}(b_{22} - b_{33})^2 + b_{23}b_{32}\right]^{1/2} \right\}^{1/2} \tag{3.9}$$

$$\lambda_{3,7} = \mp \left\{ \frac{1}{2}(b_{22} + b_{33}) - \left[\frac{1}{4}(b_{22} - b_{33}) + b_{23}b_{32}\right]^{1/2} \right\}^{1/2} \tag{3.10}$$

$$\lambda_{4,8} = \mp (b_{11})^{1/2} \tag{3.11}$$

The B_{ij} can be obtained from the solution of the characteristic equation. They are given by

$$B_{1j} = 1,\ B_{2j} = 0,\ B_{3j} = 0,\ B_{4j} = 0 \tag{3.12}$$

for $j = 1,5$

$$B_{1j} = \frac{(\lambda_j^2 - \hat{a}_{65})\hat{a}_{24} + \hat{a}_{25}\hat{a}_{64}}{(\hat{a}_{21} - \lambda_j^2)}, \quad B_{2j} = \hat{a}_{65} - \lambda_j^2,$$

$$B_{3j} = -\hat{a}_{64}, \quad B_{4j} = \frac{\hat{a}_{64}\hat{a}_{85} + (\lambda_j^2 - \hat{a}_{65})\hat{a}_{84}}{(\hat{a}_{21} - \lambda_j^2)} \tag{3.13}$$

for $j = 2,3,6,7$

and

$$B_{1j} = 0, \; B_{2j} = 0, \; B_{3j} = 0, \; B_{4j} = 1 \tag{3.14}$$

for $j = 4,8$

The Λ_{ij} are related to the B_{ij} by Eqs. (3.4), (3.5), (3.6) and (3.7); they are

$$\Lambda_{1j} = 1, \; \Lambda_{2j} = \lambda_j, \; \Lambda_{3j} = (\hat{a}_{31}B_{1j} + \hat{a}_{34}B_{2j} + \hat{a}_{35}B_{3j} + \hat{a}_{37}B_{4j})/\lambda_j B_{1j},$$

$$\Lambda_{4j} = B_{2j}/B_{1j}, \; \Lambda_{5j} = B_{3j}/B_{1j}, \; \Lambda_{6j} = \lambda_j B_{3j}/B_{1j}, \; \Lambda_{7j} = B_{4j}/B_{1j},$$

$$\Lambda_{8j} = (\hat{a}_{84}B_{2j} + \hat{a}_{85}B_{3j} + \hat{a}_{87}B_{4j})/\lambda_j B_{1j} \tag{3.15}$$

These eigenvectors are normalized such that

$$Z_{11} = \sum_{j=1}^{8} c_j \exp(\lambda_j y) \qquad \text{at } y = y_e$$

3.2 Boundary Conditions at Infinity

The boundary conditions (3.3) demand the constants c_5, c_6, c_7, and c_8 be zero. To set up these boundary conditions for SUPORT, we first solve Eqs. (3.4) for the $c_j\exp(\lambda_j y)$ and obtain

$$c_j \exp(\lambda_j y) = \sum_{i=1}^{8} f_{ij} Z_{1i} \quad \text{for } j = 1,2,\ldots 8 \tag{3.16}$$

where the matrix $[f_{ij}]$ is the inverse of $[\Lambda_{ij}]$. Setting $c_5=c_6=c_7=c_8=0$ in Eq. (3.16) leads to

$$\sum_{i=1}^{8} f_{ij} Z_{1i} = 0 \text{ for } j = 5,6,7, \text{and } 8 \text{ at } y = y_e \qquad (3.17)$$

Equations (3.17) replace the boundary conditions Eqs. (3.3).

3.3 Integration and Orthonormalization

With assigned values for ω, R, and two relations among α_{0_r}, α_{0_i}, β_{0_r}, and β_{0_i} and guessed values for the remaining relations, we determine the f_{ij} in Eqs. (3.17). Then, SUPORT converts the boundary-value problem into an initial-value problem. The RKF initial-value integrator in SUPORT is used with adjustable step sizes to keep measure of the local error per step below a specified tolerance. While integrating toward the wall, we are faced with two major difficulties due to the finite word length of the computer. One difficulty is the diminishing of the original linear independence of the solution vectors so that they become linearly dependent before the integration reaches the wall because the round-off dominates the solution due to the rapidly growing portions of the four solution vectors (parasitic error). The second difficulty is the frequent occurrence of cancellation errors while forming the final linear combination of the solution vectors. These difficulties are avoided by the use of an orthonormalization test that is based on the modified Gram-Schmidt procedure.

Since testing for independence after each integration step is expensive, we use a modified version of SUPORT (Darlow et al, 1977) and choose a preselected set of points where orthonormalization is per-

formed. These points are assigned a priori by using information about the points where orthonormalization is needed. We note that there is always a trade-off between integration and orthonormalization.

3.4 Boundary Conditions at the Wall

The boundary conditions (3.2) can be set up for SUPORT by writing them in the form

$$\sum_{j=1}^{8} e_{ij} Z_{1j} = 0 \text{ for } j = 1,2,\ldots,8 \qquad (3.18)$$

where the e_{ij} are the elements of an 8 x 8 matrix with only four nonzero elements.

At the wall, the values of the linearly independent solution vectors are linearly combined to satisfy all but one of the wall boundary conditions. The last wall boundary condition can only be satisfied by this combined solution when the exact remaining relations among α_{0_r}, α_{0_i}, β_{0_r}, and β_{0_i} have been found. A Newton-Raphson procedure is used to determine these relations. To speed up the search, we choose the relations such that the solution is an analytic function of a complex combination of them. For example, we assign β_0 and search for α_0 or assign α_0 and search for β_0. Thus a single integration is sufficient to compute each of the complex derivatives $\partial Z_{17}(0)/\partial\alpha_0$ and $\partial Z_{17}(0)/\partial\beta_0$. With the eigenvalue determined to within the desired accuracy, the eigenfunctions can be recovered using the stored solution vectors.

3.5 Adjoint Problem

Outside the boundary layer (at $y = y_e$), the adjoint problem, Eqs. (2.43)-(2.45), has constant coefficients and its solution can be written in the form

$$W_i = \sum_{j=1}^{8} \Lambda^*_{ij} c^*_j \exp(\lambda_j y) \quad \text{for} \quad i = 1,2,\ldots,8 \tag{3.19}$$

where the λ_j are the same as those for the first-order homogeneous problem, Eqs. (3.8)-(3.11), but the Λ^*_{ij} are different from the Λ_{ij}. The Λ^*_{ij} can be obtained analytically in the same way we obtained the Λ_{ij}. The Λ^*_{ij} components are given by

$$\Lambda^*_{1j} = 1,\ \Lambda^*_{2j} = -(B^*_{1j} + \hat{a}_{42}B^*_{2j})/\lambda_j B^*_{1j},\ \Lambda^*_{3j} = -\hat{a}_{43}B^*_{2j}/\lambda_j B^*_{1j},$$

$$\Lambda^*_{4j} = B^*_{2j}/B^*_{1j},\ \Lambda^*_{5j} = B^*_{3j}/B^*_{1j},\ \Lambda^*_{6j} = -(\hat{a}_{46}B^*_{2j} + B^*_{3j})/\lambda_j B^*_{1j},$$

$$\Lambda^*_{7j} = B^*_{4j}/B^*_{1j},\ \Lambda^*_{8j} = -(\hat{a}_{48}B^*_{2j} + B^*_{4j})/\lambda_j B^*_{1j} \tag{3.20}$$

where

$$B^*_{1j} = 1,\ B^*_{2j} = \frac{(\lambda_j^2 - \hat{a}_{65})\hat{a}_{24} + \hat{a}_{25}\hat{a}_{64}}{(\hat{a}_{65} - \lambda_j^2)(b_{22} - \lambda_j^2) - \hat{a}_{64}b_{23}},$$

$$B^*_{3j} = \frac{\hat{a}_{24}b_{23} - (b_{22} - \lambda_j^2)a}{(\hat{a}_{65} - \lambda_j^2)(b_{22} - \lambda_j^2) - \hat{a}_{64}b_{23}},\ B^*_{4j} = 0 \tag{3.21}$$

for $j = 1,5$

$$B^*_{1j} = 0,\ B^*_{2j} = -\hat{a}_{64}, B^*_{3j} = b_{22} - \lambda_j^2,\ B^*_{4j} = 0 \tag{3.22}$$

for $j = 2,3,6,7$

and

$$B^*_{1j} = 0,\quad B^*_{2j} = \frac{(\lambda_j^2-\hat{a}_{65})\hat{a}_{84} + \hat{a}_{85}\hat{a}_{64}}{(\hat{a}_{65}-\lambda_j^2)(b_{22}-\lambda_j^2)-\hat{a}_{64}b_{23}},$$

$$B^*_{3j} = \frac{\hat{a}_{84}b_{23}-(b_{22}-\lambda_j^2)\hat{a}_{85}}{(\hat{a}_{65}-\lambda_j^2)(b_{22}-\lambda_j^2)-\hat{a}_{64}b_{23}},\quad B^*_{4j} = 1 \qquad (3.23)$$

for $j = 4,8$

The solution of the adjoint problem is obtained by using the same numerical procedure used to solve the original problem except there is no need for the iteration scheme. The eigenvalue relations we found before are used in one integration to produce the adjoint solution. Thus, the solution of the adjoint problem provides also an independent check on the eigenvalues obtained earlier.

CHAPTER 4

HEATED LIQUIDS

This chapter is devoted to the investigation of the nonparallel stability of heated boundary-layer flows. Surface cooling or heating in a boundary-layer flow can be utilized to yield a mean-velocity profile on a flat plate which is more stable than the Blasius profile. The reason is that heat transfer alters the shape of the boundary-layer temperature profile which in turn alters the velocity profile through the viscosity-temperature dependence.

Linke (1942) was the first to investigate experimentally the effect of heat transfer on transition. He measured the drag on a vertical heated plate that is placed in a horizontal air stream. He found that heating the plate causes its drag to increase considerably. He concluded from this observation that heating the plate is destabilizing. Liepmann and Fila (1947) fully confirmed the destabilizing effect of heating in air boundary layers. They performed measurements on a vertical heated plate in a horizontal air stream. They found that the critical Reynolds number decreases with wall heating. The destabilizing effect of heating in an incompressible air boundary layer is due to increasing the air viscosity next to the wall, thereby producing an inflected velocity profile. On the other hand, cooling yields a fuller velocity profile and hence a more stable flow.

Since heating water decreases its viscosity, the above measurements and arguments suggest that heating the wall of a body in a water stream

is stabilizing. This has been confirmed by the analysis of Wazzan et al (1968, 1970, 1972). Their analysis is for a parallel flow and is based on the disturbance vorticity equation only; that is, it does not include the energy equation and hence the temperature fluctuations. However, their analysis includes the effects of the mean-temperature distribution on the viscosity of the fluid. With these assumptions, Wazzan et al obtained a fourth-order modified Orr-Sommerfeld problem. Their results show that the critical Reynolds number increases as the wall heating increases, reaches a maximum, and then decreases. Lowell and Reshotko (1974) reformulated the parallel stability problem and included temperature as well as vorticity fluctuations. They ended up with a sixth-order rather than a fourth-order system. They found that the solutions of the fourth- and sixth-order systems are close for all wall temperatures over the normal liquid range of water (0°-100°C).

The stabilizing effect of small amounts of wall heating in water was confirmed experimentally by Strazisar et al (1975, 1977) and Parker (1978). Parker found that the transition Reynolds number for water flowing in a tube can be increased from 10×10^6 to 42×10^6 by using a 7°C wall overheat. Strazisar et al (1975, 1977) conducted experiments for the case of uniform wall overheats. Their results show that, as the wall heating increases, the critical Reynolds number increases, the growth rates decrease, and the range of frequencies receiving amplification decreases. All of these results qualitatively compare with the parallel stability results of Wazzan et al and Lowell and Reshotko.

Since the flow over the portion of the body upstream of the critical Reynolds number is stable, no stabilization is needed on that portion, and one would need the heating on the portions downstream of the critical Reynolds number. This suggests the use of nonuniform rather than uniform wall heating, and led Strazisar and Reshotko (1978) to examine experimentally the effect of nonuniform wall heating. They conducted experiments with two types of wall heating. The first is a step-change heating and the second is a power-law heating of the form $T_w - T_e = \bar{A}x^n$, where T is the temperature, x is the distance in the streamwise direction, n is a constant, and the subscripts w and e denote conditions at the wall and the edge of the boundary layer, respectively. In their power-law case, they kept $T_w(x_{ref}) - T_e$, where x_{ref} is a reference location, fixed while they changed the exponent n. They made all their measurements at x_{ref}, which corresponds to a displacement-thickness Reynolds number of about 800. Their results show that decreasing n is stabilizing; that is, the case $n < 0$ results in lower growth rates than the case $n = 0$ (uniform case), which in turn results in lower growth rates than the case $n = 1$. Strazisar and Reshotko (1978) found that applying Lowell's analysis (1974) to the case of power-law temperature distributions yielded results that did not agree, even qualitatively, with the experimental results. This led to the speculation that an appropriate nonparallel theory may be needed to explain these results.

To compare with the experimental results and to investigate the aforementioned speculations, we analyze, in this chapter, the parallel and nonparallel stability of two-dimensional boundary layers in water on

a flat plate, taking into account uniform as well as nonuniform wall heating. For the case of uniform wall overheat, the parallel results are in full agreement with those of Lowell and Reshotko (1974). The nonparallel results are in good agreement with the experimental data.

For the case of nonuniform wall overheat we found that the nonparallel theory cannot explain even qualitatively the experimental results if a self-similar mean flow is used. Looking closely at the aforementioned parallel and nonparallel calculations, one finds that all of them employ self-similar boundary-layer profiles. For a uniform wall temperature or for a power-law temperature distribution and a fluid with constant properties, the flow is self-similar. However, for a fluid with variable properties, the flow is not self-similar if the wall temperature is not uniform. In fact the mean-flow measurements of Strazisar and Reshotko (1978) show variations of the mean flow from the similar solution. In contrast with previous analyses the nonsimilarity of the mean flow is taken into account. Both the parallel and nonparallel results qualitatively agree with the experimental results of Strazisar and Reshotko when nonsimilar profiles are used.

In this chapter, we present numerical results for uniform as well as nonuniform wall temperatures and compare our results with the experimental data of Strazisar et al (1975, 1977) and Strazisar and Reshotko (1978). When the variation of the temperature, thermodynamic, and transport properties are neglected, the present solution reduces to those of Bouthier (1973), Nayfeh et al (1974), Gaster (1974), and Saric and Nayfeh (1975, 1977).

4.1 Problem Formulation and Method of Solution

The present study is concerned with the two-dimensional, nonparallel stability of two-dimensional, viscous, heat-conducting, liquid boundary layers to small amplitude disturbances. The analysis takes into account variations in the fluid properties but neglects buoyancy, dissipation, and expansion energies. We follow the formulation introduced in Chapter 2, keeping in mind that we are dealing with two-dimensional disturbances. In this case, all theromodynamic and transport properties are assumed to be known functions of the temperature alone according to the equation of state. The stability analysis is applicable to uniform as well as nonuniform surface temperature variations. We superpose a small time-dependent disturbance on each mean flow, thermodynamic and transport quantity as in Eq. (2.4). Then, substituting Eq. (2.4) into the Navier-Stokes and energy equations, subtracting the mean quantities, and linearizing the resulting equations in the disturbance quantities, we obtain the following disturbance equations:

$$\frac{\partial \rho}{\partial t} + \frac{\partial}{\partial x}(\rho_0 u + \rho U_0) + \frac{\partial}{\partial y}(\rho_0 v + \rho V_0) = 0 \tag{4.1}$$

$$\rho_0\left(\frac{\partial u}{\partial t} + U_0 \frac{\partial u}{\partial x} + u \frac{\partial U_0}{\partial x} + V_0 \frac{\partial u}{\partial y} + v \frac{\partial U_0}{\partial y}\right) + \rho\left(U_0 \frac{\partial U_0}{\partial x} + V_0 \frac{\partial U_0}{\partial y}\right)$$

$$= -\frac{\partial p}{\partial x} + \frac{1}{R}\left\{\frac{\partial}{\partial x}\left[\mu_0\left(r \frac{\partial u}{\partial x} + s \frac{\partial v}{\partial y}\right) + \mu\left(r \frac{\partial U_0}{\partial x} + s \frac{\partial V_0}{\partial y}\right)\right]\right.$$

$$\left. + \frac{\partial}{\partial y}\left[\mu_0\left(\frac{\partial u}{\partial y} + \frac{\partial v}{\partial x}\right) + \mu\left(\frac{\partial U_0}{\partial y} + \frac{\partial V_0}{\partial x}\right)\right]\right\} \tag{4.2}$$

$$\rho_0\left(\frac{\partial v}{\partial t} + U_0 \frac{\partial v}{\partial x} + u \frac{\partial V_0}{\partial x} + V_0 \frac{\partial v}{\partial y} + v \frac{\partial V_0}{\partial y}\right) + \rho\left(U_0 \frac{\partial V_0}{\partial x} + V_0 \frac{\partial V_0}{\partial y}\right)$$

$$= -\frac{\partial p}{\partial y} + \frac{1}{R}\left\{\frac{\partial}{\partial x}\left[\mu_0\left(\frac{\partial u}{\partial y} + \frac{\partial v}{\partial x}\right) + \mu\left(\frac{\partial U_0}{\partial y} + \frac{\partial V_0}{\partial x}\right)\right]\right.$$

$$\left. + \frac{\partial}{\partial y}\left[\mu_0\left(r \frac{\partial v}{\partial y} + s \frac{\partial u}{\partial x}\right) + \mu\left(r \frac{\partial V_0}{\partial y} + s \frac{\partial U_0}{\partial x}\right)\right]\right\} \qquad (4.3)$$

$$\rho_0\left[\frac{\partial T}{\partial t} + u \frac{\partial T_0}{\partial x} + U_0 \frac{\partial T}{\partial x} + v \frac{\partial T_0}{\partial y} + V_0 \frac{\partial T}{\partial y}\right] + \left(\rho_0 \frac{c_p}{c_{p_0}} + \rho\right) \times$$

$$\left[U_0 \frac{\partial T_0}{\partial x} + V_0 \frac{\partial T_0}{\partial y}\right] = \frac{1}{R Pr_e c_{p_0}}\left[\frac{\partial}{\partial x}\left(\kappa_0 \frac{\partial T}{\partial x}\right.\right.$$

$$\left.\left. + \kappa \frac{\partial T_0}{\partial x}\right) + \frac{\partial}{\partial y}\left(\kappa_0 \frac{\partial T}{\partial y} + \kappa \frac{\partial T_0}{\partial y}\right)\right] \qquad (4.5)$$

$$\rho,\ \mu,\ \kappa,\ c_p = \text{functions } (T) \qquad (4.6)$$

Here, c_{p_0} is the liquid specific heat at constant pressure, $R = \rho_e U_e L/\mu_e$ is the Reynolds number, and $Pr_e = c_p \mu_e/\kappa_e$ is the freestream Prandtl number. Moreover, r, s and f are given by Eq. (2.11). The problem is completed by the specification of the boundary conditions; they are

$$u = v = T = 0 \text{ at } y = 0 \qquad (4.7)$$

$$u,\ v,\ T \to 0 \quad \text{as } y \to \infty \qquad (4.8)$$

We restrict our analysis to mean flows which are slightly non-parallel; that is, the normal velocity component is small compared with the streamwise velocity component. This condition demands all mean-flow variables to be weak functions of the streamwise position. These assumptions are expressed mathematically by writing the mean-flow variables in the form given by Eq. (2.14).

To determine an approximate solution to Eqs. (4.1)-(4.8), we use the method of multiple scales (Nayfeh, 1973) and seek a first-order expansion for the eight disturbance variables u, v, p, T, ρ, c_p, μ, and κ in the form of a traveling harmonic wave; that is, we expand each disturbance flow quantity in the form

$$q(x_1,y,t) = [q_1(x_1,y) + \varepsilon q_2(x_1,y) + \ldots]\exp(i\theta) \qquad (4.9)$$

where

$$\frac{\partial\theta}{\partial x} = \alpha_0(x_1), \quad \frac{\partial\theta}{\partial t} = -\omega \qquad (4.10)$$

For the case of spatial stability, α_0 is the complex wavenumber for the quasi-parallel flow problem and ω is the disturbance circular frequency which is taken to be real.

Substituting Eqs. (4.9) and (4.10) into Eqs. (4.1)-(4.8), transforming the time and the spatial derivatives from t and x to θ and x_1, and equating the coefficients of ε^0 and ε on both sides, we obtain problems describing the q_1 and q_2 flow quantities. These problems are referred to as the first- and second-order problems and they are solved in the next two sections.

4.1.1 The First-Order Problem

Substituting Eqs. (4.9) and (4.10) into Eqs. (4.1)-(4.8) and equating the coefficients of ε^0 on both sides, we obtain the following problem:

$$L_1(u_1,v_1,p_1,T_1) = i\alpha_0[\rho_0 u_1 + (U_0 - \frac{\omega}{\alpha_0})\rho_1] + \frac{\partial}{\partial y}(\rho_0 v_1) = 0 \qquad (4.11)$$

$$L_2(u_1,v_1,p_1,T_1) = [i\rho_0\alpha_0(U_0 - \frac{\omega}{\alpha_0}) + \frac{r}{R}\mu_0\alpha_0^2]u_1 + (\rho_0 \frac{\partial U_0}{\partial y}$$

$$- \frac{i}{R}\frac{\partial \mu_0}{\partial y}\alpha_0)v_1 + i\alpha_0 p_1 - \frac{T_1}{R}\frac{\partial}{\partial y}(\frac{d\mu_0}{dT_0}\frac{\partial U_0}{\partial y}) - \frac{1}{R}\frac{\partial \mu_0}{\partial y}\frac{\partial u_1}{\partial y}$$

$$- \frac{if}{R}\mu_0\alpha_0\frac{\partial v_1}{\partial y} - \frac{1}{R}\frac{d\mu_0}{dT_0}\frac{\partial U_0}{\partial y}\frac{\partial T_1}{\partial y} - \frac{1}{R}\mu_0\frac{\partial^2 u_1}{\partial y^2} = 0 \qquad (4.12)$$

$$L_3(u_1,v_1,p_1,T_1) = [i\rho_0\alpha_0(U_0 - \frac{\omega}{\alpha_0}) + \frac{1}{R}\mu_0\alpha_0^2]v_1 - \frac{is}{R}\alpha_0\frac{\partial \mu_0}{\partial y}u_1$$

$$- \frac{i}{R}\alpha_0\frac{d\mu_0}{dT_0}\frac{\partial U_0}{\partial y}T_1 - \frac{if}{R}\mu_0\alpha_0\frac{\partial u_1}{\partial y} - \frac{r}{R}\frac{\partial \mu_0}{\partial y}\frac{\partial v_1}{\partial y}$$

$$+ \frac{\partial p_1}{\partial y} - \frac{r}{R}\mu_0\frac{\partial^2 v_1}{\partial y^2} = 0 \qquad (4.13)$$

$$L_4(u_1,v_1,p_1,T_1) = [i\rho_0\alpha_0(U_0 - \frac{\omega}{\alpha_0}) + \frac{1}{RPr_e c_{p_0}}(\kappa_0\alpha_0^2 - \frac{\partial^2 \kappa_0}{\partial y^2})]T_1$$

$$+ \rho_0\frac{\partial T_0}{\partial y}v_1 - \frac{2}{RPr_e c_{p_0}}\frac{\partial \kappa_0}{\partial y}\frac{\partial T_1}{\partial y} - \frac{1}{RPr_e c_{p_0}}\kappa_0\frac{\partial^2 T_1}{\partial y^2} = 0 \qquad (4.14)$$

The boundary conditions are:

$$u_1 = v_1 = T_1 = 0 \quad \text{at } y = 0 \qquad (4.15)$$

$$u_1,\ v_1,\ T_1 \to 0 \quad \text{as } y \to \infty \qquad (4.16)$$

Equations (4.11)-(4.16) constitute an eigenvalue problem, which is solved numerically. It is convenient to express it as a set of six first-order equations by introducing the new variables Z_{1_n} defined by

$$Z_{11} = u_1, \qquad Z_{12} = \frac{\partial u_1}{\partial y}, \qquad Z_{13} = v_1,$$

$$Z_{14} = p_1, \qquad Z_{15} = T_1, \qquad Z_{16} = \frac{\partial T_1}{\partial y} \qquad (4.17)$$

Then Eqs. (4.11)-(4.16) can be rewritten in the compact form

$$\frac{\partial Z_{1i}}{\partial y} - \sum_{j=1}^{6} a_{ij} Z_{1j} = 0 \quad \text{for } i = 1,2,\ldots,6 \tag{4.18}$$

$$Z_{11} = Z_{13} = Z_{15} = 0 \quad \text{at } y = 0 \tag{4.19}$$

$$Z_{11},\ Z_{13},\ Z_{15} \to 0 \quad \text{as } y \to \infty \tag{4.20}$$

where the a_{ij} are the elements of a 6 x 6 variable-coefficient matrix. The nineteen nonzero elements of this matrix are

$$a_{12} = 1$$

$$a_{21} = \frac{i\rho_0\alpha_0 R}{\mu_0}\left(U_0 - \frac{\omega}{\alpha_0}\right) + \alpha_0^2$$

$$a_{22} = -\frac{1}{\mu_0}\frac{\partial \mu_0}{\partial y}$$

$$a_{23} = \frac{\rho_0 R}{\mu_0}\frac{\partial U_0}{\partial y} - i\alpha_0\left(\frac{1}{\mu_0}\frac{\partial \mu_0}{\partial y} - \frac{f}{\rho_0}\frac{\partial \rho_0}{\partial y}\right)$$

$$a_{24} = \frac{i\alpha_0 R}{\mu_0}$$

$$a_{25} = -\frac{f\alpha_0^2}{\rho_0}\frac{d\rho_0}{dT_0}\left(U_0 - \frac{\omega}{\alpha_0}\right) - \frac{1}{\mu_0}\frac{\partial}{\partial y}\left(\frac{d\mu_0}{dT_0}\frac{\partial U_0}{\partial y}\right)$$

$$a_{26} = -\frac{1}{\mu_0}\frac{d\mu_0}{dT_0}\frac{\partial U_0}{\partial y}$$

$$a_{31} = -i\alpha_0$$

$$a_{33} = -\frac{1}{\rho_0}\frac{\partial \rho_0}{\partial y}$$

$$a_{35} = -\frac{i\alpha_0}{\rho_0}\frac{d\rho_0}{dT_0}\left(U_0 - \frac{\omega}{\alpha_0}\right)$$

$$a_{41} = -\frac{i\alpha_0\mu_0}{R}\left(\frac{2}{\mu_0}\frac{\partial \mu_0}{\partial y} - \frac{r}{\rho_0}\frac{\partial \rho_0}{\partial y}\right)$$

$$a_{42} = -\frac{i\alpha_0\mu_0}{R}$$

$$a_{43} = \frac{\alpha_0\mu_0}{R}\left\{ - \alpha_0 - \frac{r}{\alpha_0\mu_0\rho_0}\frac{\partial\mu_0}{\partial y}\frac{\partial\rho_0}{\partial y} - \frac{r}{\alpha_0\rho_0}\left[\frac{\partial^2\rho_0}{\partial y^2} - \frac{2}{\rho_0}\left(\frac{\partial\rho_0}{\partial y}\right)^2\right] - \frac{i\rho_0 R}{\mu_0}\left(U_0 - \frac{\omega}{\alpha_0}\right)\right\}$$

$$a_{45} = \frac{i\alpha_0\mu_0}{R}\left\{ \frac{1}{\mu_0}\frac{d\mu_0}{dT_0}\frac{\partial U_0}{\partial y} - \frac{r}{\mu_0\rho_0}\frac{d\rho_0}{dT_0}\frac{\partial\mu_0}{\partial y}\left(U_0 - \frac{\omega}{\alpha_0}\right) - \frac{r}{\rho_0}\left[\frac{d\rho_0}{dT_0}\frac{\partial U_0}{\partial y} + \left(U_0 - \frac{\omega}{\alpha_0}\right)\left(\frac{\partial}{\partial y}\frac{d\rho_0}{dT_0} - \frac{2}{\rho_0}\frac{d\rho_0}{dT_0}\frac{\partial\rho_0}{\partial y}\right)\right]\right\}$$

$$a_{46} = - \frac{i\alpha_0\mu_0 r}{R\rho_0}\frac{d\rho_0}{dT_0}\left(U_0 - \frac{\omega}{\alpha_0}\right)$$

$$a_{56} = 1$$

$$a_{63} = \frac{RPr_e c_{p_0}\rho_0}{\kappa_0}\frac{\partial T_0}{\partial y}$$

$$a_{65} = \frac{iRPr_e c_{p_0}\alpha_0\rho_0}{\kappa_0}\left(U_0 - \frac{\omega}{\alpha_0}\right) + \alpha_0^2 - \frac{1}{\kappa_0}\frac{\partial^2\kappa_0}{\partial y^2}$$

$$a_{66} = - \frac{2}{\kappa_0}\frac{\partial\kappa_0}{\partial y}$$

The eigenvalue problem, Eqs. (4.18)-(4.20), is numerically solved using SUPORT (Scott and Watts, 1977). A detailed discussion of setting up the numerical problem is given in Chapter 3. The numerical solution leads to a value for α_0. The eigenfunction solutions are recovered using the stored solution vectors. This solution can be expressed in the form

$$Z_{1_i} = A(x_1)\zeta_i(x\ ,y) \text{ for } i = 1,2,\ldots,6 \qquad (4.21)$$

Following the analysis given in Chapter 2, we determine the amplitude function $A(x_1)$ by imposing the solvability condition at the next level of approximation.

4.1.2 The Second-Order Problem

With the solution of the first-order problem given by Eq. (4.21), the second-order problem becomes

$$\frac{\partial Z_{2_i}}{\partial y} - \sum_{j=1}^{6} a_{ij} Z_{2_j} = G_i \frac{dA}{dx_1} + D_i A \quad \text{for } i = 1,2,\ldots,6 \tag{4.22}$$

$$Z_{21} = Z_{23} = Z_{25} = 0 \qquad \text{at } y = 0 \tag{4.23}$$

$$Z_{21},\ Z_{23},\ Z_{25} \to 0 \qquad \text{as } y \to \infty \tag{4.24}$$

where the G_i and D_i are known functions of the ζ_i, α_0, and the mean-flow quantities. They are defined as follows

$$G_1 \frac{dA}{dx_1} + D_1 A = 0, \tag{4.25a}$$

$$G_2 \frac{dA}{dx_1} + D_2 A = -\frac{i f \alpha_0}{\rho_0} I_m - \frac{R}{\mu_0} I_x, \tag{4.25b}$$

$$G_3 \frac{dA}{dx_1} + D_3 A = \frac{1}{\rho_0} I_m, \tag{4.25c}$$

$$G_4 \frac{dA}{dx_1} + D_4 A = \frac{r}{R} \frac{\mu_0}{\rho_0} \left(\frac{1}{\mu_0} \frac{\partial \mu_0}{\partial y} - \frac{2}{\rho_0} \frac{\partial \rho_0}{\partial y}\right) I_m + \frac{r}{R} \frac{\mu_0}{\rho_0} \frac{\partial}{\partial y} I_m + I_y, \tag{4.25d}$$

$$G_5 \frac{dA}{dx_1} + D_5 A = 0, \tag{4.25e}$$

$$G_6 \frac{dA}{dx_1} + D_6 A = -\frac{R Pr_e c_{p_0}}{\kappa_0} I_e \tag{4.25f}$$

where I_m, I_x, I_y, and I_e represent the nonparallel terms in the continuity, x-momentum, y-momentum, and energy equations, respectively. They are defined in Appendix I.

Since the homogeneous parts of Eqs. (4.22)-(4.24) are the same as Eqs. (4.18)-(4.20) and since the latter have a nontrivial solution, the

inhomogeneous Eqs. (4.22)-(4.24) have a solution if, and only if, a solvability condition is satisfied. In this case the solvability condition demands the inhomogeneities be orthogonal to every solution of the adjoint homogeneous problem; that is,

$$\int_0^\infty \sum_{i=1}^{6} [G_i \frac{dA}{dx_1} + D_i A] W_i dy = 0 \tag{4.26}$$

where the $W_i(x_1,y)$ are the solutions of the adjoint homogeneous problem corresponding to the eigenvalue α_0. Thus, they are the solutions of

$$\frac{\partial W_i}{\partial y} + \sum_{j=1}^{6} a_{ji} W_j = 0 \quad \text{for } i = 1,2,\ldots,6 \tag{4.27}$$

$$W_2 = W_4 = W_6 = 0 \qquad \text{at } y = 0 \tag{4.28}$$

$$W_2,\ W_4,\ W_6 \to 0 \qquad \text{as } y \to \infty \tag{4.29}$$

Substituting for the G_i and D_i from Eq. (4.25) into Eq. (4.26), we obtain the following equation for the evolution of the amplitude A:

$$Q_1 \frac{\partial A}{\partial x_1} = Q_3 A \tag{4.30}$$

This equation has the same form as Eq. (2.46) derived in Chapter 2, when $Q_2 = 0$. For a two-dimensional disturbance in a two-dimensional mean flow, the wave propagates and amplifies in the direction of the mean flow, which is the x-direction. The functions Q_1 and Q_3 are given by Eqs. (2.47) and (2.49).

Equation (4.30) can be written as

$$\frac{1}{A} \frac{dA}{dx_1} = i\alpha_1(x_1) \tag{4.31}$$

where

$$i\alpha_1 = -\left[\int_0^\infty \sum_{j=1}^{6} D_j W_j dy\right] / \left[\int_0^\infty \sum_{j=1}^{6} G_j W_j dy\right] \tag{4.32}$$

The solution of Eq. (4.31) can be written as

$$A = A_0 \exp[i\varepsilon \int \alpha_1(x_1)dx] \tag{4.33}$$

where A_0 is a constant of integration.

To determine $\alpha_1(x_1)$, we need to evaluate $d\alpha_0/dx_1$ and the $\partial\zeta_i/\partial x_1$. To accomplish this, we differentiate Eqs. (4.18)-(4.20) with respect to x_1 and obtain

$$\frac{\partial}{\partial y}\left(\frac{\partial \zeta_i}{\partial x_1}\right) = \sum_{j=1}^{6} a_{ij}\left(\frac{\partial \zeta_j}{\partial x_1}\right) + G_i \frac{d\alpha_0}{dx_1} + S_i \quad \text{for } i = 1,2,\ldots,6 \tag{4.34}$$

$$\frac{\partial \zeta_1}{\partial x_1} = \frac{\partial \zeta_3}{\partial x_1} = \frac{\partial \zeta_5}{\partial x_1} = 0 \quad \text{at } y = 0 \tag{4.35}$$

$$\frac{\partial \zeta_1}{\partial x_1}, \frac{\partial \zeta_3}{\partial x_1}, \frac{\partial \zeta_5}{\partial x_1} \to 0 \text{ as } y \to \infty \tag{4.36}$$

The initial conditions for the computational procedure are chosen to exclude any multiple of the homogeneous solution. The G_i and S_i are known functions of ζ_i, α_0, and the mean-flow quantities and their derivatives; they are given by

$$G_i = \sum_{j=1}^{6} \zeta_j \frac{\partial a_{ij}}{\partial x_1} \quad \text{for } i = 1,2,\ldots,6 \tag{4.37}$$

$$S_i = \sum_{j=1}^{6} \zeta_j \left.\frac{\partial a_{ij}}{\partial x_1}\right|_{\alpha_0} \quad \text{for } i = 1,2,\ldots,6 \tag{4.38}$$

Using the solvability condition of Eqs. (4.34)-(4.36), we find that

$$\frac{d\alpha_0}{dx_1} = -\left[\int_0^\infty \sum_{i=1}^{6} S_i W_i dy\right] / \left[\int_0^\infty \sum_{i=1}^{6} G_i W_i dy\right] \tag{4.39}$$

Therefore, to the first approximation

$$Z_{1\,1}=A_0\zeta_1(x_1,y)\exp[i\int(\alpha_0+\varepsilon\alpha_1)dx - i\omega t] + O(\varepsilon) \qquad (4.40)$$

where the $Z_{1\,i}$ are related to the disturbance variables by Eq. (4.17) and the constant A_0 is determined from the initial conditions. It is clear from Eq. (4.40) that, in addition to the dependence of the eigensolution on x, the eigenvalue α_0 is modified by $\varepsilon\alpha_1$. The present solution reduces to those obtained by Nayfeh et al (1974) and Saric and Nayfeh (1975) for the case of nonheat-conducting flows.

4.2 The Mean Flow

An accurate solution to the mean-flow equations is essential for solving the disturbance equations. For flows whose thermodynamic and transport properties are functions of temperature, the two-dimensional boundary-layer equations for zero-pressure gradient are

$$\frac{\partial}{\partial x}(\rho u) + \frac{\partial}{\partial y}(\rho v) = 0 \qquad (4.41)$$

$$\rho u \frac{\partial u}{\partial x} + \rho v \frac{\partial u}{\partial y} = \frac{\partial}{\partial y}\left(\mu \frac{\partial u}{\partial y}\right) \qquad (4.42)$$

$$\rho u\, c_p \frac{\partial T}{\partial x} + \rho v c_p \frac{\partial T}{\partial y} = \frac{\partial}{\partial y}\left(\kappa \frac{\partial T}{\partial y}\right) \qquad (4.43)$$

The temperature dependence of ρ and μ couples the momentum and the energy equations. We note that buoyancy and viscous dissipation effects are neglected.

For the case of constant wall temperature, the velocity and the temperature profiles are self-similar. However, for the case of a power-law wall-temperature distribution, the flow is self-similar only

if the flow properties are constants. As the thermodynamic and transport properties of the flow are functions of temperature, a nonsimilar solution is obtained and used in this analysis. The mean-flow solution will be applicable for power-law as well as general wall temperature distributions. Similar and nonsimilar mean-flow solutions are introduced in Chapter 7. The dependence of the thermodynamic and transport properties of water on the temperature is given in Appendix II.

4.3 Analytical Results and Comparison with Experiments

Strazisar et al (1975, 1977) and Strazisar and Reshotko (1978) performed their experiments in a water tunnel whose test section is 15.5" (39.37 cm) long, 9" (22.86 cm) wide, and 6" (15.24 cm) high. The freestream turbulence was 0.1 -0.2% for U_e < 11 ft/sec. (3.35 m/sec.). They measured the boundary-layer characteristics on a flat plate that is 13.6" (34.54 cm) long, 9" (22.86 cm) wide, and 0.625" (1.59 cm) thick. It was suspended from a frame that fit the top of the test section. The plate was fitted with a rounded leading edge [1/32 inch (0.079 cm) radius] located 0.425" (1.08 cm) below the top of the test section.

Disturbances were artificially introduced in the boundary layer by using a vibrating ribbon that was stretched across the plate surface 3.75" (9.53 cm) behind the leading edge. The amplitudes of the generated disturbances were measured at five stations spaced 0.25" (0.64 cm) apart between x = 5" (12.7 cm) and x = 6" (15.24 cm). They searched the boundary layer in the normal direction using temperature-compensated hot-film anenometer and recorded the peak amplitude. Then, they deter-

mined the growth rates at x = 5.5" (13.97 cm) by using a polynomial curve fit of the peak-amplitude data.

The plate heating was provided by 11 electric heaters distributed along the plate. The wall temperature was monitored by using 11 thermistors imbedded in the surface of the plate at its centerline. However, because of the large temperature gradients involved, the thermistors did not accurately yield the plate temperature. Consequently, they had to determine the wall temperature from boundary-layer profiles measured with a hot-film anemometer operating as a resistance thermometer. Due to equipment limitations, the wall temperature could not be monitored or maintained near the leading edge. Since the thermal boundary is too thin near the leading edge, temperature profiles using the hot film were impractical in that region and the first indication of the wall temperature was provided by a thermistor imbedded 1.2" (3.05 cm) from the leading edge. Since the upstream wall-temperature distribution is essential for calculating nonsimilar boundary layers, we are unable to compare quantitatively our theory with the data of Strazisar and Reshotko for the case of power-law distributions.

Care must be made when comparing the nonparallel stability theory with the experimental data. For a parallel mean flow, $\alpha_1 = 0$, α_0 and A are constants and the ζ_n are function of y only. Hence, one can unambiguously define the growth rate σ of the disturbance as the imaginary part of $\bar{\alpha}_0$ where $\bar{\alpha}_0$ is the complex conjugate of α_0; that is

$$\sigma = - \mathrm{Im}(\alpha_0) \tag{4.44}$$

This definition is equivalent to

$$\sigma = Re(\frac{\partial}{\partial x} \ln u) = Re(\frac{\partial}{\partial x} \ln v) = Re(\frac{\partial}{\partial x} \ln p) = Re(\frac{\partial}{\partial x} \ln T) \quad (4.45)$$

On the other hand, for a nonparallel mean flow, $\alpha_1 \neq 0$, A and α_0 are functions of x, and the ζ_n are functions of both x and y. Thus, if one generalizes (4.44) to take into account $\varepsilon\alpha_1$, one obtains

$$\sigma = - Im(\alpha_0 + \varepsilon\alpha_1) \quad (4.46)$$

which is not equivalent to (4.45). Moreover, the quantity α_1 and hence σ depend on the normalization of the ζ_n because part of the ζ_n can be absorbed in A and α_1. If one generalizes the definition (4.45) and uses (4.40), one obtains

$$\sigma = - Im(\alpha_0 + \varepsilon\alpha_1) + \varepsilon Re(\frac{\partial}{\partial x_1} \ln \zeta_n) \quad (4.47)$$

Thus, the growth rate in (4.47) depends on the choice of ζ_n because the axial and transverse variations of the ζ_n are not the same. Since the ζ_n are functions of both y and x, one may term a stable flow unstable or vice versa.

Since there are many possible definitions of the growth rate in a nonparallel flow, one must be careful in comparing analytical with experimental results. Saric and Nayfeh (1975, 1977) found that the best correlation between the nonparallel theory and available experimental data for the Blasius flow is obtained if one uses the definition (4.46). In this investigation, we compare the definitions (4.46) and (4.47) evaluated at a distance y/L from the wall where ζ_1 is a maximum.

4.3.1 Uniform Wall Heating

A mean-velocity profile that is fuller than the unheated one is produced with wall heating. On this basis we may conclude that

increasing the wall temperature above the freestream value always stabilizes the flow. However, we must consider the changes in the stability equations due to wall heating in addition to the changes in the velocity profile. Since it is not known how the different terms influence the stability calculations, it is not possible to predict the effect of wall heating on the stability from only velocity-profile considerations.

Since the thermal boundary layer is much thinner than the velocity boundary layer, thermal influences are restricted to regions close to the wall. Lowell and Reshotko (1974) found that the stability characteristics are insensitive to temperature disturbances due to the limited region in which such disturbances are important for fluids of large Prandtl numbers.

In the experiments, the measured disturbance amplification rates (growth rates) were made dimensionless with respect to the boundary-layer displacement thickness δ^*. Moreover, it is presented in the form σ^*/R^* (both based on δ^*). We present our results of the disturbance amplification rates in the form σ/R (both based on L^*), where $\sigma/R = \sigma^*/R^*$. The amplification rates are given as a function of the frequency F defined as $F = \omega^*/R^* = \omega/R$. Figure 4.1 shows the variation of the calculated disturbance growth rates with frequency for T_w-T_e = 0, 3,5, and 8°F (1.67, 2.78 and 4.44°C) [T_e = 75°F (23.89°C)] and for the displacement-thickness Reynolds number R^* = 800. This range of T_w-T_e is chosen for comparison with existing experimental results. The growth rate is calculated by using the definition (4.46) and by normalizing ζ_1

so that $\zeta_1 \to \exp(-\alpha_0 y)$ as $y \to \infty$. This figure indicates that the disturbance growth rate decreases with increasing T_w-T_e. The maximum growth rate is reduced by approximately 56% by increasing the wall temperature by 5°F (2.78°C). The maximum growth rate is very small when the wall temperature is increased by 8°F (4.44°C) at R* = 800. Figure 4.1 shows that the range of unstable frequencies decreases with increasing T_w-T_e. A shift of the maximum amplified frequency to a lower value is also observed with increasing T_w-T_e.

Figure 4.2 shows the variation of the maximum growth rate with T_w-T_e obtained from this analysis over all frequencies. It shows that the maximum growth rate decreases with increasing wall temperature at all Reynolds numbers. Figures 4.1 and 4.2 indicate that the neutral stability curves for this range of wall-temperature difference are nested.

Figures 4.1 and 4.2 show a comparison between the growth rates based on the parallel, Eq. (4.44), and nonparallel, Eq. (4.46), stability theories. The nonparallel maximum growth rates are approximately 30% larger than the parallel ones. A maximum nonparallel effect occurs for the unheated wall, and the nonparallel effect decreases as the wall temperature increases. Moreover, the nonparallel critical Reynolds number is approximately 20% lower than the parallel one for all the values of T_w-T_e considered, as shown in Fig. 4.2.

These nonparallel results are compared with the experimental results of Strazisar et al (1975, 1977) for uniformly heated boundary-layer flows in Figs. 4.3-4.6. They show comparisons of the growth rates defined by (4.44), (4.46), and (4.47) for different values of T_w-T_e and

different displacement thickness Reynolds numbers. These figures show good agreement between the growth rate defined by (4.46) and the experimental results, in contrast with the parallel theory which underpredicts the experimental results by large amounts. Figures 4.3 - 4.6 show that there is no relative shift between the calculated and measured neutral points, in disagreement with Strazisar et al (1977). A possible explanation of the observed shift by Strazisar et al (1977) is that their calculations are based on a mean profile that is different from the experimental mean profile used to calculate R*.

4.3.2 Nonuniform Wall Heating

In the case of the power-law distribution $T_w - T_e = \bar{A}x^n$, Strazisar and Reshotko (1978) held the temperature difference fixed at $x_{ref.}$, while n and x were varied as shown in Fig. 4.7. They presented growth data at $x_{ref.}$ = 5.5" (13.97 cm) only (corresponding to $R_{ref.}$ = 475). Their results show that decreasing n is stabilizing.

Using a similar mean profile for a power-law temperature distribution, we find that neither the parallel nor the nonparallel theories can explain, even qualitatively, the experimental results. Thus the nonsimilarity of the mean flow must be taken into account.

Fiugres 4.8-4.10 show parallel and nonparallel growth rates calculated for the power-law distributions shown in Fig. 4.17 for T_w-T_e = 3° (1.57), 5° (2.78), and 8°F (4.44°C) at $x_{ref.}$ = 5.5" (13.97 cm). In each figure, we show the results for n = - 0.5, 0, and 1 as well as the results for the unheated case. The nonparallel growth rates do not

include the distortion effects of the mode shapes, the last term in (4.47). Including these distortions modifies the results quantitatively but not qualitatively. Both parallel and nonparallel theories predict that decreasing the exponent n results in a stabilizing effect at $x_{ref.}$, in agreement with the experimental results of Strazisar and Reshotko. This stabilizing effect can be explained as follows. As n decreases, Fig. 4.7 shows that T_w-T_e increases at all locations upstream of $x_{ref.}$. But increasing T_w-T_e results in a fuller velocity profile and hence a more stable flow. Therefore, the stabilizing effect produced at $x_{ref.}$ is cumulative of all upstream stabilizing effects. However, downstream of $x_{ref.}$, as n decreases T_w-T_e decreases, resulting in less full velocity profiles. Therefore, at some location downstream of $x_{ref.}$, a distribution with a larger exponent will be more stabilizing as shown in Fig. 4.11.

CHAPTER 5

SUBSONIC FLOWS

This chapter is devoted to the study of the nonparallel stability of a two-dimensional disturbance in a two-dimensional subsonic laminar boundary-layer mean flow. To study the effect of compressibility of the mean flow, stability characteristics are examined for boundary-layer flows on an adiabatic wall for the range of Mach numbers from 0.0 to 1.0. We use the linear stability theory and the e^N criterion to evaluate suction through porous strips for laminar flow control and compare the results with the case of continuous suction.

5.1 Problem Formulation and Method of Solution

The present study is concerned with the two-dimensional, nonparallel stability of two-dimensional, viscous, perfect-gas boundary layers to small-amplitude disturbances. The equation of state for a perfect gas is

$$p = \rho \bar{R} T \tag{5.1}$$

where $\bar{R}$ is the gas constant for air. The linearized dimensionless disturbance equations are

$$\frac{\partial \rho}{\partial t} + \frac{\partial}{\partial x}(\rho_0 u + \rho U_0) + \frac{\partial}{\partial y}(\rho_0 v + \rho V_0) = 0 \tag{5.2}$$

$$\rho_0\left(\frac{\partial u}{\partial t} + U_0 \frac{\partial u}{\partial x} + u \frac{\partial U_0}{\partial x} + V_0 \frac{\partial u}{\partial y} + v \frac{\partial U_0}{\partial y}\right) + \rho\left(U_0 \frac{\partial U_0}{\partial x} + V_0 \frac{\partial U_0}{\partial y}\right)$$

$$= -\frac{\partial p}{\partial x} + \frac{1}{R}\left\{\frac{\partial}{\partial x}\left[\mu_0\left(r \frac{\partial u}{\partial x} + s \frac{\partial v}{\partial y}\right) + \mu\left(r \frac{\partial U_0}{\partial x} + s \frac{\partial V_0}{\partial y}\right)\right]\right.$$

$$\left. + \frac{\partial}{\partial y}\left[\mu_0\left(\frac{\partial u}{\partial y} + \frac{\partial v}{\partial x}\right) + \mu\left(\frac{\partial U_0}{\partial y} + \frac{\partial V_0}{\partial x}\right)\right]\right\} \tag{5.3}$$

$$\rho_0\left(\frac{\partial v}{\partial t} + U_0\frac{\partial v}{\partial x} + u\frac{\partial V_0}{\partial x} + V_0\frac{\partial v}{\partial y} + v\frac{\partial V_0}{\partial y}\right) + \rho\left(U_0\frac{\partial V_0}{\partial x} + V_0\frac{\partial V_0}{\partial y}\right)$$

$$= -\frac{\partial p}{\partial y} + \frac{1}{R}\left\{\frac{\partial}{\partial x}\left[\mu_0\left(\frac{\partial u}{\partial y} + \frac{\partial v}{\partial x}\right) + \mu\left(\frac{\partial U_0}{\partial y} + \frac{\partial V_0}{\partial x}\right)\right]\right.$$

$$\left. + \frac{\partial}{\partial y}\left[\mu_0\left(r\frac{\partial v}{\partial y} + s\frac{\partial u}{\partial x}\right) + \mu\left(r\frac{\partial V_0}{\partial y} + s\frac{\partial U_0}{\partial x}\right)\right]\right\} \qquad (5.4)$$

$$\rho_0\left[\frac{\partial T}{\partial t} + u\frac{\partial T_0}{\partial x} + U_0\frac{\partial T}{\partial x} + v\frac{\partial T_0}{\partial y} + V_0\frac{\partial T}{\partial y}\right] + \left(\rho_0\frac{c_p}{c_{p_0}} + \rho\right)\left[U_0\frac{\partial T_0}{\partial x}\right.$$

$$\left. + V_0\frac{\partial T_0}{\partial y}\right] = (\gamma - 1)M_e^2\left[\frac{\partial p}{\partial t} + u\frac{\partial p_0}{\partial x} + U_0\frac{\partial p}{\partial x} + V_0\frac{\partial p}{\partial y}\right.$$

$$\left. + \frac{1}{R}\phi\right] + \frac{1}{RPr_e c_{p_0}}\left[\frac{\partial}{\partial x}\left(\kappa_0\frac{\partial T}{\partial x} + \kappa\frac{\partial T_0}{\partial x}\right) + \frac{\partial}{\partial y}\left(\kappa_0\frac{\partial T}{\partial y}\right.\right.$$

$$\left.\left. + \kappa\frac{\partial T_0}{\partial y}\right)\right] \qquad (5.5)$$

$$\frac{p}{p_0} = \frac{T}{T_0} + \frac{\rho}{\rho_0} \qquad (5.6)$$

where ϕ is the perturbation dissipation function defined as

$$\phi = \mu_0\left\{2r\left(\frac{\partial U_0}{\partial x}\frac{\partial u}{\partial x} + \frac{\partial V_0}{\partial y}\frac{\partial v}{\partial y}\right) + 2s\left(\frac{\partial U_0}{\partial x}\frac{\partial v}{\partial y} + \frac{\partial V_0}{\partial y}\frac{\partial u}{\partial x}\right)\right.$$

$$\left. + 2\left(\frac{\partial u}{\partial y} + \frac{\partial v}{\partial x}\right)\left(\frac{\partial U_0}{\partial y} + \frac{\partial V_0}{\partial x}\right)\right\} + \mu\left\{r\left[\left(\frac{\partial U_0}{\partial x}\right)^2 + \left(\frac{\partial V_0}{\partial y}\right)^2\right]\right.$$

$$\left. + 2s\frac{\partial U_0}{\partial x}\frac{\partial V_0}{\partial y} + \left(\frac{\partial U_0}{\partial y} + \frac{\partial V_0}{\partial x}\right)^2\right\} \qquad (5.7)$$

Here, γ is the specific-heat ratio, c_{p_0} is the air specific heat at constant pressure (it is taken constant in the stability analysis), $R = \rho_e U_e L/\mu_e$ is the Reynolds number, and $Pr_e = c_{p_e}\mu_e/\kappa_e$ is the free-stream Prandtl number. Moreover, r, s, and f are given by Eq. (2.11). The ratio of the second to the first viscosity coefficients ℓ is taken to be 0.8.

The problem is completed by the specification of the boundary conditions; they are

$$u = v = T = 0 \text{ at } y = 0 \tag{5.8}$$

$$u, v, T \to 0 \quad \text{as } y \to \infty \tag{5.9}$$

We restrict our analysis to mean flows which are slightly nonparallel; that is, the normal velocity component is small compared with respect to the streamwise velocity component. This condition demands all mean-flow variables be weak functions of the streamwise position. These assumptions are expressed mathematically by writing the mean-flow variables in the form given by Eqs. (2.14).

To determine an approximate solution of Eqs. (5.2) - (5.9), we use the method of multiple scales (Nayfeh, 1973) and seek a first-order expansion for the eight disturbance variables u, v, p, T, ρ, c_p, μ, and κ in the form of a traveling harmonic wave; that is, we expand each disturbance flow quantity in the form

$$q(x_1,y,t) = [q_1(x_2,y) + \varepsilon q_2(x_1,y) + \ldots]\exp(i\theta) \tag{5.10}$$

where

$$\frac{\partial\theta}{\partial x} = \alpha_0(x_1), \quad \frac{\partial\theta}{\partial t} = -\omega \tag{5.11}$$

For the case of spatial stability, α_0 is the complex wavenumber for the quasi-parallel flow problem and ω is the disturbance circular frequency which is taken to be real.

Substituting Eqs. (5.10) and (5.11) into Eqs. (5.2)-(5.9), transforming the time and the spatial derivatives from t and x to θ and x_1, and equating the coefficients of ε^0 and ε on both sides, we obtain

problems describing the q_1 and q_2 flow quantities. These problems are referred to as the first- and second-order problems and they are solved in the next two sections.

5.1.1 The First-Order Problem

Substituting Eqs. (5.10) and (5.11) into Eqs. (5.2)-(5.9) and equating the coefficients of ε^0 on both sides, we obtain the following problem:

$$L_1(u_1,v_1,p_1,T_1) = i\alpha_0[\rho_0 u_1 + (U_0 - \frac{\omega}{\alpha_0})\rho_1] + \frac{\partial}{\partial y}(\rho_0 v_1) = 0 \tag{5.12}$$

$$L_2(u_1,v_1,p_1,T_1) = [i\rho_0\alpha_0(U_0 - \frac{\omega}{\alpha_0}) + \frac{r}{R}\mu_0\alpha_0^2]u_1 + (\rho_0 \frac{\partial U_0}{\partial y} - \frac{i}{R}\frac{\partial \mu_0}{\partial y}\alpha_0)v_1 + i\alpha_0 p_1 - \frac{T_1}{R}\frac{\partial}{\partial y}(\frac{d\mu_0}{dT_0}\frac{\partial U_0}{\partial y}) - \frac{1}{R}\frac{\partial \mu_0}{\partial y}\frac{\partial u_1}{\partial y} - \frac{if}{R}\mu_0\alpha_0\frac{\partial v_1}{\partial y} - \frac{1}{R}\frac{d\mu_0}{dT_0}\frac{\partial U_0}{\partial y}\frac{\partial T_1}{\partial y} - \frac{1}{R}\mu_0\frac{\partial^2 u_1}{\partial y^2} = 0 \tag{5.13}$$

$$L_3(u_1,v_1,p_1,T_1) = [i\rho_0\alpha_0(U_0 - \frac{\omega}{\alpha_0}) + \frac{1}{R}\mu_0\alpha_0^2]v_1 - \frac{is}{R}\alpha_0\frac{\partial \mu_0}{\partial y}u_1 - \frac{i}{R}\alpha_0\frac{d\mu_0}{dT_0}\frac{\partial U_0}{\partial y}T_1 - \frac{if}{R}\mu_0\alpha_0\frac{\partial u_1}{\partial y} - \frac{r}{R}\frac{\partial \mu_0}{\partial y}\frac{\partial v_1}{\partial y} + \frac{\partial p_1}{\partial y} - \frac{r}{R}\mu_0\frac{\partial^2 v_1}{\partial y^2} = 0 \tag{5.14}$$

$$L_4(u_1,v_1,p_1,T_1) = [i\rho_0\alpha_0(U_0 - \frac{\omega}{\alpha_0}) - \frac{(\gamma-1)M_e^2}{R}\frac{d\mu_0}{dT_0}(\frac{\partial U_0}{\partial y})^2 + \frac{1}{RPr}(\mu_0\alpha_0^2 - \frac{\partial^2 \mu_0}{\partial y^2})]T_1 + (\rho_0\frac{\partial T_0}{\partial y} - \frac{2i(\gamma-1)M_e^2}{R}\mu_0\alpha_0\frac{\partial U_0}{\partial y})v_1 - i(\gamma-1)M_e^2\alpha_0(U_0 - \frac{\omega}{\alpha_0})p_1 - \frac{2}{RPr}\frac{\partial \mu_0}{\partial y}\frac{\partial T_1}{\partial y} - \frac{2(\gamma-1)M_e^2}{R}\mu_0\frac{\partial U_0}{\partial y}\frac{\partial u_1}{\partial y} - \frac{\mu_0}{RPr}\frac{\partial^2 T_1}{\partial y^2} = 0 \tag{5.15}$$

$$\gamma M_e^2 p_1 = \rho_0 T_1 + \rho_1 T_0 \tag{5.16}$$

The boundary conditions are

$$u_1 = v_1 = T_1 = 0 \quad \text{at } y = 0 \tag{5.17}$$

$$u_1, v_1, T_1 \to 0 \quad \text{as } y \to \infty \tag{5.18}$$

Equations (5.12)-(5.18) constitute an eigenvalue problem, which is solved numerically. It is convenient to express Eqs. (5.12)-(5.16) as a set of six first-order equations by introducing the new variables Z_{1_n} defined by

$$\begin{aligned} Z_{11} &= u_1, \qquad Z_{12} = \frac{\partial u_1}{\partial y}, \qquad Z_{13} = v_1, \\ Z_{14} &= p_1, \qquad Z_{15} = T_1, \qquad Z_{16} = \frac{\partial T_1}{\partial y} \end{aligned} \tag{5.19}$$

Then, Eqs. (5.12)-(5.18) can be rewritten in the compact form

$$\frac{\partial Z_{1_i}}{\partial y} - \sum_{j=1}^{6} a_{ij} Z_{1_j} = 0 \text{ for } i = 1,2\ldots,6 \tag{5.20}$$

$$Z_{11} = Z_{13} = Z_{15} = 0 \qquad \text{at } y = 0 \tag{5.21}$$

$$Z_{11}, Z_{13}, Z_{15} \to 0 \qquad \text{as } y \to \infty \tag{5.22}$$

where the a_{ij} are the elements of a 6 x 6 variable-coefficient matrix. The twenty three nonzero elements of this matrix are

$$a_{12} = 1$$

$$a_{21} = \frac{i\alpha_0 R}{T_0 \mu_0}\left(U_0 - \frac{\omega}{\alpha_0}\right) + \alpha_0^2$$

$$a_{22} = -\frac{1}{\mu_0}\frac{\partial \mu_0}{\partial y}$$

$$a_{23} = \frac{R}{T_0 \mu_0}\frac{\partial U_0}{\partial y} - i\alpha_0\left(\frac{1}{\mu_0}\frac{\partial \mu_0}{\partial y} + \frac{f}{T_0}\frac{\partial T_0}{\partial y}\right)$$

$$a_{24} = \frac{i\alpha_0 R}{\mu_0} - f\gamma M_e^2 \alpha_0^2\left(U_0 - \frac{\omega}{\alpha_0}\right)$$

$$a_{25} = \frac{f\alpha_0^2}{T_0}\left(U_0 - \frac{\omega}{\alpha_0}\right) - \frac{1}{\mu_0}\frac{\partial}{\partial y}\left(\frac{d\mu_0}{dT_0}\frac{\partial U_0}{\partial y}\right)$$

$$a_{26} = -\frac{1}{\mu_0}\frac{d\mu_0}{dT_0}\frac{\partial U_0}{\partial y}$$

$$a_{31} = -i\alpha_0$$

$$a_{33} = \frac{1}{T_0}\frac{\partial T_0}{\partial y}$$

$$a_{34} = -i\gamma M_e^2\alpha_0(U_0 - \frac{\omega}{\alpha_0})$$

$$a_{35} = \frac{i\alpha_0}{T_0}(U_0 - \frac{\omega}{\alpha_0})$$

$$a_{41} = -i\chi(\frac{2}{\mu_0}\frac{\partial \mu_0}{\partial y} + \frac{r}{T_0}\frac{\partial T_0}{\partial y})$$

$$a_{42} = -i\chi$$

$$a_{43} = \chi[-\alpha_0 + \frac{r}{\alpha_0\mu_0 T_0}\frac{\partial \mu_0}{\partial y}\frac{\partial T_0}{\partial y} + \frac{r}{\alpha_0 T_0}\frac{\partial^2 T_0}{\partial y^2} - \frac{iR}{T_0\mu_0}(U_0 - \frac{\omega}{\alpha_0})]$$

$$a_{44} = -i\chi r\gamma M_e[(\frac{1}{\mu_0}\frac{\partial \mu_0}{\partial y} + \frac{1}{T_0}\frac{\partial T_0}{\partial y})(U_0 - \frac{\omega}{\alpha_0}) + \frac{\partial U_0}{\partial y}]$$

$$a_{45} = i\chi[(\frac{1}{\mu_0}\frac{d\mu_0}{dT_0} + \frac{r}{T_0})\frac{\partial U_0}{\partial y} + \frac{r}{\mu_0 T_0}\frac{\partial \mu_0}{\partial y}(U_0 - \frac{\omega}{\alpha_0})]$$

$$a_{46} = \frac{i\chi r}{T_0}(U_0 - \frac{\omega}{\alpha_0})$$

$$a_{56} = 1$$

$$a_{62} = -2Pr(\gamma - 1)M_e^2\frac{\partial U_0}{\partial y}$$

$$a_{63} = \frac{RPr}{T_0\mu_0}\frac{\partial T_0}{\partial y} - 2iPr\alpha_0(\gamma - 1)M_e^2\frac{\partial U_0}{\partial y}$$

$$a_{64} = -\frac{i\alpha_0 RPr}{\mu_0}(\gamma - 1)M_e^2(U_0 - \frac{\omega}{\alpha_0})$$

$$a_{65} = \frac{i\alpha_0 RPr}{T_0\mu_0}(U_0 - \frac{\omega}{\alpha_0}) + \alpha_0^2 - \frac{1}{\mu_0}\frac{\partial^2 \mu_0}{\partial y^2} - \frac{Pr}{\mu_0}(\gamma-1)M_e^2\frac{d\mu}{dT_0}(\frac{\partial U_0}{\partial y})^2$$

$$a_{66} = -\frac{2}{\mu_0}\frac{\partial \mu_0}{\partial y}$$

where

$$\chi = 1/[\frac{R}{\mu_0\alpha_0} + ir\gamma M_e^2(U_0 - \frac{\omega}{\alpha_0})]$$

The eigenvalue problem, Eqs. (5.20)-(5.22), is solved numerically using the computer code SUPORT developed by Scott and Watts (1977). A detailed discussion of setting up the numerical problem is given in Chapter 3. The numerical solution leads to a value for α_0 and a solution vector that can be expressed in the form

$$Z_{1_i} = A(x_1)\zeta_i(x\ ,y) \text{ for } i = 1,2,\ldots,6 \tag{5.23}$$

Following the analysis given in Chapter 2, we determine the amplitude function $A(x_1)$ by imposing the solvability condition at the next level of approximation.

5.1.2 The Second-Order Problem

With the solution of the first-order problem given by Eq. (5.23), the second-order problem becomes

$$\frac{\partial Z_{2i}}{\partial y} - \sum_{j=1}^{6} a_{ij}Z_{2j} = G_i \frac{dA}{dx_1} + D_iA \quad \text{for } i = 1,2,\ldots,6 \tag{5.24}$$

$$Z_{21} = Z_{23} = Z_{25} = 0 \qquad \text{at } y = 0 \tag{5.25}$$

$$Z_{21},\ Z_{23},\ Z_{25} \to 0 \qquad \text{as } y \to \infty \tag{5.26}$$

where the G_i and D_i are known functions of the ζ_i, α_0, and the mean-flow quantities. They are defined as

$$G_1 \frac{dA}{dx_1} + D_1A = 0, \tag{5.27a}$$

$$G_2 \frac{dA}{dx_1} + D_2A = -\, if\alpha_0T_0I_m - \frac{R}{\mu_0} I_x, \tag{5.27b}$$

$$G_3 \frac{dA}{dx_1} + D_3A = T_0I_m, \tag{5.27c}$$

$$G_4 \frac{dA}{dx_1} + D_4 A = \frac{r\chi}{\alpha_0}\left(\frac{T_0}{\mu_0}\frac{\partial \mu_0}{\partial y} + 2\frac{\partial T_0}{\partial y}\right) I_m + \frac{r\chi T_0}{\alpha_0}\frac{\partial}{\partial y} I_m + \frac{R\chi}{\mu_0 \alpha_0} I_y, \tag{5.27d}$$

$$G_5 \frac{dA}{dx_1} + D_5 A = 0, \tag{5.27e}$$

$$G_6 \frac{dA}{dx_1} + D_6 A = -\frac{RPr}{\mu_0} I_e \tag{5.27f}$$

where I_m, I_x, I_y, and I_e represent the nonparallel effects in the continuity, x-momentum, y-momentum, and energy equation, respectively. They are defined in Appendix III.

Since the homogeneous parts of Eqs. (5.24)-(5.26) are the same as Eqs. (5.20)-(5.22) and since the latter have a nontrivial solution, the inhomogeneous Eqs. (5.24)-(5.26) have a solution if, and only if, a solvability condition is satisfied. In this case the solvability condition demands the inhomogeneities be orthogonal to every solution of the adjoint homogeneous problem; that is,

$$\int_0^\infty \sum_{i=1}^{6} \left[G_i \frac{dA}{dx} + D_i A\right] W_i dy = 0 \tag{5.28}$$

where the $W_i(x_1,y)$ are the solutions of the adjoint homogeneous problem corresponding to the eigenvalue α_0. Thus, they are the solutions of

$$\frac{\partial W_i}{\partial y} + \sum_{j=1}^{6} a_{ji} W_j = 0 \text{ for } i = 1,2,\ldots,6 \tag{5.29}$$

$$W_2 = W_4 = W_6 = 0 \qquad \text{at } y = 0 \tag{5.30}$$

$$W_2, W_4, W_6 \to 0 \qquad \text{as } y \to \infty \tag{5.31}$$

Substituting for the G_i and D_i from Eq. (5.27) into Eq. (5.28), we obtain an equation for the evolution of the amplitude A given by Eq. (4.31) whose solution is given by Eq. (4.33).

To determine $\alpha_1(x_1)$, we need to evaluate $d\alpha_0/dx_1$ and the $\partial\zeta_j/\partial x_1$. To accomplish this, we follow the procedure described in Chapter 4 by differentiating Eqs. (5.20)-(5.22) with respect to x_1 and using the solvability condition of the inhomogeneous set.

Therefore, to the first approximation

$$Z_{11} = A_0\zeta_1(x_1,y)\exp[i\int(\alpha_0 + \varepsilon\alpha_1)dx - i\omega t] + O(\varepsilon) \qquad (5.32)$$

where the Z_{1j} are related to the disturbance variables by Eq. (5.19) and the constant A_0 is determined from the initial conditions. The present solution reduces to those obtained by Nayfeh, Saric, and Mook (1974) and Saric and Nayfeh (1975) for the case of incompressible flows (i.e., $M_e = 0$).

5.2 The Mean Flow

The boundary-layer stability analysis requires an accurate solution of the mean laminar boundary layer. It is necessary to have mean-flow solutions available as input to the stability program. These solutions are provided in tabular form from a separate program that yields solutions of the boundary-layer equations over an adiabatic flat plate.

For a zero pressure-gradient flow, the two-dimensional boundary-layer equations with all thermodynamic and transport properties being functions of temperature are

$$\frac{\partial}{\partial x}(\rho u) + \frac{\partial}{\partial y}(\rho v) = 0 \tag{5.33}$$

$$\rho u \frac{\partial u}{\partial x} + \rho v \frac{\partial u}{\partial y} = \frac{\partial}{\partial y}\left(\mu \frac{\partial u}{\partial y}\right) \tag{5.34}$$

$$\rho u \frac{\partial h}{\partial x} + \rho v \frac{\partial h}{\partial y} = \frac{\partial}{\partial y}\left(\kappa \frac{\partial T}{\partial y}\right) + \mu\left(\frac{\partial u}{\partial y}\right)^2 \tag{5.35}$$

$$p = \rho \bar{R} T \tag{5.36}$$

The solution of Eqs. (5.33)-(5.36) is discussed in Chapter 7. Non-similar mean profiles are used for the case of nonuniform suction. The variations of the properties of the perfect gas with temperature are given in Appendix IV. The freestream stagnation temperature is held constant at 311°K unless otherwise noted.

5.3 Effect of Compressibility on Growth Rates

The effect of compressibility or increasing Mach number on the stability is better illustrated by investigating the behavior of the growth rates of given frequencies rather than by investigating the critical Reynolds number. Mack (1969) showed that the latter calculations are often misleading, while the growth rate is a good measure of the relative instability of different boundary-layer profiles.

Figure 5.1 shows the variation of the spatial amplification rate with the streamwise direction at a low frequency, $F = 10 \times 10^{-6}$. The effect of the freestream Mach number M_e is included. Figure 5.2 shows the variation of the same parameters at a high frequency, $F = 100 \times 10^{-6}$. Both figures indicate the strong effect of compressibility of the mean flow on its stability, a result known for a long time for the case of parallel stability (e.g. Lees 1947).

The effect of the Reynolds number on the amplification rates for different Mach numbers is shown in Figs. 5.3 and 5.4. These figures demonstrate the stabilizing effect of compressibility of the mean flow. A 25% reduction in the disturbance maximum growth rate occurs as the Mach number increases from 0.0 to 1.0 at R = 450. The stabilizing effect of compressibility increases with Reynolds number. The reduction in the maximum growth rate reaches 43% as the Mach number increases from 0.0 to 1.0 at R = 1500. As the Mach number increases, the unstable frequency band as well as the maximum unstable frequency are shifted to lower frequencies and the unstable frequency bandwidth slightly decreases.

5.4 Effect of Compressibility on Amplitude Ratios (Amplification Factors)

The growth of a constant frequency disturbance measured by the amplitude ratio a/a_0 (amplification factor) appears to be the most available useful quantity for the correlation of transition. The ratio of the amplitude a at the Reynolds number R to the amplitude a_0 at the Reynolds number R_0 can be obtained from Eq. (4.31). The result is

$$\ln(a/a_0) = - 2 \int_{R_0}^{R} \mathrm{Im}(\alpha_0 + \varepsilon\alpha_1) dR \qquad (5.37)$$

where the integration is carried along the mean-flow direction for constant dimensionless frequency F, and R_0 corresponds to the first neutral stability point.

Figures 5.5 and 5.6 show the variation of the amplitude ratios with the streamwise direction for the two frequencies $F = 10 \times 10^{-6}$ and 100×10^{-6}. The maximum amplification factor reduces from about 22 to about

10 as the Mach number increases from 0.0 to 1.0 for $F = 10 \times 10^{-6}$. A similar effect of compressibility is shown for $F = 100 \times 10^{-6}$ in Fig. 5.6; the amplification factor reduces from about 2.0 to 1.0. We should note that the critical Reynolds number decreases with increasing Mach number. Thus, using the critical Reynolds number as measure of degree of stability would lead to false results in this case.

Figures 5.7 - 5.9 summarize the effects of increasing Mach number on the stability characteristics of a compressible mean flow. The variation of the maximum amplification rate with Mach number for a given Reynolds number is shown in Fig. 5.7. The maximum amplification rate decreases with increasing Mach number. Figure 5.8 shows how the frequency of the most unstable disturbance (in this case the parallel and nonparallel results coincide) at a given Reynolds number decreases with increasing Mach number. The variation of the maximum amplification factor with Mach number for a constant frequency disturbance is summarized in Fig. 5.9. Again, the maximum amplification factor decreases with increasing Mach number. The reduction is higher for the lower frequency.

5.5 Nonparallel Effects in Compressible Mean Flows

Both results of nonparallel and parallel stability theories based on the definitions (4.44) and (4.46) are included in all figures from 5.1 to 5.9 for comparison. The nonparallel effects are best illustrated in Figs. 5.7 and 5.9. A slight nonparallelism of the mean flow has a destabilizing effect in this range of Mach numbers. For R = 450, Fig. 5.7 shows an increase in the maximum growth rate by 48% at $M_e = 0.0$ due

to nonparallel effects. As the Mach number increases to $M_e = 1.0$, the percentage increase in the maximum growth rate reaches 60% due to nonparallel effects. These effects decrease as the Reynolds number increases. Figure 5.9 demonstrates the destabilizing effect of nonparallelism as indicated by the maximum amplification factor for a low and a high frequency. For $F = 100 \times 10^{-6}$, the percentage increase in the amplification factor is about 50% at $M_e = 0.0$ and it increases to about 85% at $M_e = 1.0$. The nonparallel effect decreases as the disturbance frequency decreases.

Although the percentage increase in the maximum growth rate and in the amplitude ratio due to nonparallelism increases as the Mach number increases, a nearly constant $\Delta\sigma$ is observed for the Mach number range shown in Figs. 5.7 and 5.9. This suggests that the nonparallel effects for an incompressible mean flow can be used to modify the parallel stability solution of a compressible mean flow in this range of Mach numbers.

5.6 Stability Characteristics with Suction Through Porous Strips

The aerodynamic efficiency of aircraft and hence its fuel consumption can be improved by an increase in the lift and/or a decrease in the total drag. In this section, we consider the improvement of the aerodynamic efficiency through drag reduction. The drag sources are skin friction, drag due to lift, wave drag, roughness, afterbody separation, and interfaces. The relative magnitude of the various drag sources depends on the aircraft configuration and speed. The main point, however, is that skin-friction drag contributes as much as 40-50%

of the total drag for subsonic and supersonic aircraft and hence has the greatest potential for reduction.

Since transition Reynolds numbers are generally the order of 4-7 x 10^6 and the aircraft Reynolds numbers are the order of 50 - 100 x 10^6, the usual state of the boundary layer is turbulent. An obvious drag reduction scheme is to reduce the turbulent shear but let the flow stay turbulent. The possible payoff in this approach is generally low. Another scheme, which is technically more advanced, is that of laminar flow control (LFC), which keeps the flow laminar.

LFC can be achieved by using different approaches. These include suction (Gregory, 1961), favorable pressure gradient (Schlichting, 1977), wall cooling for gases (Mack, 1969), wall heating for liquids (Linke, 1942), MHD forces (Wu and Anderson, 1972), and compliant walls (Kaplan, 1964; Babanko and Kozlov, 1973). Among all of these approaches the most promising one is LFC by the use of suction in which substantial reductions in local drag occur, even up to quite high Reynolds numbers. The continuous removal of a part of the growing boundary layer by applying suction to the surface can produce two results. First, the thickness of the boundary layer is decreased. Second, the mean profile is improved to a more stable one. It is the combined effect of these suction results that can lead to laminarization of the flow. Pfenninger (1977) and Edwards (1977) gave critical reviews of the achievements and current activities in the design of practical suction surfaces for laminar flow as well as discussions of unsolved problems and difficulties.

The main elements of an LFC system are special suction surfaces, ducting, pumping installations and discharge nozzles, and controls and instrumentation. A surface with continuous area suction is the optimum for LFC, where the inflow velocities required for laminarization are very small and have no direct effect on the external pressure distribution. However, for practical design aspects, suction at suitable discrete intevals, which produces an approximation to continuous area suction, has been devised. It is essential that the air be sucked through the surface in such a way that large disturbances are not introduced into the boundary layer. Continuous area suction is preferred in cases where secondary flows are present, as on swept wings. By this means, there can be no possibility of a loss in effectiveness of control if the flow is nearly parallel to the direction of a series of suction openings. In practice, continuous area suction is provided through a fully porous surface that has many very small pores. In spite of the successful results obtained by Braslow et al (1951) and Head et al (1955), they encountered difficulties due to roughness, weight, and surface clogging in their tests.

Maintaining laminar flow by suction through slots, the order of .005" (1.25 mm) wide, has been explored in several experiments by Burrows and Schwartzberg (1952), Loftin and Horton (1952). The disadvantage of slots operating at relatively high slot Reynolds numbers is that they require extremely close manufacturing tolerances, which are difficult to achieve on a small scale. Pfenninger and Groth (1961) used a slitted surface (narrow slots) cut through the skin without lip shaping. This

is easier to construct, but it imposes a limitation on the maximum allowable slot Reynolds number of about 100. If the slot Reynolds number is higher than 100, suction induced disturbances may be introduced within the slot. Thus a large number of slots are needed to keep the slot Reynolds number low. Closely spaced slots provide better boundary- layer control because the flow field approaches that of area suction. However, this complicates the cellular and throttle hole substructure needed to control the inflow distribution.

Suction through perforated surfaces, distributed uniformly or in single or multiple spanwise rows, has been tested. Information on permissible patterns has been obtained by Gregory and Walker (1955) and Butler (1955). All perforated surfaces introduce three-dimensional disturbances into the boundary layer. Head (1961) found that the alignment of holes parallel to the stream direction could cause transition. This can be avoided on unswept wings by suitably orienting the hole pattern with respect to the flight direction. The use of perforations on swept wings is not recommended because large changes in flow direction take place over the surface. Perforated surfaces have structural advantages over slots because they can be introduced more easily into regions of compound curvature. The possibility of using strips of perforations was explored experimentally by Gregory and Walker (1955). Despite the fact that laminar flow was obtained over most of the chord, their experiment showed that the surface exhibited some sensitivity to changes in the flow direction similar to that of uniform perforations.

A surface with porous strips was developed by Lachmann et al (1952). It appears to be a better load-carrying structure. The porous strips were relatively thick and the pressure drop through them was sufficient to achieve a good inflow distribution. The relatively concentrated inflow through the strips produced a very stable boundary-layer profile. Fourteen porous strips, 0.75" (1.9 cm) wide, were inserted between the 15% and 83.5% chord stations on an 8 ft. (2.44 m) chord model. Laminar flow up to 95% chord was achieved at a chord Reynolds number of 15 x 10^6. Flight tests showed difficulties in maintaining smooth joints at the edges of the strips.

Different criteria (Gregory, 1961) were suggested to determine the amount of suction required to keep the flow laminar. One of these criteria demands that the surface suction maintain the boundary-layer Reynolds number less than the critical value corresponding to the local mean profile. With discrete suction, another criterion allows some amplification of disturbances as the disturbed fluid is totally removed at the subsequent suction opening. These criteria require excessive suction power which reduces the overall efficiency of an aircraft with LFC. Moreover, the over-thinned boundary layer is over-sensitive to surface roughness. For smooth surfaces and relatively disturbance-free flows (usual flight case), a considerable linear regime of instability takes place before transition appears. The e^N criterion based on linear stability theory has been used to correlate transition location. The amount of suction required is determined to keep N below some semi-empirical value.

In this section, we use the linear stability theory and the e^N criterion to investigate the case of suction through porous strips and compare it with the case of continuous area suction. Present capabilities do not permit comparison with the slot configuration because the flow is not boundary-layer like, and the mean flow needs, perhaps, to be calculated from the Navier-Stokes equations. The present calculations of the mean flow are based on nonsimilar solutions of the boundary-layer equations. The boundary layer under investigation is for a flow on a flat plate 16.7 ft. (5 m) long representing the chord width of an unswept wing. The oncoming freestream has a Mach number of 0.8, a stagnation temperature of 412 °K, a stagnation pressure of 630 lb/ft^2 (3016.44 N/m^2), and a unit Reynolds number of 1.76 x 10^6/ft (3.89 x 10^6/m). For this configuration and these flow conditions, a disturbance of low frequency $F = 5 \times 10^{-6}$ is found to be the most unstable. The amplification factor N reaches a value of about 21. A continuous area suction is applied to the part of the plate between the streamwise positions corresponding to the first and second neutral stability points. With a continuous suction level of $SL = 0.4 \times 10^{-4}$, defined by $SL = (\rho V)_w/(\rho U)_e$, we can reduce the amplification factor N to 9. For the case of porous strips the total suction quantity per unit span is divided among a number of porous strips covering the same area where the continuous suction is applied.

To investigate the feasability of controlling boundary layers by suction through porous strips, we performed a number of calculations for strips of various widths and spacings, subject to the constraint of

constant total mass flow through the strips. Over a strip, the boundary layer is thinned and the mean-flow velocity profile is changed to a more stable form. After such a strip and over the solid regions (spacing between two strips) the layer grows and the profile reverts toward a less stable one. However, the effect of the suction through a strip is not limited to the region over the strip but extends both upstream (upstream influence) and downstream (downstream influence). The suction through a strip accelerates the flow ahead of the strip, thereby creating a favorable pressure gradient and hence a stabilizing influence. The extent of this upstream influence increases as the suction level increases. After a strip, the profile changes to an unstable one over a finite distance (relaxation distance). This relaxation distance increases as the suction level and/or the strip width increases.

Figure 5.10 shows the variation of the boundary-layer displacement thickness as well as the mean-velocity profiles with the streamwise position in the neighborhoods of the sixth and seventh strips in one of the configurations under investigation. The cases of no suction and continuous area suction are included for comparison in all figures in this section. Due to changes in the mean flow, a disturbance having the frequency $F = 5 \times 10^{-6}$ is amplified or damped as it propagates downstream as shown in Fig. 5.11. The growth rate of the disturbance starts to decrease at the leading edge of a suction strip and continues to decrease over the strip. The growth rate reaches a valley (minimum value) at a point quite at bit after the end of the suction strip (downstream effect) before it starts a sharp increase to a peak (maximum

value) over the solid region (relaxation effect). It is noted that, for the last few strips, when the effect of suction ceases, the growth rate overrelaxes and its value is higher than the local value which would have existed in the absence of suction. The virtual origin of the boundary layer is shifted to the left as its thickness is thinner than in the case of no suction. This has the effect of shifting the growth-rate curve to the left. As a result, after the last suction strip, the disturbance grows to a certain value before it finally decays. The same feature is observed in the case of continuous area suction. This can be avoided by slightly extending the suction area or by adding more strips. In our calcuations this growing part of the disturbance is already outside the range of the plate chord under consideration.

To investigate the effect of strip width on the stability characteristics, we consider suction through porous strips having the widths $\hat{a}$ = 0.025' (0.76 cm), 0.05' (1.52 cm), and 0.07' (2.13 cm). The distance $\hat{b}$ between the leading edges of two successive strips is constant and equal to 0.8' (24.38 cm). The suction level for these cases, under the constraint of constant total mass flow through the strips, are 12.8 x 10^{-4}, 6.4 x 10^{-4}, and 4.5 x 10^{-4}, respectively. Figure 5.11b shows the variation of the amplification rate with the streamwise position for the second configuration. We use Eq. (5.37) to integrate the growth rates and calculate the amplification factor. While carrying out intergration, we encountered cases in which the amplification factor reached zero and then negative values in regions where the attenuation rates are high. Such a negative amplification factor indicates that the

amplitude a of such a disturbance has been decreased below its initial value a_0. Since disturbances having the initial amplitudes a_0 are present at all streamwise positions the negative values of the amplification factor were set equal to zero. Figure 5.12 show that the amplification factor decreases slightly with an increase in the strip width, reaching a value of about 10.56 for a = 0.07' (2.3 cm), which is about 17% higher than that for continuous area suction.

Increasing the suction level by about 7% reduces the amplification factor by nearly the same percentage as shown in Fig. 5.13. This suggests that an increase of nearly 17% in the amount of total suction is needed if the stability characteristics of the discrete suction configuration of Fig. 5.12 are to be the same as those of the continuous area suction configuration.

For a constant ratio $\hat{a}/\hat{b}$, that is a constant suction level of 6.4×10^{-4}, Fig. 5.11 compares the variations of the growth rates with streamwise position for the two cases $\hat{a}$ = 0.05' (1.52 cm) and $\hat{b}$ = 0.8' (24.38 cm), and $\hat{a}$ = 0.025' (0.76 cm) and $\hat{b}$ = 0.4' (12.19 cm). The integrated growth rates for these cases are compared in Fig. 5.14. The reduction in the amplification factor in the second case indicates a stabilizing effect with refining the discrete strips as expected because it is approaching the case of continuous area suction. For these configurations, Fig. 5.15 compares the variations of the displacement thicknesses with streamwise position. The refined configuration has a smoother displacement thickness, and hence better mean-flow characteristics thereby producing better stability results.

The preceding results are conservative because they do not include the sink effects. Since the upstream influence (sink effect) cannot be ascertained from boundary-layer theory, one needs a solution of either the Navier-Stokes equations or the interacting boundary-layer equations. To assess the upstream influence, we present some calculations simulating the sink effect of strip suction. A Gaussian distribution for the suction level is assumed upstream and downstream of the strips. The suction level variation is taken in the form

$$SL(x) = SL(x_0)\exp[-m(x - x_0)^2] \ , \ x \leq x_0$$

where $m = \infty$ represents the case of no sink effect. Figures 5.16 and 5.17 compare the configuration $\hat{a} = 0.05'$ (1.52 cm), $\hat{b} = 0.8'$ (24.38 cm), and $m = \infty$ with a configuration where Gaussian distribution for the suction level is added, here $m = 400/ft^2$ ($4305.5/m^2$). With the constraint of constant total mass flow through the strips, the suction level reduces from 6.4×10^{-4} in the first case to 2.3×10^{-4} in the second case, due to an increase in the effective strip width [effective width $= \hat{a} + (m/\pi)^{1/2} = .139'$ (4.23 cm)]. The relaxed growth rates reach lower broad peaks for the case of $m = 400$ than for the case of $m = \infty$. These lower peaks for $m = 400$ seem to be more effective than the lower valley for $m = \infty$; the amplification factor is reduced from 10.62 to 10.20.

The preceeding results are summerized in Figs. 5.18 and 5.19 which show the variation of the growth rates in the neighborhoods of the sixth and seventh strips for the different configurations under investigation. These figures indicate the relative locations of the valleys, the re-

laxation regions, and the peaks with respect to the strips. Moreover, Fig. 5-18 shows the downstream influence and that it can be controlled by changing the suction configuration. Figure 5.19 shows the upstream influence. Since the growth rate peaks are higher and more broader than the valleys, one can increase the effectiveness of the strips by extending the upstream invluence, thereby reducing the growth rate peaks and hence reducing the amplification factor.

We should note that the valleys occur quite behind the trailing edges of the strips, indicating a strong downstream effect of the strips. This downstream effect depends on the strip width and the suction level. The relaxation region depends on the width of the solid region between the strips for the same amount of suction level.

All the preceding results are based on the parallel stability theory because the nonparallel effects are small. The parallel and nonparallel growth rates of a disturbance of frequency $F = 10 \times 10^{-6}$ are shown in Fig. 5.20. This figure shows the results for a four-strip configuration where $\hat{a}$ = .4' (12.9 cm), $\hat{b}$ = 1.6' (48.76 cm), and m = 100/ft^2 (1076.4/m^2). The results for a solid surface and a continuous area suction are also included. Thus, the parallel theory is sufficient for the forementioned comparisons because the nonparallel effect is small and becomes even more smaller for $F = 5 \times 10^{-6}$.

We should note that the stability calculations for the case of discrete suction, even the parallel ones, required long computer times.

CHAPTER 6

SUPERSONIC FLOWS

It is an interesting facet of supersonic two-dimensional boundary layers that Squire's theorem (1933) no longer holds. The most unstable first-mode wave need not be parallel to the freestream as the Mach number approaches one. At supersonic speeds the most unstable first-mode wave is oblique or three-dimensional.

As the Mach number increases, the dissipation terms become important and a three-dimensional disturbance cannot be treated by an equivalent two-dimensional method as is usually done for the incompressible case. Dunn and Lin (1955) and Reshotko (1962) showed that such a transformation applies exactly for the contuinity and momentum equations but it applies only for the leading terms of the energy equation. The dissipation terms do not all transform. Mack (1969) found out that neglecting the dissipation terms leads to at most a 10% error in the disturbance amplification rate. The analysis used here is for the complete eighth-order system so that no ambiguities in the interpretation of the results will arise.

The most important feature of the stability of supersonic laminar boundary layers is that there can be more than one mode of instability contributing to the growth of the disturbance. The first mode is similar to the Tollmien-Schlichting instability mode of incompressible flows, while the second and higher unstable modes are unique to compressible flows. For compressible flows, there are multiple values of

wavenumbers for a single disturbance phase velocity whenever there is a region of supersonic mean flow relative to the disturbance phase velocity. Whereas for incompressible flows, higher modes are associated with higher wavenumbers at different phase speeds. The conclusion of the multiplicity of unstable modes in supersonic flows was reached by Mack (1975) by examining the inviscid stability equation describing the pressure fluctuations. For an adiabatic wall, the parallel results show that the second mode appears at frequencies higher than those at which the first mode appears. Moreover, it is insignificantly weak until the Mach number increases to about 3.7. With increasing Mach number, it becomes stronger and it dominates the first mode at about $M_e = 4.8$. In contrast with the first mode, the most unstable second mode is two dimensional. As the Mach number increases to the hypersonic regime, the second mode displays growth rates that are higher than those of the three-dimensional first mode. However, the maximum growth rate is less than that of the first mode at $M_e = 0$. Mack (1965) calculated these higher modes and Lees and Gold (1966) confirmed the existance of these additional modes.

The use of direct numerical methods to investigate the stability of compressible boundary-layer flows was developed by Brown (1961a, 1961b, 1962) and Mack (1965). These stability theories treat the mean flows as quasi-parallel flows. There is some disagreement between the results of these parallel stability analyses and available experimental results. Some incomplete attempts to account for the nonparallel flow effects by including either the normal velocity or some of the streamwise deriva-

tives of the mean flow were given by Brown (1967), Gunness (1968), and Boehman (1971).

There have been several attempts to measure the stability characteristics of small disturbances for zero-pressure-gradient flows at supersonic speeds. Laufer and Vrebalovich (1960) carried out measurements of the neutral stability curves, amplification rates, wave lengths, and amplitude distributions at the Mach numbers 1.6 and 2.2. They performed their measurements in the JPL 20" supersonic wind tunnel where the freestream turbulence level was reduced to about 1% by means of damping screens. For the measurements at M_e = 1.6, a 0.5" (1.25 cm) thick, 25" (62.5 cm) long flat plate with a leading-edge angle of 13° was used. At M_e = 2.2, they used a 1.0" (2.45 cm) thick, 33" (82.5 cm) long flat plate with a leading-edge angle of 24°. The leading edge radii were less than 0.001" (0.025 mm) for both plates. Laufer and Vrebalovich performed their measurements for natural as well as artificial disturbances. A high-speed valve was used as an artificial disturbance generator. This valve opened and closed a narrow slit in the surface of the plate to allow periodic air pulses of certain frequency to disturbe the boundary layer. The stability characteristics of natural disturbances in supersonic flows at Mach numbers between 1.6 and 8.5 were examined by Kendall (1975). Experiments were performed in the JPL 20" supersonic wind tunnel. The test section was 45 cm wide, 50 cm high, and the length to the throat varies from about 150 cm to 250 cm as M_e increases from 1.6 to 5.6. The flat plate experiments were carried out on a 35 cm long plate with 10° - beveled leading edge, which spanned the tunnel width. In some of these experiments, the side walls of the

tunnel were turbulent and hence radiated sound. Mack (1975) tried to compare the free oscillations in the parallel stability theory with Kendall's data. The comparison was not satisfactory. In an attempt to account for the response of the boundary layer to the incomming sound waves, Mack (1975) included a forcing term at the first neutral stability point and found a better agreement with Kendall's data. The same characterestic features of the boundary-layer response to the incomming sound waves were observed by Lebiga, et al (1977) in their experiments at $M_e = 2$. Demetriades (1960, 1974) presented experimental results for hypersonic boundary-layer flows. He studied the streamwise amplitude variation of both natural disturbances and disturbances artificially excited with a siren mechanism attached to a flat plate.

In this chapter, we analyze the linear nonparallel spatial stability of an oblique disturbance in a two-dimensional supersonic laminar boundary layer. Parallel and nonparallel stability characteristics are examined for boundary-layer flows over an adiabatic wall. We validate the transformation relating the spatial stability along any two directions introduced by Nayfeh and padhye (1978). We compare the nonparallel theory results with the experimental data of Laufer and Vrebalovich (1960) and Kendall (1975).

6.1 Problem Formulation and Method of Solution

The present investigation is concerned with the spatial three-dimensional, nonparallel stability of compressible two-dimensional,

viscous, perfect-gas boundary layers to small-amplitude disturbances. The formulation of the stability theory is the same as that presented in Chapter 2. After introducing the equation of state for a perfect gas, Eq. (5.1), one obtains the following linearized disturbance equations:

$$\frac{\partial \rho}{\partial t} + \frac{\partial}{\partial x}(\rho_0 u + \rho U_0) + \frac{\partial}{\partial y}(\rho_0 v + \rho V_0) + \rho_0 \frac{\partial w}{\partial z} = 0 \tag{6.1}$$

$$\rho_0\left(\frac{\partial u}{\partial t} + U_0 \frac{\partial u}{\partial x} + u \frac{\partial U_0}{\partial x} + V_0 \frac{\partial u}{\partial y} + v \frac{\partial U_0}{\partial y}\right) + \rho\left(U_0 \frac{\partial U_0}{\partial x} + V_0 \frac{\partial U_0}{\partial y}\right) = -\frac{\partial p}{\partial x} + \frac{1}{R}\left\{\frac{\partial}{\partial x}\left[\mu_0\left(r \frac{\partial u}{\partial x} + s \frac{\partial v}{\partial y} + s \frac{\partial w}{\partial z}\right) + \mu\left(r \frac{\partial U_0}{\partial x} + s \frac{\partial V_0}{\partial y}\right)\right] + \frac{\partial}{\partial y}\left[\mu_0\left(\frac{\partial u}{\partial y} + \frac{\partial v}{\partial x}\right) + \mu\left(\frac{\partial U_0}{\partial y} + \frac{\partial V_0}{\partial x}\right)\right] + \mu_0 \frac{\partial}{\partial z}\left(\frac{\partial w}{\partial x} + \frac{\partial u}{\partial z}\right)\right\} \tag{6.2}$$

$$\rho_0\left(\frac{\partial v}{\partial t} + U_0 \frac{\partial v}{\partial x} + u \frac{\partial V_0}{\partial x} + V_0 \frac{\partial v}{\partial y} + v \frac{\partial V_0}{\partial y}\right) + \rho\left(U_0 \frac{\partial V_0}{\partial x} + V_0 \frac{\partial V_0}{\partial y}\right) = -\frac{\partial p}{\partial y} + \frac{1}{R}\left\{\frac{\partial}{\partial x}\left[\mu_0\left(\frac{\partial u}{\partial y} + \frac{\partial v}{\partial x}\right) + \mu\left(\frac{\partial U_0}{\partial y} + \frac{\partial V_0}{\partial x}\right)\right] + \frac{\partial}{\partial y}\left[\mu_0\left(s \frac{\partial u}{\partial x} + r \frac{\partial v}{\partial y} + s \frac{\partial w}{\partial z}\right) + \mu\left(r \frac{\partial V_0}{\partial y} + s \frac{\partial U_0}{\partial x}\right)\right] + \mu_0 \frac{\partial}{\partial z}\left(\frac{\partial v}{\partial z} + \frac{\partial w}{\partial y}\right)\right\} \tag{6.3}$$

$$\rho_0\left(\frac{\partial w}{\partial t} + U_0 \frac{\partial w}{\partial x} + V_0 \frac{\partial w}{\partial y}\right) = -\frac{\partial p}{\partial z} + \frac{1}{R}\left\{\frac{\partial}{\partial x}\left[\mu_0\left(\frac{\partial w}{\partial x} + \frac{\partial u}{\partial z}\right)\right] + \frac{\partial}{\partial y}\left[\mu_0\left(\frac{\partial v}{\partial z} + \frac{\partial w}{\partial y}\right)\right] + \mu_0 \frac{\partial}{\partial z}\left(s \frac{\partial u}{\partial x} + s \frac{\partial v}{\partial y} + r \frac{\partial w}{\partial z}\right) + \frac{\partial \mu}{\partial z}\mu\left(s \frac{\partial U_0}{\partial x} + s \frac{\partial V_0}{\partial y}\right)\right\} . \tag{6.4}$$

$$\rho_0\left[\frac{\partial T}{\partial t} + u\frac{\partial T_0}{\partial x} + U_0\frac{\partial T}{\partial x} + v\frac{\partial T_0}{\partial y} + V_0\frac{\partial T}{\partial y}\right] + \left(\rho_0\frac{c_p}{c_{p_0}} + \rho\right)\times$$

$$\left[U_0\frac{\partial T_0}{\partial x} + V_0\frac{\partial T_0}{\partial y}\right] = (\gamma-1)M_e^2\left[\frac{\partial p}{\partial t} + u\frac{\partial p_0}{\partial x} + U_0\frac{\partial p}{\partial x} + V_0\frac{\partial p}{\partial y}\right.$$

$$\left. + \frac{1}{R}\phi\right] + \frac{1}{RPr_e c_{p_0}}\left[\frac{\partial}{\partial x}\left(\kappa_0\frac{\partial T}{\partial x} + \kappa\frac{\partial T_0}{\partial x}\right) + \frac{\partial}{\partial y}\left(\kappa_0\frac{\partial T}{\partial y} + \kappa\frac{\partial T_0}{\partial y}\right)\right.$$

$$\left. + \kappa_0\frac{\partial}{\partial z}\left(\frac{\partial T}{\partial z}\right)\right] \qquad (6.5)$$

$$\frac{P}{P_0} = \frac{T}{T_0} + \frac{\rho}{\rho_0} \qquad (6.6)$$

where ϕ, the perturbation dissipation function, is defined as

$$\phi = \mu_0\left\{2r\left(\frac{\partial U_0}{\partial x}\frac{\partial u}{\partial x} + \frac{\partial V_0}{\partial y}\frac{\partial v}{\partial y}\right) + 2s\left[\frac{\partial U_0}{\partial x}\left(\frac{\partial v}{\partial y} + \frac{\partial w}{\partial z}\right) + \frac{\partial V_0}{\partial y}\left(\frac{\partial u}{\partial x} + \frac{\partial w}{\partial z}\right)\right]\right.$$

$$\left. + 2\left(\frac{\partial u}{\partial y} + \frac{\partial v}{\partial x}\right)\left(\frac{\partial U_0}{\partial y} + \frac{\partial V_0}{\partial x}\right)\right\} + \mu\left\{r\left[\left(\frac{\partial U_0}{\partial x}\right)^2 + \left(\frac{\partial V_0}{\partial y}\right)^2\right]\right.$$

$$\left. + 2s\frac{\partial U_0}{\partial x}\frac{\partial V_0}{\partial y} + \left(\frac{\partial U_0}{\partial y} + \frac{\partial V_0}{\partial x}\right)^2\right\} \qquad (6.7)$$

Here, γ is the specific heat ratio, c_{p_0} is the air specific heat at constant pressure (it will be taken constant in the stability analysis), $R = \rho_e U_e L/\mu_e$ is the Reynolds number, and $Pr_e = c_{p_e}\mu_e/\kappa_e$ is the free-stream Prandtl number. Moreover, r, s, and f are given by Eq. (2.11). The ratio ℓ of the second to the first viscosity coefficients is taken to be 0.8.

The problem is completed by the specification of the boundary conditions; they are

$$u = v = w = T = 0 \quad \text{at } y = 0 \qquad (6.8)$$

$$u, v, w, T \to 0 \quad \text{as } y \to \infty \qquad (6.9)$$

We restrict our analysis to mean flows which are slightly non-parallel; that is, the normal velocity component is small compared with

the streamwise velocity component. This condition demands all mean-flow variables to be weak functions of the streamwise position. These assumptions are expressed mathematically by writing the mean-flow variables in the form given by Eq. (2.14).

To determine an approximate solution of Eqs. (6.1)-(6.9), we use the method of multiple scales (Nayfeh, 1973) and seek a first-order expansion for the eight variables u, v, p, T, ρ, c_p, μ, and κ in the form of a traveling harmonic wave; that is, we expand each disturbance-flow quantity in the form

$$q(x_1,y,z_1,t) = [q_1(x_1,y,z_1) + \varepsilon q_2(x_1,y,z_1) + \ldots]\exp(i\theta) \tag{6.10}$$

where

$$\frac{\partial\theta}{\partial x} = \alpha_0(x_1,z_1) \ , \quad \frac{\partial\theta}{\partial z} = \beta_0(x_1,z_1), \quad \frac{\partial\theta}{\partial t} = -\omega \tag{6.11}$$

For the case of spatial stability, α_0 and β_0 are the streamwise and spanwise components of the complex quasi-parallel wavenumber vector and ω is the disturbance frequency which is a real.

Substituting Eqs. (6.10) and (6.11) into Eqs. (6.1) - (6.9), transforming the time and spatial derivatives from t,x, and z to θ,x_1, and z_1, and equating the coefficients of ε^0 and ε on both sides, we obtain problems describing the q_1 and q_2 quantities. These problems are referred to as the first- and second-order problems, and they are solved in the next two sections.

6.1.1 The First-Order Problem

Substituting Eqs. (6.41) and (6.11) into Eqs. (6.1)-(6.9) and equating the coefficients of ε^0 on both sides, we obtain

$$L_1(u_1,v_1,w_1,p_1,T_1) = i\rho_0(\alpha_0 u_1 + \beta_0 w_1) + i(\alpha_0 U_0 - \omega)\rho_1 + \frac{\partial}{\partial y}(\rho_0 v_1) = 0 \tag{6.12}$$

$$L_2(u_1,v_1,w_1,p_1,T_1) = [i\rho_0(\alpha_0 U_0 - \omega) + \frac{\mu_0}{R}(r\alpha_0^2 + \beta_0^2)]u_1 + (\rho_0 \frac{\partial U_0}{\partial y} - \frac{i}{R}\frac{\partial \mu_0}{\partial y}\alpha_0)v_1 + \frac{h}{R}\mu_0\alpha_0\beta_0 w_1 + i\alpha_0 p_1 - \frac{T_1}{R}\frac{\partial}{\partial y}(\frac{d\mu_0}{dT_0}\frac{\partial U_0}{\partial y}) - \frac{1}{R}\frac{\partial \mu_0}{\partial y}\frac{\partial u_1}{\partial y} - \frac{ih}{R}\mu_0\alpha_0\frac{\partial v_1}{\partial y} - \frac{1}{R}\frac{d\mu_0}{dT_0}\frac{\partial U_0}{\partial y}\frac{\partial T_1}{\partial y} - \frac{1}{R}\mu_0\frac{\partial^2 u_1}{\partial y^2} = 0 \tag{6.13}$$

$$L_3(u_1,v_1,w_1,p_1,T_1) = [i\rho_0(\alpha_0 U_0 - \omega) + \frac{\mu_0}{R}(\alpha_0^2 + \beta_0^2)]v_1 - \frac{is}{R}\alpha_0\frac{\partial \mu_0}{\partial y}u_1 - \frac{is}{R}\beta_0\frac{\partial \mu_0}{\partial y}w_1 - \frac{i}{R}\alpha_0\frac{d\mu_0}{dT_0}\frac{\partial U_0}{\partial y}T_1 - \frac{ih}{R}\mu_0\alpha_0\frac{\partial u_1}{\partial y} - \frac{r}{R}\frac{\partial \mu_0}{\partial y}\frac{\partial v_1}{\partial y} - \frac{ih}{R}\mu_0\beta_0\frac{\partial w_1}{\partial y} + \frac{\partial p_1}{\partial y} - \frac{r}{R}\mu_0\frac{\partial^2 v_1}{\partial y^2} = 0 \tag{6.14}$$

$$L_4(u_1,v_1,w_1,p_1,T_1) = [i\rho_0(\alpha_0 U_0 - \omega) + \frac{\mu_0}{R}(\alpha_0^2 + r\beta_0^2)]w_1 + \frac{h}{R}\mu_0\alpha_0\beta_0 u_1 - \frac{i}{R}\beta_0\frac{\partial \mu_0}{\partial y}v_1 + i\beta_0 p_1 - \frac{ih}{R}\mu_0\beta_0\frac{\partial v_1}{\partial y} - \frac{1}{R}\frac{\partial \mu_0}{\partial y}\frac{\partial w_1}{\partial y} - \frac{\mu}{R}\frac{\partial^2 w_1}{\partial y^2} = 0 \tag{6.15}$$

$$L_5(u_1,v_1,w_1,p_1,T_1) = \left\{ i\rho_0(\alpha_0 U_0 - \omega) - \frac{(\gamma-1)M_e^2}{R}\frac{d\mu_0}{dT_0}\left(\frac{\partial U_0}{\partial y}\right)^2 + \frac{1}{RPr}\left[\mu_0(\alpha_0^2+\beta_0^2) - \frac{\partial^2\mu_0}{\partial y_2}\right]\right\} T_1 + \left(\rho_0\frac{\partial T_0}{\partial y} - \frac{2i(\gamma-1)M_e^2}{R}\mu_0\alpha_0\frac{\partial U_0}{\partial y}\right)v_1 - i(\gamma-1)M_e^2(\alpha_0 U_0 - \omega)p_1 - \frac{2}{RPr}\frac{\partial\mu_0}{\partial y}\frac{\partial T_1}{\partial y} - \frac{2(\gamma-1)M_e^2}{R}\mu_0\frac{\partial U_0}{\partial y}\frac{\partial u_1}{\partial y} - \frac{\mu_0}{RPr}\frac{\partial^2 T_1}{\partial y^2} = 0 \quad (6.16)$$

$$\gamma M_e^2 p_1 = \rho_0 T_1 + \rho_1 T_0 \quad (6.17)$$

The boundary conditions are

$$u_1 = v_1 = w_1 = T_1 = 0 \quad \text{at } y = 0 \quad (6.18)$$

$$u_1 , v_1, w_1, T_1 \to 0 \quad \text{as } y \to \infty \quad (6.19)$$

Equations (6.12)-(6.19) constitute an eigenvalue problem, which is solved numerically. It is convenient to introduce the new variables Z_{1_n} defined by

$$Z_{11} = u_1, \quad Z_{12} = \frac{\partial u_1}{\partial y}, \quad Z_{13} = v_1, \quad Z_{14} = p_1,$$
$$Z_{15} = w_1, \quad Z_{16} = \frac{\partial w_1}{\partial y}, \quad Z_{17} = T_1, \quad Z_{18} = \frac{\partial T_1}{\partial y} \quad (6.20)$$

Then, Eqs. (6.12)-(6.19) can be rewritten in the compact form

$$\frac{\partial Z_{1_i}}{\partial y} - \sum_{j=1}^{8} a_{ij} Z_{1_j} = 0 \quad \text{for } i = 1,2,\ldots,8 \quad (6.21)$$

$$Z_{11} = Z_{13} = Z_{15} = Z_{17} = 0 \quad \text{at } y = 0 \quad (6.22)$$

$$Z_{11}, Z_{13}, Z_{15}, Z_{17} \to 0 \quad \text{as } y \to \infty \quad (6.23)$$

where the a_{ij} are the elements of an 8 x 8 variable-coefficient matrix. The thirty one nonzero elements of this matrix are

$$a_{12} = 1$$

$$a_{21} = \frac{i\alpha_0 R}{T_0\mu_0}\left(U_0 - \frac{\omega}{\alpha_0}\right) + \alpha_0^2 + \beta_0^2$$

$$a_{22} = -\frac{1}{\mu_0}\frac{\partial \mu_0}{\partial y}$$

$$a_{23} = \frac{R}{T_0\mu_0}\frac{\partial U_0}{\partial y} - i\alpha_0\left(\frac{1}{\mu_0}\frac{\partial \mu_0}{\partial y} + \frac{f}{T_0}\frac{\partial T_0}{\partial y}\right.$$

$$a_{24} = \frac{i\alpha_0 R}{\mu_0} - f\gamma M_e^2\alpha_0^2\left(U_0 - \frac{\omega}{\alpha_0}\right)$$

$$a_{25} = \frac{f\alpha_0^2}{T_0}\left(U_0 - \frac{\omega}{\alpha_0}\right) - \frac{1}{\mu_0}\frac{\partial}{\partial y}\left(\frac{d\mu_0}{dT_0}\frac{\partial U_0}{\partial y}\right)$$

$$a_{26} = -\frac{1}{\mu_0}\frac{d\mu_0}{dT_0}\frac{\partial U_0}{\partial y}$$

$$a_{31} = -i\alpha_0$$

$$a_{33} = \frac{1}{T_0}\frac{\partial T_0}{\partial y}$$

$$a_{34} = -i\gamma M_e^2\alpha_0\left(U_0 - \frac{\omega}{\alpha_0}\right)$$

$$a_{35} = \frac{i\alpha_0}{T_0}\left(U_0 - \frac{\omega}{\alpha_0}\right)$$

$$a_{37} = -i\beta_0$$

$$a_{41} = -i\chi\alpha_0\left(\frac{2}{\mu_0}\frac{\partial \mu_0}{\partial y} + \frac{r}{T_0}\frac{\partial T_0}{\partial y}\right)$$

$$a_{42} = -i\chi\alpha_0$$

$$a_{43} = \chi\left[-\alpha_0^2 - \beta_0^2 + \frac{r}{T_0\mu_0}\frac{\partial \mu_0}{\partial y}\frac{\partial T_0}{\partial y} + \frac{r}{T_0}\frac{\partial^2 T_0}{\partial y^2} - \frac{i\alpha_0 R}{T_0\mu_0}\left(U_0 - \frac{\omega}{\alpha_0}\right)\right]$$

$$a_{44} = -i\chi\alpha_0 r\gamma M_e^2\left[\left(\frac{1}{\mu_0}\frac{\partial \mu_0}{\partial y} + \frac{1}{T_0}\frac{\partial T_0}{\partial y}\right)\left(U_0 - \frac{\omega}{\alpha_0}\right) + \frac{\partial U_0}{\partial y}\right]$$

$$a_{45} = i\chi\alpha_0\left[\left(\frac{1}{\mu_0}\frac{d\mu_0}{dT_0} + \frac{r}{T_0}\right)\frac{\partial U_0}{\partial y} + \frac{r}{T_0\mu_0}\frac{\partial \mu_0}{\partial y}\left(U_0 - \frac{\omega}{\alpha_0}\right)\right]$$

$$a_{46} = \frac{i\chi\alpha_0 r}{T_0}\left(U_0 - \frac{\omega}{\alpha_0}\right)$$

$$a_{47} = -\, i\chi\beta_0\left(\frac{2}{\mu_0}\frac{\partial\mu_0}{\partial y} + \frac{r}{T_0}\frac{\partial T_0}{\partial y}\right)$$

$$a_{48} = -\, i\chi\beta_0$$

$$a_{56} = 1$$

$$a_{62} = -\, 2Pr(\gamma - 1)M_e^2\frac{\partial U_0}{\partial y}$$

$$a_{63} = \frac{RPr}{T_0\mu_0}\frac{\partial T_0}{\partial y} - 2iPr\alpha_0(\gamma - 1)M_e^2\frac{\partial U_0}{\partial y}$$

$$a_{64} = -\frac{i\alpha_0 RPr}{\mu_0}(\gamma - 1)M_e^2\left(U_0 - \frac{\mu}{\alpha_0}\right)$$

$$a_{65} = \frac{i\alpha_0 RPr}{T_0\mu_0}\left(U_0 - \frac{\omega}{\alpha_0}\right) + \alpha_0^2 + \beta_0^2 - (\gamma - 1)M_e^2\frac{Pr}{\mu_0}\frac{d\mu_0}{dT_0}\left(\frac{\partial U_0}{\partial y}\right)^2 - \frac{1}{\mu_0}\frac{\partial^2\mu_0}{\partial y^2}$$

$$a_{66} = -\frac{2}{\mu_0}\frac{\partial\mu_0}{\partial y}$$

$$a_{83} = -\, i\beta_0\left(\frac{1}{\mu_0}\frac{\partial\mu_0}{\partial y} + \frac{f}{T_0}\frac{\partial T_0}{\partial y}\right)$$

$$a_{84} = \frac{iR\beta_0}{\mu_0} - f\alpha_0\beta_0\gamma M_e^2\left(U_0 - \frac{\omega}{\alpha_0}\right)$$

$$a_{85} = \frac{f\alpha_0\beta_0}{T_0}\left(U_0 - \frac{\omega}{\alpha_0}\right)$$

$$a_{87} = \frac{iR\alpha_0}{T_0\mu_0}\left(U_0 - \frac{\omega}{\alpha_0}\right) + \alpha_0^2 + \beta_0^2$$

$$a_{88} = -\frac{1}{\mu_0}\frac{\partial\mu_0}{\partial y}$$

where

$$\chi = 1/\left[\frac{R}{\mu_0} + ir\alpha_0\gamma M_e^2\left(U_0 - \frac{\omega}{\alpha_0}\right)\right]$$

The eigenvalue problem, Eqs. (6.21) - (6.23), is solved numerically using the computer code SUPORT developed by Scott and Watts (1977). For a wave whose amplification direction is the x-axis, the numerical solution leads to a value for α_0 and a solution vector that can be expressed in the form

$$Z_{1_i} = A(x_1,z_1)\zeta_i(x_1,y,z_1) \quad \text{for } i = 1,2,\ldots,8 \tag{6.24}$$

The amplitude function $A(x_1,z_1)$ is determined by imposing the solvability condition at the next level of approximation.

6.1.2 The Second-Order Problem

With the solution of the first-order problem given by Eq. (6.24), the second-order problem becomes

$$\frac{\partial Z_{2_i}}{\partial y} - \sum_{j=1}^{8} a_{ij}Z_{2_j} = G_i \frac{\partial A}{\partial x_1} + E_i \frac{\partial A}{\partial z_1} + D_i A \quad \text{for } i = 1,2,\ldots,8 \tag{6.25}$$

$$Z_{21} = Z_{23} = Z_{25} = Z_{27} = 0 \qquad \text{at } y = 0 \tag{6.26}$$

$$Z_{21},\ Z_{23},\ Z_{25},\ Z_{27} \to 0 \qquad \text{as } y \to \infty \tag{6.27}$$

where the G_i, E_i, and D_i are known functions of the ζ_i, α_0, β_0, and the mean-flow quantities. They are defined by

$$G_1 \frac{\partial A}{\partial x_1} + E_1 \frac{\partial A}{\partial z_1} + D_1 A = 0, \tag{6.28a}$$

$$G_2 \frac{\partial A}{\partial x_1} + E_2 \frac{\partial A}{\partial z_1} + D_2 A = -\,i f \alpha_0 T_0 I_m - \frac{R}{\mu_0} I_x, \tag{6.28b}$$

$$G_3 \frac{\partial A}{\partial x_1} + E_3 \frac{\partial A}{\partial z_1} + D_3 A = T_0 I_m, \tag{6.28c}$$

$$G_4 \frac{\partial A}{\partial x_1} + E_4 \frac{\partial A}{\partial z_1} + D_4 A = r\chi\left(\frac{T_0}{\mu_0}\frac{\partial \mu_0}{\partial y} + 2\frac{\partial T_0}{\partial y}\right) I_m + r\chi T_0 \frac{\partial}{\partial y} I_m + \frac{R\chi}{\mu_0} I_y, \tag{6.28d}$$

$$G_5 \frac{\partial A}{\partial x_1} + E_5 \frac{\partial A}{\partial z_1} + D_5 A = 0, \tag{6.28e}$$

$$G_6 \frac{\partial A}{\partial x_1} + E_6 \frac{\partial A}{\partial z_1} + D_6 A = - \frac{RPr}{\mu_0} I_e, \tag{6.28f}$$

$$G_7 \frac{\partial A}{\partial x_1} + E_7 \frac{\partial A}{\partial z_1} + D_7 A = 0 \tag{6.28g}$$

$$G_8 \frac{\partial A}{\partial x_1} + E_8 \frac{\partial A}{\partial z_1} + D_8 A = - if\beta_0 T_0 I_m - \frac{R}{\mu_0} I_z \tag{6.28h}$$

where I_m, I_x, I_y, I_z, and I_e represent the nonparallel effects in the continuity, x-momentum, y-momentum, z-momentum, and energy equations, respectively. They are defined in Appendix V.

Since the homogeneous parts of Eqs. (6.25)-(6.27) are the same as Eqs. (6.21)-(6.23) and since the latter have a nontrivial solution, the inhomogeneous Eqs. (6.25)-(6.27) have a solution if, and only if, a solvability condition is satisfied. In this case the solvability condition demands the inhomogenous terms be orthogonal to every solution of the adjoint homogeneous problem; that is

$$\int_0^\infty \sum_{i=1}^{8} \left[G_i \frac{\partial A}{\partial x_1} + E_i \frac{\partial A}{\partial z_1} + D_i A\right] W_i \, dy = 0 \tag{6.29}$$

where the $W_i(x_1, y, z_1)$ are the solutions of the adjoint homogeneous problem corresponding to the same eigenvalue. Thus, they are the solutions of

$$\frac{\partial W_i}{\partial y} + \sum_{j=1}^{8} a_{ji} W_j = 0 \quad \text{for } i = 1,2,\ldots,8 \tag{6.30}$$

$$W_2 = W_4 = W_6 = W_8 = 0 \qquad \text{at } y = 0 \tag{6.31}$$

$$W_2, W_4, W_6, W_8 \to 0 \qquad \text{as } y \to \infty \tag{6.32}$$

Substituting for the G_i, E_i, and D_i from Eqs. (6.28) into Eq. (6.29), we obtain Eq. (2.69) for the evolution of the amplitude A; its solution is given by (2.70).

Since the streamwise direction is chosen to be the direction of the wave amplification (see Chapter 2), Eqs. (2.66)-(2.68) govern the amplitude A and the streamwise derivatives of α_0 and β_0.

6.2 The Mean Flow

Equations (5.33)-(5.36) are the two-dimensional boundary-layer equations that govern a zero-pressure gradient flow whose thermodynamic and transport properties are functions of temperature. The solution of Eqs. (5.33)-(5.36) along with the equation of state for a perfect gas is treated in Chapter 7. Tabulated solutions of the laminar boundary-layer equations are used as input to the stability program. The dependence of the perfect-gas properties on the temperature is given in Appendix IV.

6.3 Effect of Mach Number on Wave Angle

The fact that a two-dimensional disturbance is the most unstable one for incompressible and slightly subsonic flows is illustrated in Figure 6.1. This figure shows the maximum amplification rate with respect to frequency versus the wave angle ψ at R = 1500 for different subsonic Mach numbers. It is clear that, for this range of Mach numbers, the maximum amplification rate with respect to wave angle occurs when $\psi = 0$; that is, for a two-dimensional wave. The importance of oblique-wave instability comes into the picture as the Mach number

increases. A wide range of unstable wave orientations appears for M_e = 0.8, and at M_e = 1.0 the most unstable wave is already three dimensional. It should be noted that, although the maximum amplification rate at a given Reynolds number with respect to both frequency and wave orientation occurs for a two-dimensional wave, Mack (1978) showed for the incompressible case that the maximum amplification rate occurs for a three-dimensional wave if the frequency is less than the most unstable one. Figure 6.2 shows this behavior for M_e = 0.8 and 1.0 at R = 1500 where the most unstable frequencies are $F = 20 \times 10^{-6}$ and $F = 19 \times 10^{-6}$, respectively. We note that the sharpness of the maximum decreases with increasing Mach number.

For the supersonic regime, Fig. 6.3 shows the effect of Mach number on the variation of the amplification rate with wave angle for the most unstable disturbance frequency with wave angle at R = 1500. These curves are calculated by using the nonparallel stability theory with σ defined by Eq. (4.46). For the range of Mach numbers, M_e = 1.6-4.5, an oblique (three-dimensional) disturbance is the most unstable according to both parallel and nonparallel stability theories.

The second mode depends primarily on the thickness of the relative supersonic flow region and only secondarily on the boundary-layer profile. Since the thickness of the relative supersonic flow region decreases with $\tilde{M}_e$ where $\tilde{M}_e = M_e/\cos\psi$, increasing the wave angle ψ has a stabilizing effect on the second and higher modes.

6.4 Relation Between Spatial Stabilities Along Two Directions

In Chapter 2, we applied three solvability conditions and derived Eqs. (2.46), (2.59), and (2.60) that govern the evolutions of the disturbance amplitude A and the wavenumber vector $\vec{K}_0 = (\alpha_0, \beta_0)$. For a parallel mean flow these equations reduce to

$$Q_1 \frac{\partial A}{\partial x} + Q_2 \frac{\partial A}{\partial z} = 0 \tag{6.33}$$

$$Q_1 \frac{\partial \alpha_0}{\partial x} + Q_2 \frac{\partial \alpha_0}{\partial z} = 0 \tag{6.34}$$

$$Q_1 \frac{\partial \beta_0}{\partial x} + Q_2 \frac{\partial \beta_0}{\partial z} = 0 \tag{6.35}$$

where Q_1 and Q_2 are proportional to the components of the complex group velocity $(\frac{\partial \omega}{\partial \alpha_0}, \frac{\partial \omega}{\partial \beta_0})$. Equations (6.33)-(6.35) can be solved along any arbitrary direction. To the first approximation, the solution of the eigenvalue problem (6.21)-(6.23) can be written as

$$Z_{1_i} = a(x,z)\zeta_i(y)\exp[i(\alpha_{0_r}x + \beta_{0_r}z - \omega t)] \tag{6.36}$$

where

$$a = A \exp[-(\alpha_{0_i}x + \beta_{0_i}z)] \tag{6.37}$$

Using Eq. (6.37) to change the dependent variable from A to a in Eq. (6.33), we obtain

$$\cos\hat{\phi}\,\frac{\partial a}{\partial x} + (\sin\hat{\phi} + iC_i\cos\hat{\phi})\frac{\partial a}{\partial z} = -\cos\hat{\phi}(\alpha_{0_i} + C\beta_{0_i})a \tag{6.38}$$

where

$$C = Q_2/Q_1 = C_r + iC_i \tag{6.39}$$

$$\hat{\phi} = \tan^{-1}C_r \tag{6.40}$$

To determine the growth rate of the disturbance in the $\bar{\psi}$ direction, we introduce the transformation

$$\bar{\xi} = x\cos\bar{\psi} + z\sin\bar{\psi} \tag{6.41}$$

$$\bar{\eta} = -x\sin\bar{\psi} + z\cos\bar{\psi} \tag{6.42}$$

where $\bar{\xi}$ and $\bar{\eta}$ are the coordinates along and normal to the $\bar{\psi}$ direction. Using Eqs. (6.41) and (6.42) we rewrite Eq. (6.38) as

$$[\cos(\bar{\psi}-\hat{\phi}) + iC_i\sin\bar{\psi}\cos\hat{\phi}]\frac{\partial a}{\partial\bar{\xi}} - [\sin(\bar{\psi}-\hat{\phi}) - iC_i\cos\bar{\psi}\cos\hat{\phi}]\frac{\partial a}{\partial\bar{\eta}} = -\cos\hat{\phi}(\alpha_{0_i} + C\beta_{0_i})a \tag{6.43}$$

If we restrict a to be independent of $\bar{\eta}$, then

$$\frac{da}{d\bar{\xi}} = -\left[\frac{(\alpha_{0_i} + C\beta_{0_i})\cos\hat{\phi}}{\cos(\bar{\psi}-\hat{\phi}) + iC_i\sin\bar{\psi}\cos\hat{\phi}}\right]a \tag{6.44}$$

whose solution is

$$a(x,z) = a_0\exp[\bar{\sigma}_0(\bar{\psi})\bar{\xi}] \tag{6.45}$$

The real part of $\bar{\sigma}_0(\bar{\psi})$ gives the following growth rate σ_0 of the disturbance in the direction $\bar{\xi}$:

$$\sigma_0(\bar{\psi}) = -\left[\frac{(\alpha_{0_i}\cos\hat{\phi} + \beta_{0_i}\sin\hat{\phi})\cos(\bar{\psi}-\hat{\phi}) + C_i^2\beta_{0_i}\sin\bar{\psi}\cos^2\hat{\phi}}{\cos^2(\bar{\psi}-\hat{\phi}) + C_i^2\sin^2\bar{\psi}\cos\hat{\phi}}\right] \tag{6.46}$$

while the imaginary part of $\bar{\sigma}_0(\bar{\psi})$ gives the following correction to the real wavenumber vector:

$$\delta k_0(\bar{\psi}) = \frac{[(\alpha_{0_i}\cos\hat{\phi}+\beta_{0_i}\sin\hat{\phi})\cos\bar{\psi} - \beta_{0_i}\cos(\bar{\psi}-\hat{\phi})]C_i\cos\hat{\phi}}{\cos^2(\bar{\psi}-\hat{\phi}) + C_i^2\sin^2\bar{\psi}\cos\hat{\phi}} \tag{6.47}$$

Nayfeh and Padhye (1978) derived Eqs. (6.46) and (6.47) and validated them for incompressible flows. Mack (1978) applied an approximation of this transformation to incompressible flows. Here, we show, using numerical results, that this transformation is valid for compressible flows.

Tables 6.1 - 6.6 show numerical results for a compressible two-dimensional mean flow for the Mach numbers M_e = .0, .4, .8, 1.6, 2.2 and 4.5. Each table is given for a specified Mach number, Reynolds number, frequency, and wave angle. For different growth-rate directions $\bar{\psi}$ (column 1), the magnitudes of the wavenumber k_0 and the growth rate σ_0 are calculated from the eigenvalue problem (columns 2 and 3). The corresponding values of k_0, σ_0, and ψ predicted from the transformation (6.46) and (6.47) are given in columns 4, 5, and 6. The latter values are calculated based on k_0, σ_0, and ψ at $\bar{\psi}$ = 0°. Comparison of the growth rates and wavenumbers calculated from the eigenvalue problem and those calculated using the transformation shows that the transformation is fairly accurate for subsonic and supersonic flows and for large included angles between the original and transformed directions.

6.5 Nonparallel Effects on First Mode

In this section the stability characteristics of an oblique disturbance in a two-dimensional supersonic mean flow are calculated using both nonparallel and parallel stability theories. For the Mach number 1.6, the variation of the spatial growth rate of an oblique disturbance at ψ = 50° with frequency is shown in Fig. 6.4. This figure shows the

parallel and nonparallel growth rates, where the latter is defined by Eq. (4.46), for different Reynolds numbers. An oblique disturbance at ψ = 50° is almost the most unstable in the specified range of Reynolds numbers. Figure 6.5 gives the variation of the maximum spatial growth rates with respect to frequency of an oblique disturbance at ψ = 50° and a two-dimensional disturbance with streamwise position. For the oblique disturbance, the maximum nonparallel growth rate is approximately 25% larger than the parallel one, while for the two-dimensional case the nonparallel growth rate is almost 50% larger than the parallel one.

Figure 6.6 shows the variation of the parallel and nonparallel growth rates with wave angle for a supersonic mean flow with the Mach number 1.6 at a Reynolds number of 400 and a frequency of 100×10^{-6} The nonparallel effects are the greatest for a two-dimensional disturbance.

Since the flow is two-dimensional and if the initial disturbance is independent of the spanwise position, the dimensional spanwise component $\beta^*_{\delta^*_r}$ of the wavenumber vector is constant in the streamwise direction. Hence the wave angle of the disturbance varies downstream because $\alpha^*_{\delta^*_r}$ decreases downstream. Then the wave angle ψ increases as the disturbance moves downstream.

The effect of frequency on the spatial growth rate of an oblique disturbance as the disturbance moves downstream is shown in Fig. 6.7. These curves are calculated for the initial wave angle ψ_0 = 60° corresponding to the first neutral-stability point. An oblique disturbance at

$\psi = 60°$ is almost the most unstable in the specified range of frequencies. An increase of the wave angle between the two neutral-stability points is about 4° for $F = 120 \times 10^{-6}$ and 8° for $F = 10 \times 10^{-6}$. This slight change in wave orientation as the Reynolds number increases has a considerable effect on the behavior of the amplitude-ratio curves. By integrating Eq. (2.69) in Chapter 2, we have

$$\ln(a/a_0) = -2\int_{R_0}^{R} I_m(\alpha_0 + \varepsilon\alpha_1)dR \qquad (6.48)$$

where $(\alpha_0 + \varepsilon\alpha_1)$ is calculated for the actual wave angle ψ whose initial value is ψ_0 and a_0 is the disturbance amplitude at the Reynolds number R_0, corresponding to the first neutral-stability point. The integration is carried along the streamwise direction. Figure 6.8 shows the variation of the amplitude ratio given by Eq. (6.48) with the Reynolds number for $F = 20 \times 10^{-6}$. The corresponding amplitude-ratio curves for a wave with the constant angle $\psi = 60°$ and for a two-dimensional wave are included for comparison. The amplitude ratio decreases from 4.18 in the case of constant ψ to 3.72 when the change in ψ (an increase of about 5°) is taken into account. Figure 6.8 also shows that the nonparallel amplitude ratio is about 28% higher than the parallel one.

6.6 Nonparallel Effects on Second Mode

For an adiabatic wall, the second mode appears at frequencies much higher than those at which the first mode appears. Hence, the nonparallelism is expected to influence the second mode more than the first mode, especially at low Reynolds numbers. At the Mach number $M_e = 4.2$,

Fig. 6.9 shows the parallel and nonparallel spatial growth rates for a two-dimensional second-mode at three different Reynolds numbers. In addition to increasing the range of frequencies which receive amplification, the nonparallelism increases the growth rate to a value about 60% higher than the parallel one at R = 1000. The percentage increase in the growth rate increases as the Reynolds number decreases. We note that at R = 400 the parallel theory predicts damped first-mode disturbances at M_e = 4.2. While the parallel stability theory predicts that second-mode disturbances with frequencies less than 520×10^{-6} are always damped, the nonparallel stability theory shows that these frequencies are amplified due to merging of the second- and first-mode unstable regions. Figure 6.9 shows that the most unstable frequency predicted by the nonparallel theory for a given Reynolds number is higher than that predicted by the parallel theory, in contrast with the first-mode results where they are equal. This shift in the most unstable frequency depends on the Reynolds number. The shift increases as the Reynolds number decreases. This result is illustrated in Fig. 6.10 for the second mode at a different Mach number.

For the whole range of Mach numbers under investigation, Fig. 6.11 summerizes the nonparallel effects. The parallel and nonparallel maximum spatial growth rates with respect to frequency and wave angle are shown for the first and second modes at R = 1500. The maximum spatial growth rate for the first mode drops sharply as the Mach number increases to $M_e \simeq 3$, where it starts to increase again due to increasing inviscid instability. For R = 1500, the second mode appears for $M_e >$

3.5 and is highly Mach-number dependent. The maximum growth rate for the second mode increases to a maximum that is less than that at $M_e = 0$. The nonparallel effects have a large influence on the second mode. They increase the maximum growth rate of the second mode by about 30%, while they increase the maximum growth rate of the first mode by about 18% at the same Mach number.

6.7 Comparison of Numerical and Experimental Results

As discussed in Section 4.5, the growth rate in a parallel flow can be unambiguously defined, while it cannot be unambiguously defined in a nonparallel flow. The first term (between brackets) in Eq. (4.47) is independent of y. The second term is the effect of mode-shape distortion. The normal structure of the different mode shapes ζ_n evolves differently as the wave travels downstream. Hence, the streamwise variation of each flow quantity depends on its distance from the wall. Moreover, at each distance from the wall, the different flow quantities vary differently in the streamwise direction. Because of this behavior, the growth rate of a disturbance is a function of both x and y. Moreover, it is different for different flow quantities. Consequently, a stability criterion based on definition (4.47) is not unique and does not define a unique neutral curve. Thus, unless these factors are taken into account in conducting the stability experiments, meaningful comparisons cannot be made between theoretical and experimental results.

The non-uniqueness of the disturbance growth rate defined by Eq. (4.47) suggests the use of a quantity that is integrated across the

boundary layer, such as the total energy of the disturbance, or the use of the streamwise rate of change of this quantity as a general measure of the growth of the disturbance. Unfortunately, the total energy of the disturbance cannot be measured directly. One obviously needs to use the measured quantities when comparing theory with experiment.

It is worth noting that, like the theory, the experiment also gives different stability conditions depending on the normal location of the measurements. The question remains how can we correlate existing experimental data with our analysis, regardless of how the stability criterion is defined.

Almost all measurements reported on experimental stability of boundary layers were made by means of hot-wire anemometers following disturbances in these boundary layers. The hot-wire response is a combination of velocity, density, and temperature fluctuations. The hot-wire response when operated at high constant overheat is proportional to the mean square of the mass-flow fluctuations. To describe the disturbance fully, one needs measurements of all fluctuation characteristics such as the rms amplitude, spectra, and propagation speed as functions of both y and x. Almost all reported experiments for compressible flows measured $|\rho u|$ at various x-stations by placing hot wires at a normal location where the mean-flow conditions are the same. Laufer and Vrebalovich (1960) reported measurements at different constant y/L positions, while Kendall (1967, 1975), Demetriades (1960, 1974), and Lebiga et al (1977) reported measurements at one constant y/L located in the wideband energy peak.

It is worth noting that the experimental measurements account for all the terms in Eq. (4.47). The measurement technique includes the amount of streamwise distortion of the eigenfunction in the growth rate. Since the eigenfunctions ζ_n are not solutions of the boundary-layer equations, they cannot be cast in a similar form. Thus, if measurements are carried out at various x-stations following constant y/L locations (for similar mean flows), the mode shape is expected to distort considerably. Saric and Nayfeh (1977) found that all the experimental data (neutral curves or growth rates) for the Blasius flow ($M_e = 0$) obtained at the value of y/L corresponding to the maximum of $|u|$ can be correlated with the nonparallel results if the growth rate is defined as in (4.46). For the case where neutral stability was determined at different values of constant y/L, Saric and Nayfeh (1977) correlated the experimental data of Kachanov et al (1975) using Eq. (4.47), which includes the profile distortion. For the heated-liquid problem, treated in Chapter 4, we arrived at the same conclusion. Including the distortion of the eigenfunction with streamwise position calculated at y/L where $|u|$ is maximum, the definition (4.47), underpredicts the experimental growth rates measured following the maximum of $|u|$.

It is interesting to investigate the effect of Mach number on the structure of the mode shape across the layer. Also, by studying the behavior of the distortion of the mode shape across the layer, we gain some insight into how much the distortion effect contributes to the growth rate at different y/L locations. In this study, we use the quantity $|\rho u|$ which is usually measured in the experiments. Figures

6.12-6.15 show theoretical results for different Mach numbers for the distributions of $|\rho u|$ across the boundary layer together with the distributions of the distortion effect $|\rho u|$ defined by $[(\partial|\rho u|/\partial x)/|\rho u|]$ at typical streamwise locations, frequencies, and wave orientations. The mode distribution indicates a remarkably sharp peak at a point somewhere across the layer. Whereas in the incompressible case the peak is always located near the wall, Figs. 6.12-6.15 show that the peak moves far away from the wall as the Mach number increases. The same effect occurs as the wave shifts its orientation (higher or lower) from that corresponding to the most unstable wave orientation. This is illustrated in Figs. 6.13 and 6.14.

Like the incompressible case, at $M_e = 0.8$ the distribution of the distortion of $|\rho u|$ across the layer exhibits a singularity at the location where $|\rho u| = 0$. As the Mach number increases, the temperature and density fluctuations become more important and $|\rho u|$ is no longer always zero within the layer. Consequently, the singularity diminishes or disappears in some cases. Figures 6.12-6.15 show that for all cases under investigation, the distortion effect of $|\rho u|$ can have an apparent stabilizing or destabilizing effect depending on the normal location where the growth rate is calculated. The distortion effect is relatively small at the normal location where $|\rho u|$ has a maximum. It is almost negligable at normal vertical location very near to that corresponding to the maximum of $|\rho u|$.

We present theoretical results at $M_e = 0.8$, 1.6, 2.2, and 4.5 for the growth rates of disturbances with different orientations. In all

figures the profile distortion is calculated at a constant value of y/L that is very near the position corresponding to the maximum of $|\rho u|$. The results shown in Fig. 6.14 for M_e = 0.8 are typical of incompressible (results in Chapter 4) and subsonic flows, where the profile distortion (curve 3) produces apparent stablilizing effects. For supersonic flows, Figs. 6.17 and 6.18 show that the profile distortion produces apparent instability effects. Two-dimensional calculations are included in Figs. 6.17 and 6.18 to show that the wave orientation is not the cause for this apparent instability for supersonic flows.

As a matter of practicality, almost all stability measurements for supersonic flows were conducted following a contour of constant y/L in the streamwise direction to avoid changes in the sensitivity of the hot-wire due to changes in the mean-flow conditions. Laufer and Vrebalovich (1960) measured the growth rates of natural as well as artificial disturbances for M_e = 2.2 and different Reynolds numbers. They performed their measurements at the normal locations y/L = 3.6, 5.6, and 6.4. At the time of their experiments, oblique disturbances were not completely understood. Laufer and Vrebalovich noted that their stability results for artificial and natural disturbances are the same. Since the natural disturbances were certainly three dimensional, and the artificial ones were thought to be predominately two dimensional, they concluded in agreement with Dunn and Lin (1955) that at least up to M_e = 2.2 the stability of the boundary layer with respect to two- and three-dimensional disturbances does not change measurably. Mack (1968) using parallel-stability calculations, concluded that the natural and the

artificial disturbances in the experiments of Laufer and Vrebalovich were three dimensional.

The lack of information about the exact orientation of a natural wave makes it difficult to interpret several of the experimental results. Figure 6.18 compares the experimental results of Laufer and Vrebalovich at R = 793 with the theoretical growth rates for a 60° wave, which is the most unstable wave, and a two-dimensioanl wave. Like the experimental measurements, the profile distortion of $|\rho u|$ is calculated at y/L = 3.60, while the location of the maximum of $|\rho u|$ changes from y/L = 4.08 to y/L = 3.84 within the unstable frequency range. First of all, Fig. 6.18 shows that the two-dimensional results, parallel and nonparallel, are far from the experimental data, confirming Mack's interpretation of the obliqueness of the artificial disturbances used. Second, while the parallel oblique results underpredict the measured growth rates by large amounts, the nonparallel results with or without the distortion effect agree better with the experimental data. The same conclusion can be drawn from Fig. 6.19, which shows another comparison at R = 390 with a 60° wave. The measurements and the calculated distortion effects are at y/L = 3.60, while the location of the maximum of $|\rho u|$ changes from y/L = 4.32 to y/L = 4.08 within the unstable frequency range. While the nonparallel theory predicts the measured growth rates at y/L = 3.60, the measurements of Laufer and Vrebalovich at y/L = 5.6 and 6.4 for R = 793 and R = 390 are largley scattered and cannot be predicted by the theory. Figure 6.20 gives the comparison at R = 793 as an example.

The measurements of Kendall (1975) were carried out at a constant value of y/L near the location corresponding to the maximum of $|\rho u|$ for natural disturbances. Again, it is difficult to interpret his results due to the lack of information about the exact orientation of the natural disturbances and the exact y/L location where the measurements were taken. Figures 6.21a and 6.21b show comparisons of the experimental growth rates of a natural disturbance at $M_e = 2.2$ and R = 1000 with the theoretical results for a 60° wave (the most unstable wave at R = 1000) and a 45° wave. For the comparison with the 60° wave, Fig. 6.21a, the profile distortion effects are calculated at the constant normal location y/L = 3.84, while the location of the maximum of $|\rho u|$ changes from y/L = 3.84 to y/L = 3.60 within the unstable frequency range. While the parallel results in Fig. 6.21a underpredict the measured growth rates, the nonparallel results with or without the distortion effects are in better agreement with the experimetnal data. Both the growth rates and the range of unstable frequencies are predicted, while there is a slight shift of the predicted most-unstable frequency. In Fig. 6-21b where the comparison is made with the 45° wave, the profile distortion effects are calculated at the constant normal location y/L = 4.08. The location of the maximum of $|\rho u|$ changes from y/L = 4.08 to y/L = 3.84 within the unstable frequency range. It seems that a 45° wave cannot account for neither the measured growth rates nor the most unstable frequency. Figures 6-21a and 6.21b show that the frequency at which the peak growth rate occurs is a strong function of the profile distortion effects.

Figure 6.20 shows another comparison of the experimental growth rates (Kendall, 1975) of a natural disturbance at $M_e = 4.5$ and $R = 1000$ with the theoretical results for a 45° wave. The profile distortion effects are calculated at the constant normal location $y/L = 12.60$, while the location of the maximum of $|\rho u|$ changes from $y/L = 12.60$ to $y/L = 12.24$ within the unstable frequency range. While the parallel results underpredict the measurements, the nonparallel results with the profile distortion effects included overpredict the measurements by a great amount. It is believed that this is a reason of the high sound intensity radiated from the turbulent boundary layers on the tunnel side walls. This sound can constitute an important source of disturbance energy to the laminar layer. Laufer (1961, 1964), Stainback et al (1972), and Donaldson and Wallace (1971) studied this sound field and concluded that it is proportional to $M_e^2 R_u^{-0.3}$ for $1.6 \leq M_e \leq 8$, where R_u is the unit Reynolds number. Moreover, Kendall (1975) by cross-correlating the signals of the probe placed in the freestream and of one in the boundary layer, found that for high Mach numbers disturbances are almost certainly caused by the freestream sound. Kendall's correlation was rather low at $M_e = 1.6$ and 2.2 indicating that the sound is less effective in disturbing the boundary layer at these speeds.

Because of the mode-shape distortion, neutral-stability points are a function of both the normal and streamwise location. The experiments of Laufer and Vrebalovich (1960) clearly show that the growth of the disturbances and the neutral curves obtained depend on the value of y/L

at which the observations were made. Figure 6.23 shows the measured normal locations of the neutral stability points as a function of streamwise position. It also shows the theoretical results generated from calculations using the zeros of Eq. (4.47) for a 60° wave. There is good agreement between experiment and theory at $y/L = 3.6$ and 4.8 for both branches. At $y/L = 5.6$ and 6.4, there is good agreement between experiment and theory for the right branch. However, we were unable to determine the neutral points at these locations corresponding to the left branch.

CHAPTER 7

THE MEAN FLOW

To study the stability of steady laminar boundary-layers one must have an accurate solution to the mean-flow equations. While the total flow satisfies the equation of state and the time-dependent conservation laws of mass, momentum, and energy, the mean flow satisfies a more restricted set of equations; namely, the steady laminar boundary-layer equations. We consider a steady two-dimensional mean flow with a zero freestream pressure gradient.

7.1 Governing Equations

For flows whose thermodynamic and transport properties are functions of temperature, the two-dimensional boundary-layer equations for a zero-pressure gradient are

$$\frac{\partial}{\partial x}(\rho u) + \frac{\partial}{\partial y}(\rho v) = 0 \tag{7.1}$$

$$\rho u \frac{\partial u}{\partial x} + \rho v \frac{\partial u}{\partial y} = \frac{\partial}{\partial y}\left(\mu \frac{\partial u}{\partial y}\right) \tag{7.2}$$

$$\rho u \frac{\partial h}{\partial x} + \rho v \frac{\partial h}{\partial y} = \frac{\partial}{\partial y}\left(\frac{\mu}{Pr}\right)\frac{\partial h}{\partial y} + \mu\left(\frac{\partial u}{\partial y}\right)^2 \tag{7.3}$$

where h is the fluid enthalpy. These equations are completed with the equation of state. Treating air as perfect gas, we take the equation of state

$$P = \rho \bar{R} T \tag{7.4}$$

We restrict our analysis to the range of Mach numbers in which the fluid can still be assumed to obey this perfect-gas law; in air this corres-

ponds to a range of Mach numbers less than six. In the case of heated liquids, all fluid properties are assumed to be known functions of the temperature alone. The buoyancy effect is neglected in Eqs. (7.1) - (7.3), and the viscous dissipation term (last term in the energy equation) is neglected for heated-liquid mean flows.

We introduce the Levy-Lees transformation, see Hayes et al (1959), to transform the independent variables from x and y to ξ and η. This transformation can be written as

$$d\xi = \rho_e U_e \mu_e dx \tag{7.5}$$

$$d\eta = \rho U_e (2\xi)^{-1/2} dy \tag{7.6}$$

Then, the derivatives are transformed according to

$$\frac{\partial}{\partial x} = \rho_e U_e \mu_e \frac{\partial}{\partial \xi} + \frac{\partial \eta}{\partial x} \frac{\partial}{\partial \eta} \tag{7.7}$$

$$\frac{\partial}{\partial y} = \rho U_e (2\xi)^{-1/2} \frac{\partial}{\partial \eta} \tag{7.8}$$

Substituting Eqs. (7.5)-(7.8) into Eqs. (7.1)-(7.3) and defining the new dependent variables

$$U = \frac{u}{U_e}, \quad H = \frac{h}{h_e} \quad \text{and}$$

$$V = \frac{2\xi}{\rho_e U_e \mu_e} \left[U \frac{\partial \eta}{\partial x} + \frac{\rho v}{(2\xi)^{1/2}} \right] \tag{7.9}$$

We rewrite Eqs. (7.1)-(7.3) as

$$2\xi \frac{\partial U}{\partial \xi} + \frac{\partial V}{\partial \eta} + U = 0 \tag{7.10}$$

$$2\xi U \frac{\partial U}{\partial \xi} + V \frac{\partial U}{\partial \eta} - \frac{\partial}{\partial \eta} \left(c \frac{\partial U}{\partial \eta} \right) = 0 \tag{7.11}$$

$$2\xi U \frac{\partial H}{\partial \xi} + V \frac{\partial H}{\partial \eta} - \frac{\partial}{\partial \eta} \left(\frac{c}{Pr} \frac{\partial H}{\partial \eta} \right) - \frac{U_e^2}{H_e} c \left(\frac{\partial U}{\partial \eta} \right)^2 = 0 \tag{7.12}$$

where

$$c = \frac{\rho\mu}{\rho_e\mu_e} \quad , \quad Pr = \frac{c_p}{\kappa} \quad , \text{ and } \frac{U_e^2}{h} \simeq (\gamma-1)M_e^2$$

Note that all fluid properties are made dimensionless by using their freestream values. Equations (7.10)-(7.12) are supplemented with the following boundary conditions:

$$U(\xi,0) = 0,\ V(\xi,0) = V_w(\xi),\ \text{and } H(\xi,0) = H_w(\xi)$$

$$\text{or } \frac{\partial H}{\partial \eta}(\xi,0) = 0 \qquad (7.13)$$

$$u(\xi,\eta) \to 1,\ \text{and } H(\xi,\eta) \to \infty \quad \text{as} \quad \eta \to \eta_e \qquad (7.14)$$

There are two different cases for the thermal boundary condition at the surface. The first one is used for the heated-liquid problem where the distribution of the surface temperature is specified. The other is used for the flow of compressible boundary-layers over adiabatic flat plates.

7.2 Self-Similar Mean-Flow Solution

Equations (7.10)-(7.14) admit self-similar solutions when the freestream stagnation temperature is constant and the boundary conditions do not vary with ξ. Then, all dependent variables are functions of η only and Eqs. (7.10)-(7.14) reduce to

$$\frac{dV}{d\eta} + U = 0 \qquad (7.15)$$

$$V\frac{dU}{d\eta} - \frac{d}{d\eta}\left(c\frac{dU}{d\eta}\right) = 0 \qquad (7.16)$$

$$V\frac{dH}{d\eta} - \frac{d}{d\eta}\left(\frac{c}{Pr}\frac{dH}{d\eta}\right) - \frac{U_e^2}{h_e}c\left(\frac{\partial U}{\partial \eta}\right)^2 = 0 \qquad (7.17)$$

$$U(0) = 0,\ V(0) = V_w,\ \text{and}\ H(0) = H_w \qquad (7.18)$$

$$\text{or}\ \frac{dH}{d\eta}(0) = 0$$

$$U(\eta) \to 1,\ \text{and}\ H(\eta) \to 1\ \text{as}\ \eta \to \eta_e \qquad (7.19)$$

Equations (7.15)-(7.17) are written as five first-order equations and then numerically integrated by using a combination of a shooting technique and a Runge-Kutta and Adam-Moulten integrator. The thermodynamic and transport properties of the fluid are computed at each integration step. The variation of water properties with temperature is given in Appendix II, while the variations of perfect-gas properties with temperature are given in Appendix IV.

The self-similar solution is used to supply the stability program with mean-flow profiles for compressible boundary-layer flows without suction and for uniformly heated liquid layers.

7.3 Nonsimilar Mean-Flow Solution

Stability calcuations are performed for plates with nonuniform suction $V_w = V_w(\xi)$, and for plates that are nonuniformly heated, $H_w = H_w(\xi)$. In these cases, self-similar solutions do not exist, even with power-law temperature distributions on the surface if the fluid properties vary with temperature.

The system of equations (7.10)-(7.14) are numerically integrated using a step-by-step procedure in the streamwise direction. A three-point implicit finite-difference technique is used to reduce the trans-

formed momentum and energy equations to finite-difference form. The method of solution used in this analysis is closely parallel to that of Harris (1971), Flügge-Lotz and Blottner (1962), and Davis and Flügge-Lotz (1963).

For a laminar boundary-layer on a flat plate, the grid-point spacings in both the η- and ξ-directions are taken to be constants. The dependent variables U, H, and V are assumed known at all the η-grid points along the stations m-1 and m-2 in the ξ-direction. The self-similar solution given by Eqs. (7.15)-(7.19) is used for this purpose.

For typical variables A and B, we write Taylor-series expansions about the grid point (m,n) in the η- and ξ-directions to yield the relations

$$\left(\frac{\partial A}{\partial \eta}\right)_{m,n} = \frac{A_{m,n+1} - A_{m,n-1}}{2\Delta\eta} + O(\Delta\eta^2) \tag{7.20}$$

$$\left(\frac{\partial^2 A}{\partial \eta^2}\right)_{m,n} = \frac{A_{m,n+1} - 2A_{m,n} + A_{m,n-1}}{\Delta\eta^2} + O(\Delta\eta^2) \tag{7.21}$$

$$A_{m,n} = 2A_{m-1,n} - A_{m-2,n} + O(\Delta\xi^2) \tag{7.22}$$

$$\left(\frac{\partial A}{\partial \xi}\right)_{m,n} = \frac{3A_{m,n} - 4A_{m-1,n} + A_{m-2,n}}{2\Delta\xi} + O(\Delta\xi^2) \tag{7.23}$$

We linearize the nonlinear terms in the governing equations in order to obtain a system of linear algebaic equations. The nonlinear products such as AB, are linearized following Flügge-Lotz and Blottner (1962); that is,

$$(AB)_{m,n} = A_{m-1,n}B_{m,n} + B_{m-1,n}A_{m,n} - A_{m-1,n}B_{m-1,n} \tag{7.24}$$

Substituting the different quotients, Eqs. (7.20)-(7.24), into Eqs. (7.11) and (7.12), we obtain

$$A_1F_{n+1} + B_1F_n + C_1F_{n-1} + D_1G_{n+1} + E_1G_n + I_1G_{n-1} = J_1 \quad (7.25)$$

$$A_2F_{n+1} + B_2F_n + C_2F_{n-1} + D_2G_{n+1} + E_2G_n + E_2G_{n-1} = J_2 \quad (7.26)$$

These equations are written for the grid point (m,n). The coefficients A_1, B_1,...,J_1 and A_2, B_2,..., and J_2 are functions of known quantities at stations m-1 and m-2. With four boundary conditions on U and H and the 2(N-2) equations given by (7.25) and (7.26), we have a set of 2N simultaneous tridiagonal equations. The Thomas algorithm is used to solve this set of equations for the unknowns U and H at state m.

At each station m, the continuity equation (7.10) is numerically integrated using the trapezoidal rule and the relation

$$V_n = V_w - \int_0^{\eta_n} (2\xi \frac{\partial U}{\partial \xi} + U)d\eta \quad (7.27)$$

where $V_w = V(0)$.

CHAPTER 8

SUMMARY AND CONCLUSIONS

We present an analysis of the effects of heating, suction, and compressibility on the stability characteristics of boundary-layer flows within the framework of a complete nonparallel, linear, spatial stability theory. Included in the theory are disturbances due to velocity, pressure, temperature, density, and transport properties as well as variations of the fluid properties with temperature. The method of multiple scales is used to account for the nonparallelism of the mean flow and equations are derived for the evolution of the disturbance amplitude and wavenumber vector.

The eigenvalue problem and its adjoint arising from the linearized disturbance equations with the appropriate boundary conditions are solved numerically using a combination of a Newton-Raphson iterative scheme and a variable-step-size integrator based on the Runge-Kutta-Fehlburg fifth-order formulas. The integrator is used in conjunction with a modified Gram-Schmidt orthonormalization procedure. Self-similar mean-flow solutions are obtained by numerically integrating the steady laminar boundary-layer equations using a combination of a shooting technique and a Runge-Kutta and Adam-Moulton integrator. For plates with nonuniform suction or temperature nonsimilar mean-flow solutions are obtained by using a three-point implicit finite-difference technique and numerically integrating the steady laminar boundary-layer equations using a step-by-step procedure in the streamwise direction.

On the basis of the present investigation, the following conclusions can be made:

1. The nonparallel results for the case of water flowing past a uniformly heated flat plate are in good agreement with the experimental results of Strazisar et al (1975, 1977).
2. Both parallel and nonparallel results are in qualitative agreement with the experimental results of Strazisar and Reshotko (1978) for power-law temperature distributions when the nonsimilarity of the mean flow is taken into account. Since the upstream wall temperature distribution is essential for calculating nonsimilar boundary layers, the wall temperature should be measured at all upstream positions for quantitative comparisons with the theory.
3. For subsonic flows over an adiabatic flat plate, the nonparallelism produces a nearly constant $\Delta\sigma$. This suggests that the nonparallel growth rates calculated for an incompressible flow can be used to modify the parallel stability growth rates of subsonic mean flows.
4. For supersonic flows over an adiabatic flat plate, oblique first-mode waves are more unstable than two-dimensional waves according to both parallel and nonparallel theories.
5. The nonparallel effect on the growth rate of a disturbance is a function of the wave angle. Nonparallel effects are the greatest for a two-dimensional disturbance.
6. The nonparallelism has a larger influence on the second mode than on the first mode.

7. For the second mode the most unstable frequency predicted by the nonparallel theory for a given Reynolds number is higher than that predicted by the parallel theory, in contrast with the first mode when they are the same.
8. In contrast with the parallel results, the nonparallel results that include the profile distortion are in good agreement with the experimental results of Laufer and Vrebalovich (1960) and Kendall (1974) for all cases where the boundary-layer fluctuations were not produced by sound.
9. The question of determining the direction of wave amplification is still open. The question becomes critical in the case of three-dimensional mean flows. This question may be answered by experiments in which disturbances of known orientations are introduced and their amplification rates along different directions are measured.
10. An evaluation is presented of suction through porous strips for laminar flow control. The results show that the number of strips and their widths and spacings can be optimized so that the total suction levels needed are about 5-10% larger than those needed to achieve the same stability characteristics using area suction.
11. It appears that the effectiveness of a strip can be increased considerably by increasing the extent of the upstream influence (sink effect). This upstream influence needs to be assessed by determining the mean flow from either the Navier-Stokes or the interacting boundary-layer equations.

REFERENCES

Babenko, V. V. and L. F. Kozlov (1973). Experimental investigation of hydrodynamic stability at rigid and elastic-damping surfaces (in Russian). Izv. Akad. Nauk SSSR, Mek. Zhid i Gaza, 122.

Barry, M. D. J. and M. A. S. Ross (1970). The flat plate boundary layer, Part 2. The effect of increasing thickness on stability. J. Fluid Mech. 43, 813.

Boehman, L. I. (1971). Reclaculation of Brown's stability results. In: Proc. of the 12th Midwest Mechanics Conf., Univ. of Notre Dame Press, Notre Dame, Indiana, 6, 193.

Bouthier, M. (1972). Stabilité linéaire des écoulements presque paralléles, I. J. Meć. 11, 1.

Bouthier, M. (1973). Stabilité linéaire des écoulements presque paralléles. II - La couche limite de Blasius. J. Meć. 12, 75.

Braslow, A. L., D. L. Burrows, N. Tetervin, and F. Visconti (1951). Experimental and theoretical studies of area suction for the control of the laminar boundary layer on an NACA 64A010 airfoil. NACA Rep. 1025.

Brown, W. B. (1961a). A stability criterion for three-dimensional laminar boundary layers. In: Boundary Layer and Flow Control. ed. G. V. Lachmann, Pergamon Press, London, 913.

Brown, W. B. (1961b). Exact solution of the stability equations for laminar boundary layers in compressible flow. In: Boundary Layer and Flow Control, ed. G. V. Lachmann, Pergamon Press, London, 1033.

Brown, W. B. (1962). Exact numerical solutions of the complete linearized equations for the stability of compressible boundary layers. Northrop Aircraft Inc., Norair Div., Rep. NOR-62-15.

Brown, W. B. (1967). Stability of compressible boundary layers. AIAA J. 5, 1753.

Burrows, D. L. and M. A. Schwartzberg (1952). Experimental investigation of an NACA 64A010 airfoil secton with 41 suction slots on each surface for control of laminar boundary layer. NACA TN 2644.

Butler, S. F. J. (1955). Current tests on laminar boundary-layer control by suction through perforations. ARC R & M 3040.

Darlow, B. L., M. R. Scott, and H. A. Watts (1977). Modifications of SUPORT, a linear boundary value problem solver, Part I - Preassigning orthonormalization points, auxilary initial value problem, disk or tape storage, SAND 77-1328, Sandia Laboratories, Albuquerque, New Mexico.

Davis, R. T. and I. Flügge-Lotz (1963). Laminar compressible flow past axisymmetric blunt bodies (results of a second-order theory). Div. Eng. Mech., Stanford Univ., Tech. Rep. 143.

Demetriades, A. (1960). An experiment on the stability of hypersonic laminar boundary layers. J. Fluid Mech. 7, 385.

Demetriades, A. (1974). Hypersonic viscous flow over a slender cone, Part III: Laminar instability and transition. AIAA Paper No. 74-535.

Donaldson, J. C. and J. P. Wallace (1971). Flow fluctuations measurements at Mach 4 in the test section of the 12-inch supersonic wind tunnel (D). AEDC-TR-71-143, Arnold Engineering Development Center, Arnold Air Force Station, Tenn.

Dryden, H. L. (1955). Transition from laminar to turbulent flow at subsonic and supersonic speeds. Proc. Conference on High-Speed Aeronautics, Polytech. Inst. of Brooklyn, New York, 41.

Dunn, D. W. and C. C. Lin (1955). On the stability of the laminar boundary layer in a compressible fluid. J. Aero. Sci. 22, 455.

Edward, B. (1977). Laminar flow control - concepts, experiences, speculations. In: AGARD Rep. 654.

Flügge-Lotz, I. and F. G. Blottner (1962). Computations of the compressible laminar boundary-layer flow including displacement thickness interaction using finite-difference methods. U. S. Air Force AFOSR 2206.

Gaponov, S. A. (1971). Influence of the characteristics of a porous wall on the stability of a bounday layer (in Russian). Izv. Sib. Otd. Akad. Nauk. SSSR, 3, 21.

Gaponov, S. A. (1975). Stability of a boundary layer of an incompressible fluid over a slotted surface (in Russian). Izv. Sib. Otd. Akad. Nauk. SSSR, 8, 37.

Gaster, M. (1974). On the effects of boundary-layer growth on flow stability. J. Fluid Mech. 66, 465.

Godunov, S. (1961). On the numerical solution of boundary-vlaue problems for systems of linear ordinary differential equations (in Russian) Zapiski Mat. Nauk. SSSR, 16, 171.

Gregory, N. (1961) Research on suction surfaces for laminar flow. In: Boundary Layer and Flow Control, ed. G. V. Lachmann; Pergamon Press, 924.

Gregory, N. and W. S. Walker (1955). Experiments on the use of suction through perforated strips for maintaining laminar flow-transition and drag measurements. ARC R & M 3083.

Gunness, R. C. (1968). The stability equations for high Mach number boundary-layer flow. Boeing Document D6-20652, Boeing Corp., Seattle, Wash.

Hama, F. and J. Nutant (1963). Detailed flow-field observations in the transition process in a thick boundary layer. Proc. 1963 Heat Transfer and Fluid Mech. Inst., Stanford Univ., 77.

Harris, J. E. (1971). Numerical solution of the compressible laminar, transitional, and turbulent boundary-layer equations and comparisons with experimental data. NASA TR R-368.

Hayes, W. D., and R. F. Probstein (1959), Hypersonic Flow Theory, Acad. Press, 290.

Head, M. R. (1961). Flight experiments on maintaining laminar flow with suction applied through perforations. In: Boundary Layer and Flow Control, ed. G. V. Lachmann, Pergamon Press, 943 and 950.

Head, M. R., D. Johnson, and M. Coxon (1955). Flight experiments on boundary layer control for low drag. ARC R & M 3025.

Hilsenrath, J., C. W. Beckett, W. S. Benedict, L. Fano, H. J. Hoge, J. F. Masi, R. L. Nuttall, Y. S. Touloukian, and H. W. Woolley (1955). Tables of thermal properties of gases. Natl. Bur. Std. U.S., Circ. No. 564.

Jaffe, N. A., T. T. Okamura, and A. M. O. Smith (1970). Determination of spatial amplification factors and their application to predicting transition. AIAA J. 8, 301.

Jordinson, R. (1970). The flat plate boundary layer, Part 1. Numerical integration of the Orr-Sommerfeld equation. J. Fluid Mech. 43, 801.

Kachanov, Yu. S., V. V. Kozlov, and V. Ya. Levchenko (1975). Growth of small distrubances in a laminar-boundary layer (in Russian). Ucheniye Zapiski TSAGI 6, 137.

Kachanov, Yu. S., V. V. Kozlov, and V. Ya. Levchenko (1977) Nonlinear development of a wave in a boundary layer (in Russian). Mek. Zhid i Gaza 3, 4.

Kaplan, R. E. (1964). The stability of laminar incompressible boundary layers in the presence of compliant boundaries. MIT, Rep. ASRL TR 116-1, 1:

Kaups, K. (1975). Transition prediction onn bodies of revolution. Douglas Aircraft Co. Rep. MDC J6530, Long Beach, Calif.

Kelly, R. E. (1967). On the stability of an inviscid, shear layer which is periodic in space and time. J. Fluid Mech. 27, 657.

Kendall, J. M. (1967). Supersonic boundary-layer stability experiments. In Proc. of boundary layer transition study group meeting, ed. W. D. McCauley, Airforce Rep. BSD-TE-67-213, Aerosp. Rep. TR 0158 (S3816-63)-1 II.

Kendall, J. M. (1975). Wind tunnel experiments relating to supersonic and hypersonic boundary-layer transition. AIAA J. 13, 290.

Klebanoff, P. S., K. D. Tidstrom, and L. M. Sargent (1962). The three-dimensional nature of boundary-layer instability. J. Fluid Mech. 12, 1.

Kovasznay, L. S. G., H. Komoda, and B. R. Vasudeva (1962). Detailed flow field in transition. Proc. 1963 Heat Transfer and Fluid Mech. Inst., Stanford Univ. Press, 1.

Lachmann, G. V., N. Gregory, and W. S. Walker (1962). Handly-Page laminar flow wing with porous strips - Details of model and wind tunnel test at NPL. ARC 14, 794.

Lanchon, H. and W. Eckhaus (1964). Sur l'analyse de la stabilité des écoulements failbement divergents. J. Méc. 3, 445.

Laufer, J. (1961). Aerodynamic noise in supersonic wind tunnels. J. Aerosp. Sci. 28, 685.

Laufer, J. (1964). Some statistical properties of the pressure field radiated by a turbulent boundary layer. Phys. Fluids, 7, 1191.

Laufer, J. and T. Vrebalovich (1960). Stability and transition of a supersonic laminar boundary layer on an insulated flat plate. J. Fluid Mech. 9, 257.

Lebiga, V. A., A. A. Maslov, and V. G. Pridanov (1977). Experimental study of stability of supersonic boundary layers on a plate with blunted leading edge (in Russian). Mek. Zhid. i Gaza 4, 65.

Lees, L. (1947). The stabiity of the laminar boundary layer in a compressible fluid. NACA Tech. Rep. 876 and NACA TN1360.

Lees, L. and H. Gold (1966). Stability of laminar boundary layers and wakes at hypersonic speeds. In: Fundamental Phenomena in Hypsesonic Flow. ed. J. G. Hall, Ithaca, N. Y., Cornell Univ. Press.

Lees, L. and C. C. Lin (1946). Investigation of the stability of the laminar boundary layer in a compressible fluid. NACA TN 1115.

Lees, L. and E. Reshotko (1962). Stability of the compressible laminar boundary layer. J. Fluid Mech. 12, 555.

Lekoudis, S. G. (1978). Stability of boundary layers over permeable surfaces. AIAA Paper No. 78-203.

Levchenko, V. Ya, M. V. Volodin, and S. A. Gaponov (1975). Stability Characteristics of boundary layers (in Russian). Scientific Book.

Liepmann, H. W. (1943). Investigations on laminar boundary-layer stability and transition on curved boundaries. NACA ACR 3H30 (NACA wartime Rep. W-107).

Liepmann, H. W. and G. H. Fila (1947). Investigations of effect of surface temperature and single roughness elements on boundary layer transition. NACA TN 1196 and NACA Rep. 890.

Ling, C. H. and W. C. Reynolds (1973). Nonparallel flow corrections for the stability of shear flows. J. Fluid Mech. 59, 571.

Linke, W. (1942). Über den Strömungswiderstand einer beheizten ebenen platte. Luftfahrtforshung 19, 157.

Loftin, L. and E. Horton (1952). Experimental investigations of boundary layer suction throguh slots to obtain extensive laminar boundary layers on a 15% thick airfoil at high Reynolds numbers. NACA Research Memo. L52D02, NACA/TIB/3491.

Lowell, R. S. and E. Reshotko (1974). Numerical study of the stability of a heated water boundary layer. Dept. Fluid, Thermal and Aerospace Sci., Case Western Reserve Univ., Rep. FTAS/TR-73-95.

Mack, L. M. (1960). Numerical calcualtion of the stability of the compressible laminar boundary layer. Calif. Inst. Tech., Jet Propulsion Lab. Rep. 20-122.

Mack, L. M. (1965). The stability of the compressible laminar boundary layer according to a direct numerical solution. AGARDograph 97, Part I, 483.

Mack, L.M. (1967). Numerical solution of compressible boundary-layer stability. In: Proc. of boundary-layer transition group meeting, ed. W. D. McCauley, Air Force Rep. BSD-TR-67-213.

Mack, L. M. (1969). Boundary-layer stability theory. Jet Propulsion Lab. Document 900-277 (Rev. A), Pasadena, Calif.

Mack, L. M. (1971). Progress in Compressible boundary-layer stability computations. In: in Proc. of the boundary layer transition workshop Aerosp. Rep. TOR 0172IV: 1-1-1-35.

Mack, L. M. (1975). Linear stability theory and the problem of supersonic boundary-layer transition. AIAA J. 13, 278.

Mack, L. M. (1977). Transition prediction and linear stability theory. AGARD Conference Proceedings No. 224, Laminar-Turbulent Transition, Paper No. 1.

Mack, L. M. (1978). Three-dimensional effects in boundary-layer stability. In: Proc. of Twelfth Symposium on Naval Hydrodynamics, National Academy of Science, Washington, D. C.

Miksad, R. W. (1973). Experiments on nonlinear interactions in the transition of a free shear layer. J. Fluid Mech. 59, 1.

Morkovin, M. V. (1958). Transition from laminar to turbulent shear flow - a review of some recent advances in its understanding. Trans. ASME 80, 1121.

Morkovin, M. V. (1969). On the many faces of transition. In: Viscous Drag Reduction, ed. C. S. Wells, Plenum, N. Y.

Morkovin, M. V. (1978). Instability, transition to turbulence, and predictability, AGARDograph No. 236.

Nayfeh, A. H. (1973). Perturbation Methods, Wiley, New York, Chap. 6.

Nayfeh, A. H. and A. N. Bozatli (1978). Nonlinear interaction of waves in boundary-layer flows. Phys. Fluids, in Press.

Nayfeh, A. H. and A. Padhye (1978). The relation between temporal and spatial stability in three-dimensional flow. AIAA Paper No. 78-1126,

Nayfeh, A. H., W. S. Saric, and D. T. Mook (1974). Stability of non-parallel flows. Arch. Mech. Stosow 26, 401.

Parker, S. J. (1978). Experiments on heat-stabilized laminar boundary layers in a tube. In: Proc. Twelfth Symposium on Naval Hydrodynamics, Natioanl Academy of Sciences, Washington, D. C.

Pfenninger, W. (1977). Laminar flow control laminarization. In: AGARD Rep. 654.

Pfenninger, W. and E. Groth (1961). Low drag boundary layer suction experiments in flight on a wing glove of an F-94A airplane with suction through a large number of fine slots. In: Boundary Layer and Flow Control. ed. G. V. Lachmann, Pergamon Press, 981.

Reshotko, E. (1960). Stability of the compressible laminar boundary layer. Calif. Inst. Tech., Guggenheim Aeronautical Lab., GALCIT Mem. 52.

Reshotko, E. (1962). Stability of three-dimensional compressible boundary layers. NASA Tech. Note TN D-1220.

Reshotko, E. (1969). Stability theory as a guide to the evaluation of transition data. AIAA J. 7, 1086.

Reshotko, E. (1976). Boundary layer stability and transition. Ann. Rev. Fluid Mech. 8, 311.

Ross, J. A., F. H. Barnes, J. G. Burns, and M. A. S. Ross (1970). The flat plate boundary layer, Part 3, Comparison of theory with experiment. J. Fluid Mech. 43, 819.

Saric, W. S. and A. H. Nayfeh (1975). Nonparallel stability of boundary layer flows. Phys. Fluids 18, 945.

Saric, W. S. and A. H. Nayfeh (1977). Nonparallel stability of boundary layers with pressure gradients and suction. AGARD Conference Proceedings No. 224, Laminar-Turbulent Transition, Paper No. 6.

Sato, H. (1970). An experimental study of nonlinear interaction of velocity fluctuations in the transition region of a two-dimensional wake. J. Fluid Mech. 44, 741.

Schlichting, H. (1935). Amplitudenverteilung und Energiebilanz der kleinen Störungen bei der plattenströmung, Nachr. Ges. Wiss. Göttingen, Math. Phys. Klasse 1, 47.

Schlichting, H. (1977). Boundary Layer Theory. 7th edition, McGraw-Hill New York.

Schubauer, G. B. and H. K. Skramstad (1947). Laminar boundary layer oscillations and transition on a flat plate. J. Aero. Sci. 14, 69.

Scott, M. R. and H. A. Watts (1977). Computational solution of linear two-point boundary value problems via orthonormalization. SIAM J. Num. Anal. 14, 40.

Smith, A. M. O. and N. Gamberoni (1956). Transition, pressure gradient, and stability theory. Proc. 9th Int. Cong. Appl. Mech., Brussels, Belgium, 4, ed. Wiley, 234.

Squire, H. B. (1933). On the stability for three-dimensional disturbances of viscous fluid flow between parallel walls. Proc. Roy. Soc. London A-142, 621.

Stainback, P. C., M. C. Fischer, and R. D. Wagner (1972). Effects of wind-tunnel disturbances on hypersonic boundary layer transition. AIAA Paper No. 72-181.

Strazisar, A. J. and E. Reshotko (1978). Stability of heated laminar boundary layers in water with non-uniform surface temperature. Phys. Fluids 21, 727.

Strazisar, A. J., J. M. Prahl, and E. Reshotko (1975). Experimental study of stability of heated laminar boundary layers in water. Fluid,Thermal and Aerospace Sci., Case Western Reserve Univ., Rep. FTAS/TR-75-113.

Strazisar, A. J., E. Reshotko, and J. M. Prahl (1977). Experimental study of stability of heated laminar boundary layers in water. J. Fluid Mech. 83, 225.

Tani, I. (1969). Boundary layer transition. Ann. Rev. Fluid Mech. 1, 169.

Tollmien, W. (1929). Über die entstehung der turbulenz, Nachr. Ges. Wiss. Göttingen, Math Phys. Klasse 21 (Translated as NACA TM 609, 1931).

Van Ingen, J. L. (1956). A suggested semi-empirical method for the calculation of the boundary-layer transtion region. Dept. of Aero. Eng. Univ. of Technology, Delft, Holand, Rep. VTH- 71 and 74.

Volodin, A. G. (1973). Stability of plane boundary layer taking into account nonparallelism (in Russian). Izv. Sib. Otd. Akad. Nauk SSSR 2, 13.

Wazzan, A. R., G. Keltner, T. T. Okamura, and A. M. O. Smith (1972). Spatial stability of stagnation water boundary layer with heat transfer. Phys. Fluids 15, 2114.

Wazzan, A. R., T. T. Okamura, and A. M. O. Smith (1968). The stability of water flow over heated and cooled flat plates. J. Heat. Trans. 90, 109.

Wazzan, A. R., T. T. Okamura, and A. M. O. Smith (1970). The stability and transition of heated and cooled incompressible laminar boundary layers. In: Proc. 4th Int. Heat Transfer Conf., ed. Grigall U. and E. Hahne, Amsterdam.

Wazzan, A. R., H. Taghavi, and G. Keltner (1974). Effect of boundary-layer growth on the stability of incompressible flat plate bcundary layer with pressure gradient. Phys. Fluids 17, 1655.

Wortmann, F. X. (1955). Untersuchung instabiler Grenzschichtschwingungen in einem Wasserkanal mit der Tellurmethode, 50 Jahre Grenzschicht-forchung. Braunschweig, F. Vieweg und Sohn, 460.

Wortman, F. X. (1969). Visualization of transition, J. Fluid Mech. 38, 473.

Wu, Y. K. and G. F. Anderon (1972). Torpedo drag reduction using magnetohydrodynamic boundary-layer control. Southeastern Mass. Univ. Tech. Rep. No. 0140-69-C-0338.

TABLE 6.1 Comparison of the growth rates and wavenumbers calculated from the eigenvalue problem and those calculated from the transformation Eqs. (6.46) and (6.47) for a two-dimensional mean flow, $M_e = 0.0$, $R = 1600$, $F = 22.25 \times 10^{-6}$, and $\psi = 50°$.

	eigenvalue problem		Transformation		$\psi°$
$\overline{\psi}°$	k_0	σ_0	k_0	σ_0	(transformation)
0.	.1669	.3174 E-2	.1669	.3174 E-2	50.00
10.	.1669	.3130 E-2	.1669	.3133 E-2	50.02
20.	.1670	.3184 E-2	.1670	.3187 E-2	50.02
30.	.1670	.3343 E-2	.1670	.3346 E-2	50.02
40.	.1671	.3636 E-2	.1671	.3636 E-2	50.02
50.	.1672	.4123 E-2	.1672	.4115 E-2	50.03
60.	.1673	.4938 E-2	.1673	.4906 E-2	50.06
70.	.1674	.6415 E-2	.1677	.6293 E-2	50.14
80.	.1677	.9484 E-2	.1686	.9081 E-2	50.37

TABLE 6.2 Comparison of the growth rates and wavenumbers calculated from the eigenvalue problem and those calculated from the transformation Eqs. (6.46) and (6.47) for a two-dimensional mean flow, $M_e = 0.4$, $R = 1500$, $F = 24 \times 10^{-6}$, and $\psi = 50°$.

	eigenvalue problem		Transformation		$\psi°$
$\bar{\psi}°$	k_0	σ_0	k_0	σ_0	(transformation)
0.	.1634	.2857 E-2	.1634	.2857 E-2	50.00
10.	.1634	.2824 E-2	.1634	.2825 E-2	50.01
20.	.1635	.2877 E-2	.1635	.2880 E-2	50.01
30.	.1635	.3027 E-2	.1635	.3029 E-2	50.01
40.	.1636	.3300 E-2	.1636	.3300 E-2	50.01
50.	.1636	.3752 E-2	.1636	.3746 E-2	50.01
60.	.1637	.4509 E-2	.1638	.4486 E-2	50.04
70.	.1639	.5887 E-2	.1641	.5795 E-2	50.12
80.	.1642	.8805 E-2	.1649	.8480 E-2	50.32

TABLE 6.3 Comparison of the growth rates and wavenumbers calculated from the eigenvalue problem and those calculated from the transformation Eqs. (6.46) and (6.47) for a two-dimensional mean flow, $M_e = 0.8$, $R = 1500$, $F = 20 \times 10^{-6}$, and $\psi = 50°$.

	eigenvalue problem		Transformation		$\psi°$
$\bar{\psi}°$	k_0	σ_0	k_0	σ_0	(transformation)
0.	.1313	.3736 E-2	.1313	.3736 E-2	50.00
10.	.1314	.3711 E-2	.1314	.3712 E-2	50.01
20.	.1314	.3801 E-2	.1314	.3802 E-2	50.01
30.	.1314	.4021 E-2	.1314	.4022 E-2	50.01
40.	.1315	.4411 E-2	.1315	.4410 E-2	50.01
50.	.1315	.5057 E-2	.1315	.5051 E-2	50.01
60.	.1316	.6144 E-2	.1317	.6126 E-2	50.03
70.	.1317	.8155 E-2	.1319	.8087 E-2	50.10
80.	.1320	.1267 E-1	.1327	.1241 E-1	50.34

TABLE 6.4 Comparison of the growth rates and wavenumbers calculated from the eigenvalue problem and those calculated from the transformation Eqs. (6.46) and (6.47) for a two-dimensional mean flow, $M_e = 1.6$, $R = 1500$, $F = 16 \times 10^{-6}$, and $\psi = 55°$.

	eigenvalue problem		Transformation		$\psi°$
$\bar{\psi}°$	k_0	σ_0	k_0	σ_0	(transformation)
0.	.9735 E-1	.2571 E-2	.9735 E-1	.2571 E-2	55.00
10.	.9735 E-1	.2584 E-2	.9735 E-1	.2583 E-2	55.02
20.	.9736 E-1	.2679 E-2	.9735 E-1	.2678 E-2	55.02
30.	.9736 E-1	.2872 E-2	.9736 E-1	.2871 E-2	55.02
40.	.9737 E-1	.3201 E-2	.9736 E-1	.3198 E-2	55.02
50.	.9738 E-1	.3744 E-2	.9737 E-1	.3738 E-2	55.02
60.	.9740 E-1	.4682 E-2	.9738 E-1	.4667 E-2	55.02
70.	.9744 E-1	.6519 E-2	.9740 E-1	.6474 E-2	55.03
80.	.9759 E-1	.1130 E-1	.9750 E-1	.1112 E-1	55.06

TABLE 6.5 Comparison of the growth rates and wavenumbers calculated from the eigenvalue problem and those calculated from the transformation Eqs. (6.46) and (6.47) for a two-dimensional mean flow, $M_e = 2.2$, $R = 1500$, $F = 12 \times 10^{-6}$, and $\psi = 60°$.

	eigenvalue problem		Transformation		
$\bar{\psi}°$	k_0	σ_0	k_0	σ_0	$\psi°$ (transformation)
0.	.7364 E-1	.2291 E-2	.7364 E-1	.2291 E-2	60.00
10.	.7363 E-1	.2310 E-2	.7364 E-1	.2310 E-2	60.02
20.	.7362 E-1	.2404 E-2	.7363 E-1	.2404 E-2	60.03
30.	.7361 E-1	.2588 E-2	.7363 E-1	.2587 E-2	60.03
40.	.7360 E-1	.2899 E-2	.7361 E-1	.2897 E-2	60.03
50.	.7359 E-1	.3414 E-2	.7359 E-1	.3407 E-2	60.03
60.	.7358 E-1	.4312 E-2	.7354 E-1	.4294 E-2	60.02
70.	.7356 E-1	.6115 E-2	.7343 E-1	.6053 E-2	59.99
80.	.7363 E-1	.1110 E-1	.7297 E-1	.1080 E-1	59.83

TABLE 6.6 Comparison of the growth rates and wavenumbers calculated from the eigenvalue problem and those calculated from the transformation Eqs. (6.46) and (6.47) for a two-dimensional mean flow, $M_e = 4.5$, $R = 1500$, $F = 27 \times 10^{-6}$, and $\psi = 60°$.

	eigenvalue problem		Transformation		$\psi°$
$\bar{\psi}°$	k_0	σ_0	k_0	σ_0	(transformation)
0.	.9917 E-1	.1846 E-2	.9917 E-2	.1846 E-2	60.00
10.	.9916 E-1	.1866 E-2	.9917 E-2	.1866 E-2	60.02
20.	.9916 E-1	.1946 E-2	.9917 E-1	.1945 E-2	60.02
30.	.9916 E-1	.2099 E-2	.9917 E-1	.2099 E-2	60.02
40.	.9916 E-1	.2357 E-2	.9916 E-1	.2356 E-2	60.02
50.	.9916 E-1	.2784 E-2	.9916 E-1	.2782 E-2	60.02
60.	.9915 E-1	.3532 E-2	.9916 E-1	.3527 E-2	60.02
70.	.9915 E-1	.5042 E-2	.9914 E-1	.5025 E-2	60.02
80.	.9915 E-1	.9364 E-2	.9907 E-1	.9222 E-2	60.00

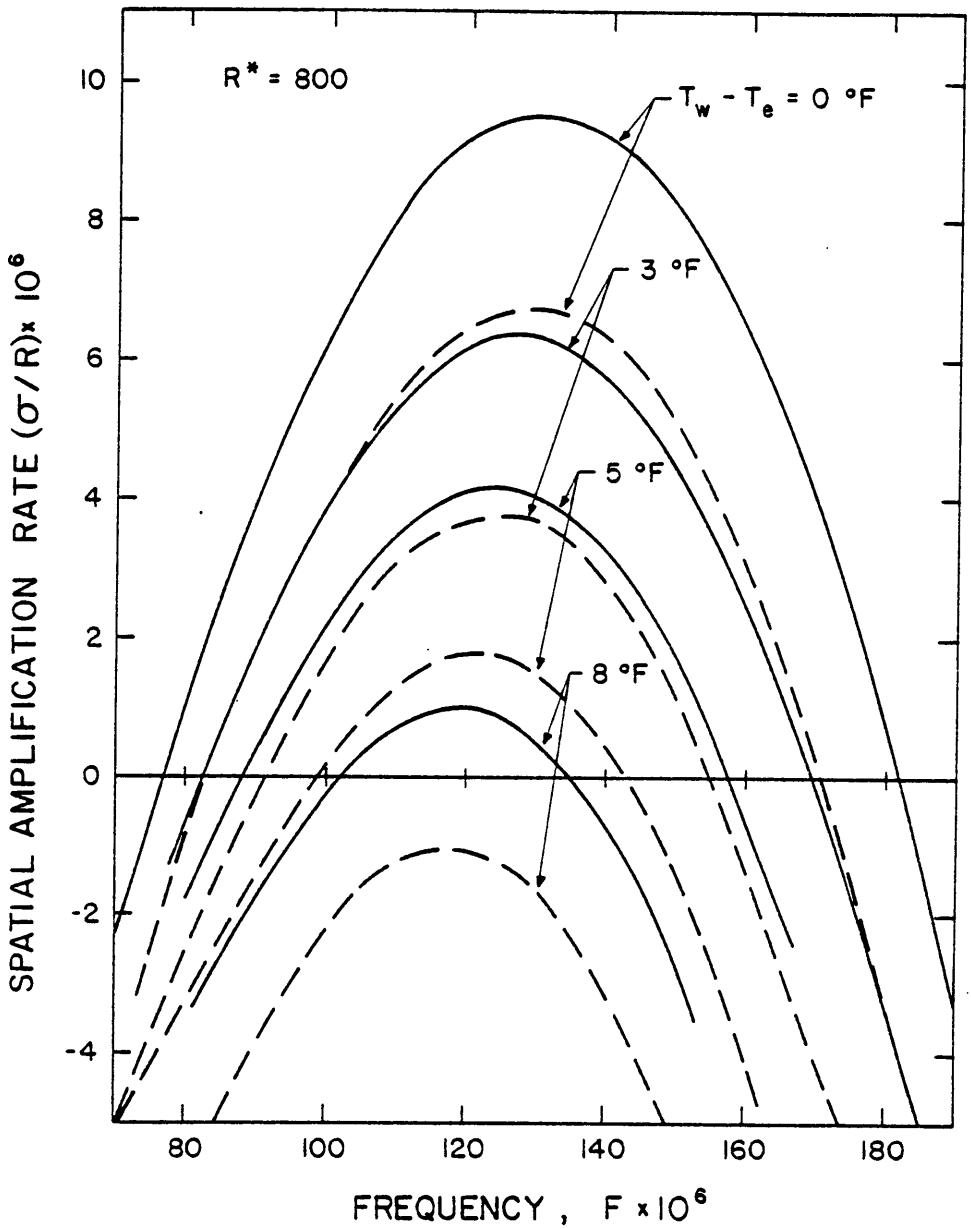

Figure 4.1 Variation of the spatial amplification rate with frequency for the unheated case and various uniform wall overheats at R* = 800. Solid lines, nonparallel $\sigma = -\mathrm{Im}(\alpha_0+\varepsilon\alpha_1)$; dashed lines, parallel.

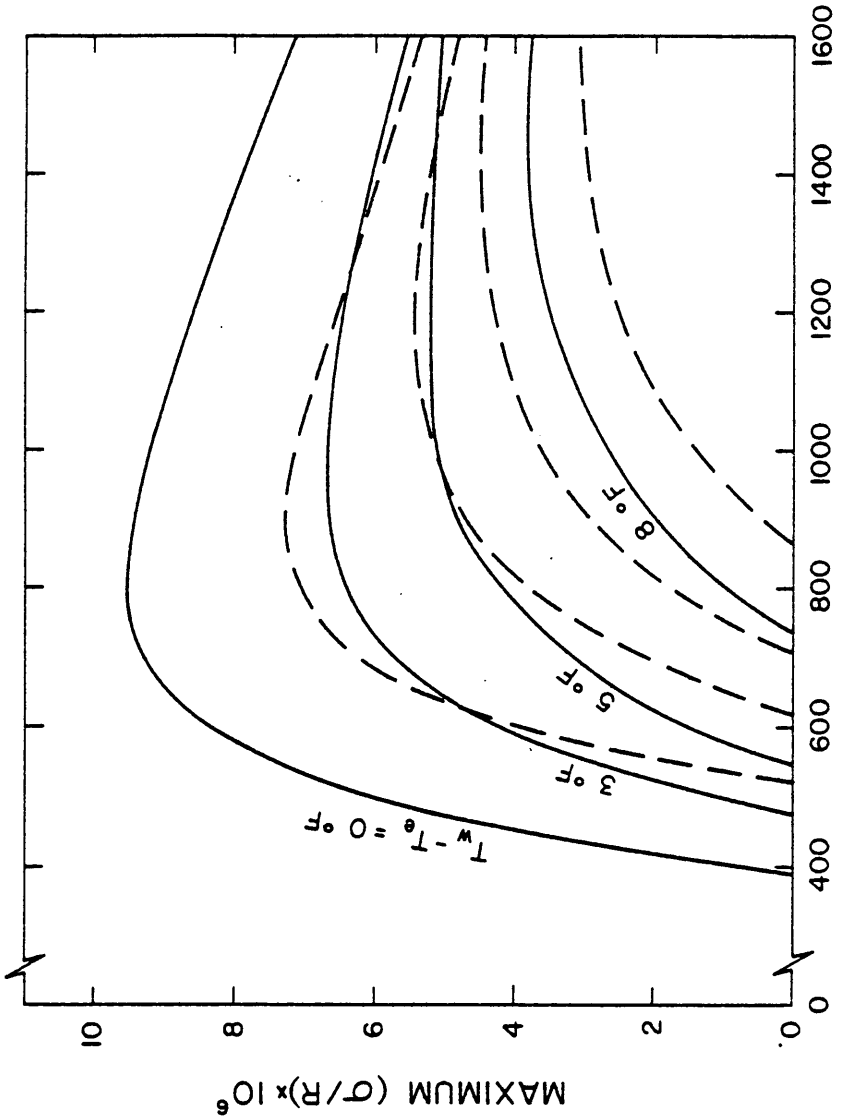

Figure 4.2 Variation of the maximum spatial amplification rate with streamwise position for the unheated case and various uniform wall overheats. Solid lines, nonparallel $\sigma = -\,\mathrm{Im}(\alpha_0+\varepsilon\alpha_1)$; dashed lines, parallel.

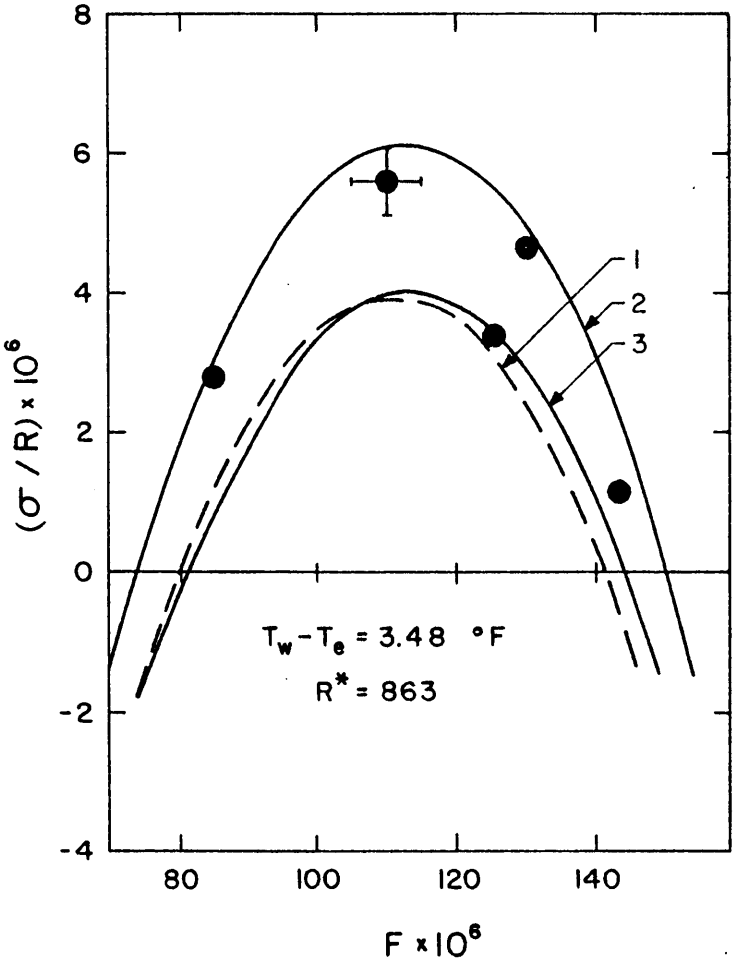

Figure 4.3

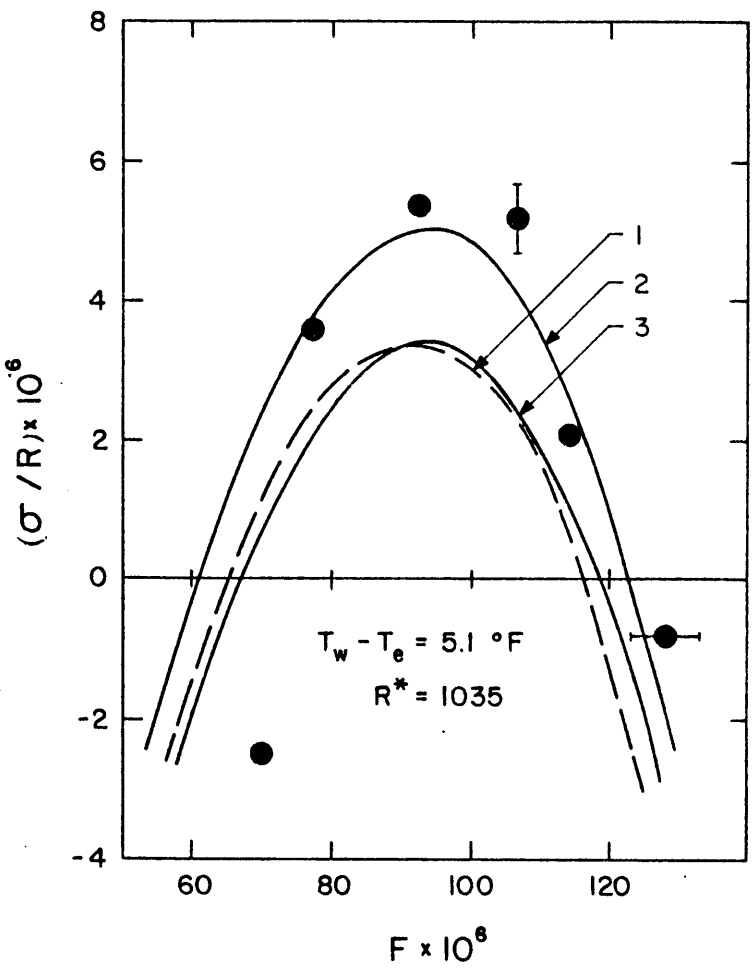

Figure 4.4

Comparison of the calculated and the measured spatial amplification rates for various uniform wall overheats and displacement thickness Reynolds numbers. Experiments, Strazisar et al (1975, 1977); (1) $\sigma = -\mathrm{Im}(\alpha_0)$, (2) $\sigma = -\mathrm{Im}(\alpha_0 + \varepsilon\alpha_1)$, (3) $\sigma = -\mathrm{Im}(\alpha_0 + \varepsilon\alpha_1) + \frac{\varepsilon}{|u|}\frac{\partial |u|}{\partial x_1}$.

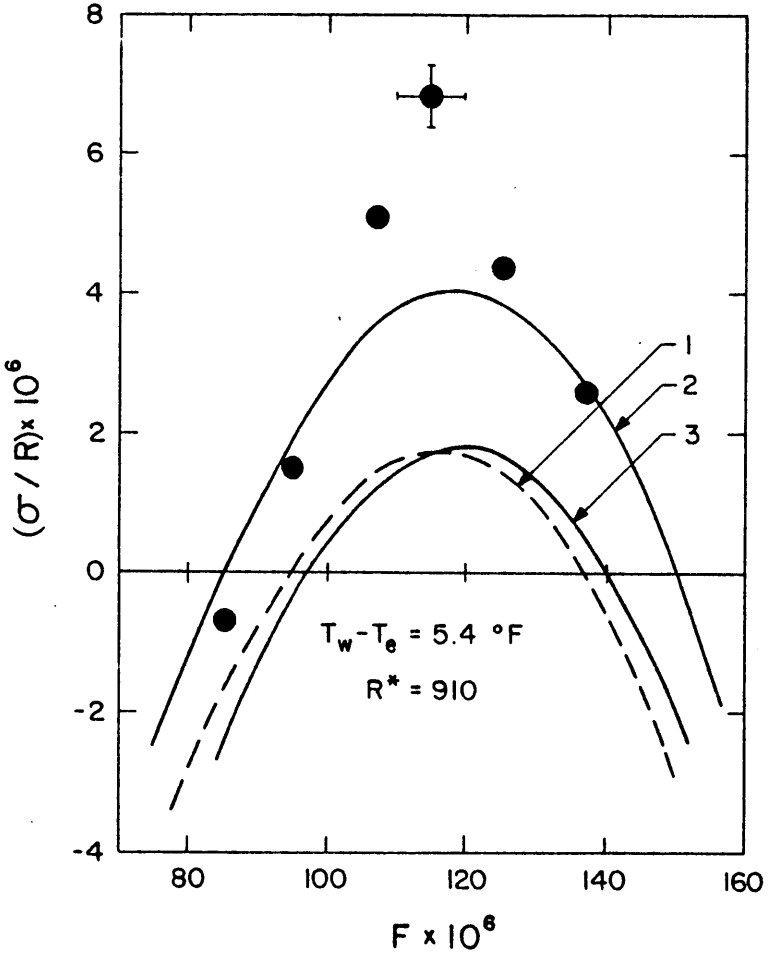

Figure 4.5

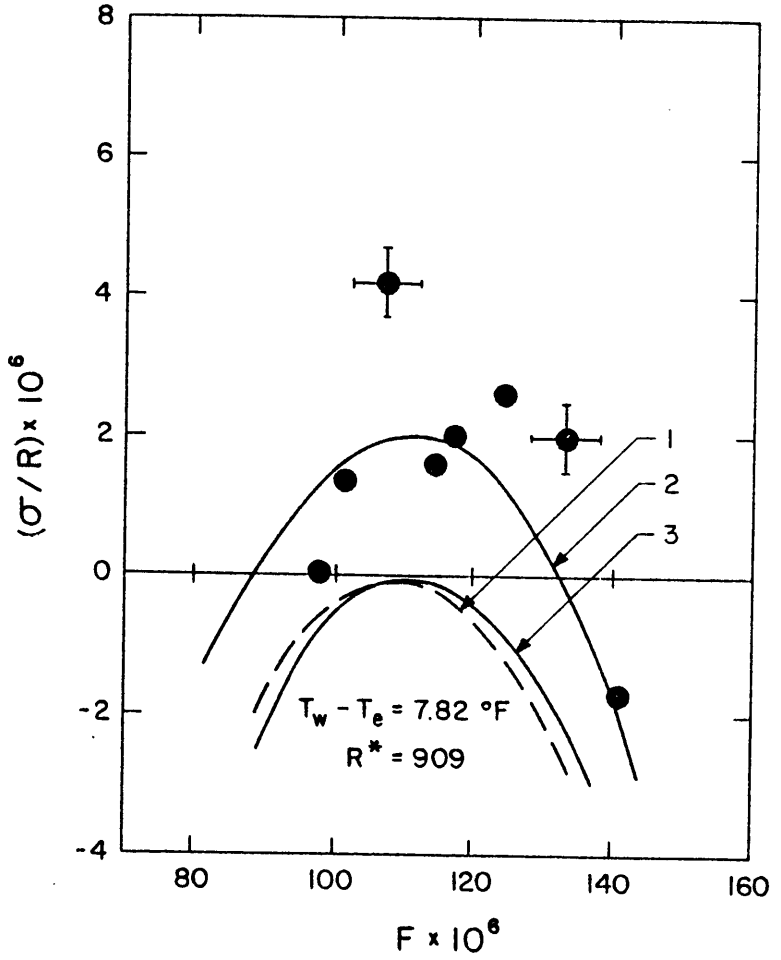

Figure 4.6

Comparison of the calculated and the measured spatial amplification rates for various uniform wall overheats and displacement thickness Reynolds numbers. Experiments, Strazisar et al (1975, 1977); (1) $\sigma = -\mathrm{Im}(\alpha_0)$, (2) $\sigma = -\mathrm{Im}(\alpha_0 + \varepsilon\alpha_1)$, (3) $\sigma = -\mathrm{Im}(\alpha_0 + \varepsilon\alpha_1) + \frac{\varepsilon}{|u|}\frac{\partial |u|}{\partial x_1}$.

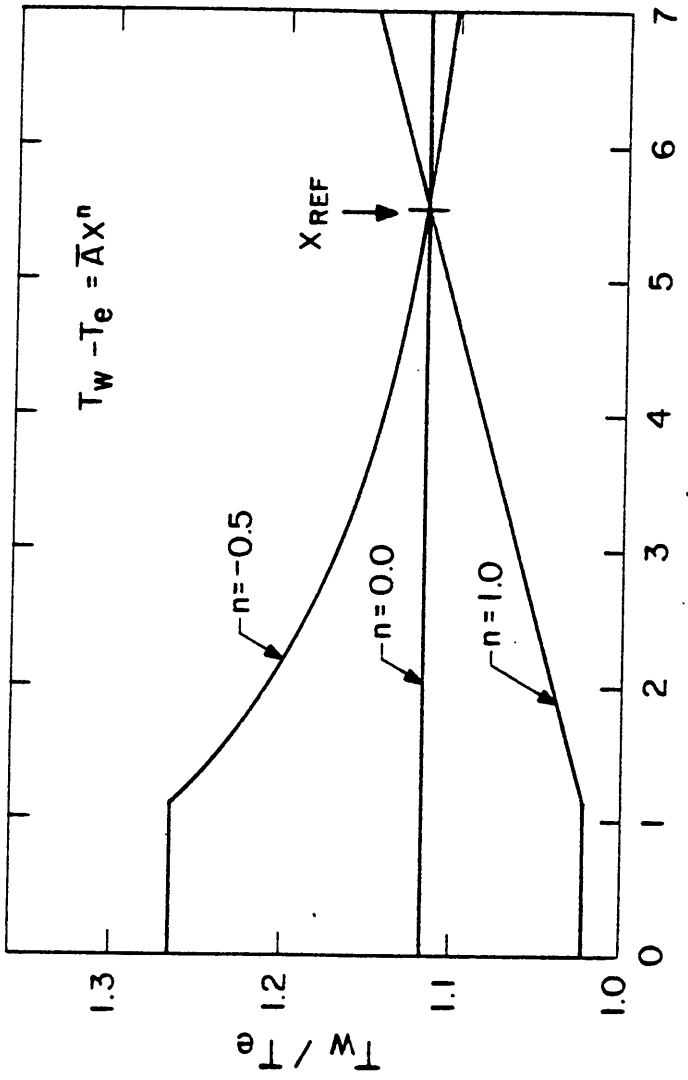

Figure 4.7 Power -law temperature distribution.

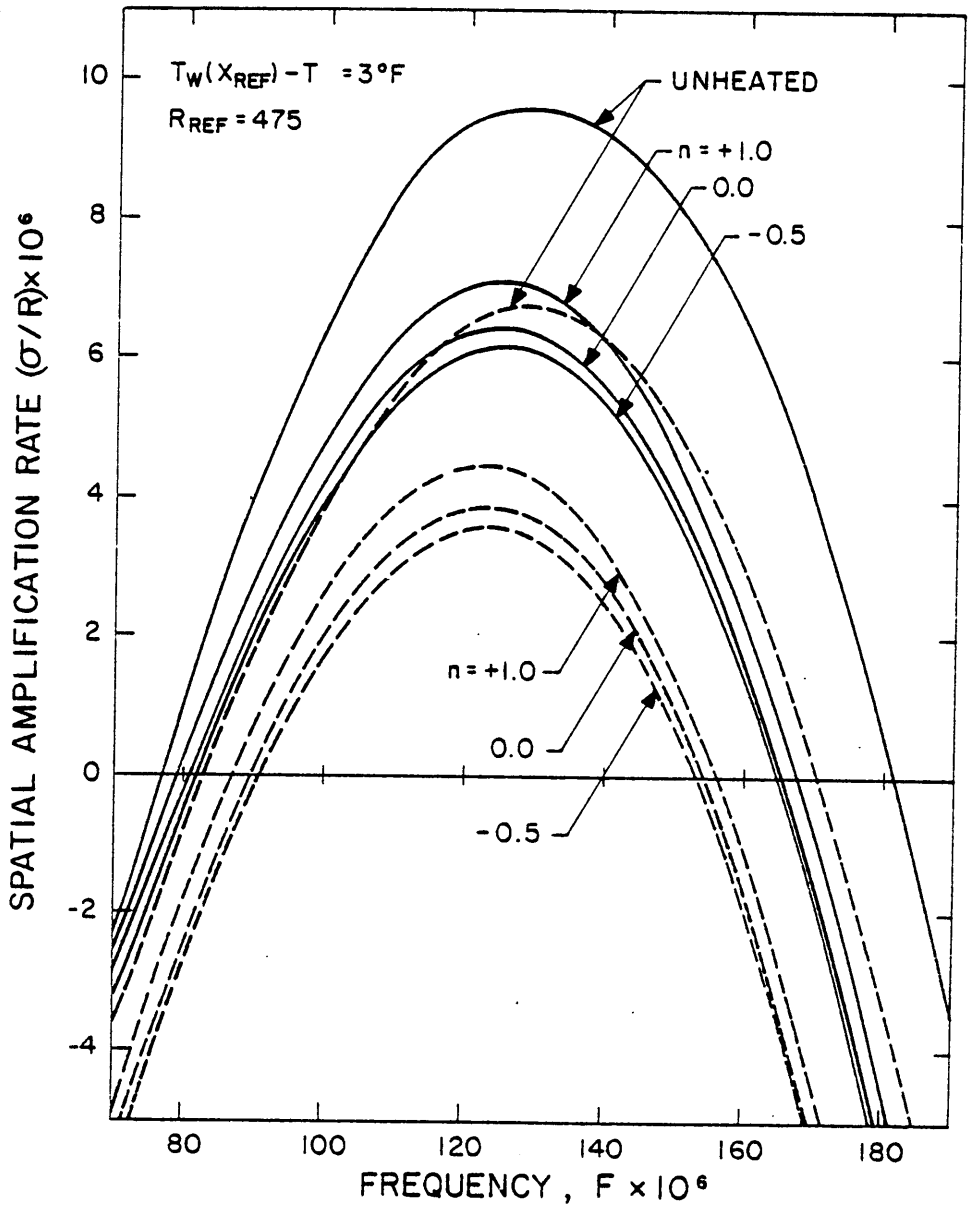

Figure 4.8 Variation of the spatial amplification rate with frequency at x_{ref} for the unheated case and the power-law temperature distributions of Fig. 4.7 for $T_w - T_e$ = 3°F at x_{ref}. Solid lines, nonparallel σ =- $Im(\alpha_0+\varepsilon\alpha_1)$; dashed lines, parallel.

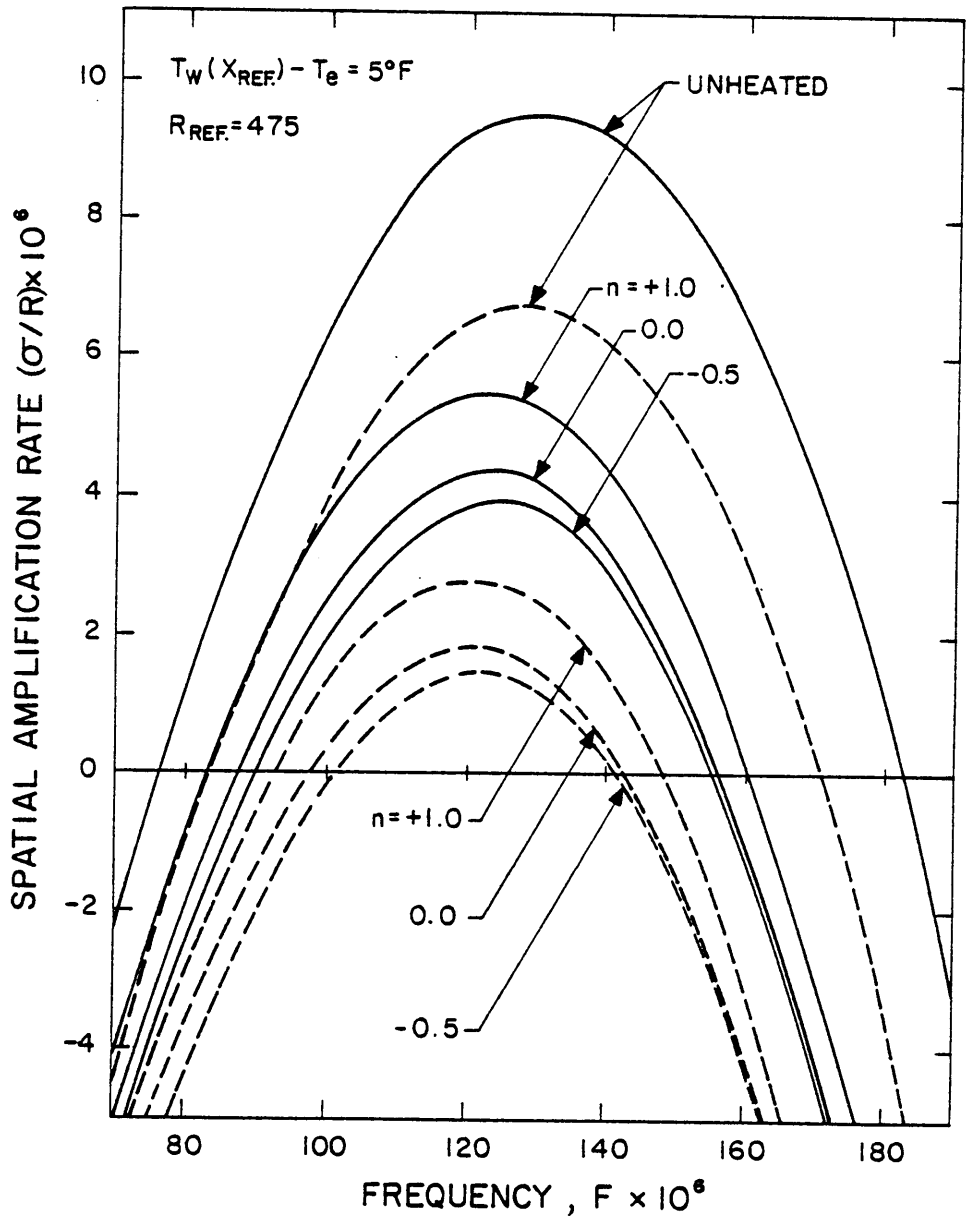

Figure 4.9 Variation of the spatial amplification rate with frequency at $x_{ref.}$ for the unheated case and the power-law temperature distribution of Fig. 4.7 for $T_w - T_e = 5°F$ at $x_{ref.}$. Solid lines, nonparallel $\sigma = -Im(\alpha_0 + \varepsilon\alpha_1)$; dashed lines, parallel.

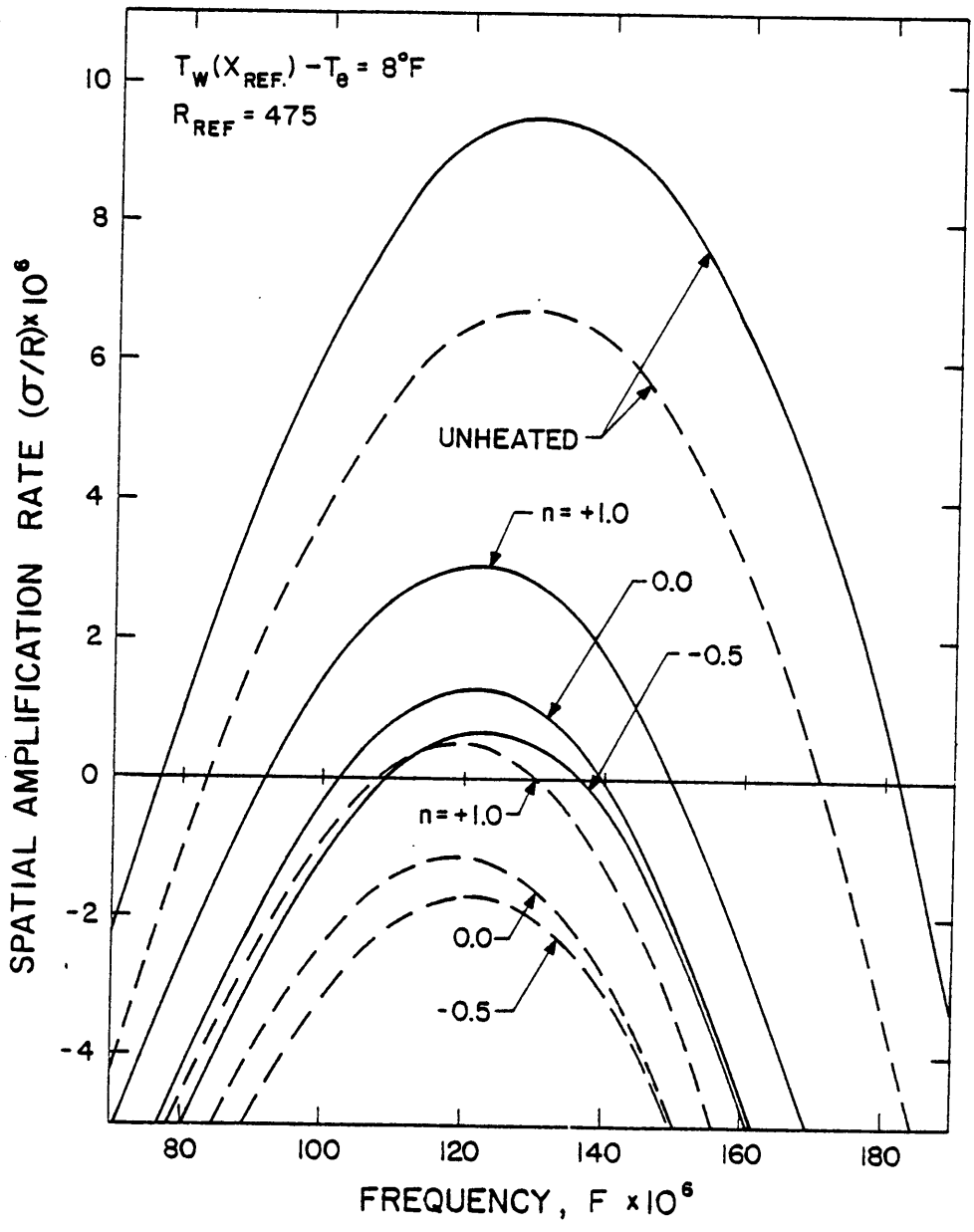

Figure 4.10 Variation of the spatial amplification rate with frequency at $x_{ref.}$ for the unheated case and the power-law temperature distribution of Fig. 4.7 for $T_w - T_e = 5°F$ at $x_{ref.}$. Solid lines, nonparallel $\sigma = -Im(\alpha_0 + \varepsilon\alpha_1)$; dashed lines, parallel.

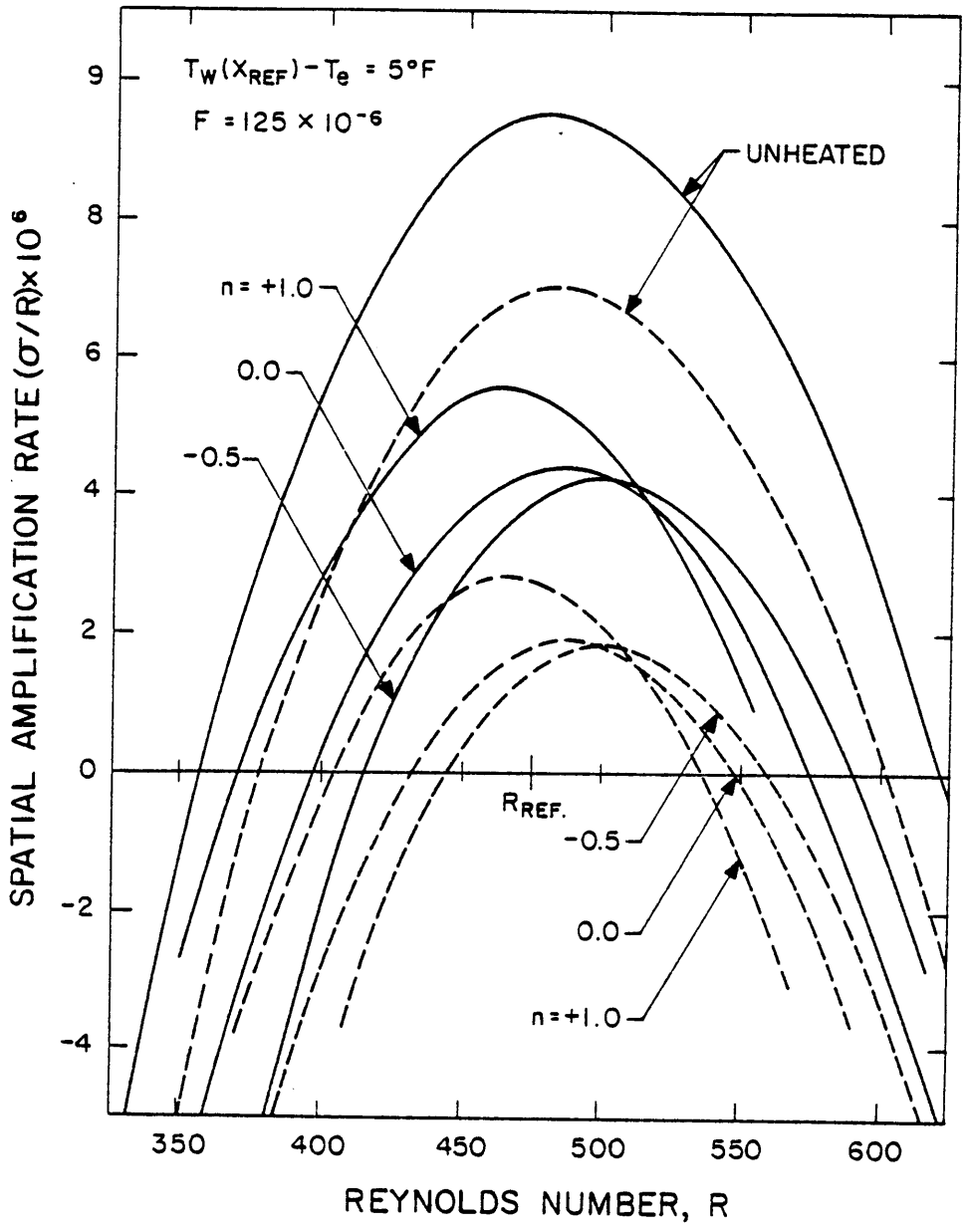

Figure 4.11 Variation of the spatial amplification rate with streamwise position for the unheated case and the power-law temperature distribution of Fig. 4.7 for $T_w - T_e$ = 5°F at $x_{ref.}$. Solid lines, nonparallel $\sigma = -\,\mathrm{Im}(\alpha_0 + \varepsilon\alpha_1)$; dashed lines, parallel.

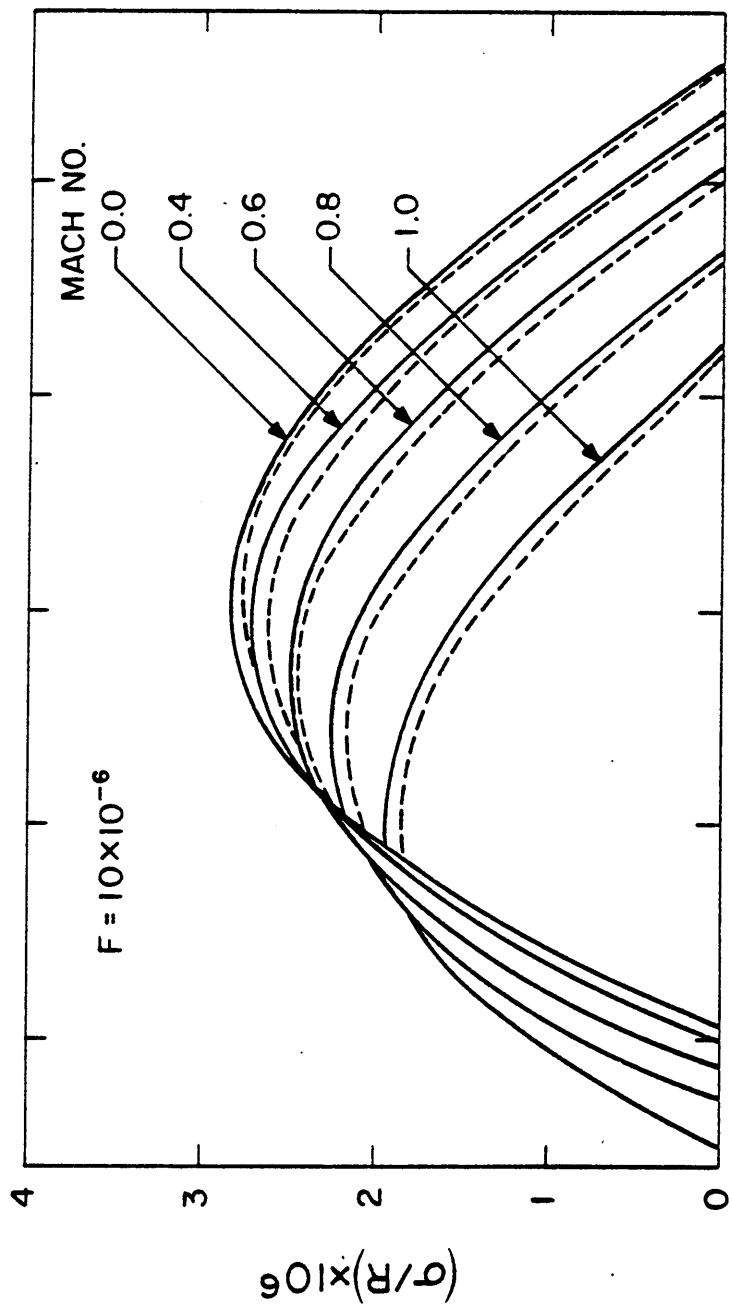

Figure 5.1 Effect of Mach number on the variation of the spatial amplification rate with streamwise position for $F = 10 \times 10^{-6}$. Solid lines, nonparallel $\sigma = -\mathrm{Im}(\alpha_0 + \varepsilon\alpha_1)$; dashed lines, parallel.

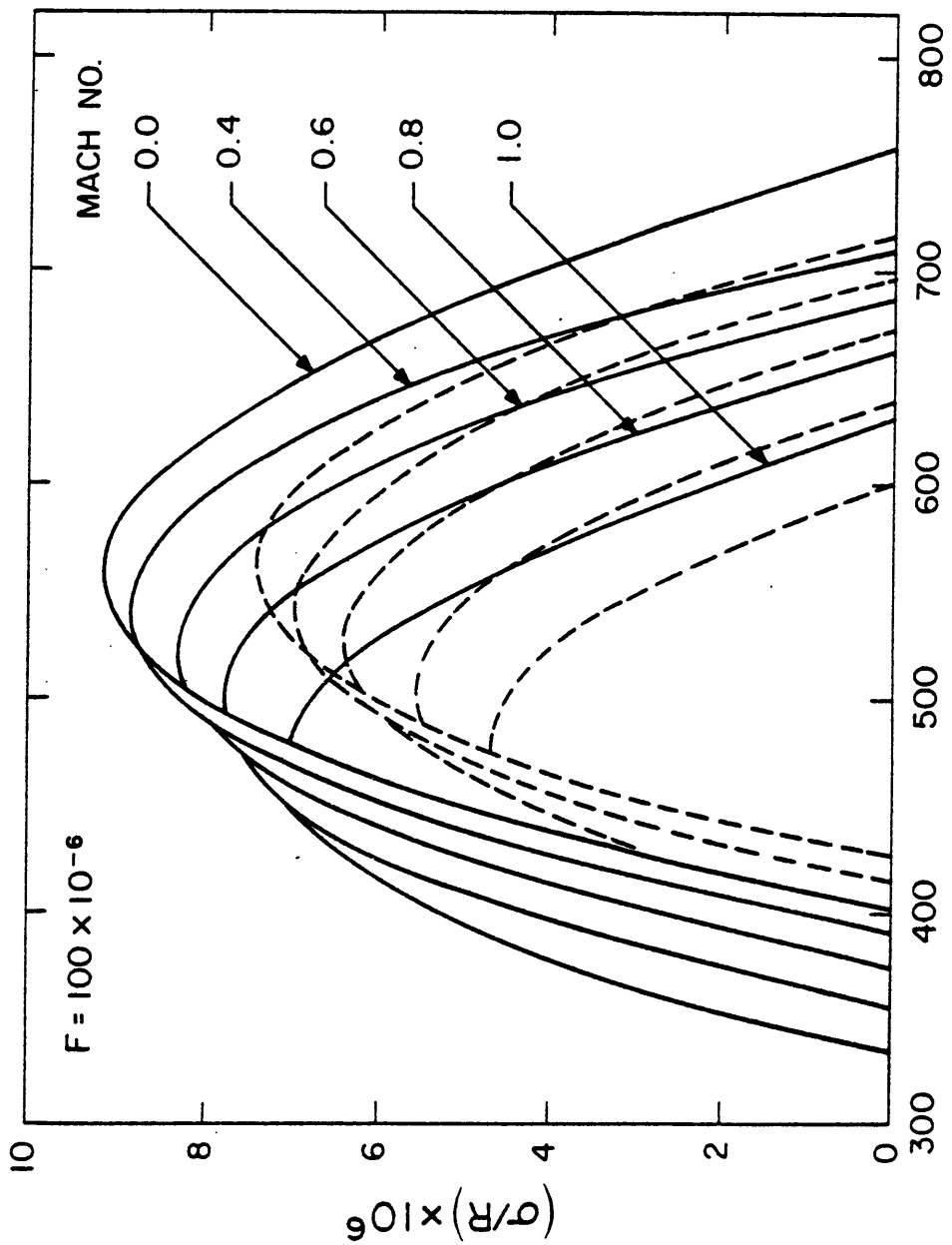

Figure 5.2 Effect of Mach number on the variation of the spatial amplification rate with streamwise position for $F = 100 \times 10^{-6}$. Solid lines, nonparallel $\sigma = \mathrm{Im}(\alpha_0 + \varepsilon\alpha_1)$; dashed lines, parallel.

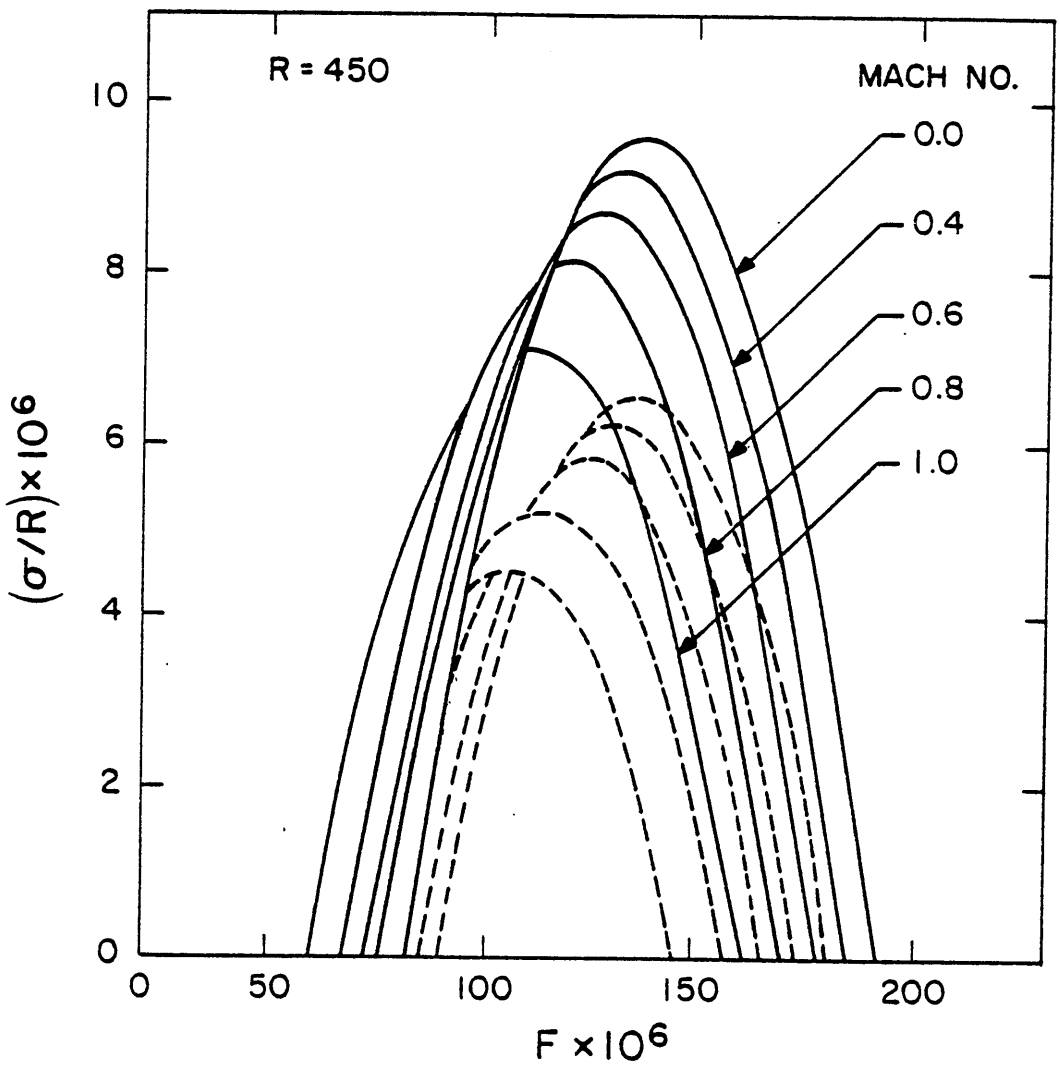

Figure 5.3 Effect of Mach number on the variation of the spatial amplification rate with frequency at R = 450. Solid lines, nonparallel $\sigma = - \mathrm{Im}(\alpha_0 + \varepsilon\alpha_1)$; dashed lines, parallel.

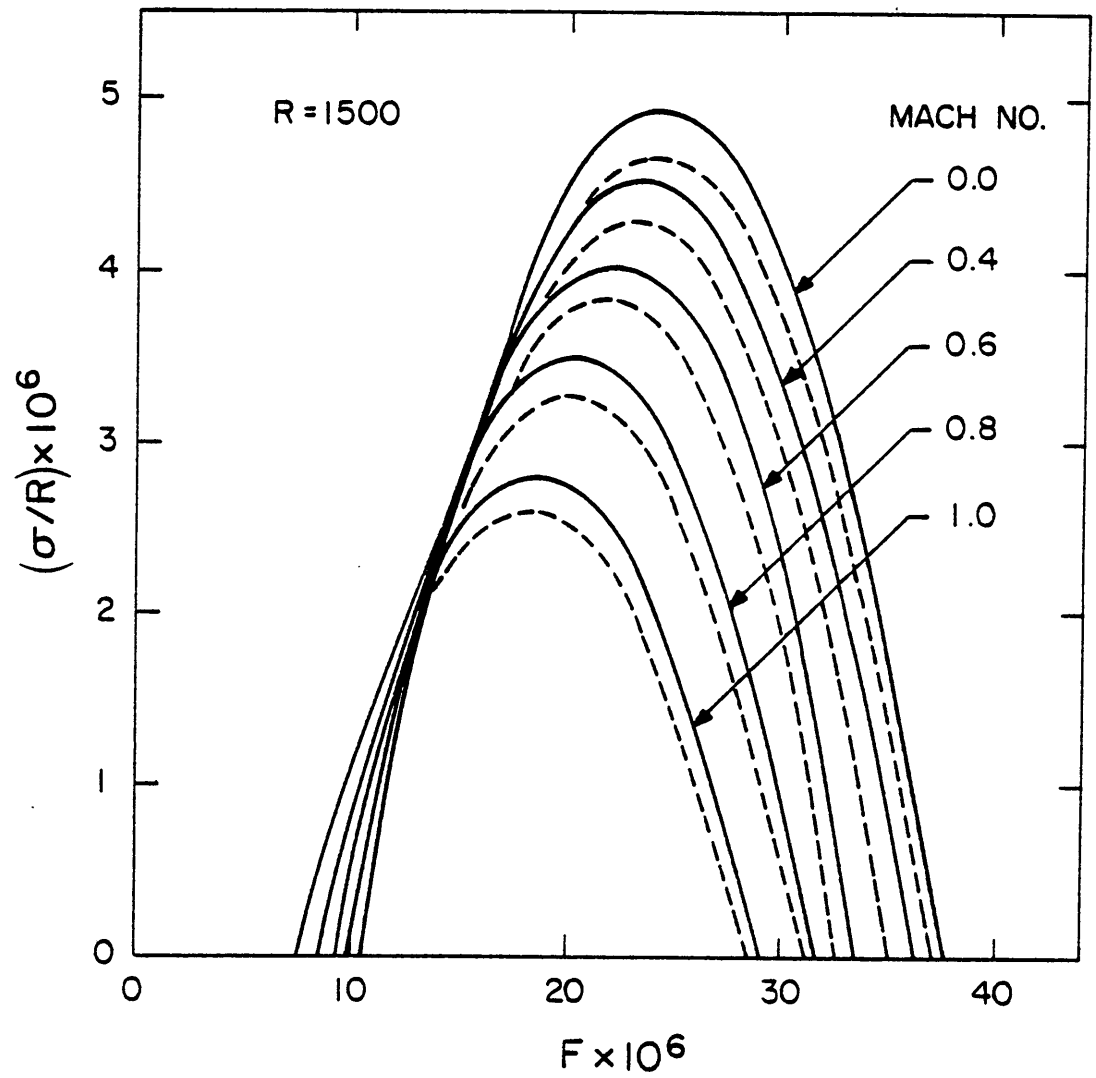

Figure 5.4 Effect of Mach number on the variation of the spatial amplification rate with frequency at R = 1500. Solid lines, nonparallel $\sigma = -\mathrm{Im}(\alpha_0 + \varepsilon\alpha_1)$; dashed lines, parallel.

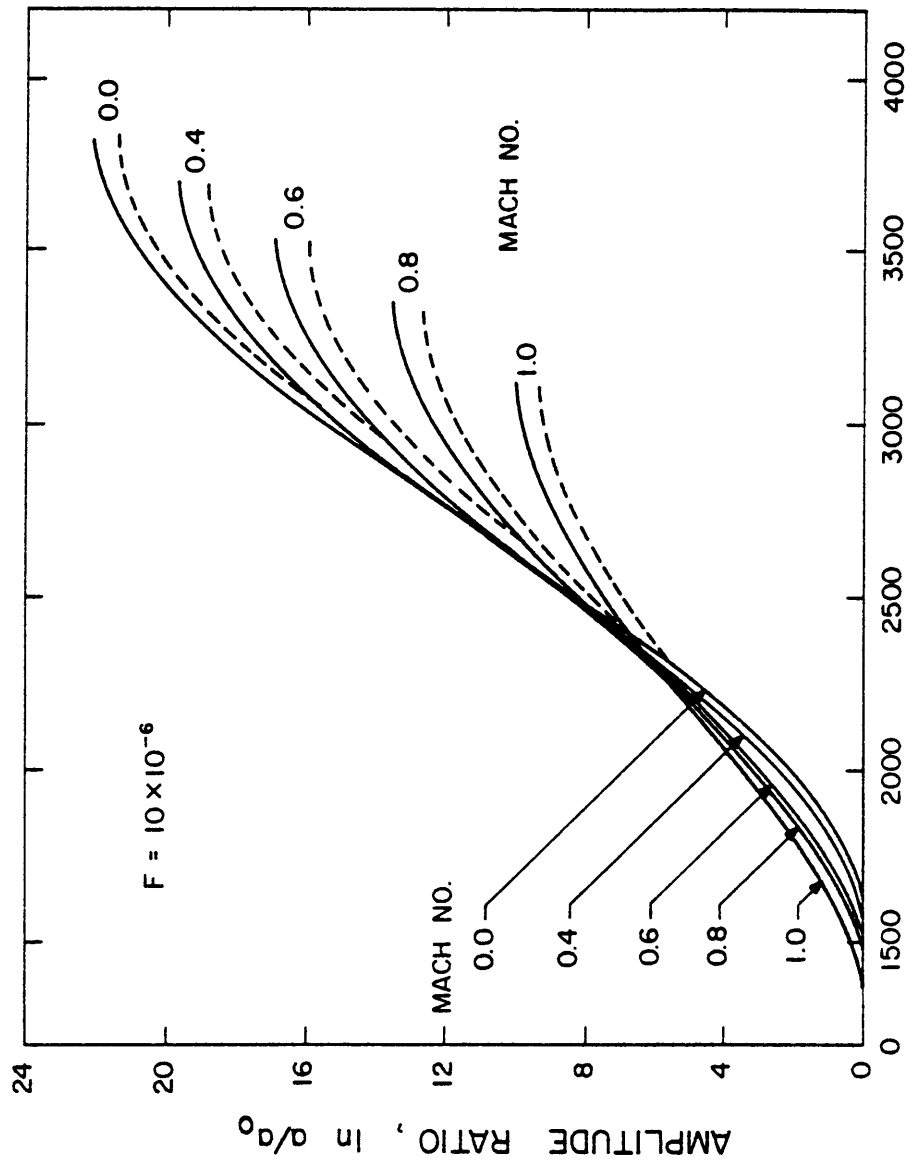

Figure 5.5 Effect of Mach number on the variation of the amplitude ratio with streamwise position for F = 10 x 10^{-6}. Solid lines, nonparallel $\sigma=-\mathrm{Im}(\alpha_0+\varepsilon\alpha_1)$; dashed lines, parallel.

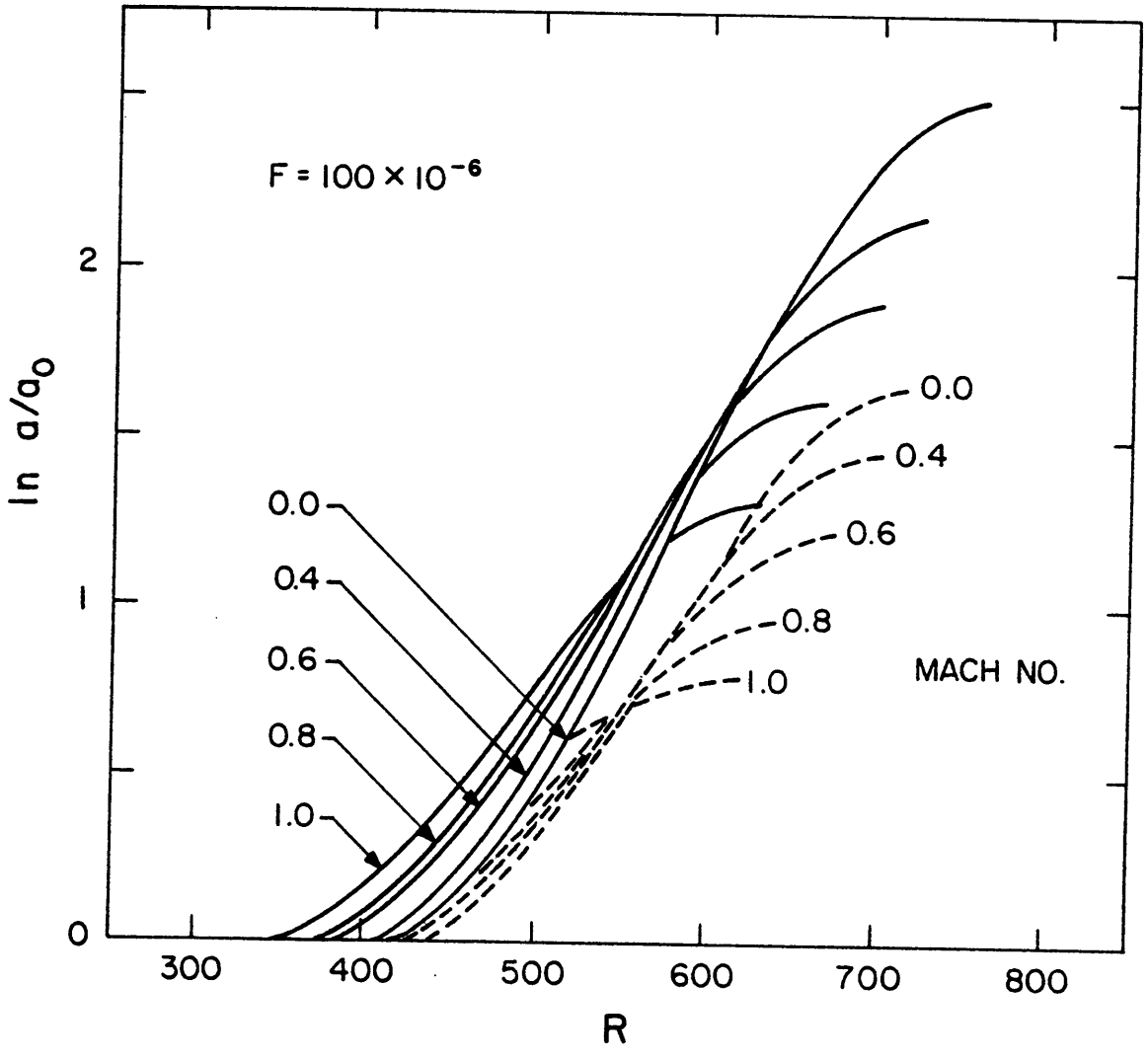

Figure 5.6 Effect of Mach number on the variation of the amplitude ratio with streamwise position for F = 100 x 10^{-6}. Solid lines, nonparallel $\sigma=-Im(\alpha_0+\varepsilon\alpha_1)$; dashed lines, parallel.

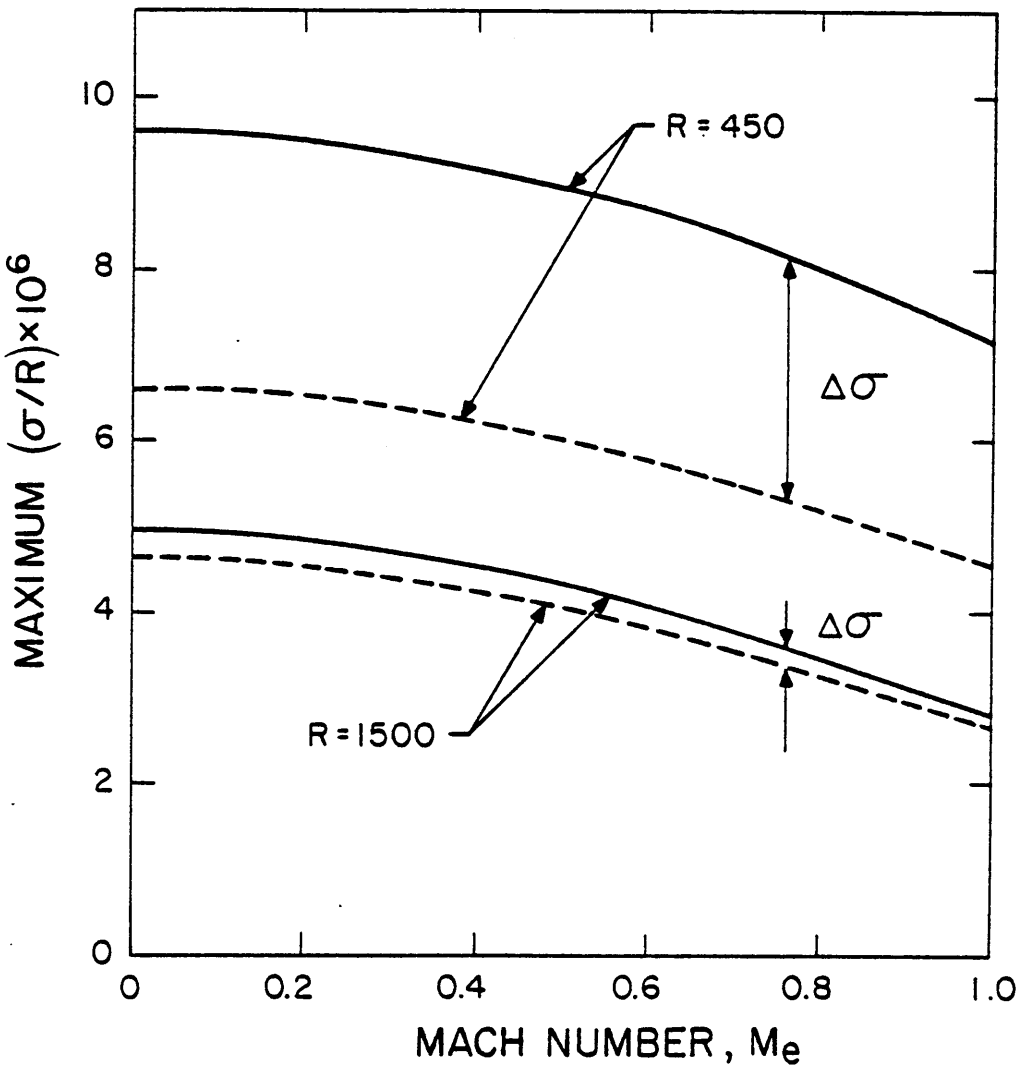

Figure 5.7 Variation of the maximum amplification rate with Mach number at R = 450 and R = 1500. Solid lines, nonparallel $\sigma = -\ \mathrm{Im}(\alpha_0 + \varepsilon\alpha_1)$; dashed lines, parallel.

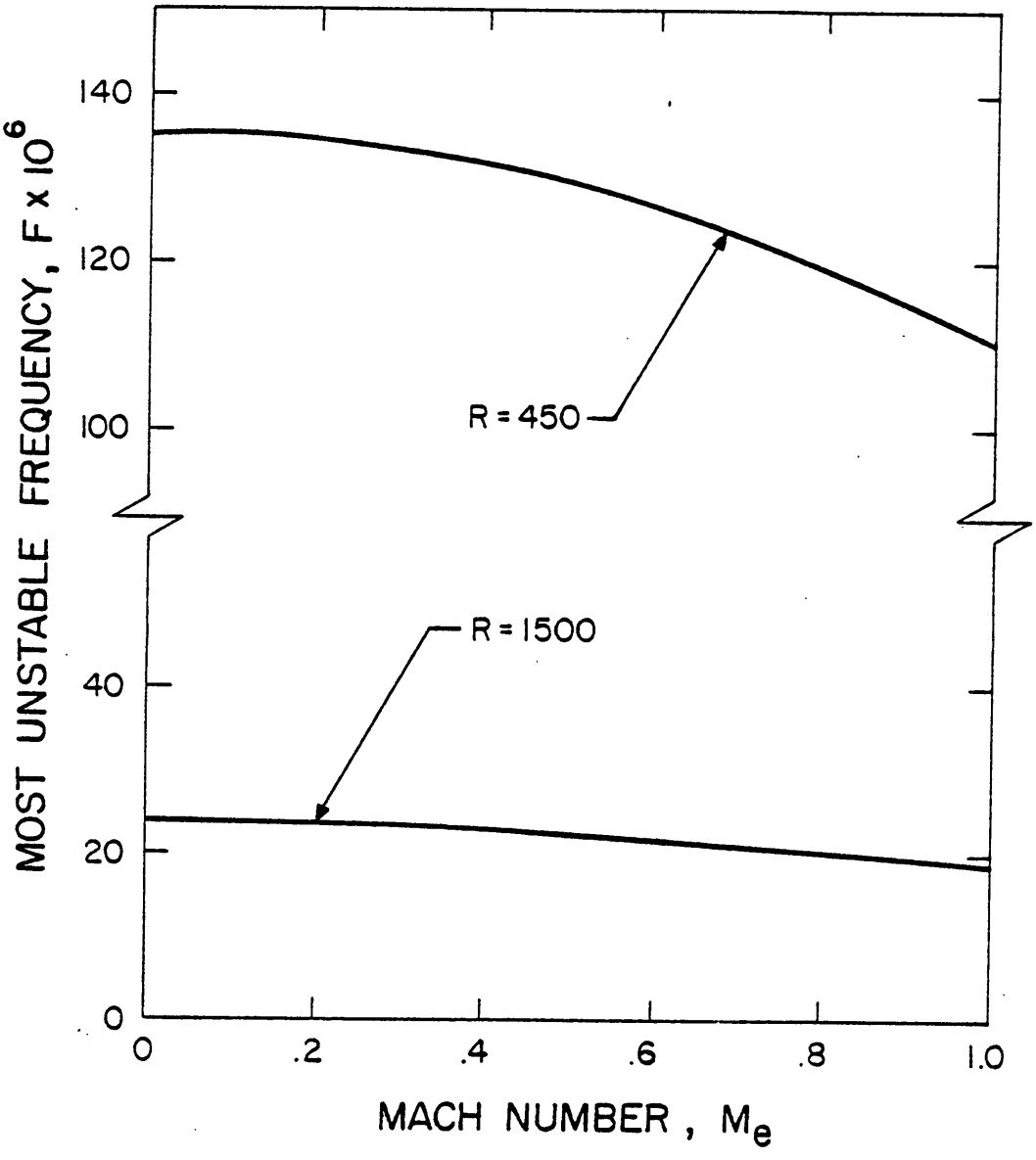

Figure 5.8 Variation of the most unstable frequency with Mach number at R = 450 and 1500.

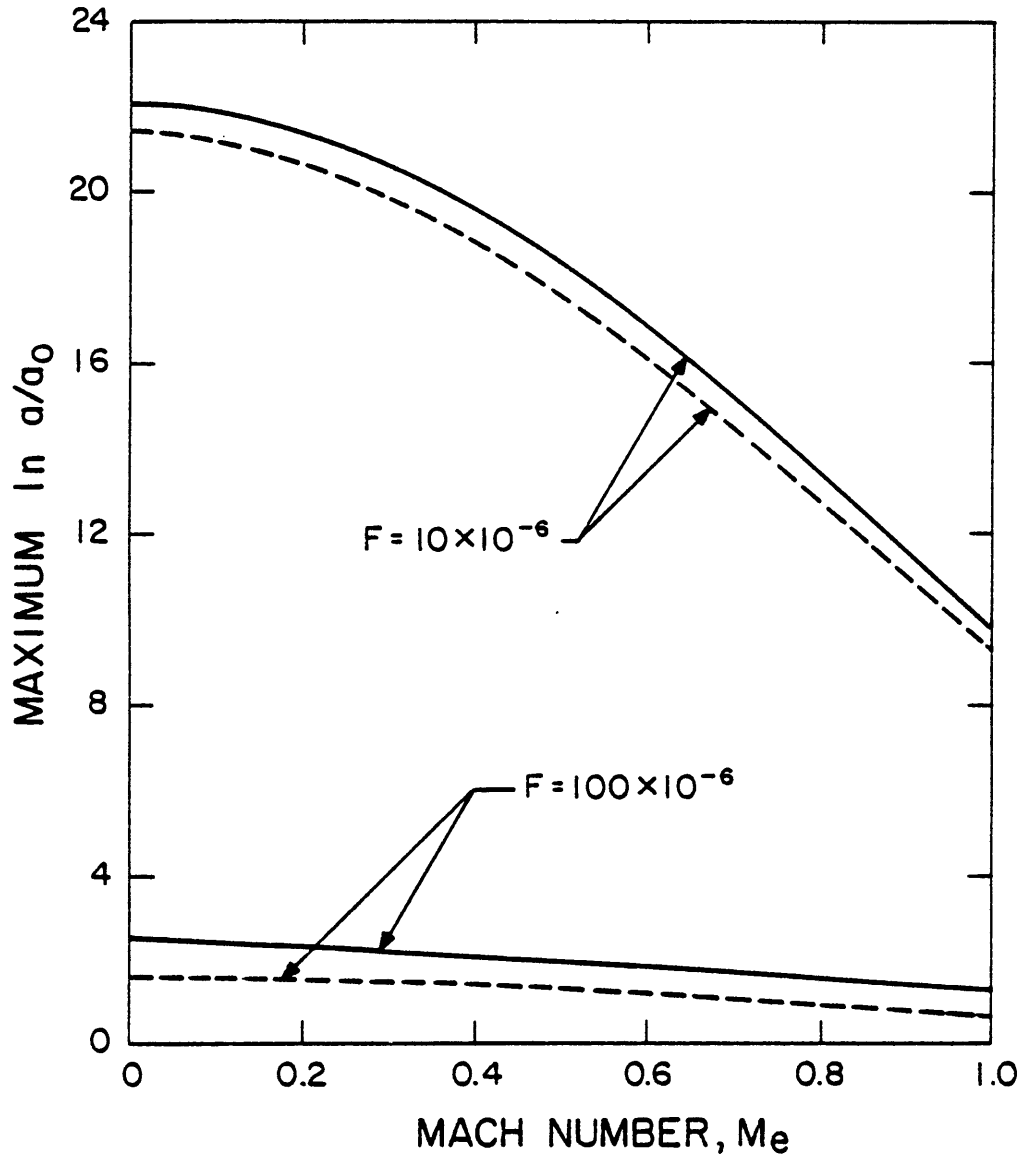

Figure 5.9 Variation of the maximum amplitude ratio with Mach number for $F = 10 \times 10^{-6}$ and 100×10^{-6}. Solid lines, nonparallel $\sigma = -\mathrm{Im}(\alpha_0 + \varepsilon\alpha_1)$; dashed lines, parallel.

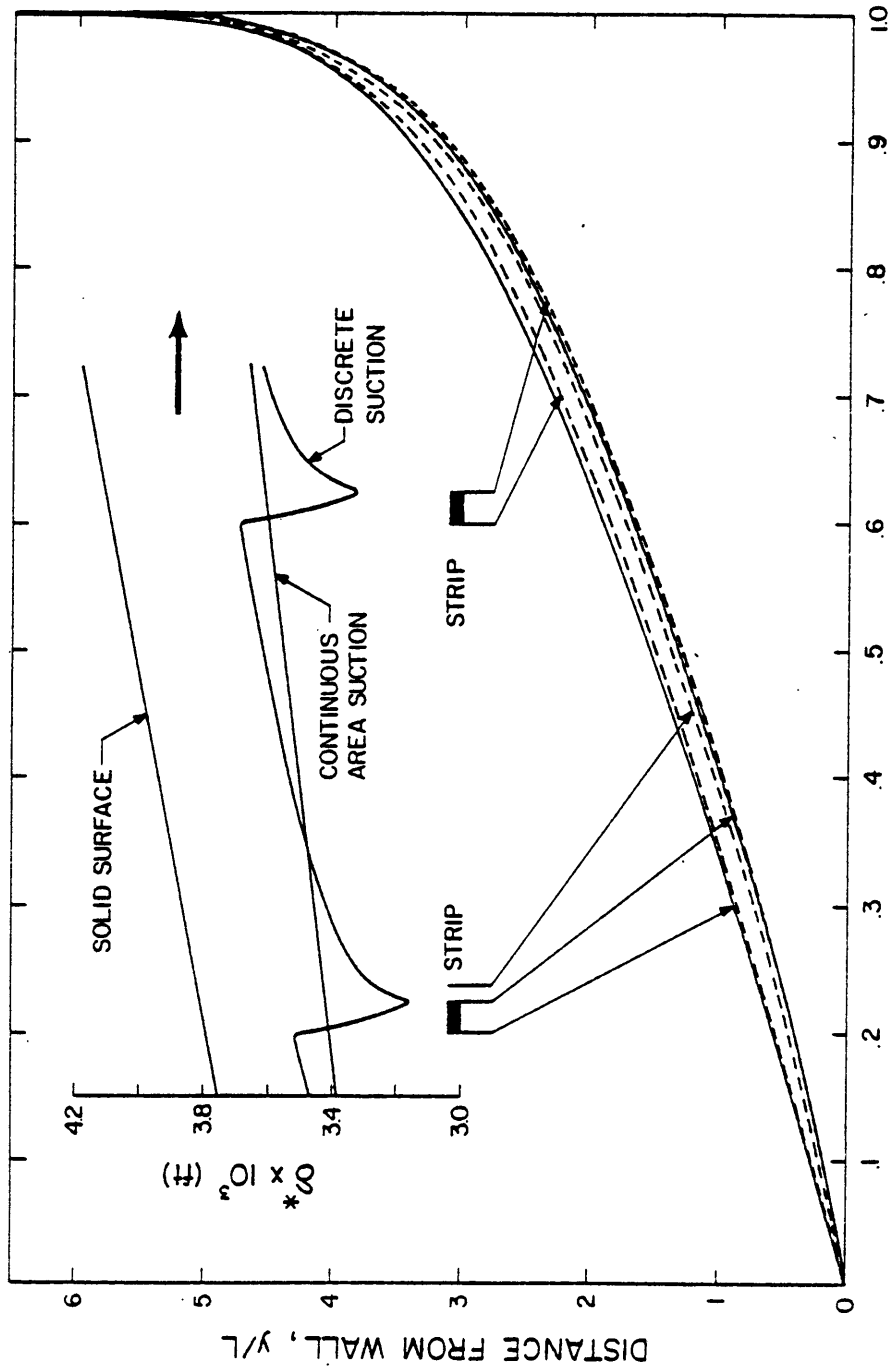

Figure 5.10 Variation of the boundary-layer displacement thickness and mean-velocity profiles with streamwise position in the neighborhoods of the sixth and seventh strips for the configuration $\hat{a}$= .05', $\hat{b}$= .8, and SL = 6.4 x 10^{-4}.

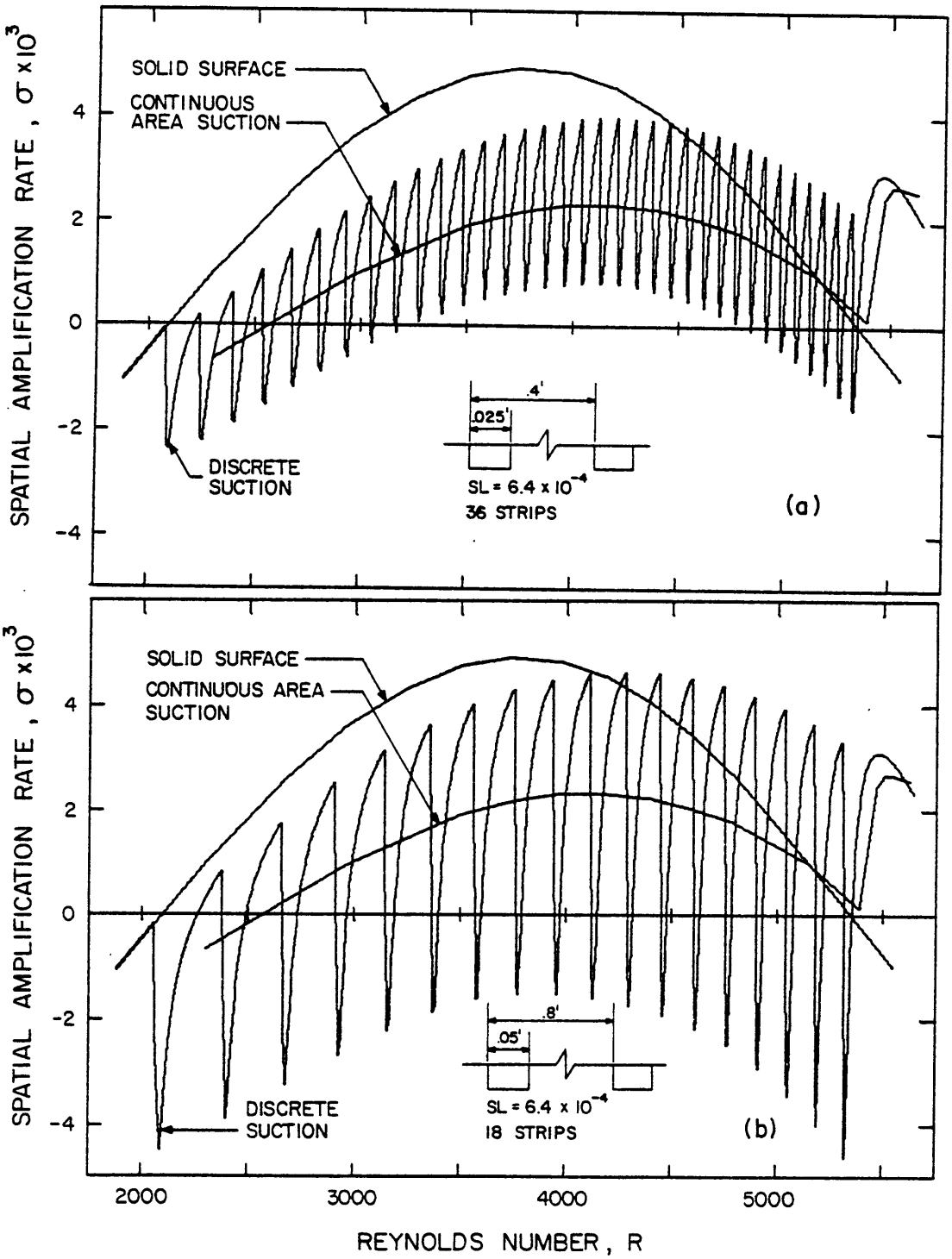

Figure 5.11 Comparison of the variations of the amplification rate with streamwise position for the cases of no suction, continuous area suction, and two strip configurations of constant $\hat{a}/\hat{b}$.

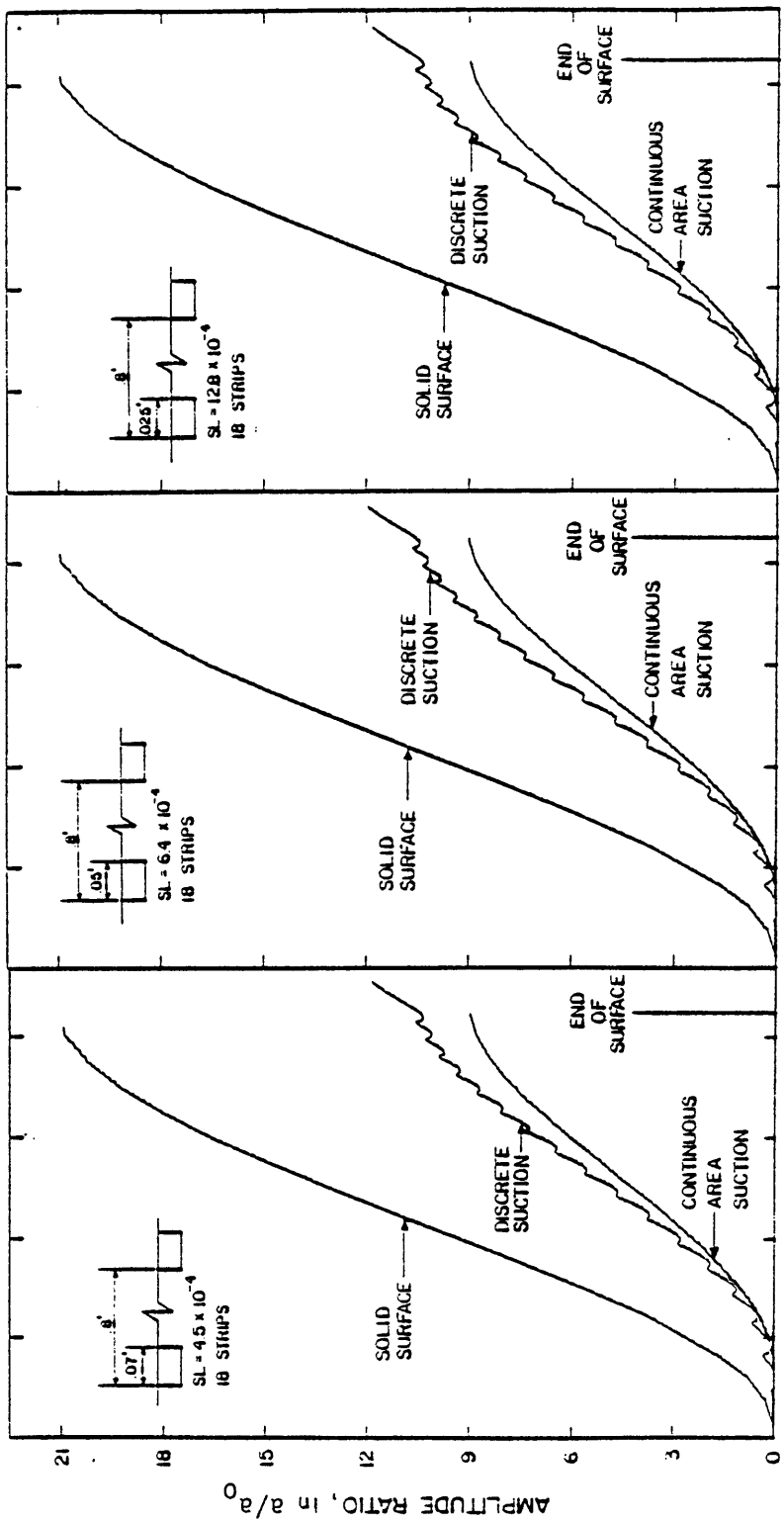

Figure 5.12 Comparison of the variation of the amplification factors with streamwise position, for the cases of no suction, continuous area suction, and three strip configurations of strip widths $\hat{a}$ = 0.025', 0.05', and 0.07'.

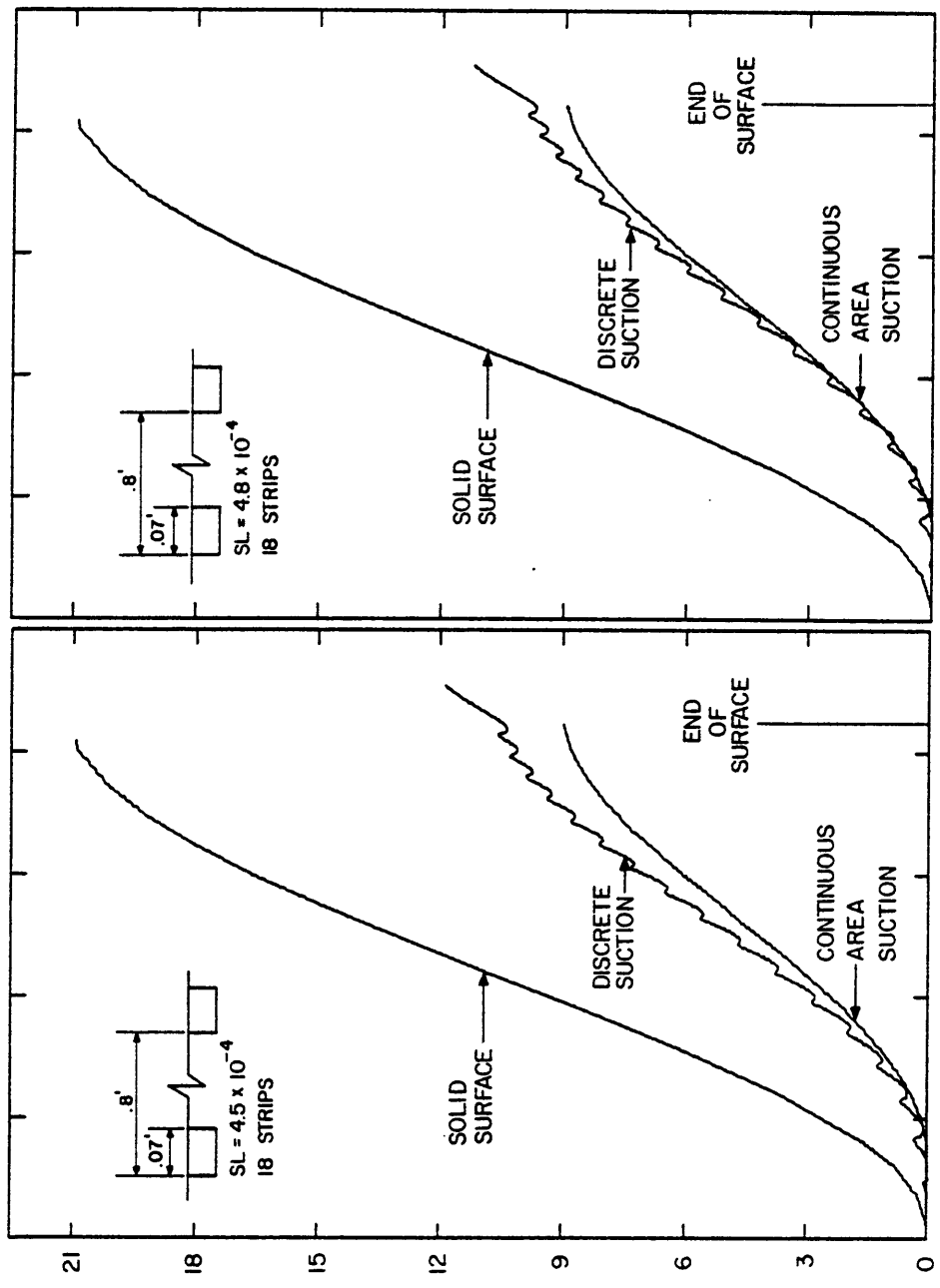

Figure 5.13 Comparison of the variation of the amplification factor with streamwise position for the cases of no suction, continuous area suction, and a strip configuration of strip width a = 0.07' with different suction levels.

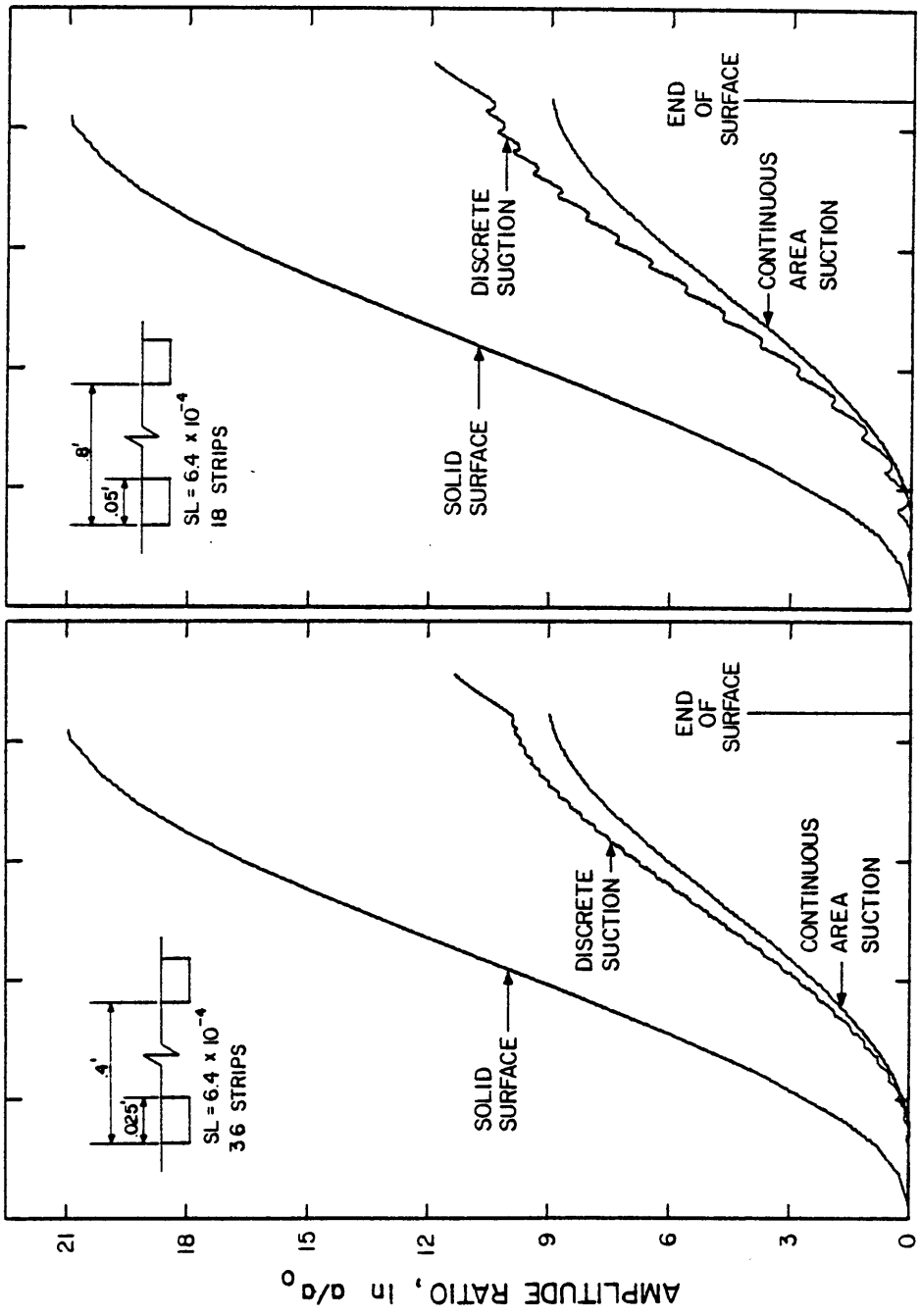

Figure 5.14 Comparison of the variation of the amplification factor with streamwise position for the cases of no suction, continuous area suction, and two strip configurations of constant $\hat{a}/\delta$.

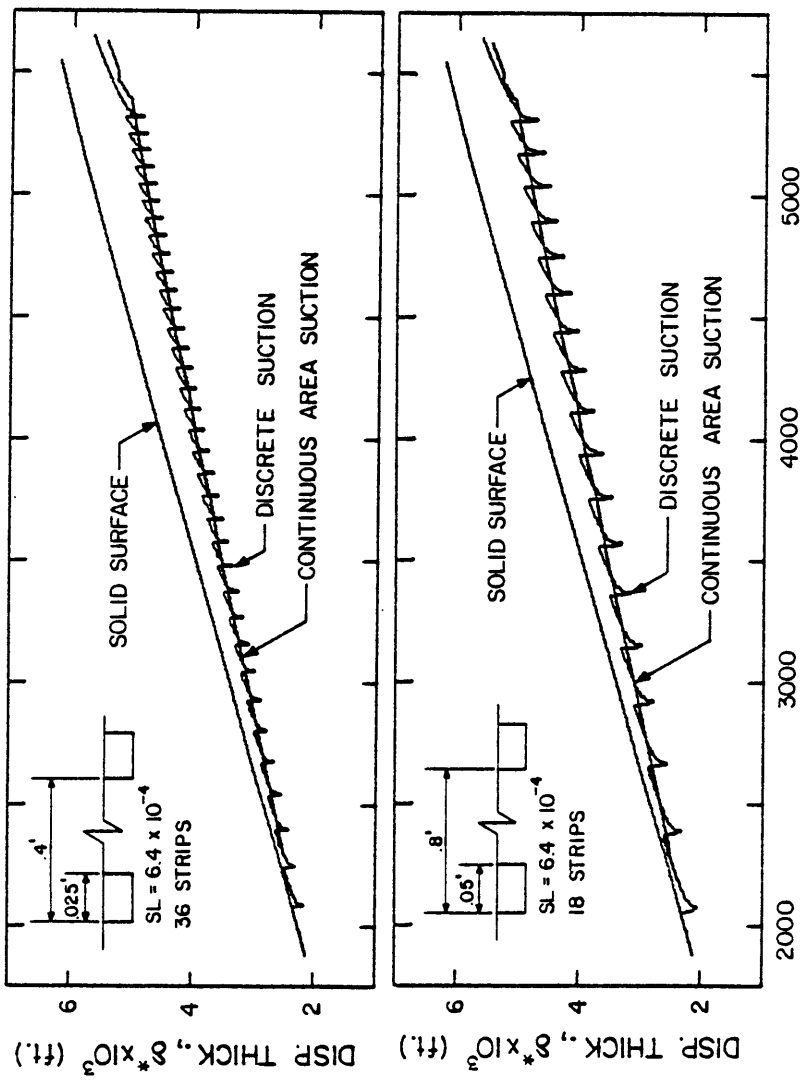

Figure 5.15 Comparison of the growth of the boundary-layer displacement thickness with streamwise position for the cases of no suction, continuous area suction, and two strip configurations of constant $\hat{a}/\hat{b}$.

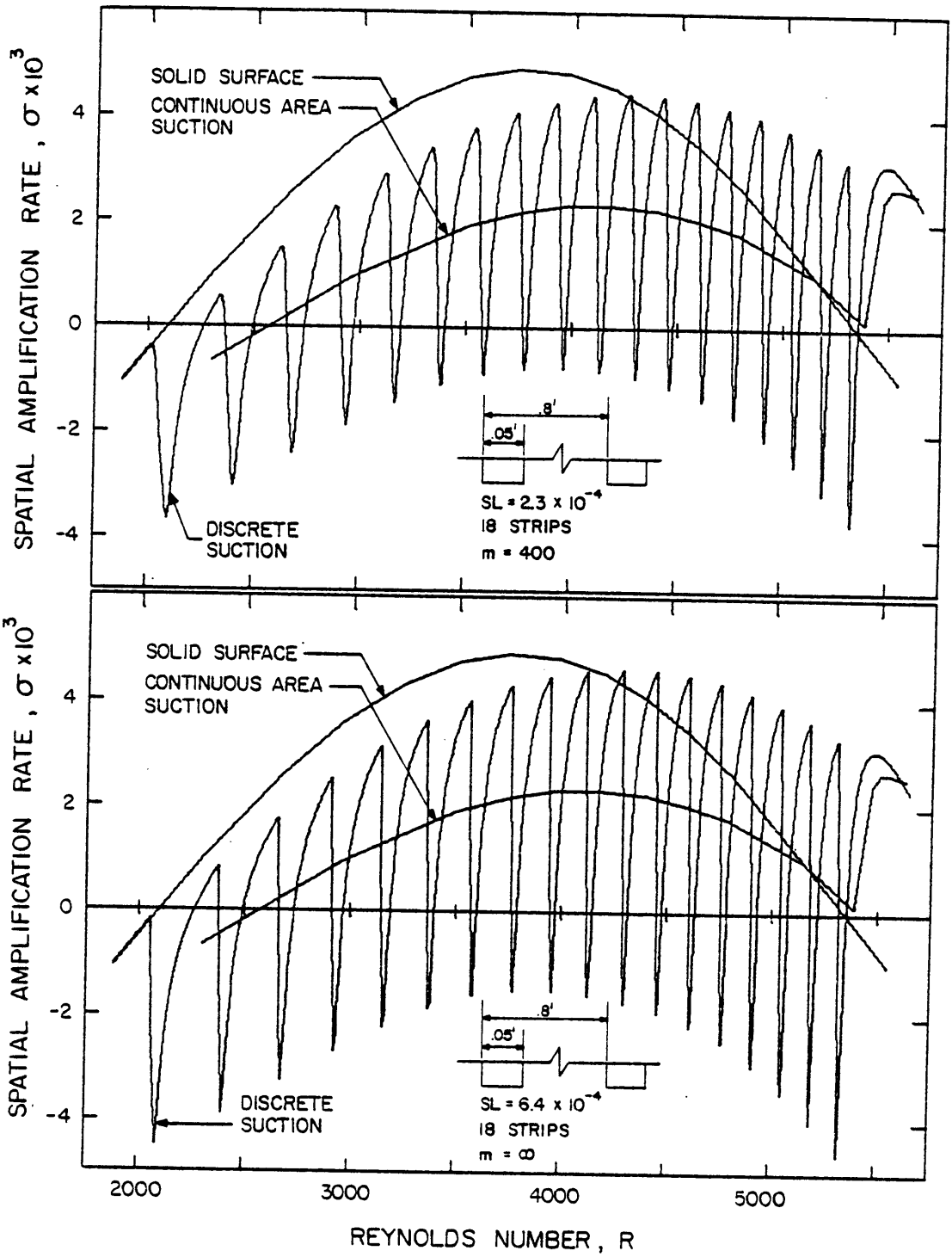

Figure 5.16 Comparison of the variation of the amplification rates with streamwise position for the cases of no suction, continuous area suction, and the strip configurations $\hat{a}$=0.05', $\hat{b}$=0.8', m=∞, SL=6.4x10^{-4} and $\hat{a}$=0.05', $\hat{b}$=0.8', m=400, SL=2.3x10^{-4}.

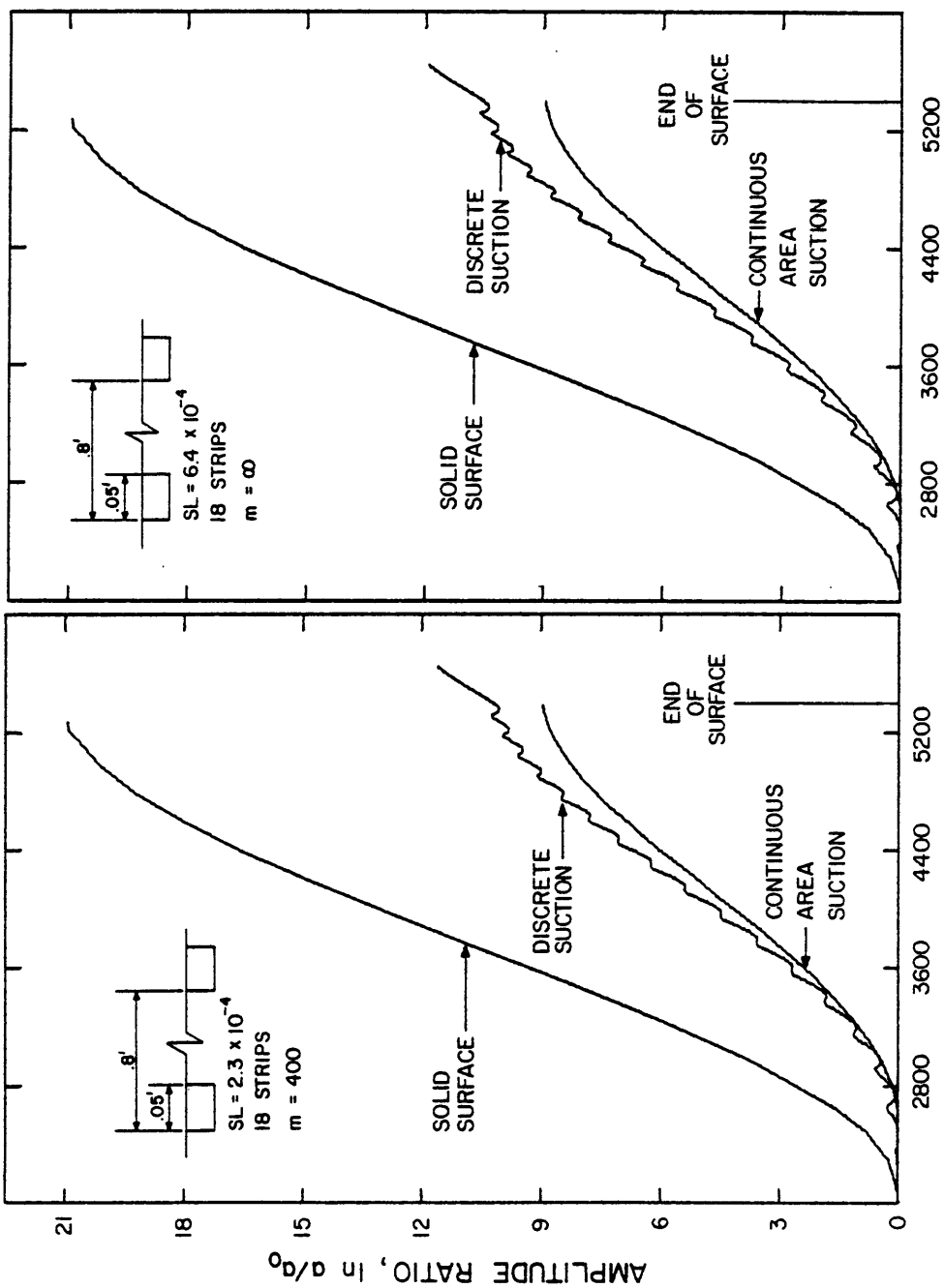

Figure 5.17 Comparison of the variation of the amplification factor with streamwise position for the cases of no suction, continuous area suction, and the strip configurations: $\hat{a}$ = 0.05', $\hat{b}$=0.8', m=∞, SL=6.4 x 10^{-4}; and $\hat{a}$=0.05', $\hat{b}$=0.8', m=400, SL=2.3 x 10^{-4}.

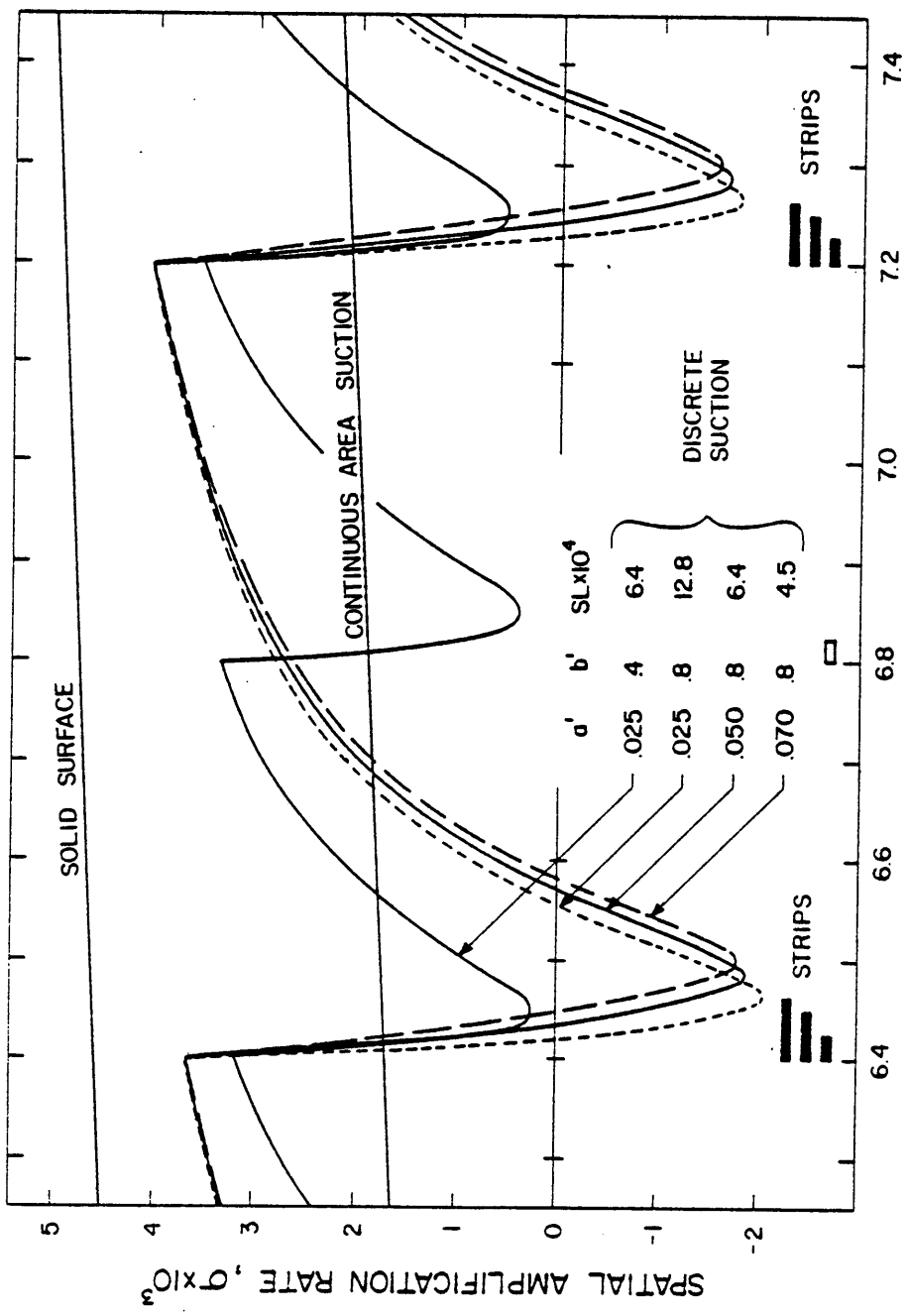

Figure 5.18 Comparison of the variation of the amplification rate with streamwise position in the neighborhoods of the sixth and seventh strips for the cases of no suction, continuous area suction, and different strip configurations.

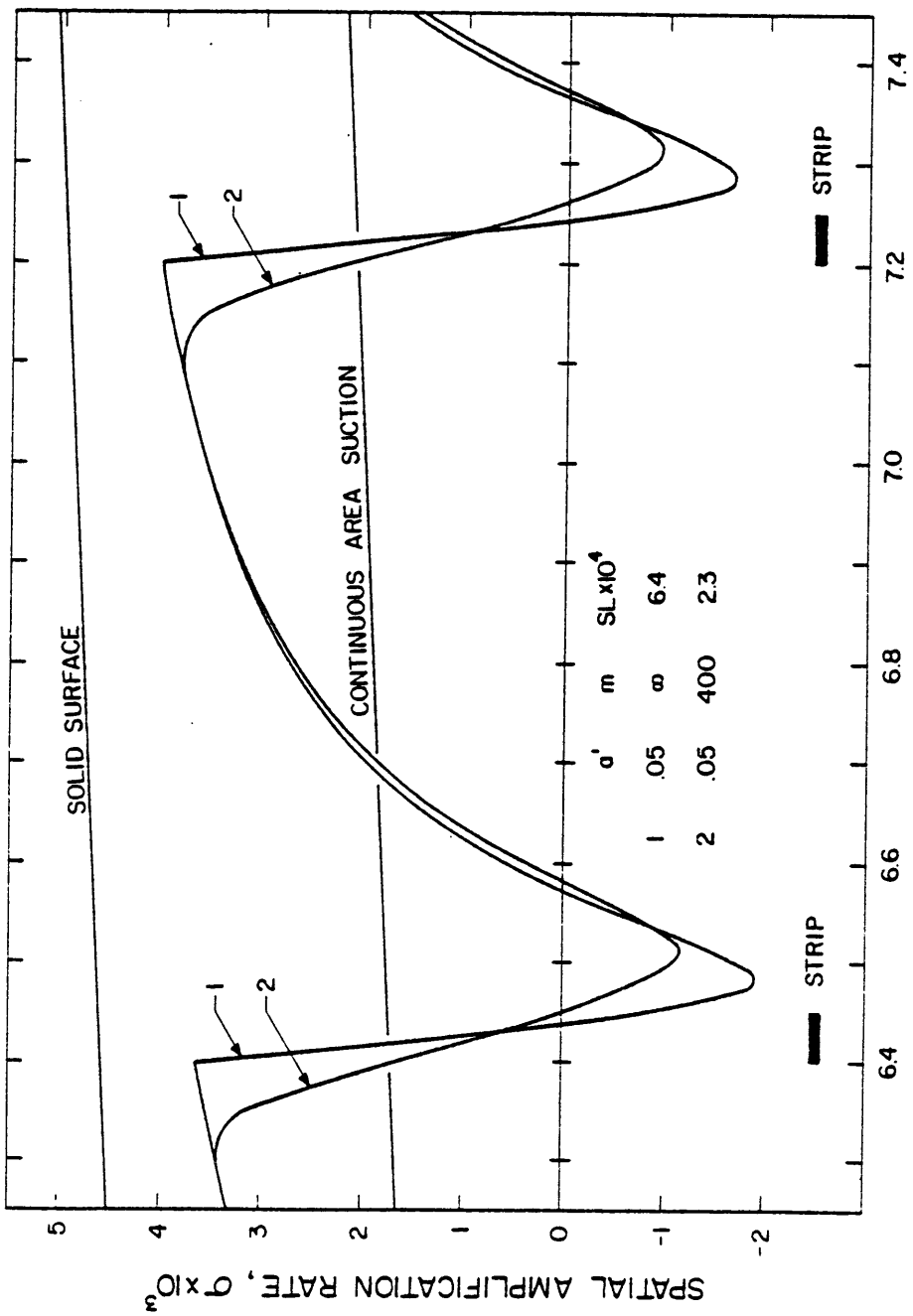

Figure 5.19 Comparison of the variation of the amplification rate with streamwise position in the neighborhoods of the sixth and seventh strips for the cases of no suction, continuous area suction, and the strip configurations: $\hat{a} = 0.05'$, $\hat{b} = 0.8'$, $m = \infty$, $SL = 6.4 \times 10^{-4}$; and $\hat{a} = 0.05'$, $\hat{b} = 0.8'$, $m = 400$, $SL = 2.3 \times 10^{-4}$.

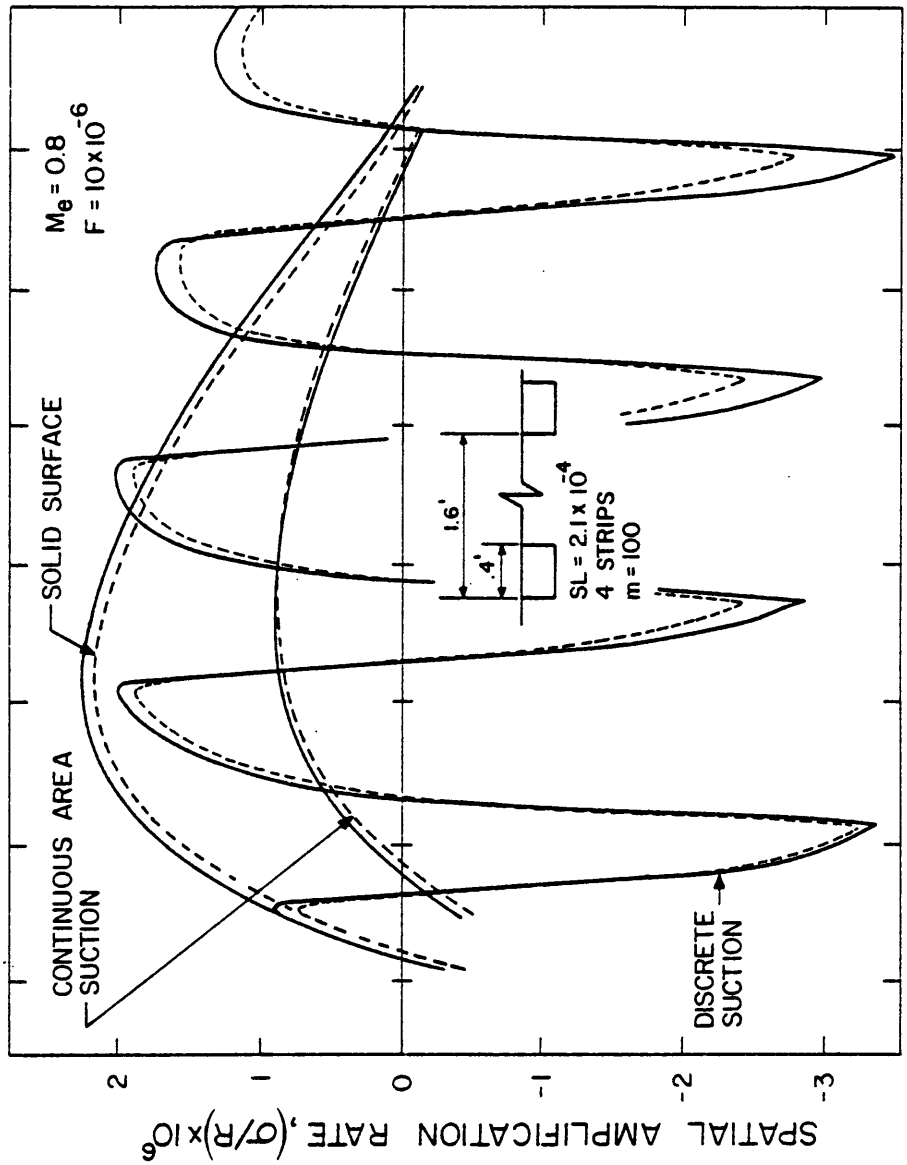

Figure 5.20 Comparison of the variation of the amplification rate with streamwise position for cases of no suction, continuous area suction, and a 4-strip configuration. Solid lines, nonparallel $\sigma = -\mathrm{Im}(\alpha_0 + \varepsilon\alpha_1)$; dashed lines, parallel.

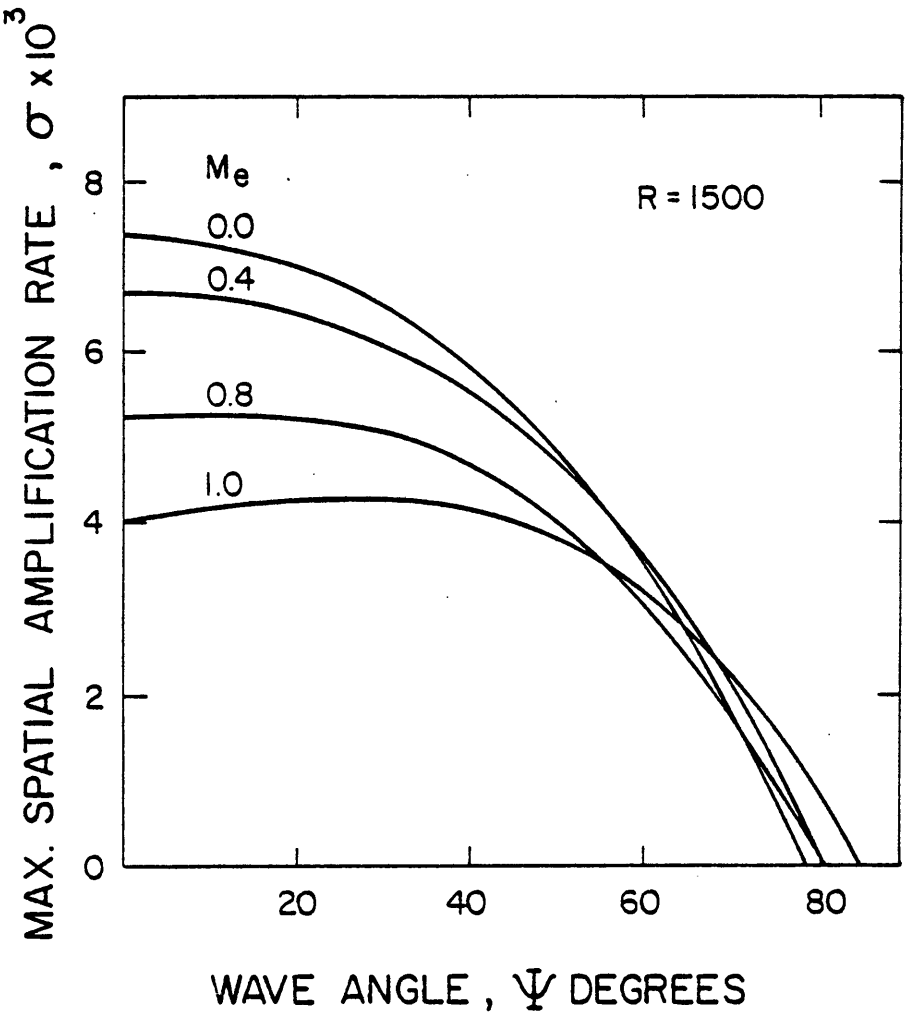

Figure 6.1 Effect of Mach number on the variation of the maximum spatial amplification rate with wave angle at R = 1500.

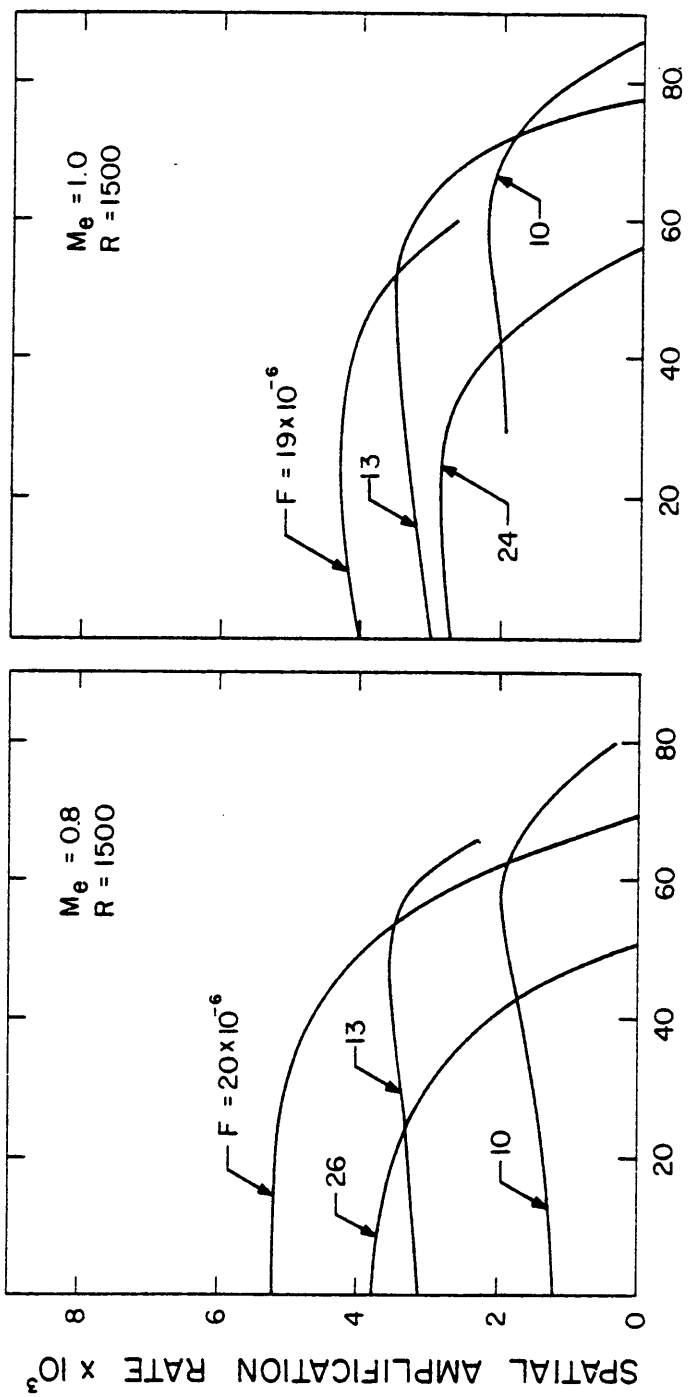

Figure 6.2 Variation of the spacial amplification rate with wave angle for various frequencies at R = 1500 for Mach numbers 0.8 and 1.0.

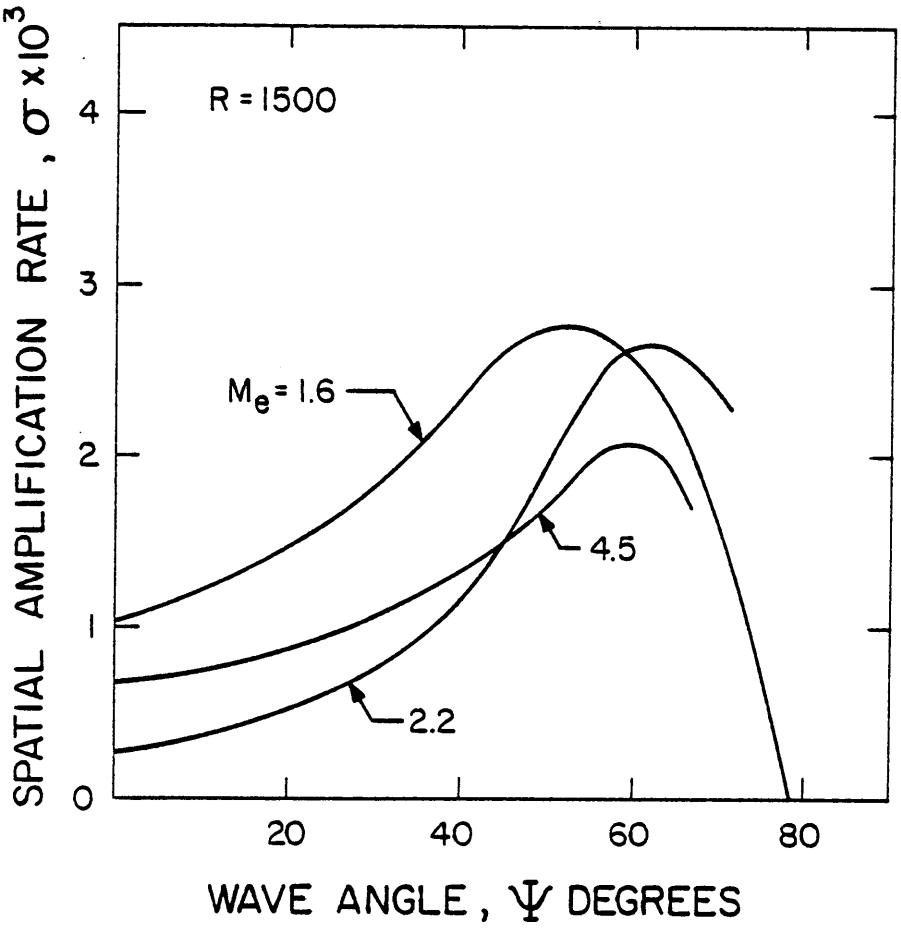

Figure 6.3 Effect of Mach number on the variations of the spatial amplification rate with wave angle, for the most unstable frequencies at R = 1500. Non-parallel results, $\sigma = -Im(\alpha_0 + \varepsilon\alpha_1)$.

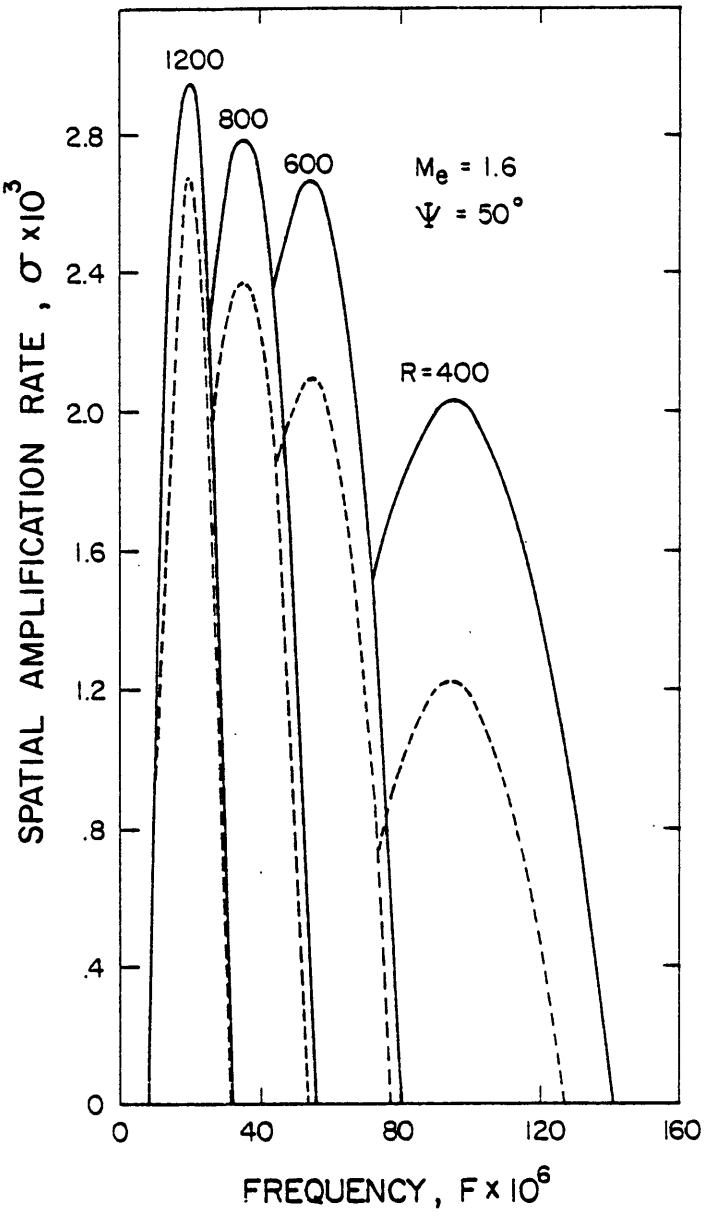

Figure 6.4 Variation of the spatial amplification rate of an oblique wave with frequency at $\psi = 50°$ at various Reynolds numbers for $M_e = 1.6$. Solid lines, nonparallel $\sigma = -\mathrm{Im}(\alpha_0 + \varepsilon\alpha_1)$, dashed lines, parallel.

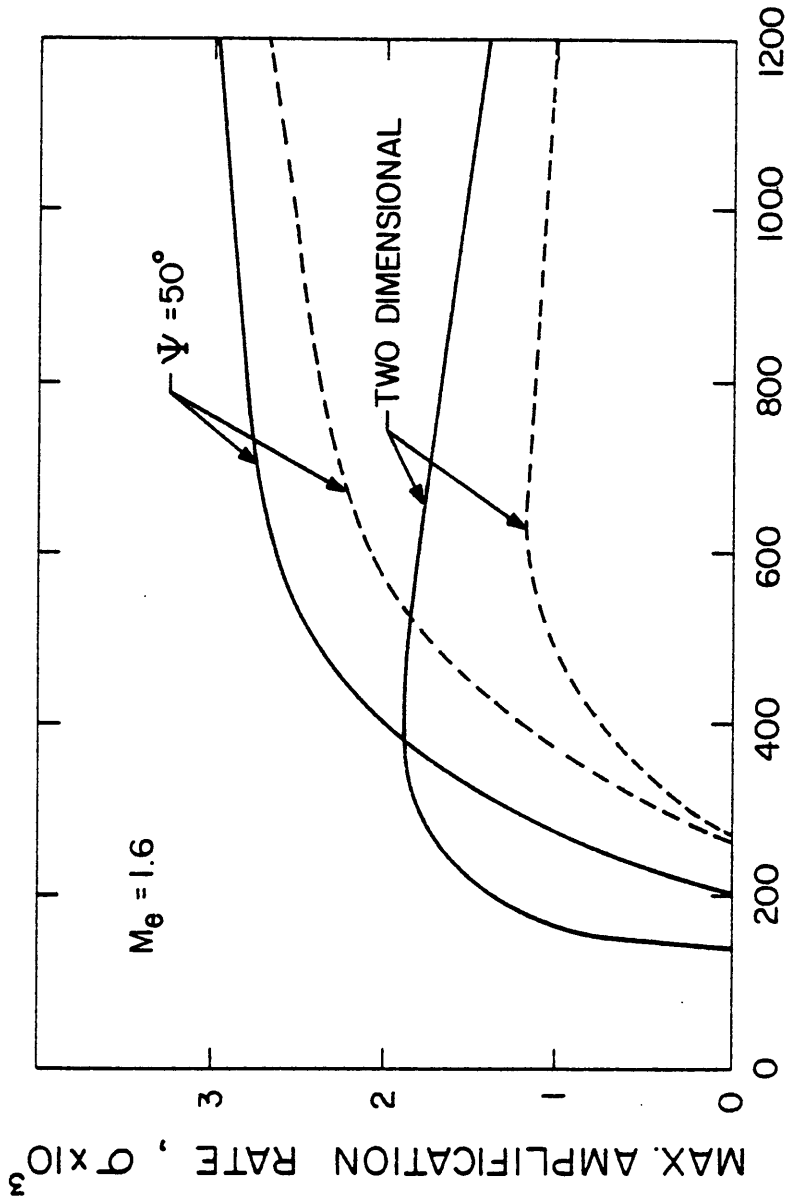

Figure 6.5 Variation of the maximum spatial amplification rate (with respect to frequency) with streamwise position at $M_e = 1.6$ for an oblique wave at $\psi = 50°$ and a two-dimensional wave. Solid lines, nonparallel $\sigma = -\mathrm{Im}(\alpha_0 + \varepsilon\alpha_1)$; dashed lines, parallel.

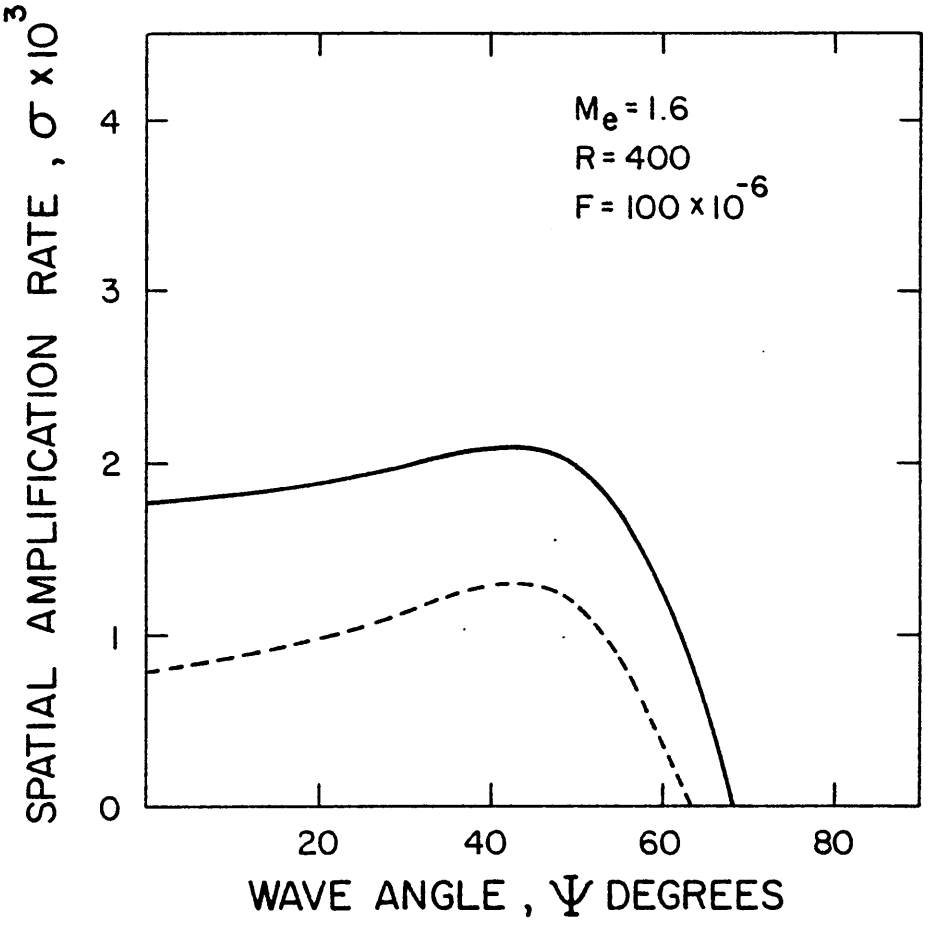

Figure 6.6 Variation of the nonparallel effect on the spatial amplification rate with wave angle for $R = 400$, $F = 100 \times 10^{-6}$, and $M_e = 1.6$. Solid line, nonparallel, $\sigma = - \mathrm{Im}(\alpha_0 + \varepsilon\alpha_1)$; dashed line, parallel.

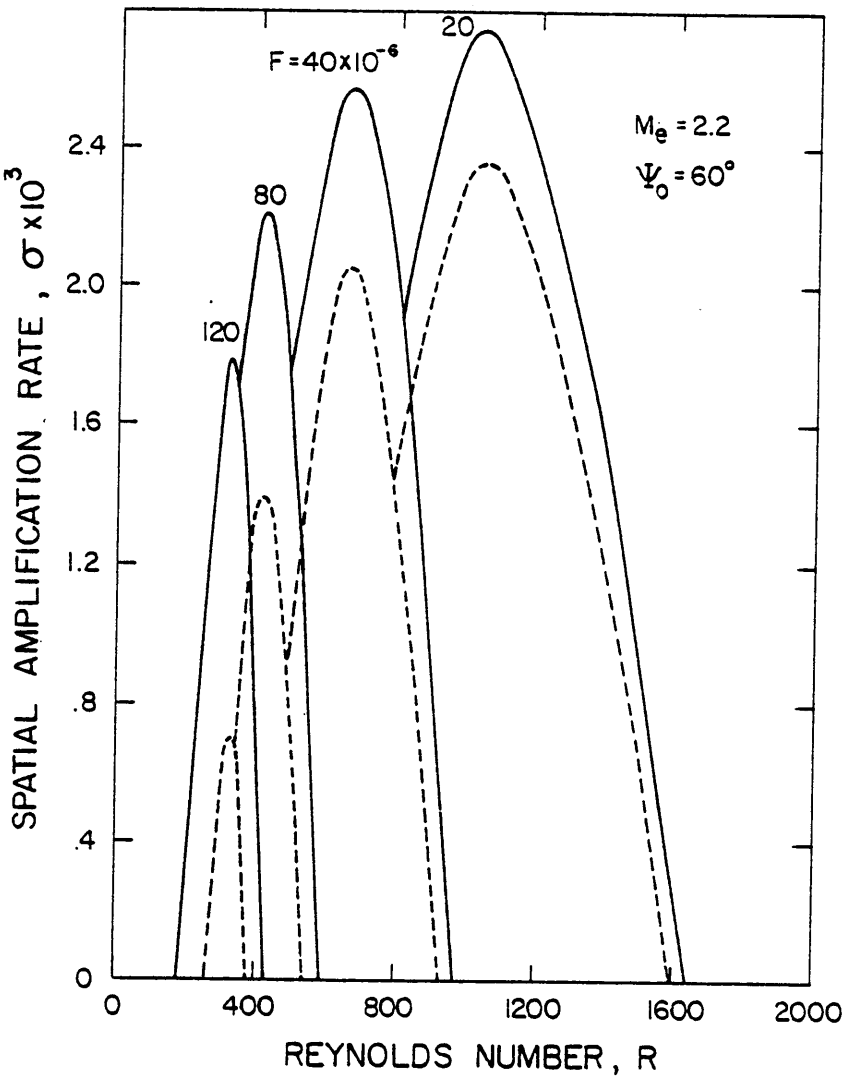

Figure 6.7 Variation of the spatial amplification rate of an oblique disturbance with streamwise position at $\psi_0 = 60°$ for different frequencies and for $M_e = 2.2$. Solid lines, nonparallel $\sigma=-Im(\alpha_0+\varepsilon\alpha_1)$; dashed lines, parallel.

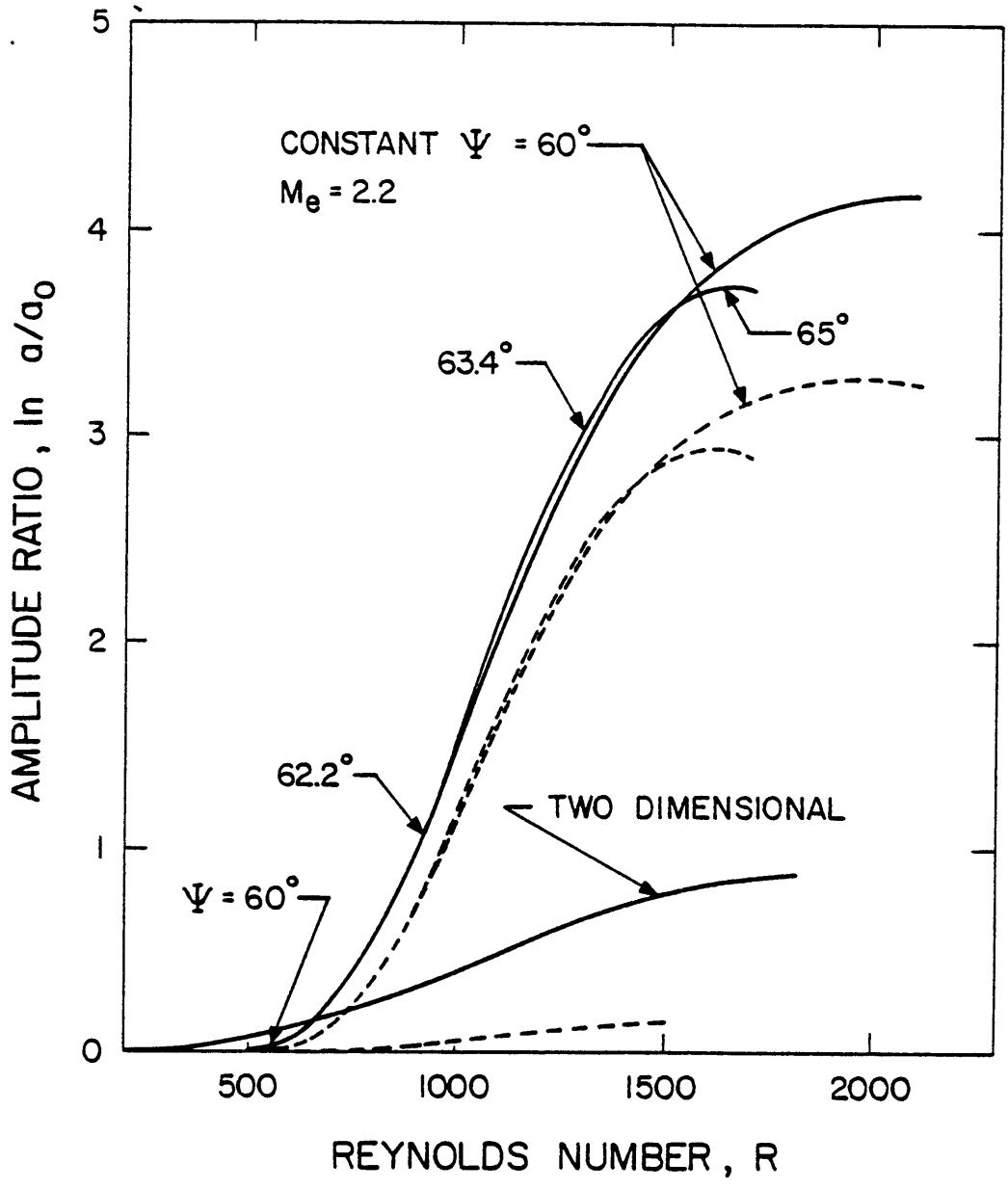

Figure 6.8 Comparison of the variation of the amplitude ratio with streamwise position for an oblique wave of variable wave angle (ψ_0 = 60°), an oblique wave of constant wave angle (ψ = 60°), and a two-dimensional wave. Solid lines, nonparallel, σ=-Im(α_0+$\varepsilon\alpha_1$); dashed lines, parallel.

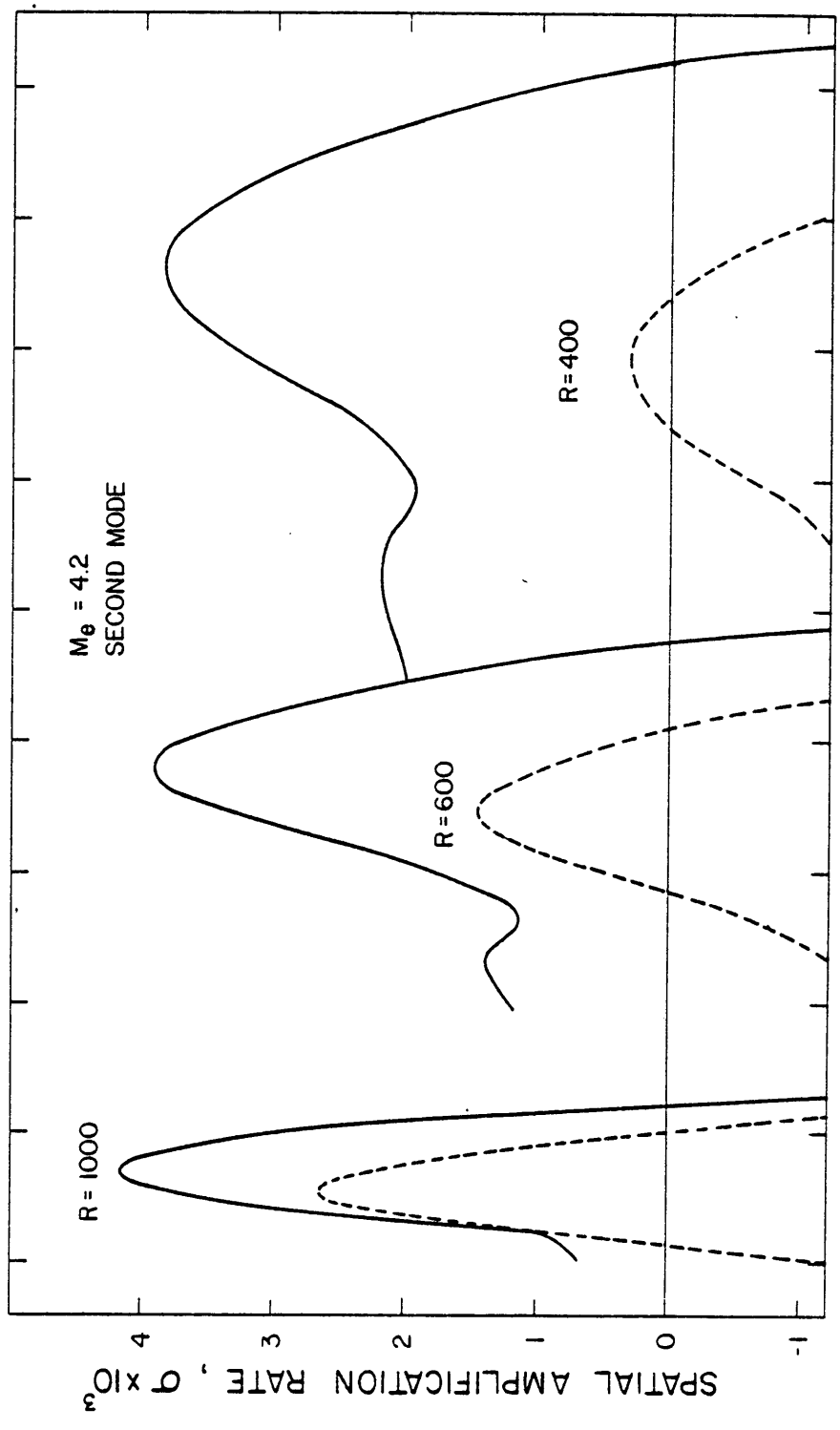

Figure 6.9 Nonparallel effects on the variation of the spatial amplification rate with frequency for a second mode at M_e = 4.2 and various Reynolds numbers. Solid lines, nonparallel, $\sigma = -\mathrm{Im}(\alpha_0 + \varepsilon\alpha_1)$; dashed line, parallel.

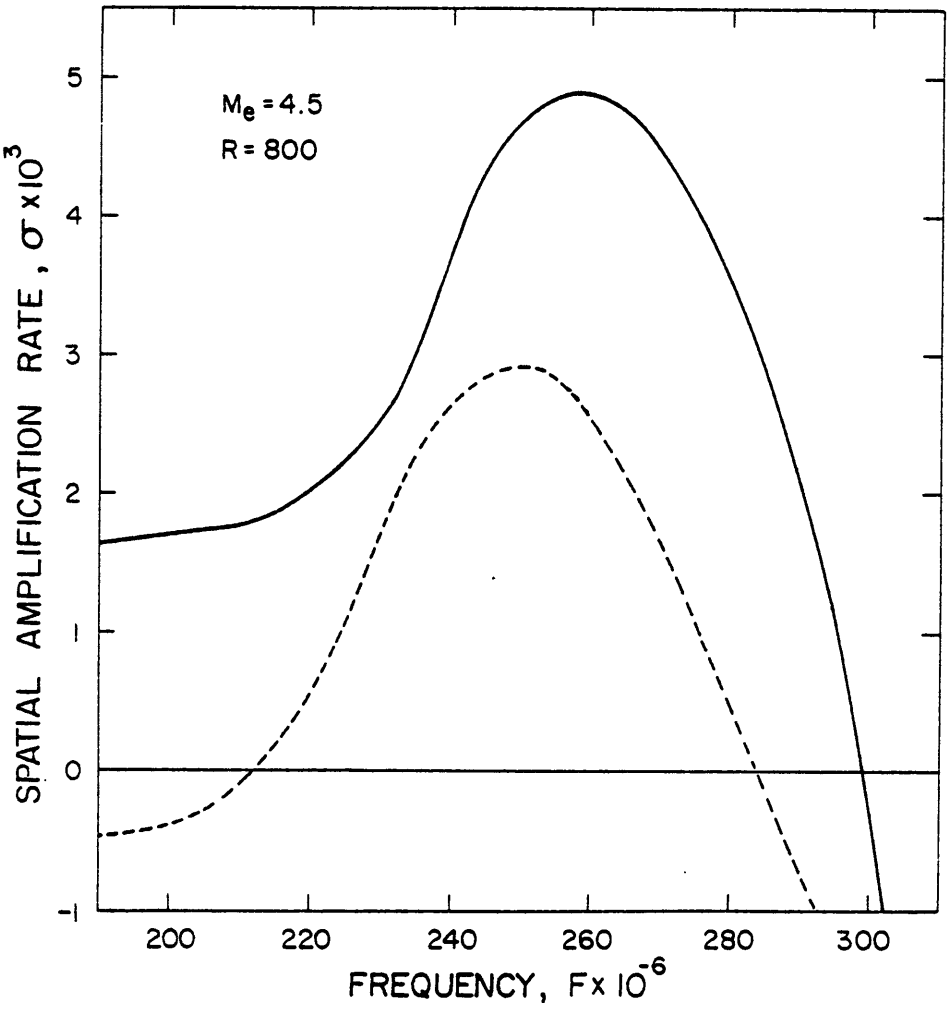

Figure 6.10 Nonparallel effects on the variation of the spatial amplification rate with frequency for a second mode at $M_e = 4.5$ and $R = 800$. Solid line, nonparallel, $\sigma = -\mathrm{Im}(\alpha_0 + \varepsilon\alpha_1)$; dashed lines, parallel.

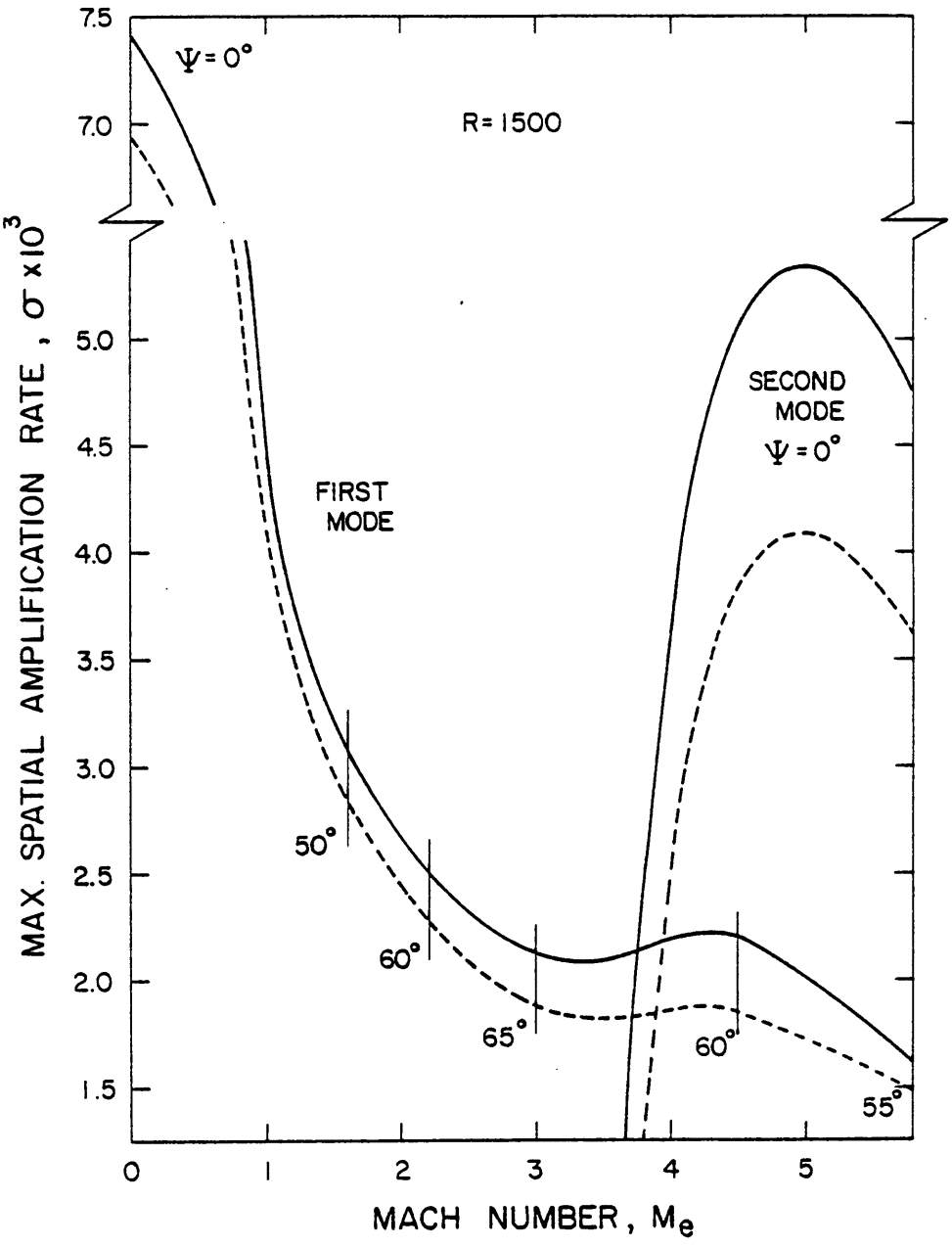

Figure 6.11 Variation of the maximum amplification rate (with respect to frequency and wave angle) with Mach number for the first and second modes at R = 1500. Solid lines, nonparallel, $\sigma = - \mathrm{Im}(\alpha_0 + \varepsilon\alpha_1)$, dashed lines, parallel.

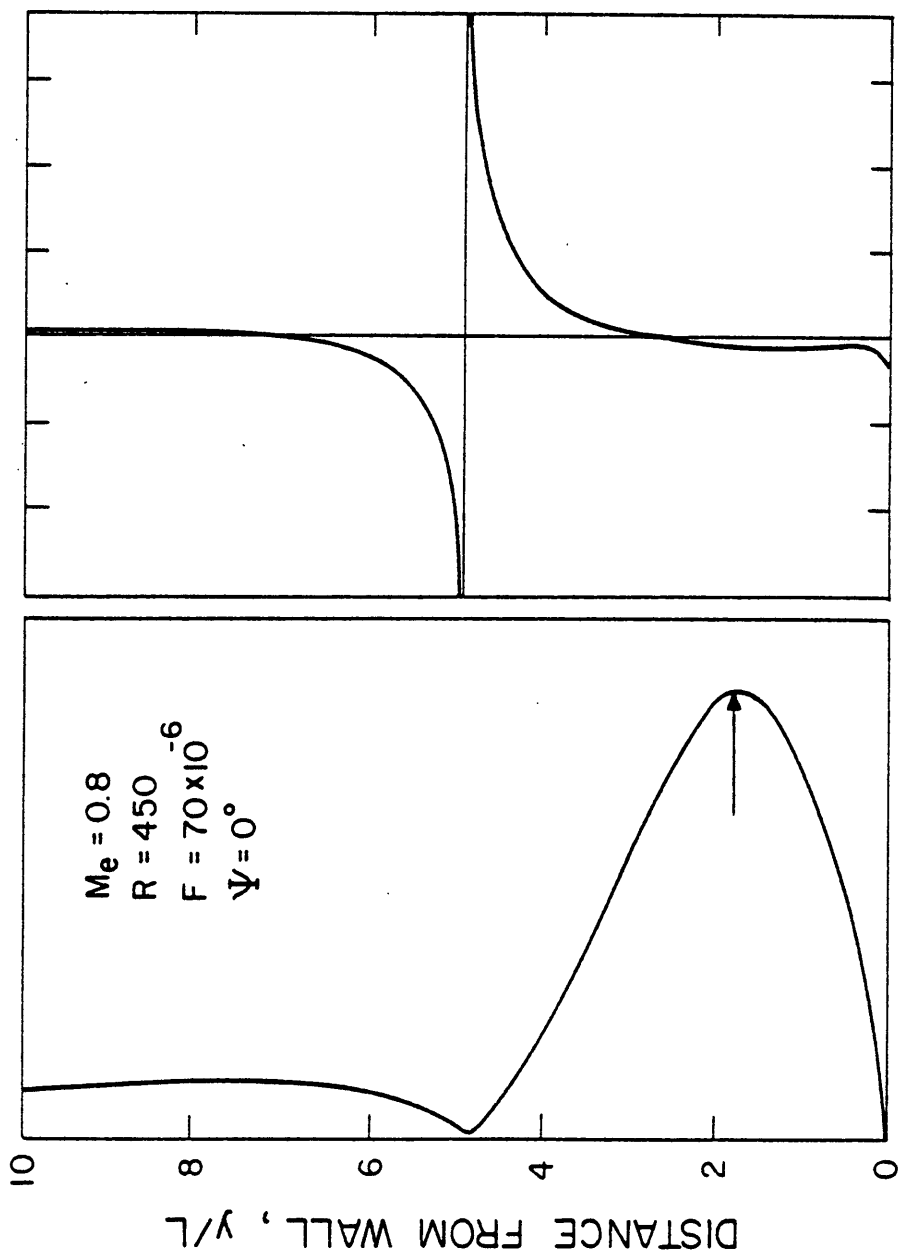

Figure 6.12 Variation of $|\rho u|$ and profile distortion of $|\rho u|$ across the boundary layer at R = 450 for a two-dimensional wave at $F = 70 \times 10^{-6}$ and $M_e = 0.8$.

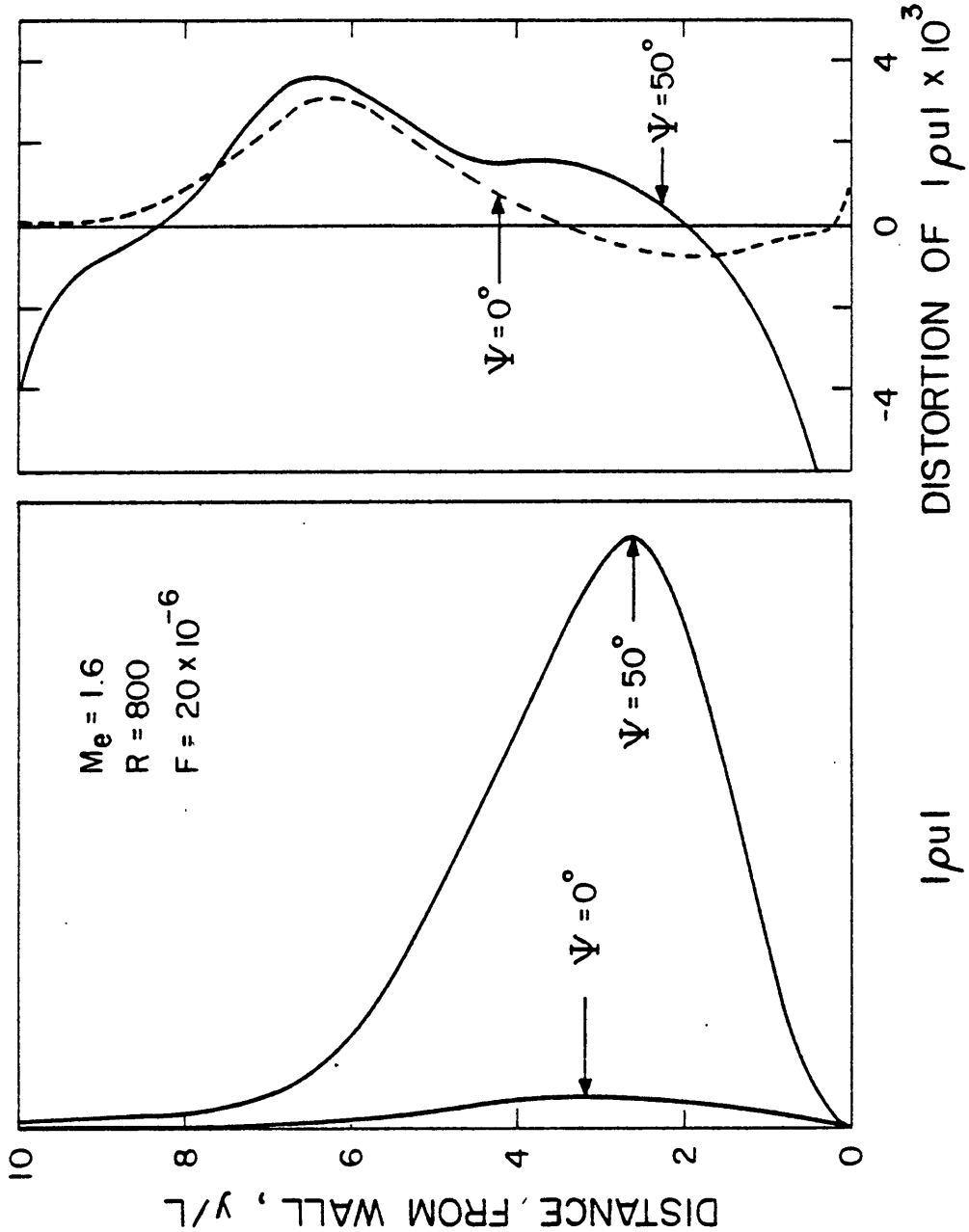

Figure 6.13 Variation of $|\rho u|$ and profile distortion of $|\rho u|$ across the boundary layer at R = 800 for a two-dimensional wave and an oblique wave ($\psi = 50°$) at $F = 20 \times 10^{-6}$ and $M_e = 1.6$.

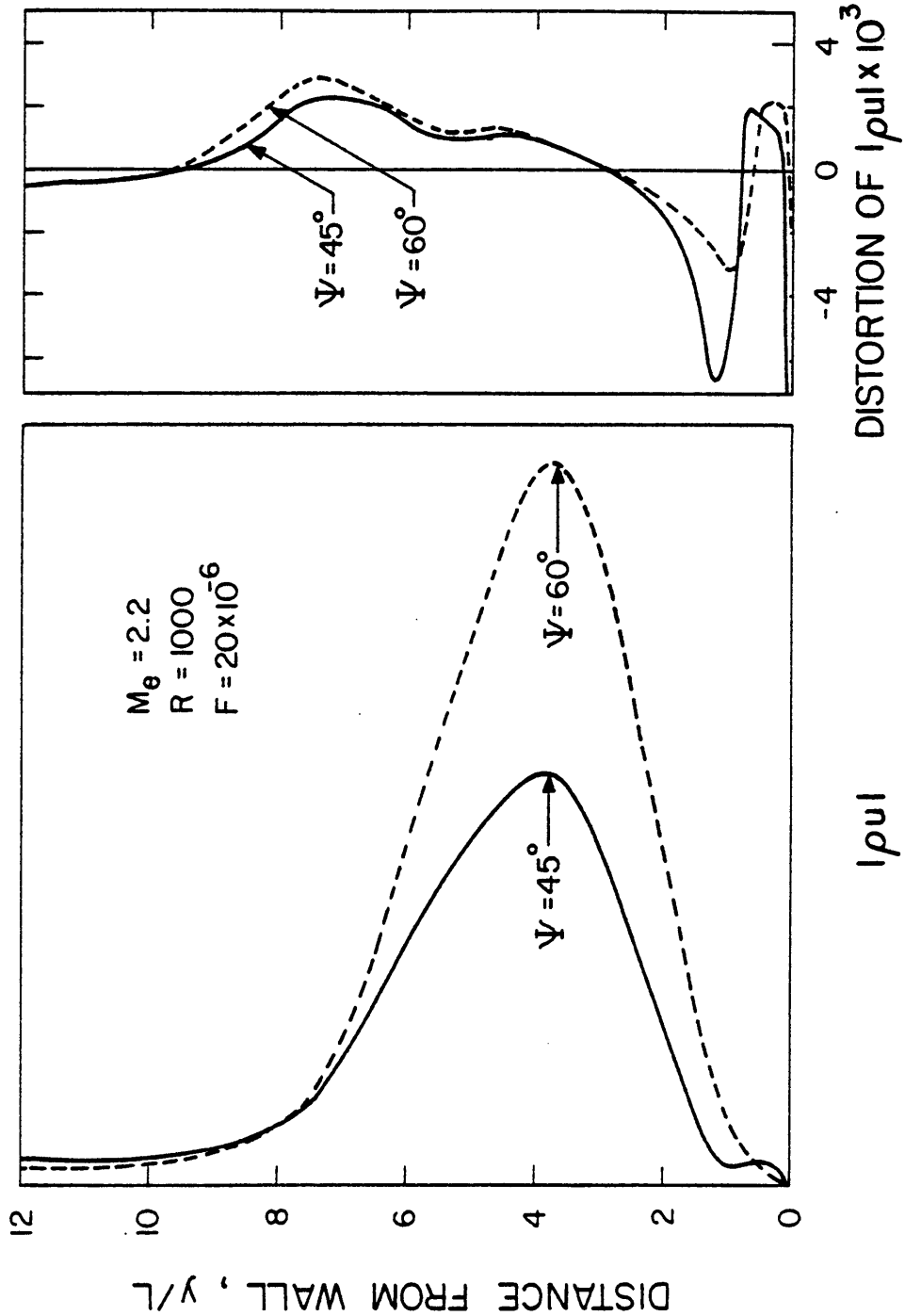

Figure 6.14 Variation of $|\rho u|$ and profile distortion of $|\rho u|$ across the boundary layer at R = 1000 for two oblique waves at ψ = 45° and ψ = 60° at $F = 20 \times 10^{-6}$ and $M_e = 2.2$.

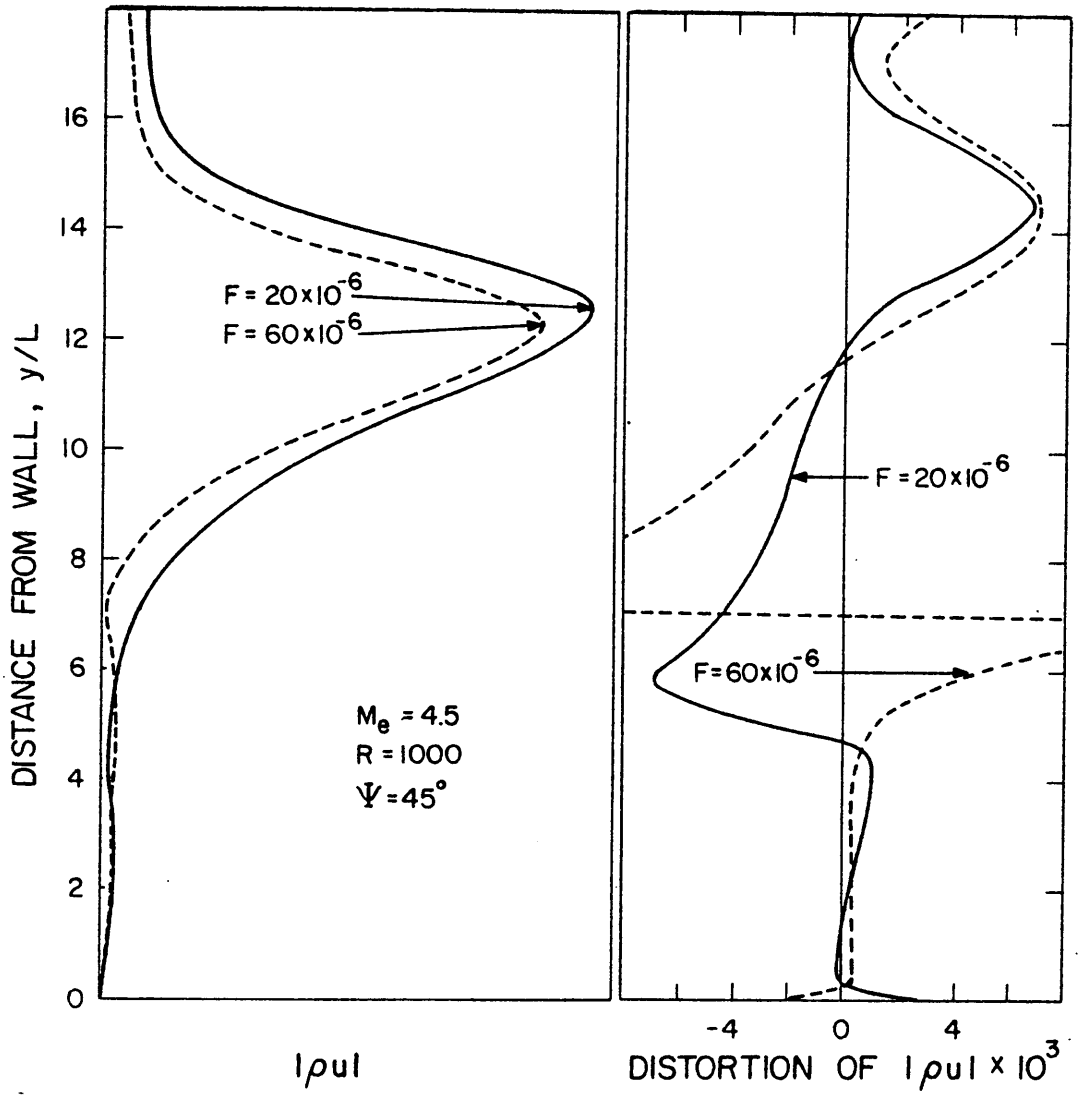

Figure 6.15 Variation of $|\rho u|$ and profile distortion of $|\rho u|$ across the boundary layer at R = 1000 for and oblique wave (ψ = 45°) at F = 20 x 10^{-6} and F = 60 x 10^{-6} and M_e = 4.5.

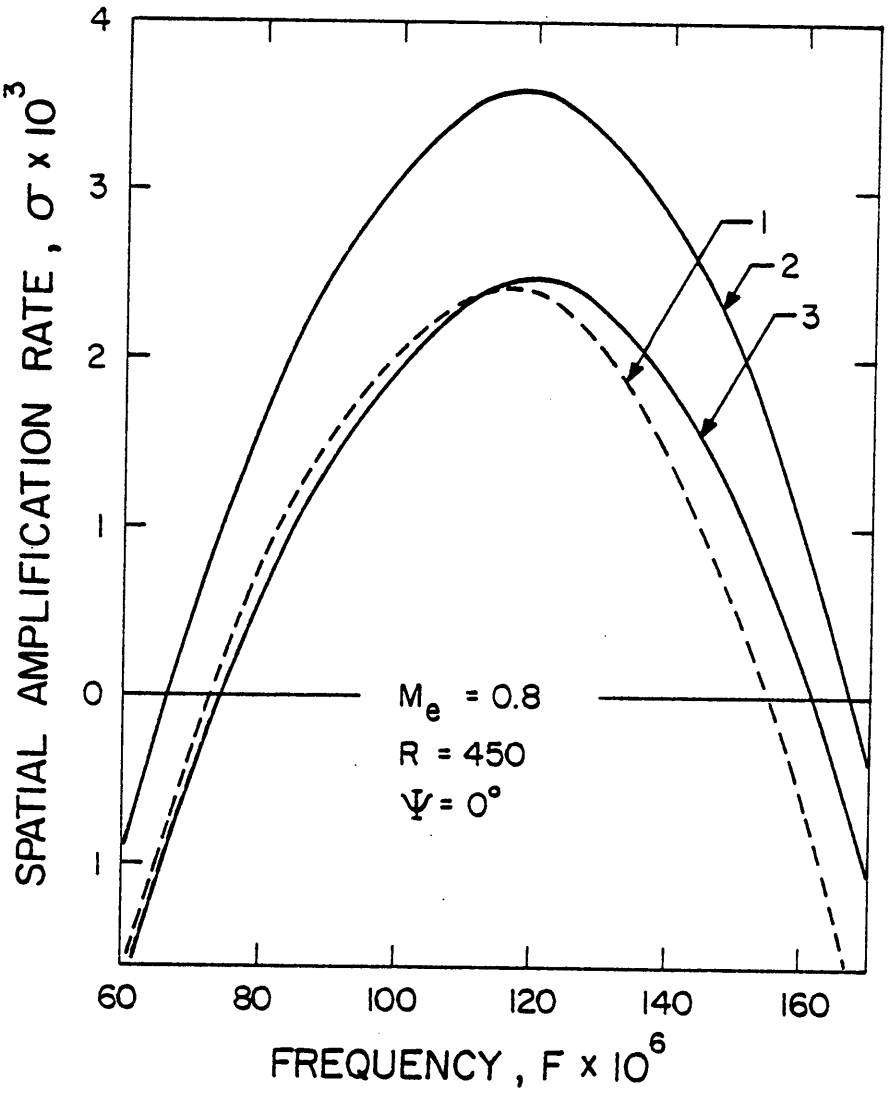

Figure 6.16 Variation of the spatial amplification rate with frequency at R = 450 for a two-dimensional wave for $M_e = 0.8$. (1) $\sigma = -\mathrm{Im}(\alpha_0)$, (2) $\sigma = -\mathrm{Im}(\alpha_0 + \varepsilon\alpha_1)$, (3) $\sigma = -\mathrm{Im}(\alpha_0 + \varepsilon\alpha_1) + \frac{\varepsilon}{|\rho u|}\frac{\partial|\rho u|}{\partial x_1}$ calculated at constant y/L near the position of the maximum of $|\rho u|$.

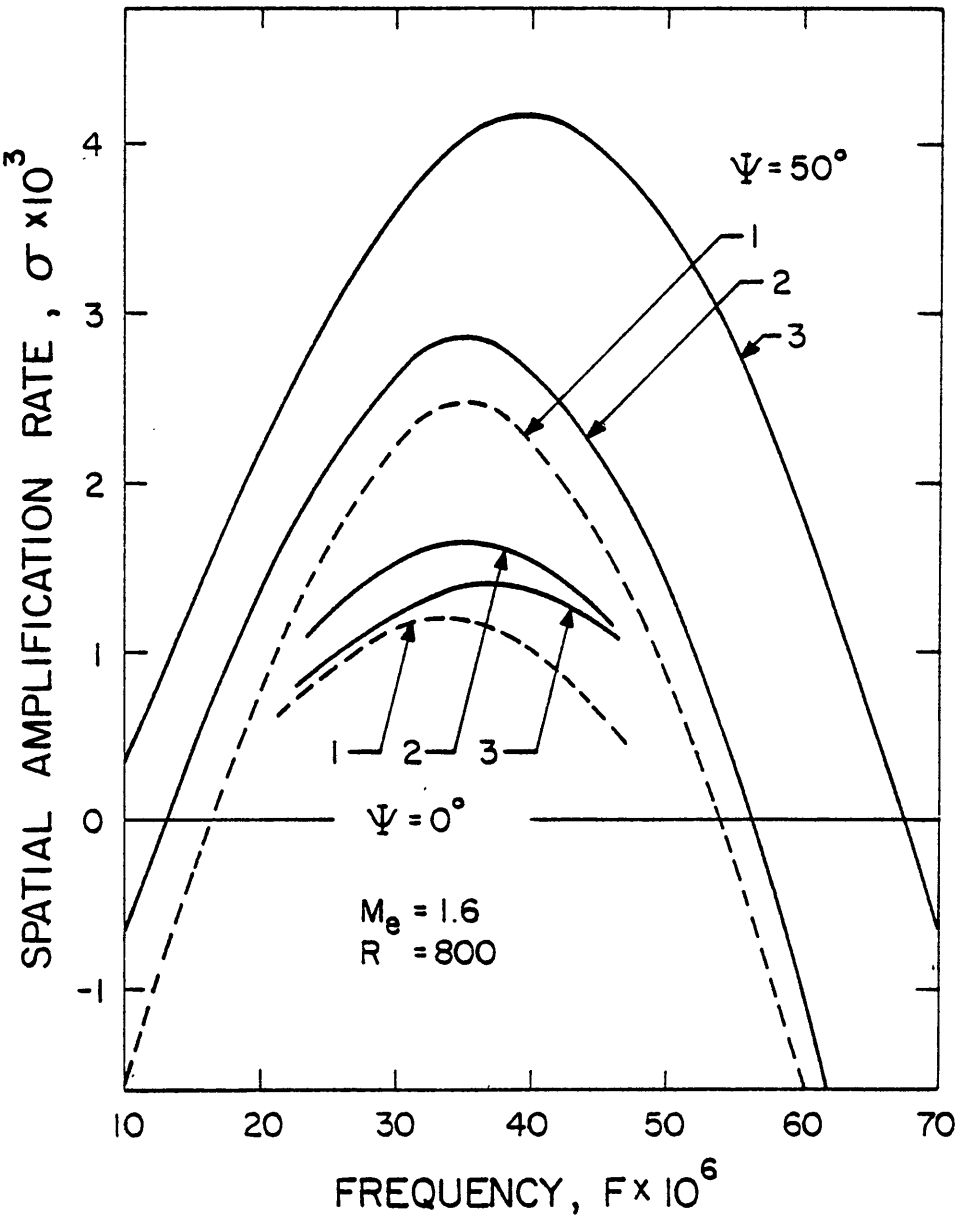

Figure 6.17 Variation of the spatial amplification rate with frequency at R = 800 for an oblique wave at $\psi = 50°$ for $M_e = 1.6$. (1) $\sigma = -\mathrm{Im}(\alpha_0)$, (2) $\sigma = -\mathrm{Im}(\alpha_0 + \varepsilon\alpha_1)$, (3) $\sigma = -\mathrm{Im}(\alpha_0 + \varepsilon\alpha_1) + \frac{\varepsilon}{|\rho u|}\frac{\partial |\rho u|}{\partial x_1}$ calculated at constant y/L near the position of the maximum of $|\rho u|$.

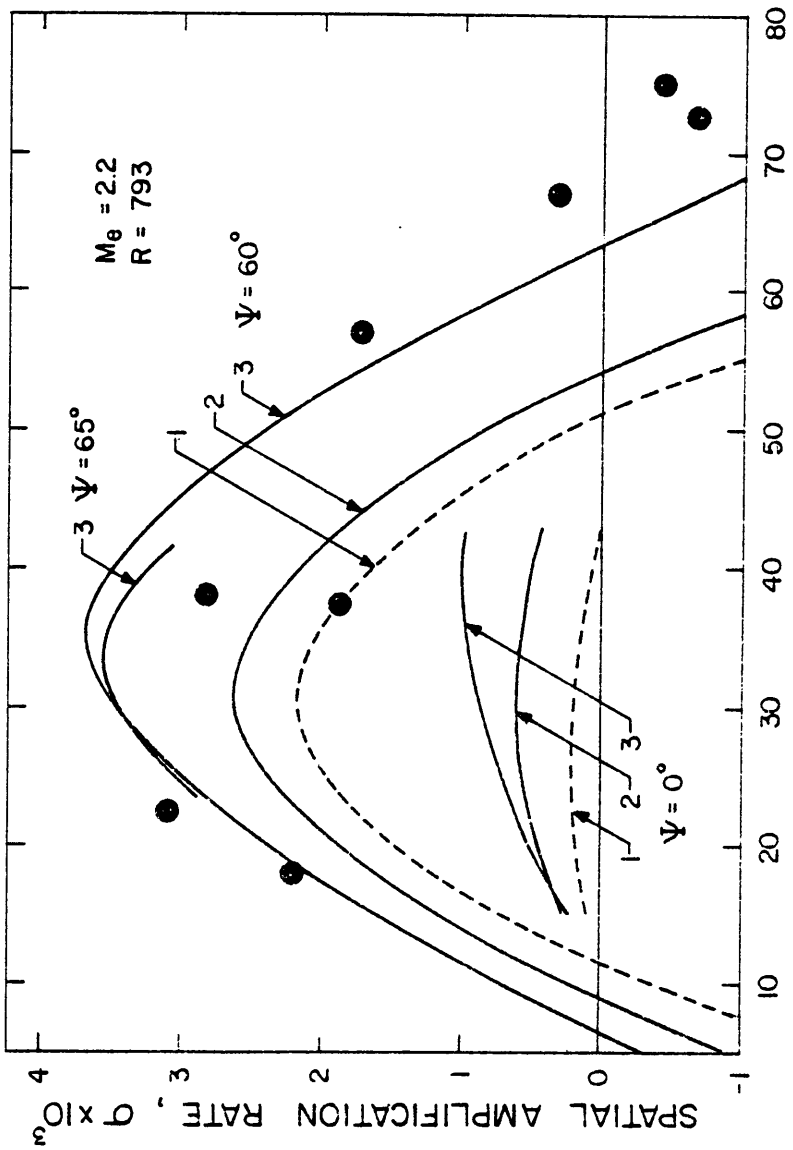

Figure 6.18 Comparison of the measured spatial amplification rates for a natural disturbance (Laufer and Vrebalovich, 1960) with the calculated spatial amplification rates for a two-dimensional and a 60°-oblique disturbance at R = 793 and M = 2.2:
(1) $\sigma = -\mathrm{Im}(\alpha_0)$, (2) $\sigma = -\mathrm{Im}(\alpha_0 + \varepsilon\alpha_1)$, (3) $\sigma = -\mathrm{Im}(\alpha_0 + \varepsilon\alpha_1) + \frac{\varepsilon}{|\rho u|}\frac{\partial |\rho u|}{\partial x_1}$
calculated at $y/L = 3.60$.

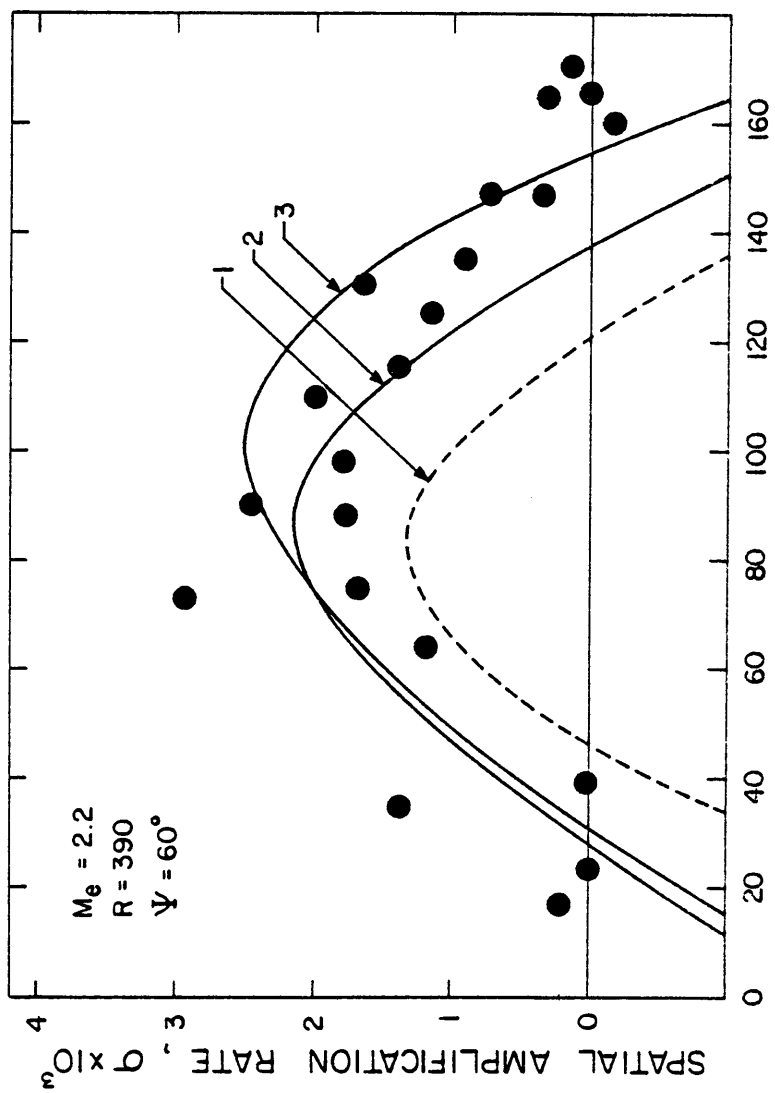

Figure 6.19 Comparison of the measured spatial amplification rates for a natural disturbance (Laufer and Vrebalovich, 1960) with the calculated spatial amplification rates for 60° - oblique disturbance at R = 390 and M_e = 2.2: (1) $\sigma = -\mathrm{Im}(\alpha_0)$, (2) $\sigma = -\mathrm{Im}(\alpha_0 + \varepsilon\alpha_1)$, (3) $\sigma = -\mathrm{Im}(\alpha_0 + \varepsilon\alpha_1) + \frac{\varepsilon}{|\rho u|}\frac{\partial|\rho u|}{\partial x_1}$ calculated at y/L = 360.

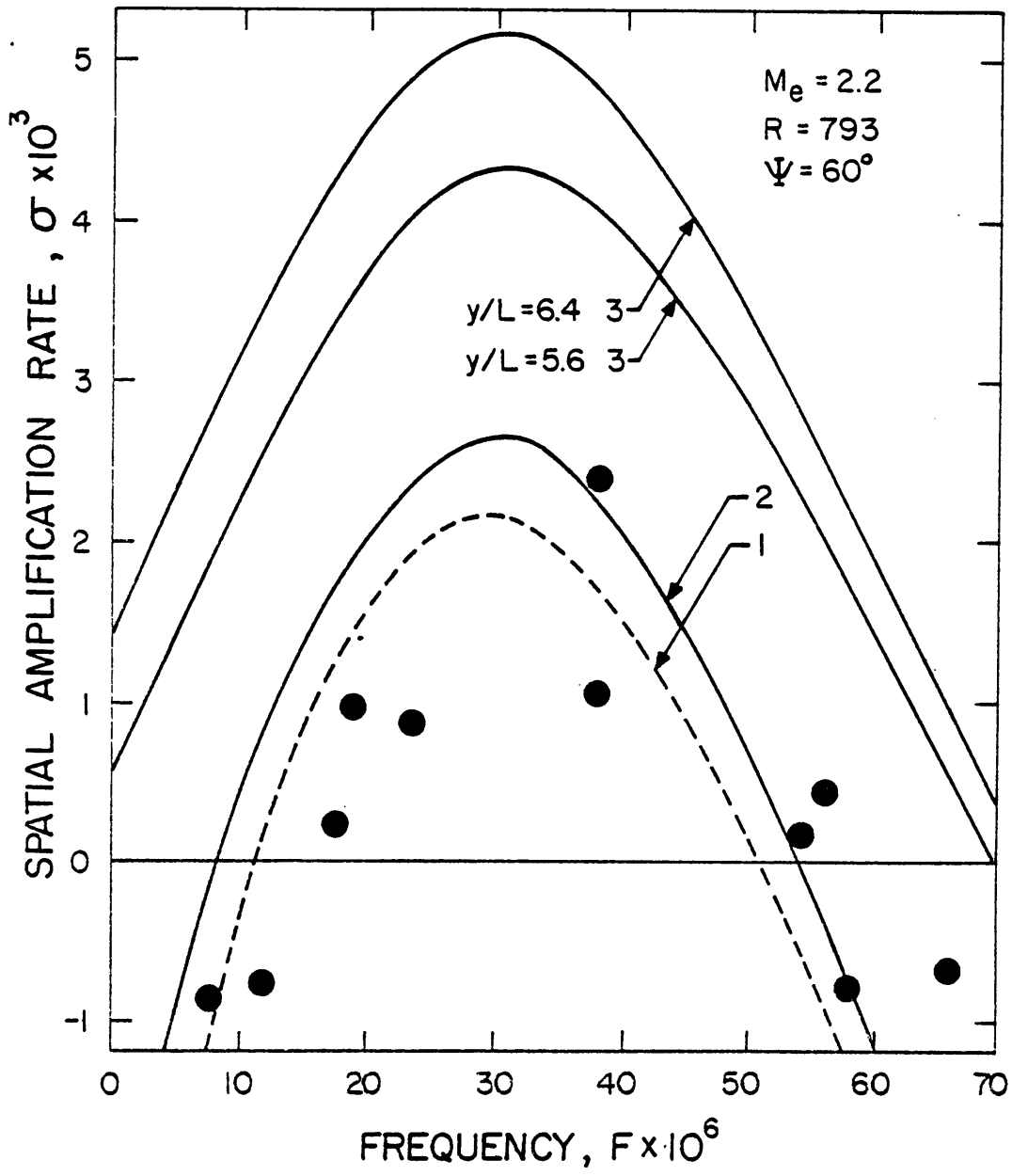

Figure 6.20 Comparison of the measured spatial amplification rates for a natural disturbance (Laufer and Vrebalovich, 1960) with the calculated spatial amplification rates for 60° - oblique disturbance at R = 793 and M_e = 2.2: (1) $\sigma = -\mathrm{Im}(\alpha_0)$, (2) $\sigma = -\mathrm{Im}(\alpha_0 + \varepsilon\alpha_1)$, (3) $\sigma = -\mathrm{Im}(\alpha_0 + \varepsilon\alpha_1) + \frac{\varepsilon}{|\rho u|}\frac{\partial |\rho u|}{\partial x_1}$ calculated at y/L = 5.6 and y/L=6.4..

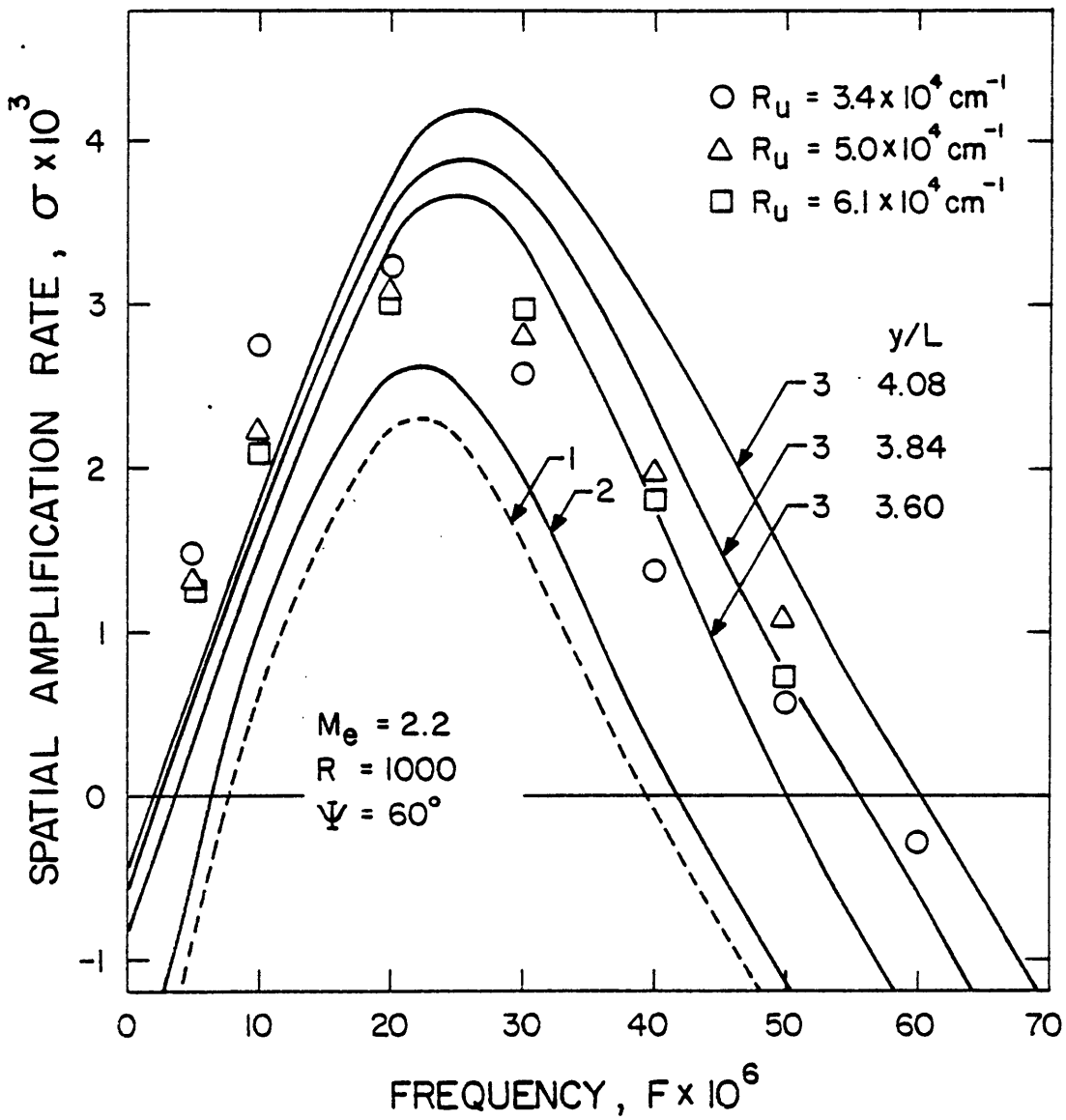

Figure 6.21a Comparison of the measured spatial amplification rates for a natural disturbance (Kendall, 1975) with the calculated spatial amplification rates for a 60° - oblique disturbance at R = 1000 and M_e = 2.2: (1) $\sigma = -\mathrm{Im}(\alpha_0)$, (2) $\sigma = -\mathrm{Im}(\alpha_0 + \varepsilon\alpha_1)$, (3) $\sigma = -\mathrm{Im}(\alpha_0 + \varepsilon\alpha_1) + \frac{\varepsilon}{|\rho u|}\frac{\partial|\rho u|}{\partial x_1}$ calculated at different y/L locations near the maximum of $|\rho u|$.

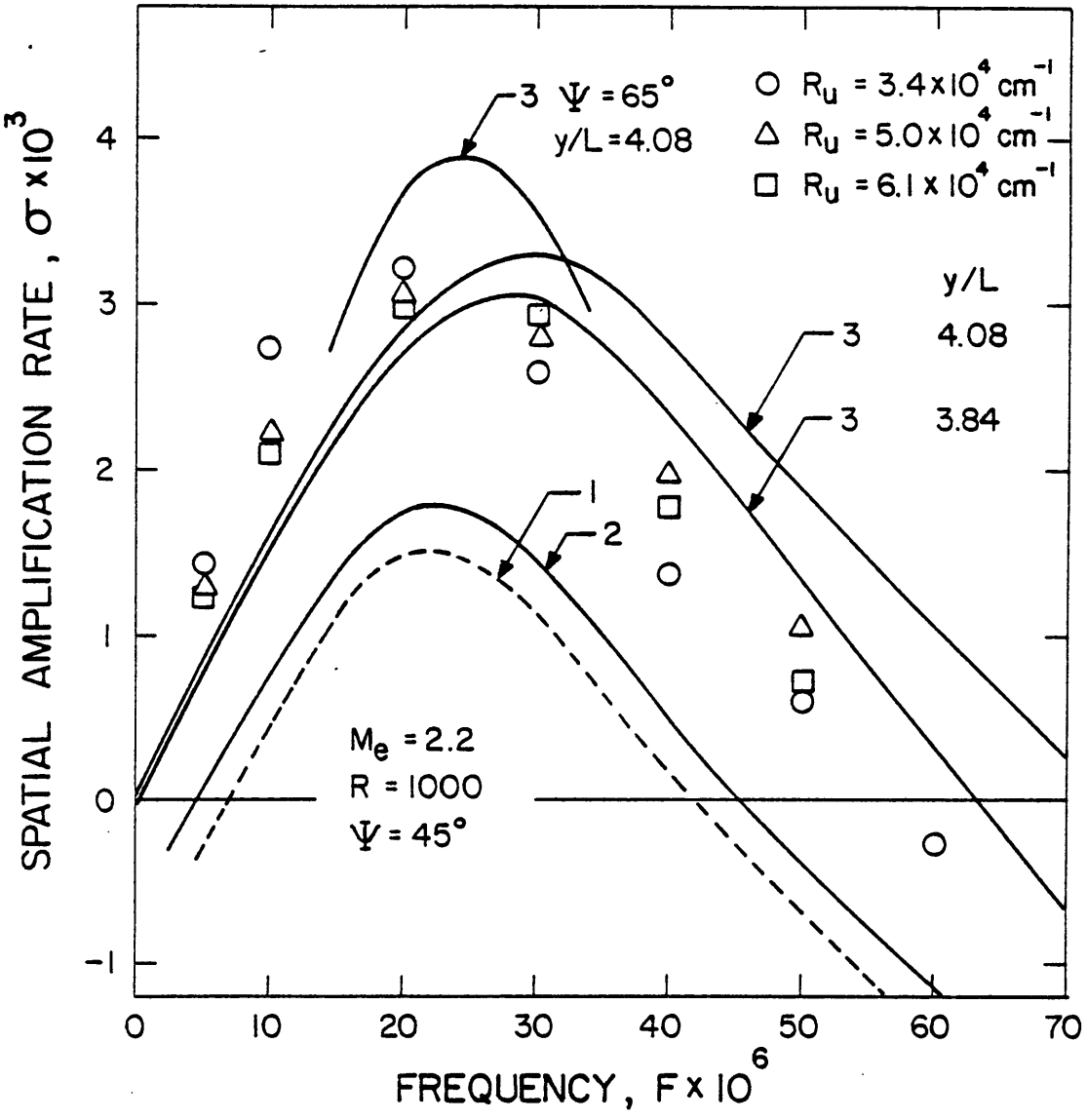

Figure 6.21b Comparison of the measured spatial amplification rates for a natural disturbance (Kendall, 1975) with the calculated spatial amplification rates for a 45° - oblique disturbance at R = 1000 and $M_e = 2.2$: (1) $\sigma = -\mathrm{Im}(\alpha_0)$, (2) $\sigma = -\mathrm{Im}(\alpha_0 + \varepsilon\alpha_1)$, (3) $\sigma = -\mathrm{Im}(\alpha_0 + \varepsilon\alpha_1) + \frac{\varepsilon}{|\rho u|}\frac{\partial|\rho u|}{\partial x_1}$ calculated at different y/L locations near the maximum of $|\rho u|$.

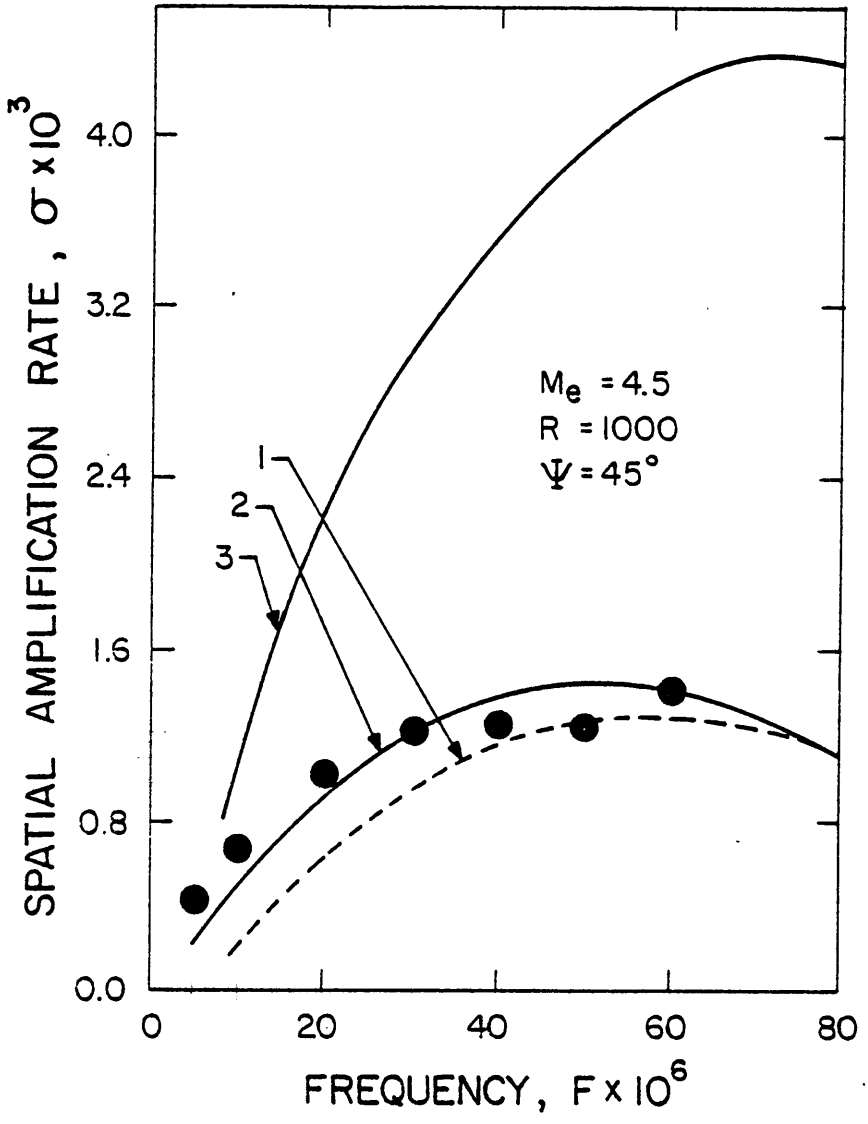

Figure 6.22 Comparison of the measured spatial amplification rates for a natural disturbance (Kendall, 1975) with the calculated spatial amplification rates for a 45°-oblique disturbance at R = 1000 and M_e = 4.5: (1) $\sigma = -\mathrm{Im}(\alpha_0)$, (2) $\sigma = -\mathrm{Im}(\alpha_0+\varepsilon\alpha_1)$, (3) $\sigma = -\mathrm{Im}(\alpha_0+\varepsilon\alpha_1) + \frac{\varepsilon}{|\rho u|}\frac{\partial|\rho u|}{\partial x_1}$ calculated at constant y/L locations near the maximum of $|\rho u|$.

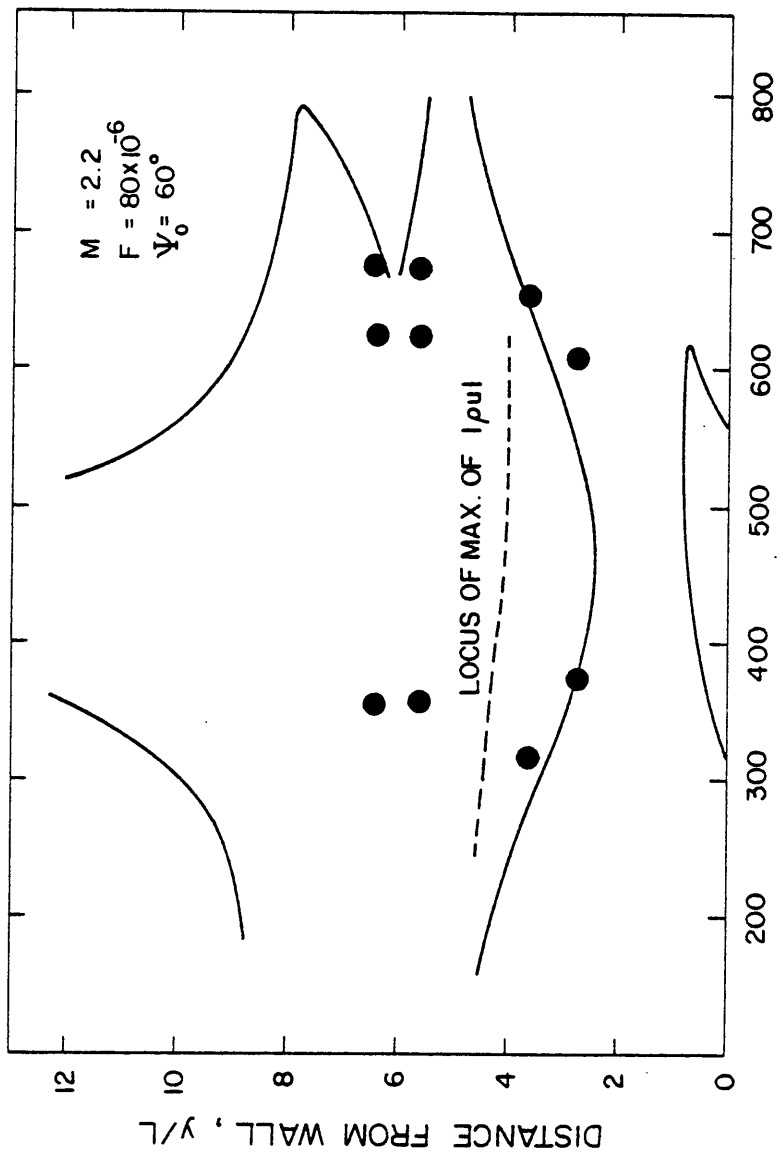

Figure 6.23 Measured (Laufer and Vrebalovich, 1960) and calculated normal locations of the neutral stability points as a function of the streamwise position for a 60°-oblique disturbance at $F = 80 \times 10^{-6}$ and $M_e = 2.2$. Solid line, the zeros of $\sigma = -\mathrm{Im}(\alpha_0 + \varepsilon\alpha_1) + \dfrac{\varepsilon}{|\rho u|}\dfrac{\partial|\rho u|}{\partial x_1}$.

APPENDIX I

$$I_m = -\left\{\rho_0\zeta_1 + U_0\frac{d\rho_0}{dT_0}\zeta_5\right\}\frac{dA}{dx_1} - \left\{\frac{\partial\rho_0}{\partial x_1}\zeta_1 + \rho_0\frac{\partial\zeta_1}{\partial x_1} + \left[\frac{d\rho_0}{dT_0}\left(\frac{\partial U_0}{\partial x_1} + \frac{\partial V_0}{\partial y}\right)\right.\right.$$

$$\left.\left. + U_0\frac{\partial}{\partial x_1}\left(\frac{d\rho_0}{dT_0}\right) + V_0\frac{\partial}{\partial y}\left(\frac{d\rho_0}{dT_0}\right)\right]\zeta_5 + U_0\frac{d\rho_0}{dT_0}\frac{\partial\zeta_5}{\partial x_1} + V_0\frac{d\rho_0}{dT_0}\frac{\partial\zeta_5}{\partial y}\right\} A$$

$$I_x = \left\{\left(\frac{2ir}{R}\mu_0\alpha_0 - \rho_0U_0\right)\zeta_1 + \frac{1}{R}\frac{\partial\mu_0}{\partial y}\zeta_3 + \frac{f}{R}\mu_0\frac{\partial\zeta_3}{\partial y} - \zeta_4\right\}\frac{dA}{dx_1}$$

$$+ \left\{\left[\frac{ir}{R}\left(\mu_0\frac{d\alpha_0}{dx_1} + \alpha_0\frac{\partial\mu_0}{\partial x_1}\right) - \rho_0\frac{\partial U_0}{\partial x_1}\right]\zeta_1 + \left(\frac{2ir}{R}\mu_0\alpha_0 - \rho_0U_0\right)\frac{\partial\zeta_1}{\partial x_1}\right.$$

$$- \rho_0V_0\zeta_2 + \frac{s}{R}\frac{\partial\mu_0}{\partial x_1}\frac{\partial\zeta_3}{\partial y} + \frac{f}{R}\mu_0\frac{\partial}{\partial x_1}\left(\frac{\partial\zeta_3}{\partial y}\right) + \frac{1}{R}\frac{\partial\mu_0}{\partial y}\frac{\partial\zeta_3}{\partial x_1} - \frac{\partial\zeta_4}{\partial x_1}$$

$$\left. + \left[\frac{i}{R}\alpha_0\frac{d\mu_0}{dT_0}\left(r\frac{\partial U_0}{\partial x_1} + s\frac{\partial V_0}{\partial y}\right) - \frac{d\rho_0}{dT_0}\left(U_0\frac{\partial U_0}{\partial x_1} + V_0\frac{\partial U_0}{\partial y}\right)\right]\zeta_5\right\} A$$

$$I_y = \left\{\frac{s}{R}\frac{\partial\mu_0}{\partial y}\zeta_1 + \frac{f}{R}\mu_0\zeta_2 + \left(\frac{2i}{R}\mu_0\alpha_0 - \rho_0U_0\right)\zeta_3 + \frac{1}{R}\frac{d\mu_0}{dT_0}\frac{\partial U_0}{\partial y}\zeta_5\right\}\frac{dA}{dx_1}$$

$$+ \left\{\frac{s}{R}\frac{\partial\mu_0}{\partial y}\frac{\partial\zeta_1}{\partial x_1} + \frac{1}{R}\frac{\partial\mu_0}{\partial x_1}\zeta_2 + \frac{f}{R}\mu_0\frac{\partial\zeta_2}{\partial x_1} + \left[\frac{i}{R}\left(\mu_0\frac{d\alpha_0}{dx_1} + \alpha_0\frac{\partial\mu_0}{\partial x_1}\right)\right.\right.$$

$$\left. - \rho_0\frac{\partial V_0}{\partial y}\right]\zeta_3 - \rho_0V_0\frac{\partial\zeta_3}{\partial y} + \left(\frac{2i}{R}\mu_0\alpha_0 - \rho_0U_0\right)\frac{\partial\zeta_3}{\partial x_1} + \frac{1}{R}\left[f\frac{d\mu_0}{dT_0}\frac{\partial}{\partial x_1}\times\right.$$

$$\left.\left(\frac{\partial U_0}{\partial y}\right) + \frac{\partial U_0}{\partial y}\frac{\partial}{\partial x_1}\left(\frac{d\mu_0}{dT_0}\right) + r\frac{d\mu_0}{dT_0}\frac{\partial^2V_0}{\partial y^2} + \left(r\frac{\partial V_0}{\partial y} + s\frac{\partial U_0}{\partial x_1}\right)\frac{\partial}{\partial y}\left(\frac{d\mu_0}{dT_0}\right)\right]\zeta_5$$

$$\left. + \frac{1}{R}\frac{d\mu_0}{dT_0}\frac{\partial U_0}{\partial y}\frac{\partial\zeta_5}{\partial x_1} + \frac{1}{R}\frac{d\mu_0}{dT_0}\left(r\frac{\partial V_0}{\partial y} + s\frac{\partial U_0}{\partial x_1}\right)\zeta_6\right\} A$$

$$I_e = \left\{\left(\frac{2i}{RPr_ec_{p_0}}\alpha_0\kappa_0 - \rho_0U_0\right)\zeta_5\right\}\frac{dA}{dx_1} - \left\{\rho_0\frac{\partial T_0}{\partial x_1}\zeta_1 - \left[\frac{i}{RPr_ec_{p_0}}\times\right.\right.$$

$$\left(\alpha_0\frac{d\kappa_0}{dT_0}\frac{\partial T_0}{\partial x_1} + \kappa_0\frac{d\alpha_0}{dx_1} + \alpha_0\frac{\partial\kappa_0}{\partial x_1}\right) - \left(\frac{d\rho_0}{dT_0} + \frac{\rho_0}{c_{p_0}}\frac{dc_{p_0}}{dT_0}\right)\left(U_0\frac{\partial T_0}{\partial x_1}\right.$$

$$\left.\left. + V_0\frac{\partial T_0}{\partial y}\right)\right]\zeta_5 + \left(\frac{2i}{RPr_ec_{p_0}}\alpha_0\kappa_0 - \rho_0U_0\right)\frac{\partial\zeta_5}{\partial x_1} - \rho_0V_0\zeta_6\right\} A$$

APPENDIX II

The variation of the water thermodynamic and transport properties with temperature is given by

$$\rho = 1 - \frac{(T - 3.9863)^2(T + 288.9414)}{508929.2\ (T + 68.12963)} + 0.011445\ \exp(-\frac{374.3}{T})$$

ρ in gm/mℓ, T in °C.

$$\text{Log}(\frac{1.002}{\mu}) = \frac{1.37023(T - 20) + 8.36 \times 10^{-4}(T - 20)^2}{109 + T}$$

μ in Cp, T in °C

$$\kappa = - 9.901090 + 0.1001982T - 1.873892 \times 10^{-4}T^2 + 1.039570 \times 10^{-7}T^3$$

κ in m watts $cm^{-1}K^{-1}$, T in °K

$$c_p = 2.13974 - 9.68137 \times 10^{-3}T + 2.68536 \times 10^{-5}T^2 - 2.42139 \times 10^{-8}T^3$$

c_p in cal $gm^{-1}K^{-1}$, T in °K

A discussion of the sources and accuracy of these formulas can be found in Lowell and Reshotko (1974).

APPENDIX III

$$I_m = -\left\{\frac{1}{T_0}\zeta_1 + \frac{\gamma M_e^2 U_0}{T_0}\zeta_4 - \frac{U_0}{T_0^2}\zeta_5\right\}\frac{dA}{dx_1} + \left\{\frac{1}{T_0^2}\frac{\partial T_0}{\partial x_1}\zeta_1 - \frac{1}{T_0}\frac{\partial \zeta_1}{\partial x_1} - \frac{\gamma M_e^2}{T_0}\left(\frac{\partial U_0}{\partial x_1} + \frac{\partial V_0}{\partial y} - \frac{U_0}{T_0}\frac{\partial T_0}{\partial x_1} - \frac{V_0}{T_0}\frac{\partial T_0}{\partial y}\right)\zeta_4 - \frac{\gamma M_e^2 U_0}{T_0}\frac{\partial \zeta_4}{\partial x_1} - \frac{\gamma M_e^2 V_0}{T_0}\frac{\partial \zeta_4}{\partial y} + \frac{1}{T^2}\left(\frac{\partial U_0}{\partial x_1} + \frac{\partial V_0}{\partial y} - 2\frac{U_0}{T_0}\frac{\partial T_0}{\partial x_1} - 2\frac{V_0}{T_0}\frac{\partial T_0}{\partial y}\right)\zeta_5 + \frac{U_0}{T_0^2}\frac{\partial \zeta_5}{\partial x_1} + \frac{V_0}{T_0^2}\zeta_6\right\} A$$

$$I_x = \left\{\left(\frac{2ir}{R}.\mu_0\alpha_0 - \frac{U_0}{T_0}\right)\zeta_1 + \frac{1}{R}\frac{\partial \mu_0}{\partial y}\zeta_3 + \frac{f}{R}\mu_0\frac{\partial \mu_3}{\partial y} - \zeta_4\right\}\frac{dA}{dx_1} + \left\{\left[\frac{ir}{R}\left(\mu_0\frac{d\alpha_0}{dx_1} + \alpha_0\frac{\partial \mu_0}{\partial x_1}\right) - \frac{1}{T_0}\frac{\partial U_0}{\partial x_1}\right]\zeta_1 + \left(\frac{2ir}{R}\mu_0\alpha_0 - \frac{U_0}{T_0}\right)\frac{\partial \zeta_1}{\partial x_1} - \frac{V_0}{T_0}\zeta_2 + \frac{s}{R}\frac{\partial \mu_0}{\partial x_1}\frac{\partial \zeta_3}{\partial y} + \frac{f}{R}\mu_0\frac{\partial}{\partial x_1}\left(\frac{\partial \zeta_3}{\partial y}\right) + \frac{1}{R}\frac{\partial \mu_0}{\partial y}\frac{\partial \zeta_3}{\partial x_1} - \frac{\gamma M_e^2}{T_0}\left(U_0\frac{\partial U_0}{\partial x_1} + V_0\frac{\partial U_0}{\partial y}\right)\zeta_4 - \frac{\partial \zeta_4}{\partial x_1} + \left[\frac{i}{R}\alpha_0\frac{d\mu_0}{dT_0}\left(r\frac{\partial U_0}{\partial x_1} + s\frac{\partial V_0}{\partial y}\right) + \frac{1}{T_0^2}\left(U_0\frac{\partial U_0}{\partial x_1} + V_0\frac{\partial U_0}{\partial y}\right)\right]\zeta_5\right\} A$$

$$I_y = \left\{\frac{s}{R}\frac{\partial \mu_0}{\partial y}\zeta_1 + \frac{f}{R}\mu_0\zeta_2 + \left(\frac{2i}{R}\mu_0\alpha_0 - \frac{U_0}{T_0}\right)\zeta_3 + \frac{1}{R}\frac{d\mu_0}{dT_0}\frac{\partial U_0}{\partial y}\zeta_5\right\}\frac{dA}{dx_1} + \left\{\frac{s}{R}\frac{\partial \mu_0}{\partial y}\frac{\partial \zeta_1}{\partial x_1} + \frac{1}{R}\frac{\partial \mu_0}{\partial x_1}\zeta_2 + \frac{f}{R}\mu_0\frac{\partial \zeta_2}{\partial x_1} + \left[\frac{i}{R}\left(\mu_0\frac{d\alpha_0}{dx_1} + \alpha_0\frac{\partial \mu_0}{\partial x_1}\right) - \frac{1}{T_0}\frac{\partial V_0}{\partial y}\right]\zeta_3 - \frac{V_0}{T_0}\frac{\partial \zeta_3}{\partial y} + \left(\frac{2i}{R}\mu_0\alpha_0 - \frac{U_0}{T_0}\right)\frac{\partial \zeta_3}{\partial x_1} + \frac{1}{R}\left[f\frac{d\mu_0}{dT_0}\frac{\partial}{\partial x_1}\times\left(\frac{\partial U_0}{\partial y}\right) + \frac{\partial U_0}{\partial y}\frac{\partial}{\partial x_1}\left(\frac{d\mu_0}{dT_0}\right) + r\frac{d\mu_0}{dT_0}\frac{\partial^2 V_0}{\partial y^2} + \left(r\frac{\partial V_0}{\partial y} + s\frac{\partial U_0}{\partial x_1}\right)\times\frac{\partial}{\partial y}\left(\frac{d\mu_0}{dT_0}\right)\right]\zeta_5 + \frac{1}{R}\frac{d\mu_0}{dT_0}\frac{\partial U_0}{\partial y}\frac{\partial \zeta_5}{\partial x_1} + \frac{1}{R}\frac{d\mu_0}{dT_0}\left(r\frac{\partial V_0}{\partial y} + s\frac{\partial U_0}{\partial x_1}\right)\zeta_6\right\} A$$

$$
\begin{aligned}
I_e = & \left\{ \left(\frac{2i}{RPr}\,\alpha_0\mu_0 - \frac{U_0}{T_0}\right)\zeta_5 + (\gamma-1)M_e^2\left(\frac{2}{R}\,\mu_0\,\frac{\partial U_0}{\partial y}\,\zeta_3 + U_0\zeta_4\right)\right\}\frac{dA}{dx_1} \\
& + \left\{\left\{(\gamma-1)M_e^2\left[\frac{\partial P_0}{\partial x_1} + \frac{2i}{R}\,\alpha_0\mu_0\left(r\,\frac{\partial U_0}{\partial x_1} + s\,\frac{\partial V_0}{\partial y}\right)\right] - \frac{1}{T_0}\,\frac{\partial T_0}{\partial x_1}\right\}\zeta_1\right. \\
& + \frac{2}{R}\,\mu_0(\gamma-1)M_e^2\left[\frac{\partial U_0}{\partial y}\,\frac{\partial \zeta_3}{\partial x_1} + \left(r\,\frac{\partial V_0}{\partial y} + s\,\frac{\partial U_0}{\partial x_1}\right)\frac{\partial \zeta_3}{\partial y}\right] \\
& - \frac{\gamma M_e^2}{T_0}\left(U_0\,\frac{\partial T_0}{\partial x_1} + V_0\,\frac{\partial T_0}{\partial y}\right)\zeta_4 + (\gamma-1)M_e^2\left(U_0\,\frac{\partial \zeta_4}{\partial x_1} + V_0\,\frac{\partial \zeta_4}{\partial y}\right) \\
& + \left[\frac{1}{T_0^2}\left(U_0\,\frac{\partial T_0}{\partial x_1} + V_0\,\frac{\partial T_0}{\partial y}\right) + \frac{i}{RPr}\left(\mu_0\,\frac{d\alpha_0}{dx_1} + 2\alpha_0\,\frac{\partial \mu_0}{\partial x_1}\right)\right]\zeta_5 \\
& \left. + \left(\frac{2i}{RPr}\,\alpha_0\mu_0 - \frac{U_0}{T_0}\right)\frac{\partial \zeta_5}{\partial x_1} - \frac{V_0}{T_0}\,\zeta_6\right\} A
\end{aligned}
$$

APPENDIX IV

The variations of the air properties with temperature is given by

$$\mu = \frac{1.458T^{3/2} \times 10^{-5}}{T + 110.4} \qquad \text{for } T > 110.4$$

$$\mu = (0.693873 \times 10^{-6})T \qquad \text{for } T \leq 110.4$$

μ in gm/cm. sec, T in °K

$$\kappa = \frac{0.6325T^{1/2} \times 10^{-5}}{1 + (245.4/T) \times 10^{-12/T}} \qquad \text{for } T > 80$$

$$\kappa = (0.222964 \times 10^{-6})T \qquad \text{for } T \leq 80$$

κ in cal/cm. sec. °C, T in °K

For the variations of the enthalpy and Prandtl number with temperature, the NBS perfect gas tables (Hilsenrath et al, 1955) are used. The specific heat c_p is computed from the definition of Prandtl number

$$Pr = \frac{c_p \mu}{\kappa}$$

using the calculated values of μ and κ and the tabulated values of Pr. The constants used in preceding relations are taken from Hilsenrath et al (1955).

APPENDIX V

$$I_m = -\left\{\frac{1}{T_0}\zeta_1 + \frac{\gamma M_e^2 U_0}{T_0}\zeta_4 - \frac{U_0}{T_0^2}\zeta_5\right\}\frac{dA}{dx_1} - \left\{\frac{1}{T_0}\zeta_7\right\}\frac{dA}{dz_1} + \left\{\frac{1}{T_0^2}\frac{\partial T_0}{\partial x_1}\zeta_1\right.$$

$$- \frac{1}{T_0}\frac{\partial \zeta_1}{\partial x_1} - \frac{\gamma M_e^2}{T_0}\left(\frac{\partial U_0}{\partial x_1} + \frac{\partial V_0}{\partial y} - \frac{U_0}{T_0}\frac{\partial T_0}{\partial x_1} - \frac{V_0}{T_0}\frac{\partial T_0}{\partial y}\right)\zeta_4 - \frac{\gamma M_e^2 U_0}{T_0}\frac{\partial \zeta_4}{\partial x_1}$$

$$- \frac{\gamma M_e^2 V_0}{T_0}\frac{\partial \zeta_4}{\partial y} + \frac{1}{T_0^2}\left(\frac{\partial U_0}{\partial x_1} + \frac{\partial V_0}{\partial y} - 2\frac{U_0}{T_0}\frac{\partial T_0}{\partial x_1} - 2\frac{V_0}{T_0}\frac{\partial T_0}{\partial y}\right)\zeta_5$$

$$\left. + \frac{U_0}{T_0^2}\frac{\partial \zeta_5}{\partial x_1} + \frac{V_0}{T_0^2}\zeta_6 - \frac{1}{T_0}\frac{\partial \zeta_7}{\partial z_1}\right\} A$$

$$I_x = \left\{\left(\frac{2ir}{R}\mu_0\alpha_0 - \frac{U_0}{T_0}\right)\zeta_1 + \frac{1}{R}\frac{\partial \mu_0}{\partial y}\zeta_3 + \frac{f}{R}\mu_0\frac{\partial \zeta_3}{\partial y} - \zeta_4 + \frac{if}{R}\mu_0\beta_0\zeta_7\right\}\frac{dA}{dx_1}$$

$$+ \left\{\frac{2i}{R}\mu_0\beta_0\zeta_1 + \frac{if}{R}\mu_0\alpha_0\zeta_7\right\}\frac{dA}{\partial z_1} + \left\{\left[\frac{ir}{R}\left(\mu_0\frac{\partial \alpha_0}{\partial x_1} + \alpha_0\frac{\partial \mu_0}{\partial x_1}\right)\right.\right.$$

$$+ \frac{i}{R}\mu_0\frac{\partial \beta_0}{\partial z_1} - \frac{1}{T_0}\frac{\partial U_0}{\partial x_1}\Big]\zeta_1 + \left(\frac{2ir}{R}\mu_0\alpha_0 - \frac{U_0}{T_0}\right)\frac{\partial \zeta_1}{\partial x_1} + \frac{2i}{R}\mu_0\beta_0\frac{\partial \zeta_1}{\partial z_1}$$

$$- \frac{V_0}{T_0}\zeta_2 + \frac{s}{R}\frac{\partial \mu_0}{\partial x_1}\frac{\partial \zeta_3}{\partial y} + \frac{f}{R}\mu_0\frac{\partial}{\partial x_1}\left(\frac{\partial \zeta_3}{\partial y}\right) + \frac{1}{R}\frac{\partial \mu_0}{\partial y}\frac{\partial \zeta_3}{\partial x_1}$$

$$- \frac{\gamma M_e^2}{T_0}\left(U_0\frac{\partial U_0}{\partial x_1} + V_0\frac{\partial U_0}{\partial y}\right)\zeta_4 - \frac{\partial \zeta_4}{\partial x_1} + \left[\frac{i}{R}\alpha_0\frac{d\mu_0}{dT_0}\left(r\frac{\partial U_0}{\partial x_1} + s\frac{\partial V_0}{\partial y}\right)\right.$$

$$\left. + \frac{1}{T_0^2}\left(U_0\frac{\partial U_0}{\partial x_1} + V_0\frac{\partial U_0}{\partial y}\right)\right]\zeta_5 + \left[\frac{is}{R}\left(\mu_0\frac{\partial \beta_0}{\partial x_1} + \beta_0\frac{\partial \mu_0}{\partial x_1}\right)\right.$$

$$\left.\left. + \frac{i}{R}\mu_0\frac{\partial \alpha_0}{\partial z_1}\right]\zeta_7 + \frac{if}{R}\mu_0\beta_0\frac{\partial \zeta_7}{\partial x_1} + \frac{if}{R}\mu_0\alpha_0\frac{\partial \zeta_7}{\partial z_1}\right\} A$$

$$I_y = \left\{\frac{s}{R}\frac{\partial\mu_0}{\partial y}\zeta_1 + \frac{f}{R}\mu_0\zeta_2 + \left(\frac{2i}{R}\mu_0\alpha_0 - \frac{U_0}{T_0}\right)\zeta_3 + \frac{1}{R}\frac{d\mu_0}{dT_0}\frac{\partial U_0}{\partial y}\zeta_5\right\}\frac{dA}{dx_1}$$

$$+\left\{\frac{2i}{R}\mu_0\beta_0\zeta_3 + \frac{s}{R}\frac{\partial\mu_0}{\partial y}\zeta_7 + \frac{f}{R}\mu_0\zeta_8\right\}\frac{dA}{dz_1} + \left\{\frac{s}{R}\frac{\partial\mu_0}{\partial y}\frac{\partial\zeta_1}{\partial x_1}\right.$$

$$+\frac{1}{R}\frac{\partial\mu_0}{\partial x_1}\zeta_2 + \frac{f}{R}\mu_0\frac{\partial\zeta_2}{\partial x_1} + \left[\frac{i}{R}\left(\mu_0\frac{\partial\alpha_0}{\partial x_1} + \alpha_0\frac{\partial\mu_0}{\partial x_1}\right) + \frac{i}{R}\mu_0\frac{\partial\beta_0}{\partial z_1}\right.$$

$$\left.-\frac{1}{T_0}\frac{\partial V_0}{\partial y}\right]\zeta_3 - \frac{V_0}{T_0}\frac{\partial\zeta_3}{\partial y} + \left(\frac{2i}{R}\mu_0\alpha_0 - \frac{U_0}{T_0}\right)\frac{\partial\zeta_3}{\partial x_1} + \frac{2i}{R}\mu_0\beta_0\frac{\partial\zeta_3}{\partial z_1}$$

$$+\frac{1}{R}\left[f\frac{d\mu_0}{dT_0}\frac{\partial}{\partial x_1}\left(\frac{\partial U_0}{\partial y}\right) + \frac{\partial U_0}{\partial y}\frac{\partial}{\partial x_1}\left(\frac{d\mu_0}{dT_0}\right) + r\frac{d\mu_0}{dT_0}\frac{\partial^2 V_0}{\partial y^2} + \left(r\frac{\partial V_0}{\partial y}\right.\right.$$

$$\left.\left.+ s\frac{\partial U_0}{\partial x}\right)\frac{\partial}{\partial y}\left(\frac{d\mu_0}{dT_0}\right)\right]\zeta_5 + \frac{1}{R}\frac{d\mu_0}{dT_0}\frac{\partial U_0}{\partial y}\frac{\partial\zeta_5}{\partial x_1} + \frac{1}{R}\frac{d\mu_0}{dT_0}\left(r\frac{\partial V_0}{\partial y}\right.$$

$$\left.+ s\frac{\partial U_0}{\partial x_1}\right)\zeta_6 + \frac{s}{R}\frac{\partial\mu_0}{\partial y}\frac{\partial\zeta_7}{\partial z_1} + \frac{f}{R}\mu_0\frac{\partial\zeta_8}{\partial z_1}\Bigg\}A$$

$$I_z = \left\{\frac{if}{R}\mu_0\beta_0\zeta_1 + \left(\frac{2i}{R}\mu_0\alpha_0 - \frac{U_0}{T_0}\right)\zeta_7\right\}\frac{dA}{dx_1} + \left\{\frac{if}{R}\mu_0\alpha_0\zeta_1 + \frac{1}{R}\frac{\partial\mu_0}{\partial y}\zeta_3\right.$$

$$\left.+\frac{f}{R}\mu_0\frac{\partial\zeta_3}{\partial y} - \zeta_4 + \frac{2ir}{R}\mu_0\beta_0\zeta_7\right\}\frac{dA}{dz_1} + \left\{\left[\frac{is}{R}\mu_0\frac{\partial\alpha_0}{\partial z_1}\right.\right.$$

$$-\left.\left.+\frac{i}{R}\left(\mu_0\frac{\partial\beta_0}{\partial x_1} + \beta_0\frac{\partial\mu_0}{\partial x_1}\right)\right]\zeta_1 + \frac{if}{R}\mu_0\beta_0\frac{\partial\zeta_1}{\partial x_1} + \frac{if}{R}\mu_0\alpha_0\frac{\partial\zeta_1}{\partial z_1}\right.$$

$$+\frac{1}{R}\frac{\partial\mu_0}{\partial y}\frac{\partial\zeta_3}{\partial z_1} + \frac{f}{R}\mu_0\frac{\partial}{\partial z_1}\left(\frac{\partial\zeta_3}{\partial y}\right) - \frac{\partial\zeta_4}{\partial z_1} + \frac{is}{R}\beta_0\frac{d\mu_0}{dT_0}\left(\frac{\partial U_0}{\partial x_1} + \frac{\partial V_0}{\partial y}\right)\zeta_5$$

$$+\left[\frac{i}{R}\left(\mu_0\frac{\partial\alpha_0}{\partial x_1} + \alpha_0\frac{\partial\mu_0}{\partial x_1}\right) + \frac{ir}{R}\mu_0\frac{\partial\beta_0}{\partial z_1}\right]\zeta_7 + \left(\frac{2i}{R}\mu_0\alpha_0 - \frac{U_0}{T_0}\right)\frac{\partial\zeta_7}{\partial x_1}$$

$$\left.+\frac{2ir}{R}\mu_0\beta_0\frac{\partial\zeta_7}{\partial z_1} - \frac{V_0}{T_0}\zeta_8\right\}A$$

$$I_e = \left\{ \left(\frac{2i}{RPr}\,\alpha_0\mu_0 - \frac{U_0}{T_0}\right)\zeta_5 + (\gamma-1)M_e^2\left(\frac{2}{R}\,\mu_0\,\frac{\partial U_0}{\partial y}\,\zeta_3 + U_0\zeta_4\right) \right\} \frac{dA}{dx_1}$$

$$+ \left\{ \frac{2i}{RPr}\,\mu_0\beta_0\zeta_5 \right\} \frac{dA}{dz_1} + \left\{ \left\{ (\gamma-1)M_e^2\left[\frac{\partial P_0}{\partial x_1} + \frac{2i}{R}\,\alpha_0\mu_0\left(r\,\frac{\partial U_0}{\partial x_1} + s\,\frac{\partial V_0}{\partial y}\right)\right] \right.\right.$$

$$\left. - \frac{1}{T_0}\,\frac{\partial T_0}{\partial x} \right\}\zeta_1 + \frac{2}{R}\,\mu_0(\gamma-1)M_e^2\left[\frac{\partial U_0}{\partial y}\,\frac{\partial \zeta_3}{\partial x_1} + \left(r\,\frac{\partial V_0}{\partial y} + s\,\frac{\partial U_0}{\partial x_1}\right)\frac{\partial \zeta_3}{\partial y}\right]$$

$$- \frac{\gamma M_e^2}{T_0}\left(U_0\,\frac{\partial T_0}{\partial x} + V_0\,\frac{\partial T_0}{\partial y}\right)\zeta_4 + (\gamma-1)M_e^2\left(U_0\,\frac{\partial \zeta_4}{\partial x_1} + V_0\,\frac{\partial \zeta_4}{\partial y}\right)$$

$$+ \left[\frac{1}{T_0^2}\left(U_0\,\frac{\partial T_0}{\partial x_1} + V_0\,\frac{\partial T_0}{\partial y}\right) + \frac{i}{RPr}\left(\mu_0\,\frac{\partial \alpha_0}{\partial x_1} + 2\alpha_0\,\frac{\partial \mu_0}{\partial x_1}\right)\right.$$

$$\left. + \frac{i}{RPr}\,\mu_0\,\frac{\partial \beta_0}{\partial z_1}\right]\zeta_5 + \left(\frac{2i}{RPr}\,\alpha_0\mu_0 - \frac{U_0}{T_0}\right)\frac{\partial \zeta_5}{\partial x_1} + \frac{2i}{RPr}\,\mu_0\beta_0\,\frac{\partial \zeta_5}{\partial z_1}$$

$$\left. - \frac{V_0}{T_0}\,\zeta_6 + \frac{2is}{R}\,\mu_0\beta_0(\gamma-1)M_e^2\left(\frac{\partial U_0}{\partial x_1} + \frac{\partial V_0}{\partial y}\right)\zeta_7 \right\} A$$

The vita has been removed from the scanned document

EFFECT OF COMPRESSIBILITY, SUCTION, AND HEAT TRANSFER ON THE NONPARALLEL STABILITY OF BOUNDARY-LAYER FLOWS

by

Nabil Mohamed El-Hady

(ABSTRACT)

We investigate the effect of heating, suction, and compressibility on the stability characteristics of boundary-layer flows within the framework of a complete nonparallel, linear, spatial stability theory. Included in the theory are disturbances due to velocity, pressure, temperature, density, and transport properties as well as variations of the fluid properties with temperature. The method of multiple scales is used to account for the nonparallelism of the mean flow and an equation is derived for the modulation of the wave amplitude with position. The nonparallel results of uniform wall heating for water flows past a flat plate are in good agreement with the experimental results of Strazisar et al (1975, 1977). Both parallel and nonparallel results are in qualitative agreement with the experimental results of Strazisar and Reshotko (1978) for power-law temperature distributions when the nonsimilarity of the mean flow is taken into account.

Stability characteristics are examined for boundary-layer flows over an adiabatic flat plate to study the effect of a slight compressibility of the mean flow. Although the percentage increase in the maximum growth rate and in the amplitude ratio due to nonparallelism in-

creases as the Mach number increase, a nearly constant $\Delta\sigma$, where σ is the growth rate, is observed for the Mach number range from 0.0 to 1.0.

The feasability of controlling boundary layers by suction through porous strips is investigated and the results are compared with the case of continuous area suction. It appears that the effectiveness of a strip can be increased considerably by increasing the extent of the upstream influence (sink effect). The results show that the strip number, widths, and spacings can be optimized so that one needs total suction levels of about 5-10% more than those needed to achieve the same stability characteristics using area suction.

For supersonic flows, oblique first-mode waves are more unstable than two-dimensional waves according to both parallel and nonparallel theories. The effect of nonparallelism on the growth rate of a disturbance is a function of the wave angle. The nonparallelism has a larger influence on the second mode than on the first mode. For the second-mode the most unstable frequency predicted by the nonparallel theory for a given Reynolds number is higher than that predicted by the parallel theory, in contrast with the first mode results where they are equal. The distortion effect of the mode shapes is relatively small at the location normal to the plate where $|\rho u|$ is maximum. The nonparallel results show good agreement with the experimental results of Laufer and Vrebalovich (1960) and Kendall (1975), in contrast with the parallel results which underpredict the experimental measurements.